DOCTOR OF PHILOSOPHY

A Systematic Approach To the Implementation of Renewable Energy Under Different Climate Change Scenarios: Achieving Sustainable and Resilient Energy Access In The East African Community

Nkurunziza, Romeo Sosthene

Award date:
2020

A Systematic Approach To the Implementation of Renewable Energy Under Different Climate Change Scenarios: Achieving Sustainable and Resilient Energy Access In The East African Community

By

Romeo Sosthène Nkurunziza

March 2019

A thesis submitted in partial fulfilment of the University's requirements for the Degree of Doctor of Philosophy

Certificate of Ethical Approval

Applicant: Romeo Nkurunziza

Project Title: A Systematic Approach To the Implementation of Renewable Energy Under Different Climate Change Scenarios: Achieving Sustainable and Resilient Energy Access In The East African Community.

This is to certify that the above named applicant has completed the Coventry University Ethical Approval process and their project has been confirmed and approved as Low Risk

Date of approval: 12 February 2019

Project Reference Number: P87228

Acknowledgements

Praise the Lord for his has given me the courage and the strength to complete this works. I am indebted and thankful to my family for being patient and supportive throughout the journey of this thesis.

My sincere gratitude goes to my Director of Study Dr Abdullahi Ahmed who supported and guided me throughout this research. Thanks to Dr George Agyekum-Mensah and Dr Andrew Arewa for their guidance and supervisory role.

This work would not have been possible without the support and guidance that I received from Dr Bastien Dieppois and Dr Jonathan Eden. Their kindness, understanding, encouragement and critically constructive discussions have supported me greatly and contributed to constructing and completing this research.

I am also thankful to the Met Office, especially David Hein for his support and guidance throughout the placement at Met Office. Many thanks to Dr Laura Burgin for all support, guidance and encouragement she gave me. Her friendship, kindness and understanding have built my research capabilities.

My thanks also go out to the Dr Liam Brierley, PhD student Moussa Sidibe, Eade Rosie and others who all helped me in numerous ways during my research.
I am also grateful to the Centre for Agroecology, Water and Resilience for hosting me during the final year of my research.

Abstract

Despite abundant renewable energy resources in the East African Community (EAC) geographical region, energy access is very low with less than 20% of the population having reliable access. Modern energy provision in the region is still heavily dependent on hydropower which contributes to the generation of more than 50% of the electricity used in the area. There is clear evidence that the hydropower plants in the region are operating below capacity due to drought. The hydropower production deficit is often met by fossil fuel power generators, which are not sustainable due to their cost and resulting environmental pollution. The existing modern energy provision in the EAC has been found to be inadequate, variable and unreliable and cannot solve the energy access problem in the region. Therefore, harnessing renewable energy from various sources will lead to a sustainable, reliable and climate-resilient energy supply by reducing dependency on fossil fuel, with its inherent costs and potential for environmental damage, as well as buffering hydropower generation shortfalls.

Even though the region has recently developed a renewable energy implementation plan, so far no comprehensive research has been carried out to explore the ways various energy sources in the EAC can be harnessed to reduce the energy access gap caused by shortfalls in hydropower generation. In response to this gap in knowledge, this research investigates a systematic approach for achieving a reliable, sustainable, and climate-resilient energy supply in the EAC under different climate change scenarios.

Data from the Co-ordinated Regional Climate Downscaling Experiment (CORDEX-AFRICA) project was used as the basis for future climate prediction. Climate data from 17 CORDEX-AFRICA Regional Climate Models for the time period of 2021 to 2100, under both representative Concentration Pathways (RCP) RCP4.5 and 8.5 climate scenarios, were used in a multi-model ensemble (MME). From 2021-2100, under both

RCP4.5 and 8.5, precipitation and wind speed are always complementary irrespective of the levels of solar irradiance. In addition, it is predicted that precipitation and solar irradiance are complementary when there is a low level of available wind, but showed little or no complementarity for the periods when the wind availability levels are higher. It is also predicted that there will be no complementarity between solar and wind speed during periods of high precipitation, but good complementarity during periods of low levels of precipitation. Moreover, hydro and wind power sources are geographically dispersed because the Western parts of the EAC have more precipitation than the Eastern parts.

This research concluded that the potential ability of hydro, wind and solar energy resources in the EAC to provide a balanced supply is strong, which could compensate for local and country level imbalances. The research developed a Decision Support Framework which provides a methodological pathway for renewable energy stakeholders when developing policy, strategies and future plans to implement a renewable energy mix at scale in the EAC.

This study has pioneered the use of a mixture of renewable energy sources and recommends that future research is commissioned for the retrofitting of the existing infrastructure with smart grids, to accommodate periods when the electricity supply is intermittent.

Abbreviations

- **EAC**: East African Community
- **IPCC**: Intergovernmental Panel on Climate Change
- **CMIP5**: Coupled Models Intercomparison Project Phase 5
- **GHG**s: Greenhouse gases
- **UNECA**: United Nations Economic Commission for Africa
- **GCM**: Global Climate Model
- **RCM**: Regional Climate Model
- **GR2M**: Génie Rural à 2 paramètres Mensuel
- **DSF**: Decision Support Framework
- **CORDEX**: Coordinated Regional Downscaling Experiment
- **EAC_RCMs**: East Africa Community Regional Climate Models
- **HOMER**: Hybrid Optimization of Multiple Energy Resources
- **PVEP**: Photovoltaic Energy Production
- **EAPP**: Eastern Africa Power Pool
- **RCP**: Representative Concentration Pathway
- **IEA**: International Energy Agency
- **UNECA**: United Nations Economic Commission for Africa
- **MAD**: Median Absolute Deviations
- **SRES:** Special Report on Emissions Scenarios
- **MME**: Multi-Model Ensemble
- **MMEM**: Multi-Model Ensemble Mean
- **EACREEE:** East African Community Renewable Energy and Energy Efficiency
- **RE:** Renewable Energy
- **Q-Q:** Quantile-Quantile

- **REN21**: Renewable Energy Policy Network for the 21st Century
- **SPEI**: Standardised Precipitation-Evapotranspiration Index
- **EDL**: Economic Distance Limit
- **ENSO**: El Niño-Southern Oscillation
- **NOAA**: National Oceanic and Atmospheric Administration
- **GDP**: Gross Domestic Products
- **DBS**: Distributed Based Scaling
- **RSDS**: Surface Downwelling Shortwaves Radiation
- **NSE**: Nash and Sutcliffe Efficiency
- **KGE**: King-Gupta Efficiency
- **GRDC**: Global Runoff Data Centre
- **GPCC**: Global Precipitation Climatological Centre
- **CRU**: Climate Research Unit
- **ITCZ**: Intertropical Convergence Zone
- **TNPC:** Total Net Present Cost
- **TAR:** Third Assessment Report
- **AR4:** Four Assessment Report
- **AR5:** Fifth Assessment Report
- **MTOE:** Million Tonnes of Oil Equivalent
- **WMO**: World Meteorological Organization
- **iHOGA**: Improved Hybrid Optimization by Genetic Algorithms
- **RETScreen**: Renewable Energy and Energy Efficiency Technology Screening
- **RAPRSIM**: Renewable Alternative Power systems Simulation
- **HybSim:** Hybrid Simulation Model
- **IPSYS:** Integrated Power System tool

- **iGRHYSO**: Improved Grid Connected Renewable Hybrid System Optimization
- **INSEL:** Integrated Simulation Environment Language
- **SOMES:** Simulation and Optimization Model for Renewable Energy Systems
- **WCRP**: World Climate Research Program
- **UNHCR:** United Nations High Commissions for Refugees
- **RC:** Refugee Camp
- **HH:** Households
- **PCA:** Paris Climate Agreement
- **PET:** Potential Evapotranspiration

Symbols

- **$C0_2$**: Carbon dioxide
- **$N0_2$**: Nitrous Oxide
- **CH_4**: Methane
- **0_3**: Ozone
- **E**: Energy density (W/m^2)
- **ρ**: Air density (Kg /$m^{3)}$
- **U**: Wind speed at hub-height (m/s)
- $\Delta\boldsymbol{E}$: Changes in potential wind energy
- $\boldsymbol{E_{Fp}}$ where F is: Future wind energy and p: corresponding periods
- $\boldsymbol{E_b}$: Wind energy based on baseline data
- η_{ref} : Photovaltaic modules reference efficiency
- $\boldsymbol{T_{ref}}$: Photovaltaic modules reference temperature
- $\boldsymbol{T_{cell}}$: Photovaltaic modules cell temperature
- **T**: Air temperature for the baseline period in ^{0}C,
- **C_1, C_2** and **C_3**: Coefficients
- $\boldsymbol{\beta}$(Beta): Temperature coefficient set by cell material and structure
- $\boldsymbol{\gamma}$(Gamma): Irradiance coefficients set by cell material and structure
- $\boldsymbol{\rho_s}$**:** Spearman correlation coefficient
- $\boldsymbol{r}$: Pearson correlation coefficient
- $\boldsymbol{\tau}$: Kendall correlation coefficient

List of Figures

List of Tables

Table of Contents

Chapter 1: Introduction

1.1 Research background

The burning of fossil fuels (*i.e.*[1] coal, oil, and gas) and the resulting emissions of greenhouse gases (GHG) is one of the most pressing environmental issues facing the planet today. The increase in the concentration of anthropogenic and naturally occurring GHG such as Carbon Dioxide ($C0_2$), Nitrous Oxide ($N0_2$), Methane (CH_4) and the depletion of Ozone (0_3), has already caused an increase in the mean global atmospheric temperature by 0.6°C by the end of the twentieth century (Anderson et al. 2016). Projections for climate warming over the course of the twenty-first century are estimated to be between 1.0°C and 3.7°C depending on future GHG emissions (Anderson et al. 2016).

As an alternative to fossil fuel, renewable energy (RE) has been identified as one of the most promising ways of reducing GHG emissions. The term RE refers to an energy resource that is replenished rapidly by natural processes (REN21 2015). For example, the power generated from, but not restricted to, solar radiation, the Earth's heat (geothermal), biomass, water and the wind. As a global resource, RE is also being considered as one of the solutions for reducing energy access difficulties, especially within developing countries (Ebinger et al. 2011a). However, whilst some researchers (e.g.Ebinger et al. 2011b, and Pryor and Barthelmie 2010) argue that most RE resources are dependent on climatic conditions, within most studies, the evidence presented when climate change and renewable energy are considered in the same context habitually focuses on the impacts of renewables in terms of reducing the GHG (Pašičko et al. 2012, Ebinger and Vergara 2011). The scope by which climatic conditions are researched with reference to RE is

[1] *i.e. is the abbreviation for id est and means "in other words."*

important because changes in precipitation, solar, temperature and wind speed could significantly impact the available energy from these resources (Pašičko et al. 2012). In this thesis, hydroclimate will be used as an umbrella term for precipitation, temperature, wind speed and solar radiation. Reliable and climate-resilient energy refer to the ability of the energy production system to deliver consistent levels of energy under different climatic conditions (Lemaire 2004). Sustainable energy refers to the provision of energy that meets current needs without compromising access and supply for the needs of future generations (Lemaire 2004). This study covers the East African Community (EAC)[2] which, for the purposes of clarity throughout this thesis, constitutes of Burundi, Rwanda, Tanzania, Uganda, Kenya and South Sudan.

1.2 Statement of the problem

The Renewable Energy Policy Network for the 21st Century (REN21) indicates that access to modern energy in the subregion of the EAC is low due to the limited coverage of the power grid (REN21-EAC 2016). The REN21 also indicated that low electricity consumption rates have resulted in electricity currently contributing less than 10% to the EAC's energy balance. According to UN-Energy (2005) and Brew-Hammond (2010), modern energy is often identified in terms that contrast it with traditional energy such as the energy derived from the burning of biomass in open fires, whereas (UNDP (2005) indicates that modern energy combines both energy carriers and associated technologies, together with the benefits to users such as lighting, cooking, heating, transportation, and etc. Access to modern energy is therefore defined by the International Energy Agency (2017) as a household which maintains reliable and affordable access to both clean cooking facilities and electricity. In terms of clarifying to what extent the household

[2] *The EAC is the regional intergovernmental organisation of the republics of Burundi, Kenya, Rwanda, the United Republic of Tanzania, the Republic of Uganda and South Sudan. South Sudan is not included as it was not part of the EAC at the onset of this research.*

would possess this access is to be considered as having energy access there should be enough energy to supply an initial basic service with a gradual increase in the level of energy over time. The household would increase their energy level with the view to the eventual attainment of regional averages. Despite the low access to modern energy mentioned by the REN21, the EAC region has immense energy sources. For example, approximately 21 trillion cubic feet of gas has been discovered across the EAC. An estimated 2.5 billion barrels of oil reserves are in Uganda, with more reserves located just off of the Kenyan coast (IEA 2014). These sources of energy constitute immense potential in terms of the opportunity it gives the EAC countries with reference to increase their energy access and rapid economic growth, thus leading to poverty reduction (where poverty refers to living on less than US$2 a day; World Bank 2008). However, in terms of energy sustainability, reliability, and climate-resilience, the aforementioned sources (oil and gas) highlight an increasing concern. As fossil fuels, the EAC cannot rely on these sources of energy. The reasons for this may be divided into two main subgroups stated as follows:

i) Fossil fuels are finite resources and will eventually become depleted (McLamb 2011);
ii) Fossil fuels are the main cause of global GHG emissions and cause irreparable damage to our ecosystem (Environmental and Energy Study Institute 2016).

In addition, it is important to note that the GHG are responsible for approximately 87% of GHG emissions (COWE 2013). Finally, as a signatory of the Paris Climate Agreement (PCA) of which more details can be found in the UNFCCC report (2015), the EAC countries have committed to strengthening the global response against the threat of climate change and, in doing so, are obliged to pursue efforts in order to limit temperature increases beyond 1.5°C.

Ultimately, it is unfeasible to honour the GHG emissions reduction target as per the PCA whilst relying on fossil fuels. Therefore, in order for developing countries including those in the EAC to create a foundation of sustainability and resilience economically, and to do so within a community which also meets its GHG emissions reduction criteria, it becomes essential to invest in RE. For contextual purposes, the EAC is a region endowed with substantial renewable energy resources such as solar, wind, geothermal, biomass, thermal and hydropower (EAC secretariat 2015). However, although extensive renewable energy resources are present, the EAC is currently heavily dependent on hydropower, with more than 50% of total electricity generation capacity coming from this singular source (Karekezi et al. 2009, Jjunju and Killingtveit 2015, REN21 2016a).

With reference to research that provides an analysis of hydropower and climate change relatively, the World Watch Institute (2010) noted that worryingly, new African dams were being built with no assessment as to how climate change would affect them. This was evidenced despite the fact that to date, many existing dams are already plagued by drought-caused power shortages. This substantiates the significance of research and analysis on the impact of climate change as undertaken by the World Watch Institute (2010) and previously observed in the EAC (Hulme et al. 2001, IPCC 2001), as a general lack of actioned research in this particular area has meant that the energy sector has subsequently been adversely affected.

With respect to the adverse effects of the relationship between the production of hydropower and climate change, in 2004 and 2006, Uganda experienced a reduction in water levels at Lake Victoria, causing a hydropower generation shortfall of 50 MW. This, in turn, reduced their Gross Domestic Product (GDP) growth rate from 6.2% to 4.9% (Karekezi et al. 2009). A similar situation in terms of a considerable decline in electrical generation also occurred within Rwanda, which saw its Mukungwa hydroelectric station, with a typical capacity of approximately 12.5MW, reduce to 1MW due to a shortage of rainfall (EAC 2011a). Similarly, Kenya has suffered several shortfalls in hydropower generation due to drought conditions between 1999 and 2002. This resulted in a reduction of 25% of Kenya’s total hydropower generation capacity and a cumulative loss of 1-1.5% of their total GDP as measured in the year 2000 (Karekezi and Kithyoma 2005). Despite the documented periods of energy crises, controversially, hydropower generation continues to be not only used but to be expanding. In Burundi, Congo, and Rwanda for example, the construction of the 145MW Ruzizi III Dam across their common border negates the fact that they have all recently suffered energy shortages due to dropping river water levels (The World Rivers Review 2012). Likewise, recent hydroelectricity generation in Tanzania has fallen 20% short of its full capacity, chiefly due to the lack of rain. On evaluation, the level of decline rendered it difficult for the dams to operate, which in turn forced Tanzania to close several of its hydroelectric plants which reduced its total electricity generation by 35% (Harris 2015).

Despite this threat to the hydro energy sector in the EAC region, little progress has been made in terms of the acknowledgement of this. Kammen et al. (2015) state that the East African Power Pool (EAPP) master plan does not include any analysis of the effects of climate change on the regional power strategy nor provide any insight into possible problems associated with climate change conditions. Because of this, Beilfuss's (2012) suggestion that hydropower plant development should be halted due to the potential impacts of climate change on future hydropower production is one that should be considered as very pressing. However, other researchers have challenged some of Beilfuss's (2012) conclusions, arguing that the generalisability of these statements are subject to certain limitations. For instance, when looking historically at hydropower production shortfalls, it should be noted that production shortfalls happened during specific years only (see above discussions). This suggests that any deficit recorded may simply be linked to the prevailing climatic conditions for that particular year, as shown in previous work (Karekezi and Kithyoma 2005, World Watch Institute 2010, Beilfuss 2012a, Carty 2017). To support this, Conway et al. (2017) present a case for future hydropower production and climatic linkage in the EAC as established, but, at the same time acknowledges that hydropower is exposed to high levels of climate variability and regional climate linkages are strong.

This is a significant case in point because by 2030, assuming completion of the dams as planned, 70% and 59% of the total hydropower capacity will be located in one cluster of rainfall variability within eastern and southern Africa respectively, thus increasing the risk of concurrent climate-related electricity supply disruption in each region (Conway et al. 2017). This statement is relevant to the EAC as it highlights the fact that its future investment for energy plans within the region are dominated by hydropower (EAPP 2015, Jjunju and Killingtveit 2015).

Drawing from the remarks of the World Watch Institute (2010), Beilfuss (2012a) and Kammen (2015) indicate that even though there is already climate change impact manifestation in place on existing hydropower plants, future energy investment plans in the East Africa region will continue to be dominated by hydropower generation capacity. In addition to these remarks, the study conducted by Conway et al (2017) stipulating a future risk of concurrent climate-related electricity supply disruption in the EAC, suggests that poor investment planning in terms of renewable energy systems may lead to shortfalls in energy supply during certain periods of the year, thus causing potential disruption in supply and hampering the EAC’s ability to meet their sustainable development goals (SDG).

In spite of the available evidence of historical and future climate change and its adverse impacts on hydropower production in the EAC, there are no corresponding comprehensive research studies pertaining to the adaptation measures for future climate change and the impact of this on energy generation in the EAC. This gap in knowledge regarding future adaptation measures that seek to buffer the effects of climate change on energy generation in the EAC constitutes the main thrust of this research.

1.3 The rationale for this research

This research provides an insight into the variability and complementarity of future hydroclimate in the EAC, relative to future renewable energy investment planning. Thus, the research is oriented towards developing a renewable energy decision support framework (DSF) for policymakers and investors. The framework will support sound energy investment decision making that considers complementary energy resources in the face of the energy production deficit currently experienced in the EAC due to the impact of climate change on hydropower production.

This research addresses the gap in knowledge as previously mentioned, by answering the questions raised in the problem statement, the responses of which will inform the development of a DSF for RE implementation in the EAC. The results of this research will provide a better understanding in terms of the ability of renewable resources to complement each other within the EAC as a basis for ensuring sustainability, resilience, and climate-resilience in terms of the energy supply, especially under an ever changing climate. Moreover, this research contributes towards the SDG for the EAC as detailed below:

i) SDG7.1 – ensure universal access to affordable, reliable and modern energy services;

ii) SDG7.2 – increase substantially the share of renewable energy in the global energy mix;

iii) SDG13.2 – to integrate climate change measures into national policies, strategies, and planning.

In addition, the result of this study works towards supporting the energy initiatives of East African Community Renewable Energy and Energy Efficiency (EACREEE), which in turn promotes renewable energies and energy efficiency in the EAC. Finally, although this research is based on the EAC as a specific location, its outcomes have implications for other developing countries who are looking to strengthen the resilience of their own renewable energy supplies.

1.4 Research questions

As a result of the potential hydroclimate changes, this research seeks to address the following questions:

1. What are the potential future hydroclimate change scenarios in the EAC?
2. Do the hydroclimate resources complement each other in renewable energy generation in the EAC?
3. How can decision-makers in the EAC achieve reliable, affordable and climate-resilient energy access through a complementary renewable energy mix?

1.5 Research aim and objectives

This research is to establish a well-balanced renewable energy generation capacity that manages the regional, country and local imbalances across the EAC. Therefore, the aim of the study is to develop a DSF for achieving reliable, sustainable, and climate-resilient energy access in the EAC under the future climate change scenario. The climate change scenarios used in this study refers to Representative Concentration Pathways (RCPs) 4.5 and RCP8.5 (van Vuuren et al. 2011). These RCP scenarios are discussed in detail in

Section 3.4.2. The potential complementarity and energy generation implications of the available hydro, wind and solar power resources will be evaluated based on the following timeline: near future (2021-2050), middle-term future (2051-2080) and long-term future (2071-2100). In this respect, the following five objectives have been formulated to achieve the research aim:

1) To explore the current status of energy access and future renewable energy implementation plans in the EAC;

2) To investigate EAC future hydroclimate changes under different climate scenarios (RCP4.5 and 8.5) for the period spanning from 2021 to 2100;

3) To study the ability of hydro, wind and solar resources to complement each other under different future climate change scenarios during the periods of 2021-2100, and its implications for energy supply balancing;

4) To propose optimal hybrid combinations of hydro, wind speed and solar power for electrification of a selected case study area;

5) To develop a systematic pathway for renewable energy implementation in the EAC.

Figure 1-1 below shows how this research is structured, and how the chapters are connected.

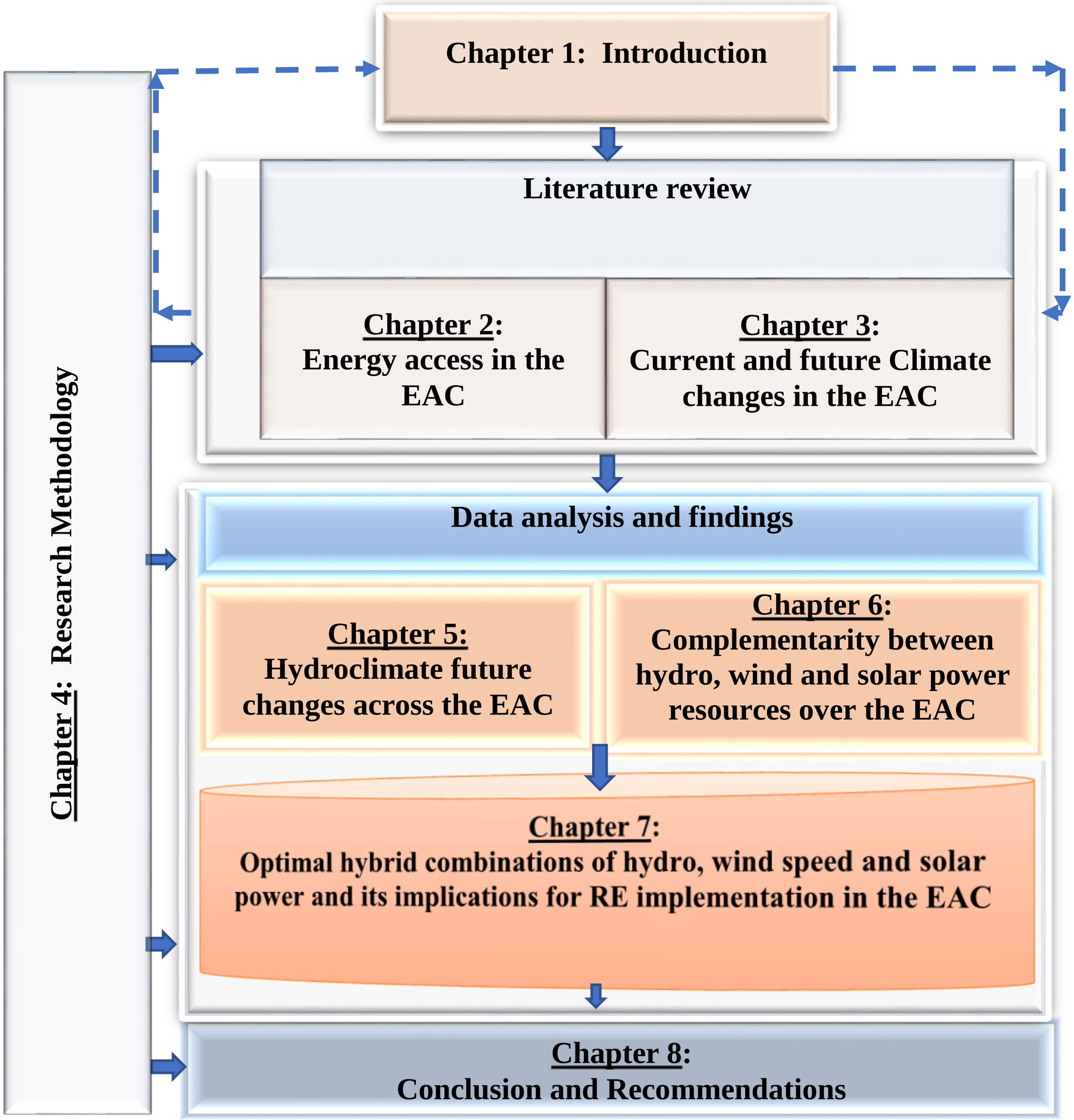

Figure 1-1: Thesis structure
Chapters connections are represented by blue arrows indicating the flow of information from one chapter to another. In this respect, Chapter 1 provides an introduction to this research, and the literature review is made of Chapters 2 and 3. The research methodology is in Chapter 4, data analysis and findings are dealt with in Chapters 5, 6 and 7. Finally, the research conclusion and recommendations are given in Chapter 8.

Chapter 2: The EAC state of energy access and production

This chapter investigates the state of energy access in the EAC. It is split into 3 main sections. It starts by exploring energy consumption in a global context and its relation to human development. Next, it compiles the evidence of energy access within the EAC. Lastly, this chapter explores the state of provision of hydro, wind and solar power in the region.

2.1 Introduction

Energy use is one of the principal factors that influence economic growth and quality of life (McVeigh and Mordue 1999, Zou et al. 2016). This is important because the empirical evidence shows that there is a positive correlation between per capita energy consumption and human development (Goldemberg 2001 and IEA 2014). In addition, the IEA (2014) also argue that energy is a fundamental prerequisite to economic development and socio-economic transformation. Supporting this perspective, the United Nations Economic Commission for Africa (UNECA 2014a) indicates that higher-income countries are associated with high energy consumption, whereas low-income countries are associated with low energy consumption. Pisupati (2019) uses a graphical representation (Figure 2-1) to explain the relationship between energy consumption (kWh per person) and quality of life , indicated by the Gross Domestic Product per year per Person (GDP/Year/Person)

Figure 2-1: Energy consumption and GDP/ year/person.
Source: Pisupati (2019)

Figure 2-1 shows that developed nations (high income) consume more energy compared to the developing nations. Looking at Figure 2-1, it can be seen that the energy consumption rate around the globe is unevenly distributed and correlates with the level of productivity in a country. Further to this, Esen and Bayrak (2017) indicate that there is a positive and statistically significant relationship between energy consumption and economic growth. In the same vein, the Africa Progress Panel (2015), indicated that, as of 2012, the USA energy consumption per capita was 12,209.7 kWh, whilst for the United Kingdom, Euro-Asia and Pacific, Latin America, and the Caribbean consumption was respectively 5,010.4 kWh, 1,285.6 kWh and 1,931.2 kWh. However, in Sub-Saharan Africa excluding South Africa, the consumption was as little as 162 kWh per year (U.S.Energy Information Administration 2016). To support this argument, an additional representation of the Sub-Saharan Africa energy consumption is given in Figure 2-2 below. This figure, which includes some of the EAC countries, indicates a very low energy consumption represented as Million Tonnes of Oil Equivalent (Mtoe) per capita.

This, in line with the aforementioned low energy consumption in Sub-Saharan Africa, reflects the low level of GDP and human development indices across the region.

Figure 2-2: Population and per capita energy consumption in sub-Saharan Africa
Source: (IEA 2014)

In Sub-Sahara Africa, energy consumption is very low (IEA 2014). This is crucial to note because as discussed, the positive correlation between energy consumption and GDP per capita is an indication that an increase in energy access/consumption could play a key part in terms of improving the living standard of the population in the EAC region. Therefore, any attempt to build robust economic growth will require an increase in energy access in the region.

2.1.1 The EAC energy access situation

This section explores the EAC energy status in terms of energy access and consumption. It looks at the sources of energy that are being used, the rate at which traditional energy (*i.e*. wood, charcoal, and biogas) is accessed and is compared with modern energy (*i.e*. hydro, wind, solar power, etc.) across the EAC country members. Finally, the initiatives for scaling up energy access in the region are also explored.

2.1.2 The EAC energy access and consumption

Regarding access to modern energy in the EAC, REN21-EAC (2016) indicates that, as of 2015, electricity access remained at less than 22% in the EAC region, which is well below the average electrification rate of 33.5% in sub-Saharan Africa as a whole. This is presented in Figure 2-3, where traditional biomass, such as that which is used for cooking and heating, is the most dominant energy consumption factor within EAC partner states.

Figure 2-3: Share of primary energy consumption in EAC partner states, by fuel source 2011-2014.

Source: REN21 (2016a)

Figure 2-3 shows that traditional biomass as the source of energy is the most dominant source of energy consumption in the EAC region and accounts for about 86.12% of total energy consumption. Approximately 98.6% of the population in rural areas use traditional biomass in the form of woody biomass for heating and cooking. This is in contrast to most urban households (85.7% of the urban population) where traditional biomass is utilised in the form of charcoal (REN21 2016a). These findings confirm the association between biomass, location and the power grid. Biomass is currently consumed as more than 90% of energy sources in the EAC, whilst electricity contributes less than 10% of the EAC's energy balance (UNECA 2014). This is due to the limited coverage of the power grid (UNECA 2014). When looking at individual countries within the EAC on a case by case basis, the IEA (2019) reported that 6.5% of the total rural population have access to electricity in Burundi compared to 35.5% of the urban population. In Rwanda, 37.2% of the rural population and 69.4% of the urban population have access to electricity, whilst 18.6% of Uganda's rural populations have access to electricity compared to 23.3% of the urban population. Kenya has the highest electricity access rate with 67.6% of the rural population compared to 89.5% of the urban population. Given this difference in the electrification rate between the rural and urban settings, it is evident that the above regions continue to rely heavily on traditional biomass which is predominantly utilised in the rural areas (EAC 2011b).

The present study provides additional evidence with respect to the fact that in addition to traditional biomass, the regions also use petroleum products. For petrolatum products, the level of consumption compared to traditional biomass was relatively small - ranging from 2.5% in Burundi to 22% in Kenya (Figure 2-3). Petroleum products are used mainly in the transport sector, but also play a vital role in the industrial sector where they are used as a back-up power source for diesel generators and play a part in the processing of tea, flowers/ horticultural commissions, coffee and agro-industries (REN21 2016b). As shown in Figure 2-4 below, the percentage of change in petroleum consumption for the period of 2000-2011 was 40.23% for Africa with a percentage of 67.09% for the Eastern Africa sub-region alone. For the same period, changes in petroleum consumption ranged from 14% in Burundi to 166% in Kenya as shown in Table 2-1.

Figure 2-4: Petroleum consumption for the period of 2000-2011
Percentage changes in petroleum consumption for the period of 2000-2011 Eastern Africa Vs. Africa. Source: (UNECA 2014a)

Table 2-1: EAC change in petroleum energy consumption (2000-2011)

Source:(Kinuthia 2014)

As indicated in Figure 2-3, electricity consumption in the region is the smallest source of energy with the use of traditional biomass and petroleum products dominating. In terms of electricity consumption, Karekezi et al. (2009), and REN21 (2016) state that the EAC region’s electricity sector is based primarily on hydropower, which contributes to more than 50% of the total electricity production in the region. Given the low energy access discussed above coupled with the overextension of the region’s energy generation capacity due to rapid population growth, growing industries and climate change (Kazoora 2014), the EAC needs to increase its energy supply to meet the pace of energy demand.

2.1.3 Drivers of energy demand

One of the energy demand drivers is population growth and it is estimated that by 2030 the EAC population (excluding South Sudan) will have increased to 237 million, of which 178 million will be children and youth (Eyakunze and Salim 2012). In addition, projections show that 31% of the total population will be living in urban areas (Eyakunze and Salim 2012). In terms of economic growth, EAC subregion has the fastest growing economy in the East Africa region. This growth is reported in the African Development Bank's (AfDB) Economic Outlook for 2019. The report indicates that East Africa is the fastest-growing region on the continent for the fifth year running. This is evidenced by the fact that the region has grown by an additional 5.7% in 2018 and is projected to grow by 5.9% in 2019, and 6.1% in 2020 (African Development Bank 2018). As a consequence of this economic growth, the urban population shows rapid expansion, and the growth of large and unplanned urban settlements have become a common feature in the EAC and major cities such as Bujumbura, Dar es Salaam, Kampala, Kigali and Nairobi (Oketch and Ngware 2015).

The EAC's growing population and urbanisation at a rapid pace not only puts pressure on local governments in terms of meeting the energy demand but will also have supplementary implications on energy demand such as changes in lifestyle in terms of the energy uptake of electrical appliances which are expected to increase (AfDB 2018). For example, as well as other electrical devices and appliances (televisions, cookers microwaves, toasters, etc.), the population using mobile phones (as of 2012) were reported at approximately 71.5% in Kenya, 58.6% in Tanzania, 48.7% in Uganda, 48.7% in Rwanda and 21.3% in Burundi (AfDB 2018).

Furthermore, the rise in the popularity, use and accessibility of mobile phones is projected to increase more in the coming years (AfDB 2018). In addition, global warming is also playing an important role in energy demand. Edwards et al. (2013) indicate that, globally, climate change is expected to increase pressure on energy demand, particularly in terms of additional power capacity required to satisfy supplementary cooling services. This is because the majority of modern buildings in most African countries including the EAC, despite experiencing tropical climates (*i.e.* where the temperature is warmer than 18°C), are a replica of building designs from western countries, which were historically designed with cold and temperate climates in mind (Kazoora 2014). In addition to this, within the EAC, the expected rise in average annual temperature is currently projected to be between 1°C and 5°C; precisely the predictions made for 2020 show a typical increase of approximately 1°C whilst a 5°C increase is predicted by 2100 (Ebinger et al. 2011b, IPCC 2014). For this reason, there will be a requirement for more additional power capacity in order for cooling within the region in line with temperature comfort expectations (Ebinger et al. 2011b). As a result of this population growth, and other drivers of energy demand such as economic growth, urban settlement, change in comfort expectations as well as an upsurge in the uptake of electrical appliances, energy demand in the EAC region is constantly increasing.

Energy demand in Kenya, Rwanda, Tanzania and Uganda are expected to grow by approximately 5.3% per year by 2020 in order to meet these changing lifestyle demands. Power generation capacity will have to increase by an estimated 37.7% in Uganda, 96.4% in Kenya, 75.3% in Tanzania and 115% in Rwanda (Roos 2014). Whilst it would be interesting to comment on the extent to which this demand is on course for being achieved, such data would require the evaluation of the generation capacity implementation progress to date against the suggested power generation capacity mentioned by Roos (2014). Due to practical constraints, this is beyond the scope of this research.

2.1.4 Potential sources of Energy in the EAC

The EAC region has immense energy sources (REN21 2016a). For instance, there has been a discovery of new oil and gas reserves across the region, with 1.2 trillion cubic feet of gas in Tanzania, and an estimated 2.5 billion barrels of oil reserves in Uganda (IEA 2014) in addition to the oil found off of the coast of Kenya (IEA 2014). The discovery of new oil and gas resources in the region is likely to play a major role in the country's renewed capacity for energy generation. It is important to note here however, that the aforementioned sources of energy are fossil fuels, which the EAC cannot rely on for three reasons as outlined in Section 1.2. Furthermore, in the recent Paris Agreement, the EAC countries have committed to a global response to the threat of climate change by keeping the rise in global temperature for this century below 2°C above pre-industrial rates (UNFCCC 2015).

The only way the EAC can commit and succeed in the reduction of GHG emissions and still ensure access to energy for all is to invest more in RE. In the context of RE, the consensus amongst researchers and reports from EAC energy stakeholders (e.g.[3] Karekezi and Kithyoma 2003, International Renewable Energy Agency 2015, Nalule 2016, Gordon 2018, Hafner et al. 2018, Wassie and Adaramola 2019) is that the EAC geographical region is endowed with plentiful RE resources. Furthermore, in its 2015 report, the EAC indicated that the region is endowed with substantial RE resources including solar, wind, geothermal, biomass, thermal and hydropower (EAC secretariat 2015). A study conducted by Gordon (2018) provided further insight on the availability of renewable

[3] e.g. *stands for exempli gratia and means "for example."*

energy in East Africa, suggesting that solar radiation levels are high due to its proximity to the equator where wind speeds are some of the strongest on the continent, hydropower resources are plentiful, and the Great Rift Valley is a promising source of geothermal power. This viewpoint from Gordon (2018), indicating the abundance of hydropower resources, however, appears contradictory to the previous statements made by Beilfuss (2012b), Worldwatch Institute (2010) and Kammen et al. (2015), which criticise the investments in hydropower within the EAC region. If there is inconsistency in the perception of availability of hydropower resources in the EAC amongst researchers, then a study is needed to reconcile these contradictions with reference to the availability of hydropower resources in the EAC (such study is beyond the scope of this research). The common agreement amongst the researchers (i.e. World Watch Institute (2010), Beilfuss (2012b), Kammen et al. (2015) and Conway et al. (2017), is that climate change will adversely affect energy supply sources.

In regards to scaling up energy access in the region, energy access targets and policies have been formulated by each of the EAC government members (EAC 2011b). In terms of these targets and policies, Kenya is leading the way, with a target of 100% energy access by 2030 (REN21 2016b). Meanwhile, other countries have different targets (REN21 2016b). Uganda has set the target of at least 98% by 2020, Rwanda targeted 70% by 2017, and Burundi aims to achieve 25% by 2020. The key points emerging from this section is that energy consumption is still currently dominated by traditional biomass (Figure 2-3). Figure 2-3 also indicates that access to modern energy resources is very low. With the expectation that the region will experience a great increase in energy demand, there is, therefore, a requirement for increased energy generation capacity in order to provide access to modern energy services (REN21 2016b). In this sense, capitalising on a mixture of RE could reduce the EAC's reliance on fossil fuels, thus increasing economic diversification and growth, as well as driving the EAC towards future sustainable energy.

2.1.5 EAC current energy investment flagship projects

This section explores the EAC's current and future major projects in an effort to scale up energy access within the EAC in response to their energy outlook master plan for 2013-2039 (cf.[4] Table 2-2). As previously mentioned, the EAC country members have undertaken ambitious projects to harness renewable energy resources. For instance, the Africa Development Bank (2015) stated that the Rusizi III Dam, a hydropower project intended to produce 145MW with an estimated cost of more than $600 million, is to serve Rwanda, Burundi, and Congo. Rwanda has completed an 8.5MW solar farm at the cost of $23.7million (Ayre 2015, Whitlock 2015). Kenya is due for completion of a wind farm in Lake Turkana which comprises of a total of 365 turbines with a total generation capacity of 310MW (Kibati 2015). Also, as of 2011, Kenya has 198MWh installed capacity of geothermal energy (Kollikho 2013). Finally, according to the National Association of Professional Environmentalists (NAPE), Uganda has completed the construction of its Bujagli Dam, the biggest dam in the EAC with a recorded 250MW generation capacity in 2012 (NAPE 2014). These projects reveal that the EAC is eager to invest in RE, hence the creation of such a vast foundation for sustainable energy.

Even though RE is preferred over fossil fuels, earlier studies have shown that climate change effects will have significant implications for renewable energy generation (Pryor and Barthelmie 2010, Ebinger et al. 2011a, Pašičko et al. 2012, REN21 2016b). Moreover, EAPP (2015), Jjunju and Killingtveit (2015) indicate that more than 50% of grid-connected electrical energy supply is sourced from hydropower and that future investment plans are similarly dominated by hydropower plants. As already stated, the hydropower in the EAC is already adversely affected by reduced rainfall due to climate

[4]cf. *(short for the Latin: confer/conferatur) refers the reader to other material to make a comparison with the topic being discussed.*

change as well as the alteration of river flows due to the deforestation in the catchment areas (World Watch Institute 2010, Beilfuss 2012b, REN21-EAC 2016).

These shortfalls in hydropower generation cause numerous power outages which are often filled by diesel generators (Adegoke 2018, IRENA 2016, UNECA 2014, Republic of Kenya 2011, Ministry of Energy and Mineral Development 2007). Furthermore, the annual sales revenue loss to firms due to the electrical outages in Eastern Africa is one of the biggest issues they face (UNECA 2014). As an example, the annual sales revenue loss to firms due to electrical outages in Uganda and Burundi is 9.4% and Tanzania 7.3% (UNECA 2014). In addition, the same report concluded that power outage is a major obstacle for executing business, affecting 49.2% of firms in sub-Saharan Africa compared to 39.2% of the world average. It should be noted that hydropower is dominant in most of the EAC countries (also shown in Table 2-3 and

Figure 2-5:9) and in the current flagship projects of the EAC. This means that in order to scale up the energy access in a sustainable way, the EAC would require deeper consideration as to how the hydrological condition has changed over the last two decades combined with a clear strategy or contingency for potential future changes.

2.1.6 EAC future energy access plan

For the EAC to meet the constant increase in energy demand shown in Table 2-2**,** the East Africa Community Power Pool (EACPP) has provided a national generation expansion plan for 2013-2039 (Table 2-3). Table 2-3 shows the current and future demand forecast plan in two year intervals, dating from 2013 to projections in 2039.

Table 2-2: Demand Forecast Plan 2013-2039 (EAC) in MWh.

Year	Burundi	Kenya	Rwanda	Tanzania	Uganda
2013	29.34	918.4	62.9	837	420.3
2015	28.42	1519	100.8	1284	551.9
2017	30.82	2808	167.7	1769	641.7

Year	Burundi	Kenya	Rwanda	Tanzania	Uganda
2019	56.849	4114	204.91	2091.6	795.09
2021	103.8	5178	237.6	2391	975
2023	114.6	5952	256.8	2740	1158
2025	117.6	6999	280.6	3098	1376
2027	126.4	8095	309.8	3503	1635
2029	139.3	9209	345.4	3945	1916
2031	155.9	10318	387	4412	2147
2033	172.83	11430	428.77	4912.1	2378.2
2035	189.27	12518	469.52	5447.9	2604.6
2037	204.91	13553	508.33	5954.9	2819.7
2039	219.29	14504	543.95	6399.3	3017.7

From Table 2-2, it can be seen that by 2039, Burundi demand forecast is 219.29MWh- the lowest in the region. Kenya has the highest demand with 14504MWh. The second highest demand is projected to come from Tanzania, with a total demand of 6399.3MWh, followed by Uganda (3017.7MWh) and then Rwanda (543.95MWh). Table 2-3 shows a commitment to the national expansion plan by 2025 for each country in the EAC.

Table 2-3: EACPP planned fossil fuel and renewable energy generation capacity by 2025

EACPP committed energy generation capacity by sources in MW by 2025									
	Coal	Oil	Natural gas	Hydro	Geo-thermal	Wind	Solar	Others*	Total
Burundi		17	0	180	0	0	20	0	217
Kenya	1,920	391	3,440	934	4,000	636	-	44	11365
Rwanda	0	55	0	76	0	0	28	297	506
Tanzania	700	100	2,901	3,299	0	100	120	19	7239
Uganda	0	150	0	2,226	250	0	20	107	2753

Source: Adapted from EACPP (2016)

Within the table above, the term *others** includes sources that are exploited in such low capacities that their contributions are combined. These sources are bagasse, methane, municipal waste, peat and wood-based generation. Figures 2-5 to Figure 2-9, denoted in Figures 2-5: 9, are visual representations of individual countries' (as presented on Table 2-3) committed energy generation capacity by 2025. Both Figures 2-5:9 and Table 2-3 are the EAC energy generation capacity in the response to the demand shown in table 2-3.

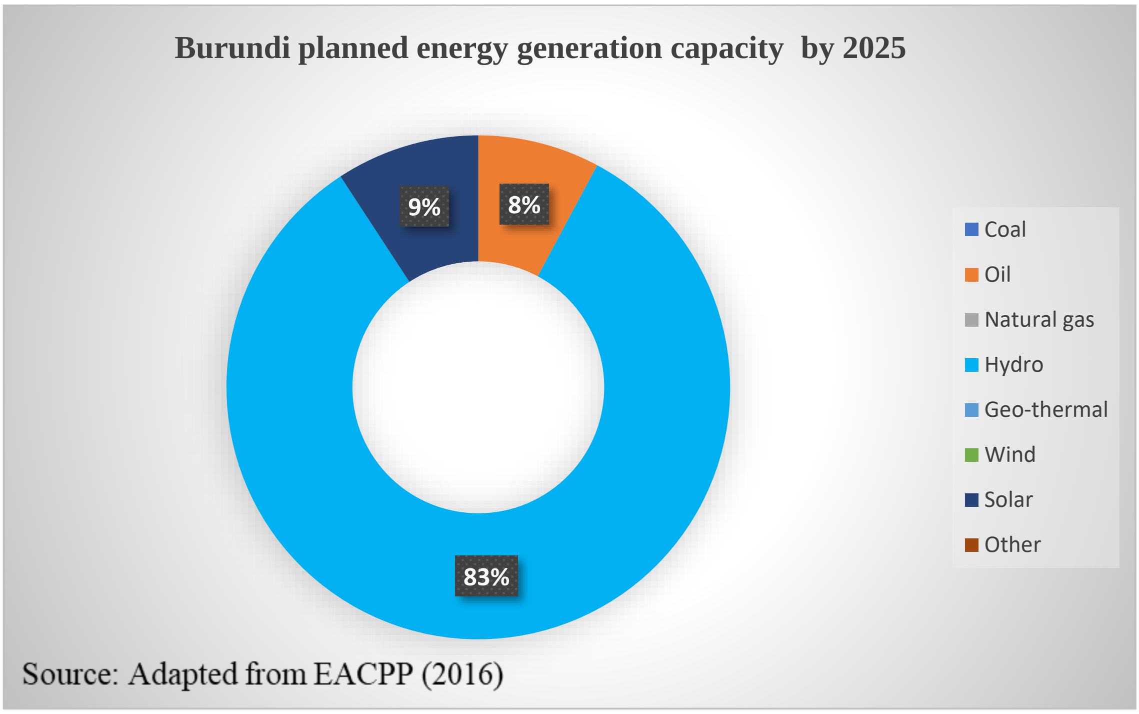

Figure 2-5: Burundi national expansion plan by 2025 and by energy source type

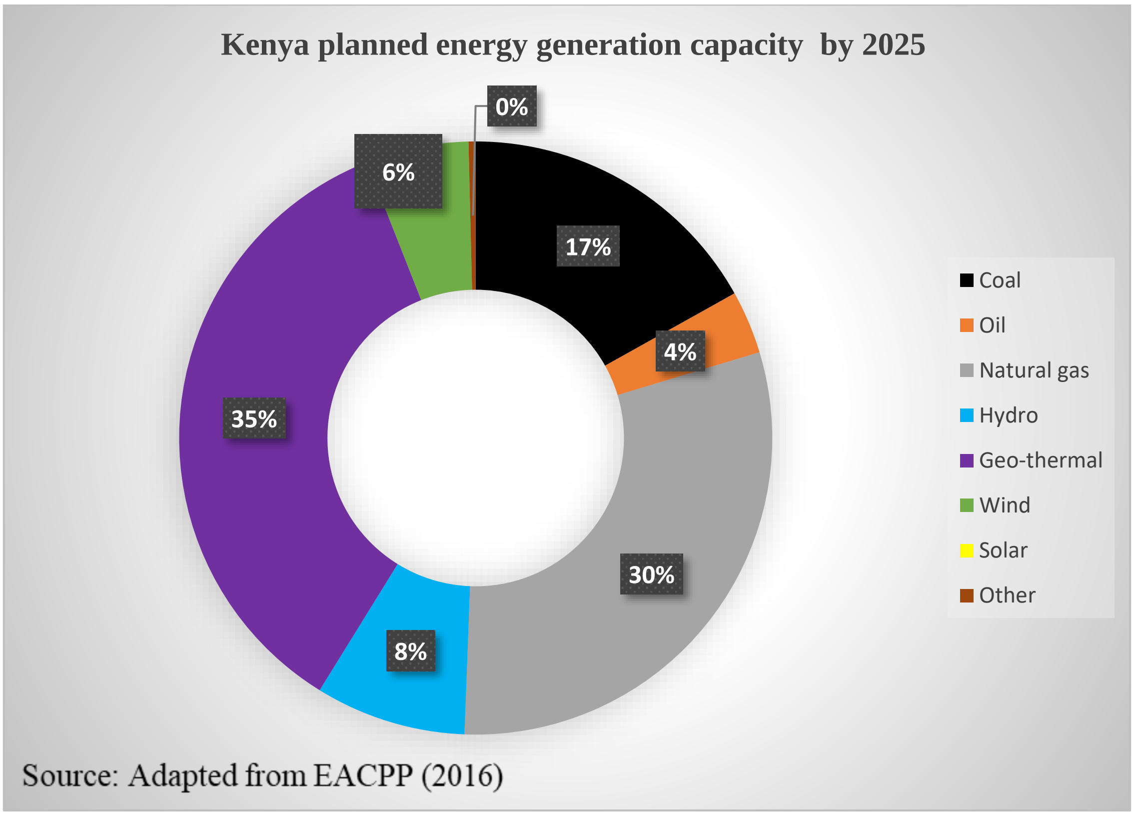

Figure 2-6: Kenya national expansion plan by 2025 and by energy source type;

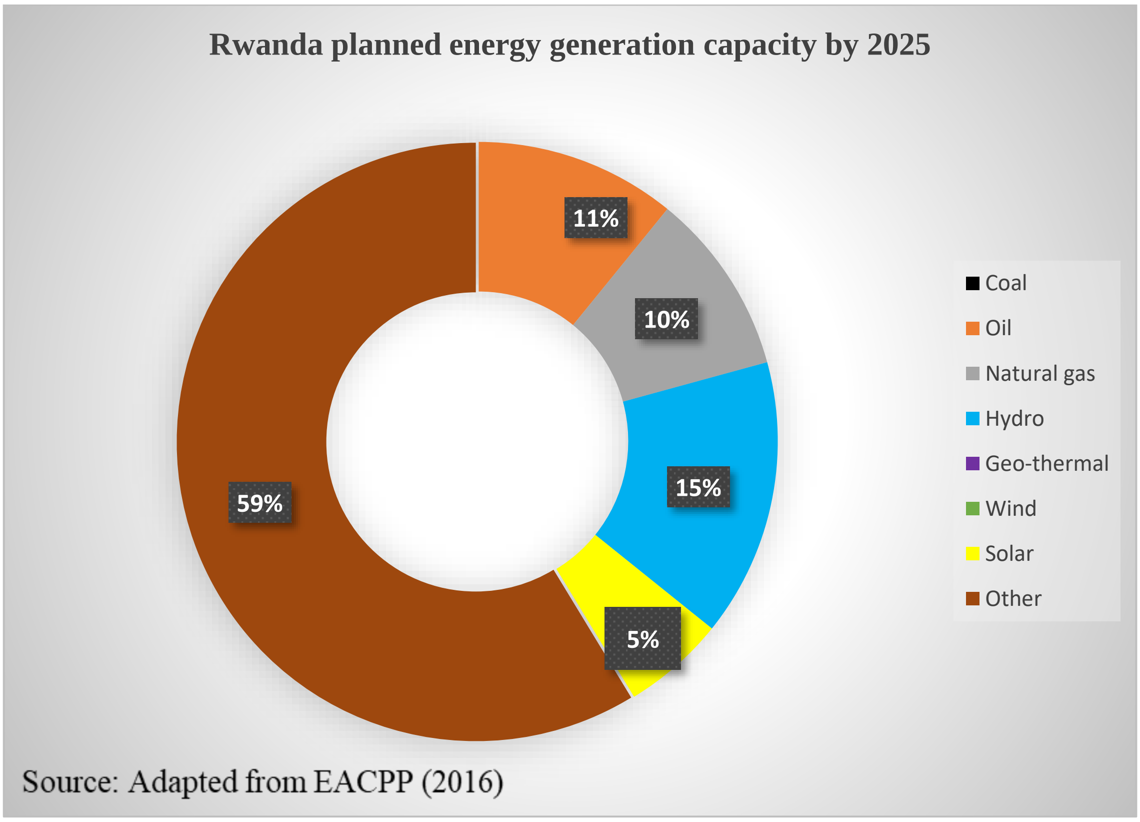

Figure 2-7: Rwanda national expansion plan by 2025 and by energy source type

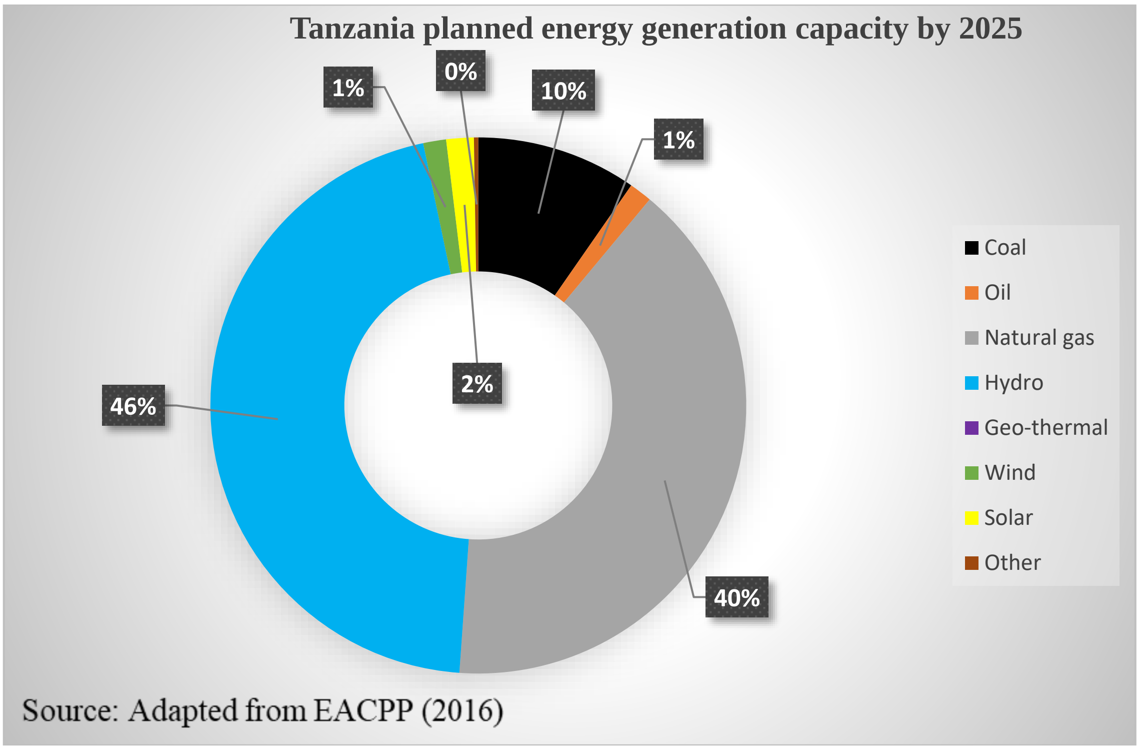

Figure 2-8: Tanzania national expansion plan by 2025 and by energy source type

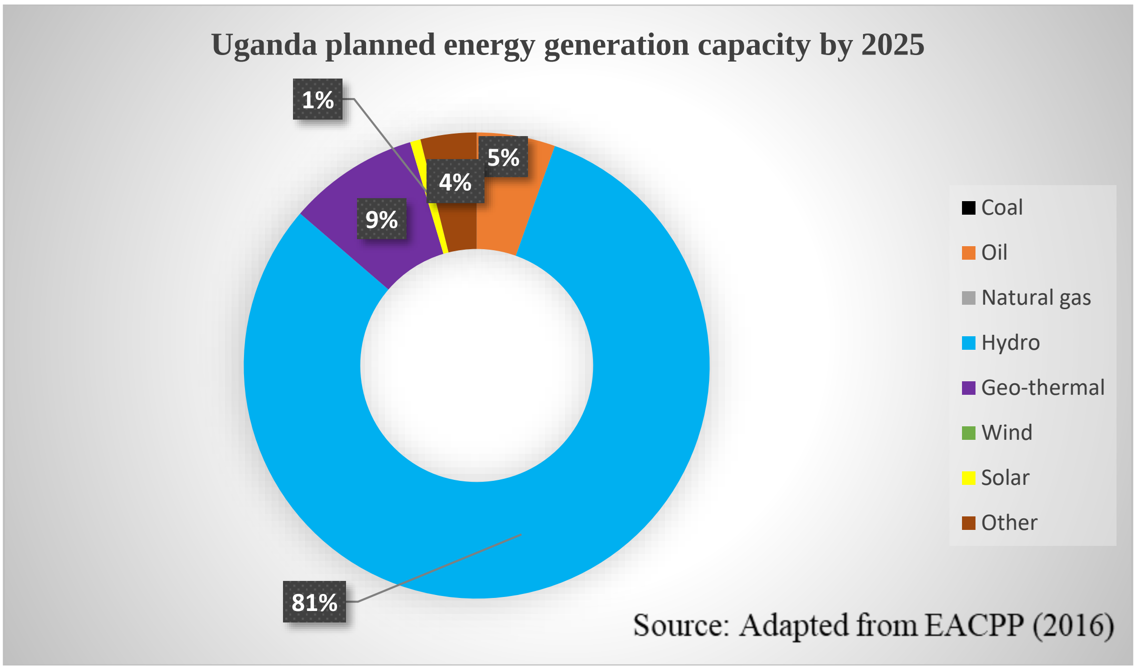

Figure 2-9: Uganda national expansion plan by 2025 and by energy source type

As illustrated in Table 2-3, the EACPP master plan contains a considerable amount of energy (both renewable and fossil fuel). In the EACPP master plan, Kenya has the highest amount of implementation with regards to the RE plan (11365MW), followed by Tanzania (7239MW), then Uganda (2753MW), Rwanda (506MW) and Burundi

(217MW; Table 2-3). Burundi's plan (see Figure 2-5) shows that hydropower constitutes 83% of all of its future planned renewable energy procurement in 2025, whilst fossil fuel makes up 9% and 8% for coal and oil respectively. From Figure 2-6, it can be noted that Kenya has a fairly wide mixture of renewable sources in its plan, with a significant amount of renewable energy to be sourced from geothermal resources. In terms of the planned total energy capacity, geothermal takes up 35% of the total planned renewable capacity, followed by hydro (8%), and wind (6%). Fossil fuel in Kenya is comprised of 17% from coal, then oil and natural gas contributing 4% and 30% respectively. The remaining countries' future renewable plans are mostly dominated by hydropower. It should be noted with regards to Figure 2-7**,** that 15% of Rwanda's energy plan is based on hydropower whilst other sources make up 59%, and solar constitutes 5%.

Fossil fuel energy in Rwanda is sourced mainly from oil and natural gases at 11% and 10% respectively. Tanzania as per Figure 2-8 has 46%, 2%, and 1% respectively from hydropower, solar and wind power. In Tanzania, 40% of its fossil fuel energy is sourced from natural gas, then coal constitutes 10% and oil constitutes 1%. As per Figure 2-9, Uganda plans for 81%, 9%, and 1% respectively from hydro, geothermal, and solar energy. Other sources contribute approximately 4% of the total planned capacity. Fossil fuel with particular reference to oil contributes to 5% of sourced energy in Uganda.

In summary, it is noted that much of the future planned energy generation, with reference to the 2025 national commitment, is to be sourced from hydropower in the majority of the EAC countries. This is with the exception of Kenya where geothermal energy is dominant (with 35% of the total planned energy expansion). This may be because renewable energy, such as wind and solar, are not yet exploited at a large scale, and certainly not as much as hydro, with the exclusion of wind energy in Kenya and solar energy in Rwanda. Fossil fuel is also featured in the future energy expansion plan as oil and natural gas make up a significant portion of the EAC's commitment to the energy expansion plan in all countries except Burundi and Uganda which possess natural gas. In addition, within Kenya and Tanzania, there is the inclusion of coal within their national commitment for expansion plan by 2025.

2.2 Hydropower, solar and wind energy resources available in the EAC

2.2.1 Hydropower

This section explores hydropower as a source of energy and investigates the current installed capacity and performance in the EAC. Hydropower is a power generated from the energy of falling water which can be harnessed to generate electricity (Reynolds 1983, Draper 2003). Globally, hydropower supplies 16.4% of the total energy from all sources and provides 76% of all renewable electricity reaching 1000GW of installed capacity in 2013 (Brower et al. 2014).

To generate electricity from water, the kinetic energy of the falling water is captured by the turbine, and the rotation of the turbine drives the generator to produce electricity. The greater the height from which the waterfalls and the more water that flows through the turbine, the more electricity is generated (Draper 2003). The hydropower is generally guided by the following equation (Reynolds 1983).

$$Hydropower(kW) = Q * g * \Delta H \qquad (1)$$

where g is the acceleration of gravity (9.81ms^{-2}), Q (m^3/s) represents the water flow rate and ΔH (m) is the falling height (in meters). REN21 (2016) points out that hydropower is currently the main electricity source in the EAC and is a leading source of renewable power in the region. As of 2014 (see Figure 2-10), the EAC shares a total generating hydropower capacity of 2,082MW (EAC 2014), in which Kenya has the largest share (36%), followed by Uganda (33%) and Tanzania (27%). Burundi and Rwanda have the lowest share in the region with 1% and 3%, respectively.

Figure 2-10: 2014 Installed hydropower capacity in the EAC (MW).

Data source: EAC (2014)

At the EAC regional level, hydro infrastructure contributes to more than 50% of electricity generation and is expected to continue playing a decisive role in the energy system (REN21 2016b, Conway et al. 2017, Sridharan et al. 2019).

2.2.2 Hydropower advantages and disadvantages

Although hydropower is an important source of clean energy with an added benefit of having the capacity to reduce global warming by cutting the world GHG emissions (Edenhofer et al. 2011), it may trigger unintended adverse consequences that developers and policymakers in the energy sector should be aware of. For instance, a large hydropower construction requires a vast area to serve as a reservoir, where interrupted water will be stored. This can have a greater impact on the ecosystem, the environment, and can create social issues (Veilleux 2017). For example, in Brazil, one of its largest hydropower plants, namely the Balbina hydroelectric plant, flooded 2,360 km^2 of tropical forest to then only generate an average of just 112.2 MW of electricity (Kemenes et al. 2007).

In addition, vegetation had been left to decompose in this reservoir, resulting in a substantial amount of methane release causing the loss of potential forest utilisation in addition to the displacement of the local population (Kemenes et al. 2007). These events understandably caused controversy and conflict. In 2017, Egypt and Ethiopia experienced political/diplomatic conflict with regards to Ethiopia's Renaissance Dam. The dam was set to utilise the Nile to become Africa's biggest power exporter whilst presenting an existential threat to Egypt who sources 90% of their water from the Nile (Veilleux 2017). In addition, hydropower is also vulnerable to climate change (Ebinger and Vergara 2011, Beilfuss 2012a, Cole et al. 2014, Savelsberg et al. 2018). Amongst other examples across the globe, just in the EAC alone, there has been clear and evident recorded shortfalls in hydropower production due to drought (Karekezi et al. 2009, EAC 2011a, World Rivers Review 2012). Nevertheless, in terms of being advantageous, a number of studies analysed and compared hydropower with the fossil fuel electricity generation technologies and concluded that hydropower is much cleaner compared to fossil fuel (Owusu and Asumadu-Sarkodie 2016, Kaygusuz 2007, Bilgen et al. 2004). Therefore, investing in hydropower will help to lower GHG emissions and reduce its negative consequences as opposed to the continued use of fossil fuels (Ebinger et al. 2011b, Shahzad 2012, Liu et al. 2013, European Climate Foundation et al. 2014, François et al. 2016). In this sense, the hydropower benefits outweigh its drawbacks, especially when it comes to comparing it with fossil fuels. The main challenge in terms of hydropower investment is the drawbacks stated for the EAC as they transition towards increased access to modern energy, whilst simultaneously developing their energy sector in a way that is both reliable and sustainable.

2.2.3 Solar power

The energy from solar radiation, commonly known as solar energy, can be converted to electrical energy, which in turn can be used to power our homes and businesses (REN21 2016b). Solar radiation can be captured through a system of photovoltaic panels (Liu and Jordan 1960, Alboteanu et al. 2015). According to Brower et al. (2014) and Jäger-Waldau

(2013), photovoltaic is currently the fastest growing renewable energy technology with a record increase in global annual capacity production from 1 to 40 GWp (where p denotes installed peak capacity) over the last decade, and annual growth rates of 40-60% were recorded between 2008 and 2013. A recent report on photovoltaics indicates that the compound annual global growth rate of PV installations measured at 24% between 2010 and 2017 (Philipps 2018). Thus, REN21 (2016) noted that the EAC member countries received solar radiation of between 4-6kWh.m^{-2}.day^{-1} demonstrating that the EAC is geographically well-placed to receive enough solar radiation throughout the years to utilise photovoltaic panels effectively. In addition, SolarGIS (2015) shows that the EAC average annual sum of Global Horizontal Irradiation (GHI) amounted to a minimum of 1200Kwh/m^2 for the period between 1994 and 2010. This is an indication that the region has an immense source of solar energy which, once harnessed, can significantly contribute to the energy solution for the fast-growing population within a region such as EAC. Despite this, however, solar energy as a resource is hitherto not well exploited in the EAC (EAC secretariat 2011).

So far, the only country that has exploited solar energy on a large scale is Rwanda which has an 8.5MW solar farm capacity, providing 6% of the country's total capacity (Whitlock 2015). Nevertheless, East African countries do have programs in place for future scaling up of renewable energy, including the harnessing of solar energy sources. For instance, Rwanda has a plan to provide rooftop solar power to 250,000 households by 2018 (Easter African BusinessWeek 2016), while Burundi is planning to build a 7.5MW solar power plant (Whitlock 2015). As of 2014, Uganda is planning to build a 20MW solar power plant (Biryabarema 2014), and Tanzania has a program to construct a solar mini-grid that will provide electricity to more than 100,000 people and 2,340 small businesses (Africa Business review 2016). In addition to this, by 2014, Kenya had already identified nine sites where 50% of the energy needs of the country could be generated solely from the use of solar energy (Njeru 2014). This study investigates how solar can be used in conjunction with hydropower and others such as wind powers in order to supply a smooth energy balance.

2.2.4 Solar power advantages and disadvantages

Harnessing solar energy may balance the energy production deficit of hydropower, caused mostly by climate-induced rainfall variations, thereby increasing energy access and reliability of electricity supply (Ebinger et al. 2011b). However, the availability of solar energy is not immune to these climatic variations, as climate change can affect solar energy resources by altering atmospheric water vapour content, cloudiness and transmissivity (Cutforth and Judiesch 2007). Change in the atmospheric water vapour content, cloudiness, and transmissivity can then reduce the efficiency of PV cells. For example, a 2% decrease in global solar radiation can result in a 6% decrease in solar cell output (Bull et al. 2007, Fidge and Martinsen 2006). This highlights the importance of the need to account for climate change impact on solar energy investment, which requires a comprehensive assessment of future climate change impacts on the solar resource.

Furthermore, solar energy is only available during the day, and it is thus intermittent. One possible way of dealing with intermittent and time-dependent availability is to use hybrid systems for generating power with reference to solar power in addition to other sources of renewable energy (Pašičko et al. 2012). Moreover, harnessing solar energy at a large scale requires land as well as the challenge of competing with land use requirements (Gulcu et al. 2006). This could prove problematic in an area where land use is an issue. If new buildings and infrastructure can be designed to accommodate PV cells, the issues that arise between land use and solar energy generation have the potential to be reduced. Another challenge is that the PV cells have a short life expectancy spanning between 20 and 25 years (Monier and Hestin 2011, Cellura et al. 2012), which is considerably short compared to a hydropower plant that can operate for up to 100 years (Briones et al. 2017). Decommissioning solar plant systems can generate waste, estimated to measure at 9.57 million tonnes in 2050 (Monier and Hestin 2011), which, if not properly managed, can cause environmental issues (Cellura et al. 2012). Despite the issues associated with a PV cell energy system, the benefits outweigh the use of fossil fuels by far as PV energy systems do not produce any direct GHGs (Ebinger et al. 2011b, Dowling 2013, Jerez et al. 2015).

2.2.5 Wind Energy

Wind energy is generated using wind turbines, which are made up of two or three blades commonly named rotor blades, attached to the top of a tall tower. As the wind blows, it forces the rotor to spin, and as it spins it generates energy that in turn, powers a generator. The generator itself is made up of magnets and a considerable amount of copper wire. As the conducting coils travel via each magnetic field, the electrons begin to shift, creating an electric current (Macgill and Ho 2009).

Empirical evidence indicates that a typical wind turbine has a characteristic power performance curve. This means that its power output varies with wind speed (Uluyol et al. 2014, Sohoni et al. 2016). The performance of a given wind-turbine generator can be related to three key points which are: cut-in speed defined as the minimum wind speed at which the machine will start generating power; rated wind speed defined as the maximum wind speed at which the maximum power output is reached; and cut-out speed, which is a wind speed threshold, beyond which the turbine is forced to stop (Manwell et al 2009).

Energy from wind power is growing on the global energy market, and, as illustrated in Figure 2-11, 2017 saw a growth of approximately 10% (539,123 MW) compared to 2016 (487,279 MW) in terms of the installed capacity for global wind power. Also in 2017, wind power installed capacity increased by approximately 23-fold compared to 2001 (Global Wind Energy Council 2018).

Figure 2-11: Global cumulative installed wind(MW) capacity between 2001 and 2017
Source: (Global Wind Energy Council 2018)

In the EAC, wind power is not extensively exploited. This is because Kenya is the only EAC member country that has grid-connected wind power (REN21 2016, Global Wind Energy Council 2018). In 2017, the Lake Turkana wind farm in Kenya, with a cumulative capacity of 310MW (Kibati 2015), was the single largest wind farm ever installed in the EAC. However, there is growing interest from another member of the EAC – Tanzania which currently has a number of wind power projects in the pipeline.

As evidenced by their growing interest in the implementation of wind power projects, Othieno and Awange (2016) stated that the Tanzanian government had initiated a feasibility study in the northern region to establish whether 50 MW wind generators could be installed. Moreover, in March 2016 Tanzania issued a wind resource assessment tender that was aimed at developing 50–100 MW from a wind power project in Tanzania's southern highlands (African Energy 2016). In Burundi, Rwanda and Uganda, wind speeds are relatively low, with an annual average wind speed of less than 4m per second ($4m.s^{-1}$), and no wind power plants are under construction (REN21 2016). In addition, energy from the wind is not featured in their 2025 energy expansion plans (cf. Table 2-3).

2.2.6 Wind power advantages and disadvantages

Although wind energy is a greener option when compared to fossil fuels, it is still necessary to balance the advantages of wind generating technology against its disadvantages. For instance, wind turbines have been reported to pose a threat to wildlife (National Wind Coordinating Committee 2010, Ellison 2012). This means that the local wildlife, for example flying birds and bats could be injured or killed if they run into the blades of a turbine. Wildlife at ground level can also be affected, for example by noise pollution as a result of the humming blades (National Wind Coordinating Committee 2010).

Wind turbines require a substantial investment in terms of upfront costs. For instance, the European Wind Energy Association indicates that approximately 75% of the total cost of energy for a wind turbine is related to upfront costs such as the cost of the turbine, foundation, electrical equipment, grid-connection and so on (European Wind Energy Association 2012). This outlay can prove expensive especially if the wind energy investment is aimed at rural areas where underground cables are required in order to connect such areas to more populated towns and cities (Manwell et al. 2010). Furthermore, wind energy supply may suffer from the varied speed of wind, which is often described as intermittent (Ogwang et al. 2014, Pašičko et al. 2012, Asrari et al. 2012, Ebinger et al. 2011b), thus making it difficult to predict the amount of energy that can be collected at any given time (Ebinger and Vergara 2011).

Though wind energy technology still has its limitations as evidenced above, it is clean energy, producing little to no GHG emissions, compared to fossil fuels. This is because wind energy is renewable and categorised as a green energy (Shahzad 2012, European Climate Foundation et al. 2014, Ebinger et al. 2011b, Carvalho et al. 2017).

2.3 Chapter Conclusion

The current energy provision in the region of EAC is dominated by traditional biomass rather than modern energy. This modern energy is sourced from both fossil fuel and hydropower. It has been noted that currently, modern energy consumption in the region is mainly supplied by hydropower and that hydropower generation shortfalls have been recorded in the last decade due to the occurrence of droughts in the region. The shortfalls are often compensated for by pollutants and expensive diesel generators.

As we know, there are now a large number of energy provision projects in the pipeline with the aim of scaling up access to modern energy in the future. These energy provision projects are dominated by hydro within most of the EAC countries. The studies undertaken on the future of hydropower plans in eastern and southern Africa highlight an increased risk of concurrent climate-related electricity supply disruptions which indicates that hydropower is vulnerable to climate variation (Conway et al, 2017). Thus, investing in hydropower without considering future changes in climate may lead to poor energy supply and poor investment planning which in return may lead to shortfalls in supply during certain periods of the years, causing potential disruption in energy access.

Energy from fossil fuels, which is not sustainable due to their cost and resultant environmental pollution, are still featured in the EAC future committed energy provision expansion plan. Given the vulnerability of hydropower to climate change and the environmental pollution associated with fossil fuel, relying heavily on the contribution of these two sources of energy (hydro and fossil fuel) towards future energy supplies in the EAC will lead the region to forego both its commitment to reducing GHG emissions and its commitment to meeting the SDG. In order to improve the sustainability and resilience of energy supply in the region, it is essential to broaden the energy mix by investing in a mixture of renewable energy sources (wind, and solar hydropower).

The advantages and disadvantages of hydro, wind and solar power generating technology have been explored and the conclusion is that their advantages outweigh their disadvantages compared to the use of fossil fuels. In respect to renewable energy sources in the EAC, we have noted that the EAC geographical region is endowed with various renewable energy resources that are largely not exploited. In light of this, individual member countries, such as Rwanda and Kenya, have already started investing heavily in RE. The rest of the EAC countries such as Tanzania, Burundi, and Uganda are also following suit with renewable energy implementation plans. However, climate change and other seasonal climate variations are not yet being taken into account. Hence, the energy generation from these renewable sources is uncertain. This challenge will be addressed here in this research. Thus, to offset this uncertainty in the face of climate change, it is necessary to have a good understanding of future climate scenarios. Further, it is important to explore the possibility of investing in a hybrid energy system. The next chapter of this thesis explores climate change and the prevailing climate in the EAC.

Chapter 3: The EAC climate system, its recent changes, and projection

This chapter presents the current studies on climate change and their implications on energy generation within the EAC. Inclusive of the findings of organisations such as the Intergovernmental Panel on Climate Change (IPCC), the first section of this chapter will discuss aspects of disseminating climate change. In addition, an introduction to climate models, regional climate models, and emission scenarios are provided. Finally, this chapter explores and discusses the EAC's past and projected climate systems.

3.1 Climate change dissemination body-IPCC

Since climate change, which refers to the flux in worldwide weather phenomena based on direct correlation with the increase in global average temperatures (e.g. Meehl et al. 2007) became worldwide scientific knowledge, it has attracted much attention around the globe. As one of the results of this increased attention, the IPCC was jointly formed. Founded in 1988 by the United Nation Environmental Programme (UNEP) and the World Meteorological Organisation (WMO), the IPCC set out with the aim to become a front line climate change dissemination body (IPCC 2013a). To date, it objectively assesses the latest scientific and technological evidence of climate change and its associated socio-economic impact. It also works towards making such information available to both the public and policymakers. Since its creation, the IPCC has made an enormous contribution to the body of knowledge about climate change (IPCC 1992, 1996, 2001, 2008, 2014).

3.2 Global and Regional Climate Models

Climate change has prompted enquiries into the processes behind climate variation (IPPC 1992), and it is because of this that scientists and academics around the globe have developed tools for climate modelling in order to better understand climate change processes. Climate modelling was first developed in the 1950s by an American, Phillip

Norman, as a way to realistically model both monthly and seasonal patterns in the troposphere (Phillips 1956). Following his pioneering work, climate modelling attracted the curiosity of scientists and climatologists who recognised the need for more sophisticated models (Cubasch et al. 2013). From then on, climate models have undergone various different stages of improvement leading to the development of the general circulation models and global climate models (GCMs). The IPCC explains GCMs as mathematical representations of the climate's physical processes in the atmosphere, ocean, cryosphere, land surface and other ecosystems (IPCC 2008). A number of climate scientists also describe GCMs as a set of equations derived from physical, chemical and biological laws that quantify the climate (Räisänen 2007, Gettelman and Rood 2016). Below, Table 3-1 charts the development of these GCMs expressed as computer codes and run on powerful computers.

Table 3-1: **GCM development**

Adapted from: (Cubasch et al. 2013)

Table 3-1 indicates how models have been improved over time due to the addition of various components, climate physical processes (e.g. heat transfers), and the ways they interact with each other. The number of processes added within each component increases over time and is represented by the size of the magnetic disk within the flowchart. As can be seen from the graph above, the bigger disks are representative of more processes having been added. Thus, between the mid-1970s and 1990 FAR (First Assessment Report), atmosphere, land surface, ocean and sea ice processes were added to the different GCM components (Table 3.1). Aerosol and carbon cycle modules were then added for the Second Assessment Report (SAR) which was published in 1995 and in the Third Assessment Report (TAR) which was published in 2001. Dynamic vegetation was added for the IPCC Assessment Report 4 (AR4) in 2007. In 2013, the atmospheric chemistry and land-ice components were added during Assessment Report 5 (AR5).

As previously mentioned, the interactions between the components (e.g. ocean, land, and atmosphere) and within the components (e.g. ocean cooling and warming, condensation of water vapour to form clouds, CO_2 uptake by plants, etc.) are mathematically represented by the set of complex equations that govern the GCMs. The variability between and within these components are referred to as the GCMs' internal variability (IPCC 2001, Jones et al. 2004), and also known as natural internal processes within the climate system (Sturman 2008, Tobergte and Curtis 2013, Lafaysse et al. 2014). According to the IPCC, GCMs are the only advanced tools currently available for simulating the response of the global climate system to increasing GHG concentrations.

3.3 How much can GCM projections of future climate change be trusted?

Climate models combine the effects of anthropogenic induced climate change and natural climate variability to determine the Earth's future climate trajectory in the coming decades (Deser et al. 2014). Because of climatic processes, such as the interaction between different components, e.g. atmosphere and land-ocean which are extremely complex, some of the processes are not yet fully understood and thus, the mathematical representation of these processes are estimated (Sturman 2008, Tobergte and Curtis 2013). In this sense, the GCM representations of climatic processes and feedbacks are potentially subject to uncertainties as the parameterisation used to represent geophysical processes are part of the simulation chain (IPCC 2001, Lafaysse et al. 2014). For example, this is evident in the case of the future of GHG and aerosol emissions as there remains uncertainty surrounding the projected socio-economic development of human societies (Lafaysse et al. 2014).

Furthermore, the IPCC (2008) indicates that due to limitations in computing, scientific understanding and the availability of detailed observations with regards to various physical processes, many important small-scale changes could not be represented explicitly in GCMs. Moreover, the IPCC recognises that the GCMs are deficient in the simulation of tropical precipitation, such as that of El-Nino Southern Oscillation (as explained in Section 3.5.1), and the observed variation in tropical wind and rainfall, within a time scale of 30 to 90 days. However, GCM limitations do not make the data produced (that is, the GCM data) unreliable for a number of reasons. For example, Gettelman and Rood (2016) argued that the physical science behind GCMs is based on physical laws that have been established for several hundred years. To be more explicit, when simulating climate processes, GCMs follow the basic fundamental laws of physics that describe the conservation of mass, energy and momentum, also known as Newton's second law of momentum (Newton 1687) in addition to gravity (Räisänen 2007, Gettelman and Rood 2016). Thus, this presents a strong reason to believe that GCMs act as valuable tools in terms of exploring future climate change. Moreover, Schwartz (2012) argues that many criticisms of climate modelling fail to reflect on the analysis of the basic science concepts behind the GCMs, as well as the extensive history of the development of radiation transfer codes in planetary modelling and atmospheres. Further to this, Hausfather (2017) postulated that even though some climate models projected either less or more warnings than previously experienced, all projected results showed a temperature increase between 1970 and 2016 that were in line with what actually occurred. Similarly, an international team of climate scientists found that until 2011, the actual global temperature continued to increase in line with the estimations of the IPCC report (Rahmstorf et al. 2012).

Although there are many reasons to believe that climate models can give useful information on future climate change, the question on model reliability has no simple quantitative justification (Räisänen 2007). To deal with GCM limitations, it is of paramount importance to assess the suitability of GCMs over the region of interest. Therefore, in terms of using GCMs, confidence in the models' capacities for accuracy must be based on the careful evaluation of their performances. Performances here refers to the comparison of each model's output against actual observations (Lupo and Kininmonth 2013). In addition, different GCMs set different priorities to deconstruct the extremely complex climate system in such a way that it can be simulated on a large-scale (Fischer and Knutti 2013). In this sense, using a Multi-Model Ensemble (MME) to investigate all the different simulations originating from various physics processes used in different institutions, is better than using a single model. Fowler et al. (2007) define an MME as the mean of a set of model simulations from structurally different models, where one or more of the initial condition ensembles are available from each model. Jones et al. (2004) argue that whilst a single model projection may provide a plausible representation of climate change, it can give no indication into the range of the possible outcomes for assessing the risks and opportunities in terms of how to respond accordingly. In addition, no one model can be chosen as best. Because of this, it is important to use results from a range of models as the mean of the ensemble can be expected to outperform individual ensemble members (Hagedorn et al. 2005; IPCC 2014; Gilvati et al. 2017). This is because of individual model errors which are compensated in the MME, and tend to match better to the observed climate (Hagedorn et al. 2005). Moreover, Givati et al. (2017) postulate that MME results outperform any results from a single model prediction due to the fact that the trend in the mean of all models is closer to that of the observed climate. Based on these differing arguments, the use of MME to account for a wide range of GCM uncertainties is adopted. Another limitation of GCMs is that the important small-scale physical processes cannot be represented explicitly and are therefore parameterised (Jones et al. 2004, Sailor, David J. et al. 2008, Weyant et al. 2009, Hazeleger et al. 2010, Rashid et al. 2015). To overcome this limitation, regional climate models (RCMs) have been developed to represent local sub-grid-scale features and dynamics which cannot be simulated on a global scale (Giorgi et al. 2009).

The recent Coupled Model Inter-comparison Project Phase 5 (CMIP5) climate models (Taylor et al. 2012) for example, which have been used in the IPCC assessment reports, have been dynamically downscaled to a high-resolution over various regions within the Coordinated Regional Climate Downscaling Experiment project (CORDEX; Giorgi et al. 2009, Nikulin et al. 2012, Endris et al. 2013, Christensen et al. 2014; Gutowski et al. 2016). CORDEX domain encompasses the majority of land areas in the world, including within the continent of Africa. In Africa, CORDEX domains are known as CORDEX-AFRICA. Within CMIP5, and thus CORDEX, historical simulations are forced by historic anthropogenic emissions of greenhouse gases and sulphate aerosols. In addition to this, they are inclusive of other anthropogenic and natural forcing. The inputs to GCMs are emission scenarios currently termed as Representative Concentration Pathways which are described in Section 3.4.2.

3.4 Emission Scenarios and Representative Concentration Pathways

3.4.1 Emission Scenarios

Climate modelling provides an understanding of the potential level of greenhouse gases, aerosol, and other pollutants concentrated in the atmosphere (IPCC 2001). Since the range of future emissions is highly uncertain, the World Meteorological Organisation (2015) argues that scenarios provide an alternative image of how the future might unfold. According to Wayne (2015), emissions scenarios provide a framework by which the process of building experiments can be streamlined.

The World Meteorological Organisation (2015) added that emission scenarios encompass assumptions about driving factors such as patterns of population growth, and economic and technological levels. Emission scenarios thus provide input for climate modelling by describing potential future releases into the atmosphere of greenhouse gases, aerosols, and other pollutants as well as providing information on land use and land cover. Emission scenarios are chief tools with which to analyse how emission from various sources (natural and man-made) may influence future emissions outcomes. Further improvements to emission scenarios have yielded Representative Concentration Pathways (RCPs) scenarios and have been referred to within the IPCC Fifth Assessment Report (AR5).

3.4.2 Representative Concentration Pathways

This study uses the RCPs scenarios, which were developed for the IPCC AR5. The RCPs are the main inputs to climate modelling which are used to analyse how emissions from various sources, both natural and man-made, may influence future emission outcomes. The pathways describe four possible climate futures, all of which are considered possible, depending on the extent of greenhouse gas concentration in the atmosphere in future (Weyant et al. 2009, van Vuuren et al. 2011). Figure 3-1 is an illustrative schematic of the four RCPs which, represent a range of possible radiative forcing values during the year 2100. These are 2.6W/m^{2,} $^{+}$4.5 W/m^2, +6.0 W/m^2, and +8.5 W/m^2 respectively for RCP2.6, RCP4.5, RCP6.0 and RCP8.5, relative to pre-industrial values. This figure also demonstrates how the RCPs are advancing our knowledge of climate change.

Figure 3-1: Global surface temperature trend from 1850 to 2300.

Results from historical data and each RCP are computed using a number of models and arrows. For each RCP and historical record, the graph points to its corresponding number of models. For example, 42 models have been used to compute the historical mean in temperature and are in black, whereas 32 and 12 models have been used to compute future projections under RCP2.6 respectively for the periods from 2005 to 2050 and 2100 to 2300.

Source: (IPCC 2013b)

As an example, under the recently developed RCPs, global warming is likely to exceed 2°C under RCP6.0 and RCP8.5 (projection with high confidence) and more likely than not global warming is likely to exceed 2°C under the RCP4.5 (projection with medium confidence) (IPCC 2013b).

In summary, the understanding of climate variability and climate change are advanced by climate modelling (i.e. GCM and RCMs). Although GCMs have limitations and deficiencies which require attention, this does not detract from the successes that they have achieved. GCMs, as well as RCMs, remain widely used and accepted as points of reference, based on the understanding that these models are founded on well-established physical laws, and are thus able to reproduce features of past climate changes and variability. One of the main advantages of climate models is that they allow the examination of potential future trajectories of climate using RCP scenarios. RCPs describe four plausible future trajectories of climate change on a global scale according to the GHG concentration in the atmosphere going forward. The next section explores the projected change over the EAC region and its potential effect on energy generation.

3.5 EAC climate system and its observed change manifestation on energy

3.5.1 The observed change in climate

The EAC has three seasons: the long rainy season which occurs during the months of March, April and May (MAM); the short rainy season which occurs during October, November and December (OND); and the dry season during the months of June, July, August and September (JJAS; Indeje et al. 2000, Yang et al. 2014, Ongoma et al. 2017). The EAC climate is governed by complex patterns of atmospheric circulations composed of the Inter-tropical convergence zone (ITCZ), sub-tropical high-pressure systems, various jet streams and easterly and westerly wave systems (Wu et al. 2013). The interdecadal variability of climates in the EAC region is known to be influenced by El Niño Southern Oscillation (ENSO) (Fer et al. 2017, McGregor and Ebi 2018). ENSO is a naturally occurring phenomenon that involves a fluctuating sea surface temperature (SST) in the equatorial Pacific Ocean and exerts a discernible impact on ecosystems and society through the alterations in climate patterns it causes (McGregor and Ebi 2018). The ENSO has two cycles. The first El Niño cycle is the ENSO warm phase associated with a band of warm ocean water that develops in the central and east-central equatorial Pacific. The second phase of the ENSO is La Niña events and is the cold ENSO phases (NOAA 2018). La Niña is characterised by SSTs in the eastern Pacific where it is colder than normal for the region. In addition, La Niña is characterised where air pressure is high within the eastern Pacific and low in the western (Niedzielski 2015). Figure 3-2 illustrates the ENSO cycle phases.

Figure 3-2: El Niño Southern Oscillation
La Niña [A](Normal Year) is referred to as the cold phase of ENSO and El Niño [B] as the warm phase of ENSO. All take place off the coast of South America.
Source: (NOAA 2018)

As stated above, the ENSO has a great influence on the East African climate. In this regard, Nicholson (1996) and Segele et al. (2009) postulate that the climate over East Africa is characterised by the frequent succession of extreme dry and wet periods due to the high interannual variations in the amount of precipitation. In East Africa, dry periods are also known to be linked to La Niña, while wet periods are associated with the El Niño shown (Nicholson and Kim 1997, Schreck and Semazzi 2004). Moreover, Shongwe et al.

(2011) noted that the number of excessive rainfall events and droughts are increasing in East Africa. A continuous decline in rainy days has also been observed in the region of East Africa in recent decades (Lyon and Dewitt 2012, Liebmann et al. 2014 and Souverijns et al. 2016). Further to this, data analysis for the period of 1940-2001 indicates an increase in temperature anomalies in the Eastern African climate variability (Scheck and Simazine 2004). Figure 3-3 below shows historical temperature variability in East African where the temperature has been constantly increasing.

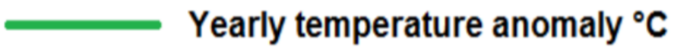

Figure 3-3: East African historical temperature variability.
Source: (Carty 2017)

Carty (2017) indicates that temperatures in the East African region have been consistently higher in recent years compared with a historic average (over the period 1940 to1981) and prolonged droughts have been observed. The increase in temperature and prolonged droughts indicate that the level of evaporation from hydropower reservoirs will increase, thus reducing the amount of water required to maintain hydropower plants at their operating capacity level.

3.5.2 Projected climate change in the East African region

According to Hulme et al. (2001) and IPCC (2008), average temperatures in Africa are predicted to increase by 1.5℃ to 3℃ by 2080, with an expected increase of 5% to 8% of arid and semi-arid lands in Africa. Furthermore, there is a likelihood of an increase in annual mean rainfall in parts of East Africa (IPCC 2007, 2014, Serdeczny et al. 2017), and an increase in runoff in equatorial Africa (Milly et al. 2005). Academics such as Shongwe et al. (2011), McSweeney et al. (2015) and Kent et al. (2015), applied various GCMs and RCMs to study precipitation in East Africa. They concluded that the areas located near the equator and the Greater Horn of Africa are most likely to experience an increase in annual precipitation. These findings contrast the current drying trend in the region, and this contradiction has been termed as the East African climate paradox by Rowell et al. (2015). This paradox refers to the internal variability of GCMs and the uncertainty associated with the reproduction of aerosol impacts.

Seager et al. (2010), Niang et al. (2014) attributed part of the future increase in precipitation throughout the region to an enhancement of water vapour and the intensified of moisture transport within the Hadley circulation. This shows that when predicting future climate change projections, the uncertainties associated with GCMs should be noted. Not enough studies have been conducted on wind energy generation within the East African region. with specific reference to future wind projections, or variations on future climate change. However, referring to the previously conducted studies (e.g. Breslow and Sailor 2002, Sailor et al. 2008, Pereira de Lucena et al. 2010, Gonçalves-Ageitos et al. 2015, Breslow and Sailor 2002, and Sailor et al. 2008) indicating future variations in wind speed, the wind speed is likely to vary in future across the EAC region. The extent to which it will vary will need to be examined.

Concerning solar radiation, Wild et al. (2015) indicated that a large part of the world is expected to experience a decrease in all-sky radiation in the coming decades. Similarly, Ebinger and Vergara (2011) stated that the distribution of global solar radiation showed that solar irradiance is likely to decrease by 5 Wm^{-2} over sub-Saharan Africa due to the increase in GHG altering atmospheric transmissivity, cloudiness and water vapour processes whereas an increase of more than 5 Wm^{-2} would be observed over the Middle-East. However, the authors, Ebinger and Vergara (2011), state that sub-Saharan Africa is well suited for concentrated solar power, despite the projected decrease in solar radiation over the region. More studies are needed to contribute to knowledge on the implications of climate change on the energy sector within the EAC region. Energy from other sources such as wind and solar power is still developing, so the relative variation in climate change could impact future studies.

3.6 Chapter conclusion

This chapter has explored the literature pertaining to the study of the EAC climate system and its manifestation in terms of hydropower generation. An increase in temperature across the region has been recorded and it has also been noted that the average temperatures in Africa are predicted to increase by 1.5℃ to 3℃ by 2080. This means that an increase in temperature across the EAC region is also expected. These projections are likely to lead to an increase in electricity demand for cooling and possibly impact on the performance of solar PV. This is because performance reduces with PV surface temperature. It has also been noted that precipitation has been characterised by the frequent succession of extreme dry and wet periods due to high inter-annual variations in precipitation numbers which have adversely impacted hydropower generation. It should be noted that observed changes in wind speed and solar radiation have not been well documented. Research on future wind speed in the EAC is extremely limited and the extent to which wind in the EAC will be affected by climate change is yet to be determined. For future solar radiation, it is expected that a decrease in all-sky radiation in the coming decades due to the increase in GHG altering atmospheric transmissivity, cloudiness, and water vapour processes will take place. In addition to this, the distribution of global solar radiation shows that solar irradiance is likely to decrease by $5Wm^{-2}$ over sub-Saharan Africa.

This chapter has explored the climate impacts on the EAC and the literature shows that hydropower production shortfalls have been recorded over the last decade in all the member countries of the EAC. The deficit in hydropower outputs is mainly due to drought-spell recurrence, which resulted in many of the EAC countries losing a considerable amount of hydropower production. It is noted that there is limited energy generation capacity from wind and solar within the EAC, even though there are some small scale projects and plans for future implementation. However, with regards to this, it should also be noted that no related climate change impact studies were undertaken during the planning of these renewable energy projects.

In more general terms, climate change could have significant impacts on hydro, wind and solar energy sources as a result of the rising temperatures, variations in the amount of precipitation, and changes in humidity, wind patterns, and the number of sunny days per year. Therefore, for the EAC to harness its renewables and ensure the reliability of energy provision, it is important to have a better understanding of climate change and the renewable energy nexus with respect to the potential complementarity of the various renewable energy resources.

Chapter 4: Research methodology

4.1 Introduction

This chapter presents the research methodology. For this, various approaches are presented to justify the selection of the most appropriate methods for the research. The main aim of this research is to develop a DSF for achieving reliable, sustainable, and climate-resilient energy access in the EAC region under different climate change scenarios. In this respect, five objectives have been formulated to achieve the aim of this research. Each objective requires a tailored research method. Hence, this chapter identifies and describes the research methodology and methods by which each objective was achieved. Archived simulated data (CORDEX-AFRICA) available at https://www.cordex.org/data-access/esgf// (list of models available for African domain) are used in this study. This list is presented on Table 4-1. Quantitative analysis of these CORDEX-AFRICA data is used throughout the course of this research. This research chapter starts by explaining the methods employed to accomplish objectives one to five of this research. The five objectives are organised respectively into five themes as follow:

1. Theme One: The status of current energy access, future renewable energy climate nexus
2. Theme Two: Assessing future climate change under RCP4.5 & 8.5 scenarios for the EAC
3. Theme Three: Hydro, wind and solar power resources joint variability in the EAC under RCP4.5 and 8.5 scenarios and the implications for energy supply balancing
4. Theme Four: Optimal hybrid combinations of hydro, wind speed and solar power for electrification of a hypothetical village within the EAC
5. Theme Five: A systematic approach for renewable energy implementation in the EAC

Table 4-1: CORDEX-AFRICA regional climate models

	Domain	RCM	RCM Centre	Driving GCM	GCM full name (Centre)
1	AFR-44	CCLM4-8-17	Climate Limited-area Modelling Community	CNRM-CERFACS-CNRM-CM5	Centre National de Recherches Météorologiques - Centre Européen de Recherche et de Formation Avancée en Calcul Scientifique
2	AFR-44	CCLM4-8-17	Climate Limited-area Modelling Community	ECMWF-ERAINT	European Centre for Medium-Range Weather Forecasts
3	AFR-44	CCLM4-8-17	Climate Limited-area Modelling Community	ICHEC-EC-EARTH	Irish Centre for High-End Computing EC-EARTH Model
4	AFR-44	CCLM4-8-17	Climate Limited-area Modelling Community	MOHC-HadGEM2-ES	Met Office Hadley Centre Global Environment Model version 2
5	AFR-44	CCLM4-8-17	Climate Limited-area Modelling Community	MPI-M-MPI-ESM-LR	Institut Pierre-Simon Laplace, France
6	AFR-44	CRCM5	Canadian Regional Climate Model	CCCma-CanESM2	Canadian Centre for Climate Modelling and Analysis
7	AFR-44	CRCM5	Canadian Regional Climate Model	ECMWF-ERAINT	Canadian Centre for Climate Modelling and Analysis
8	AFR-44	CRCM5	Canadian Regional Climate Model	MPI-M-MPI-ESM-LR	Max-Planck-Institut für Meteorologie
9	AFR-44	DMI HIRHAM5	Danmarks Meteorologiske Institut	ECMWF-ERAINT	European Centre for Medium-Range Weather Forecasts
10	AFR-44	DMI HIRHAM	Danmarks Meteorologiske Institut	ICHEC-EC-EARTH	Irish Centre for High-End Computing EC-EARTH Model

	Domain	RCM	RCM Centre	Driving GCM	GCM full name (Centre)
11	AFR-44	DMI HIRHAM	Danmarks Meteorologiske Institut	NCC-NorESM1-M	Norwegian Climate Centre-Norwegian Earth System Model
12	AFR-44	HadGEM3-RA	Hadley Centre Global Environment Model version 3	ECMWF-ERAINT	European Centre for Medium-Range Weather Forecasts
13	AFR-44	HadRM3P	Hadley Centre Regional Climate Model, version 3	ECMWF-ERAINT	European Centre for Medium-Range Weather Forecasts
14	AFR-44	KNMI-RACMO22T	Royal Netherlands Meteorological Institute	ECMWF-ERAINT	European Centre for Medium-Range Weather Forecasts
15	AFR-44	MPI-RACMO22T	Royal Netherlands Meteorological Institute	ICHEC-EC-EARTH	Irish Centre for High-End Computing EC-EARTH Model
16	AFR-44	MPI-RACMO22T	Royal Netherlands Meteorological Institute	MOHC-HadGEM2-ES	Met Office Hadley Centre Global Environment Model version 2
17	AFR-44	RCA4	Rossby Centre Atmosphere model version 4	CCCma-CanESM2	Canadian Centre for Climate Modelling and Analysis
18	AFR-44	RCA4	Rossby Centre Atmosphere model version 4	CNRM-CERFACS-CNRM-CM5	Centre National de Recherches Météorologiques - Centre Européen de Recherche et de Formation Avancée en Calcul Scientifique
19	AFR-44	RCA4	Rossby Centre Atmosphere model version 4	CSIRO-QCCCE-CSIRO-Mk3-6-0	Commonwealth Scientific and Industrial Research Organisation, Australia
20	AFR-44	RCA4	Rossby Centre Atmosphere model version 4	ECMWF-ERAINT	European Centre for Medium-Range Weather Forecasts

	Domain	RCM	RCM Centre	Driving GCM	GCM full name (Centre)
21	AFR-44	RCA4	Rossby Centre Atmosphere model version 4	ICHEC-EC-EARTH	Irish Centre for High-End Computing EC-EARTH Model
22	AFR-44	RCA4	Rossby Centre Atmosphere model version 4	IPSL-IPSL-CM5A-MR	Institut Pierre-Simon Laplace, France
23	AFR-44	RCA4	Rossby Centre Atmosphere model version 4	MIROC-MIROC5	Model for Interdisciplinary Research On Climate, Japan
24	AFR-44	RCA4	Rossby Centre Atmosphere model version 4	MOHC-HadGEM2-ES	Met Office Hadley Centre Global Environment Model version 2
25	AFR-44	RCA4	Rossby Centre Atmosphere model version 4	MPI-M-MPI-ESM-LR	Max-Planck-Institut für Meteorologie
26	AFR-44	RCA4	Rossby Centre Atmosphere model version 4	NCC-NorESM1-M	Norwegian Climate Centre-Norwegian Earth System Model
27	AFR-44	RCA4	Rossby Centre Atmosphere model version 4	NOAA-GFDL-GFDL-ESM2M	National Oceanic and Atmospheric Administration
28	AFR-44	MPI-REMO2009	Max Planck Institute for Meteorology	ECMWF-ERAINT	European Centre for Medium-Range Weather Forecasts
29	AFR-44	MPI-REMO2010	Max Planck Institute for Meteorology	ICHEC-EC-EARTH	Irish Centre for High-End Computing EC-EARTH Model
30	AFR-44	MPI-REMO2011	Max Planck Institute for Meteorology	IPSL-IPSL-CM5A-LR	Institut Pierre-Simon Laplace, France
31	AFR-44	MPI-REMO2012	Max Planck Institute for Meteorology	MIROC-MIROC5	Model for Interdisciplinary Research On Climate, Japan

	Domain	RCM	RCM Centre	Driving GCM	GCM full name (Centre)
32	AFR-44	MPI-REMO2013	Max Planck Institute for Meteorology	MOHC-HadGEM2-ES	Met Office Hadley Centre Global Environment Model version 2
33	AFR-44	MPI-REMO2014	Max Planck Institute for Meteorology	MPI-M-MPI-ESM-LR	Max-Planck-Institut für Meteorologie
34	AFR-44	MPI-REMO2015	Max Planck Institute for Meteorology	NOAA-GFDL-GFDL-ESM2G	National Oceanic and Atmospheric Administration

In the above table 4-1, The GCMs' long names are often named after their institution. The other letters signify supplementary information regarding the GCMs and are separated by a hyphen. The most frequents ones are detailed as follows: -ESMs: Earth System Models; -GFDL: Geophysical Fluid Dynamics Laboratory; -CM: coupled climate model; -HIRAM: High-Resolution Atmosphere Model; -LR: Low Resolution; -MR: Medium Resolution; -QCCCE: Queensland Climate Change Centre of Excellence; -CERFACS: Centre Européen de Recherche et de Formation Avancée en Calcul Scientifique and the domain AFR-44 means 0.44 x 0.44 degree resolution over Africa.

4.2 Exploring the status of energy access and future renewable energy implementations plans in the EAC.

The method used to achieve objective one is presented through a literature review of the status of energy access and future renewable energy implementation plans in the EAC. The analysis and discussion are presented in chapter two and chapter three.

Chapter one focuses on the status of EAC energy access and production, while chapter two presents the recent and projected changes in the EAC climate system. In chapters one and two, the literature review outlines the current theory and gaps in existing studies, which provides a basis for the formulation of research aims and objectives. This works towards developing the theoretical framework that underpins this research. The information necessary to conduct the literature review was obtained through a comprehensive, critical and objective analysis of the current knowledge of energy access and future RE implementation plans.

The literature was collected from a range of sources including from national governments, EAC publications, reports, books and articles. These were researched in conjunction with the reports and publications of the African and other international development agencies such as the United Nations Economic Commissions for Africa (UNECA), World Banks, and African Development Bank. Information on governance and values relevant and specific to the EAC were sourced from the report of various governments and donor agencies as well as scholarly publications. Readily available data on energy generation and access was obtained from individual EAC governments, the EAC data portal and donor reports, as well as energy agencies such as the Energie des Grand Lacs (EGL), the East African Community Power Pool (EACPP) and the East African Community Climate Change Master Plan 2011-2031 (EAC 2011a). The latest textbooks, publications, and reports from the World Bank, EAC, IEA and IPCC assessment reports on renewable energy and climate change were reviewed and also contributed to the literature review of this research. All sources used in completing the literature review have been referenced in the text and bibliography.

4.3 Investigating future hydroclimate change scenarios for the EAC

This section outlines the empirical research strategy employed in chapter five to achieve objective two, which is to investigate EAC future hydroclimate changes under RCP4.5 and 8.5 for the period spanning from 2021 to 2100. CORDEX-Africa (RCMs) data, with specific reference to historical and RCP scenarios, are the main source of data used in this research. The study area shown in Figure 4-1 is also described and the choice of the two RCPs and their sources of observed data are justified. Furthermore, the selection, implementation and validation processes for the RCMs used throughout this research are evaluated and described. Finally, the methods used to achieve the objectives are discussed.

CORDEX is sponsored by the World Climate Research Program (WCRP) to organise an internationally coordinated framework to produce improved regional climate projections for identified regions worldwide (CORDEX 2018). The CORDEX regional climate models (RCMs) various simulations for the Africa domain (CORDEX-Africa) shown in Figure 4-1[A] are conducted at the spatial resolutions of 0.44 degrees (AFR-44, ~50 km) (Gutowski et al. 2016). Data for this research were extracted from the CORDEX_AFRICA domain and constrained to the EAC sub-region domain (*i.e.* for the location at the coordinates of Latitude -12.0S–6.0N and Longitude: -28W–42.0E) as shown in Figure 4-1[B]. As previously stated, the resulting models are termed EAC_RCMs. Figure 4-1[C] is a selected local area used to study the optimal combinations of hydro, wind and solar power resources with the aim of finding ways to achieve a well-balanced renewable energy supply that meets local, country and regional demands.

4.3.1 Study area and CORDEX domain

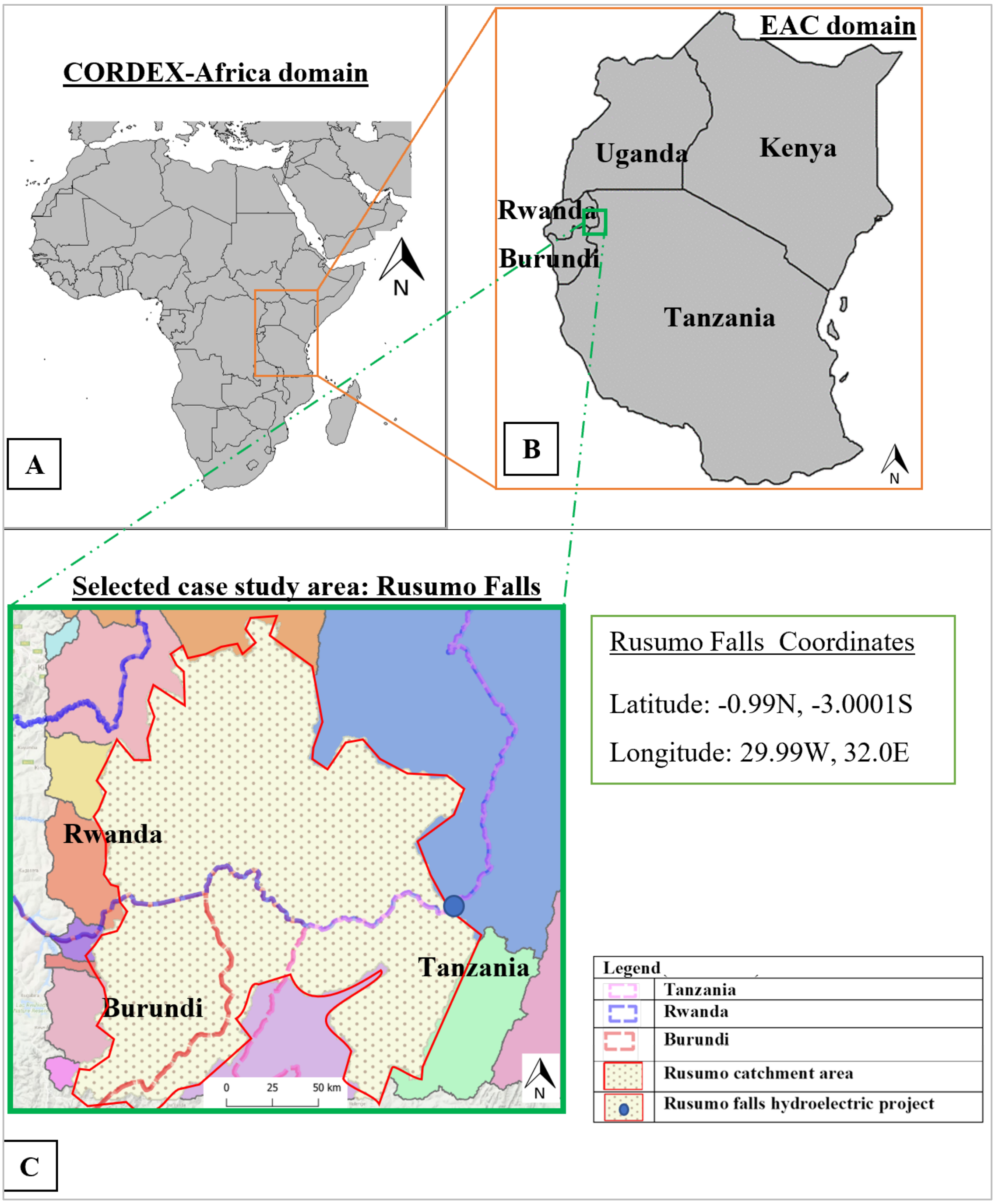

Figure 4-1[A to C]: Study domain.

Sub-figure (A) shows the regional climate models data at African domain (CORDEX-Africa) and sub-figure (B) represents the region (EAC) for which the data has been extracted for this study. Further to this, subfigure (C) represents a selected local area of 50kmx50km (green contour) and data for this local area is extracted from the regional area (EAC)in order to investigate the hydroclimate complementarity and its implications in energy balancing at the local scale. The bottom right corner is a legend for further area description.

For the electricity network to redistribute power sufficiently to meet both local and regional demand, there has to be resource sharing across the neighbouring countries (IRENA 2014, IEA 2014, REN21-EAC 2016). In addition, the logic dictates that hydro, solar and wind and other sources of power are produced where their supply is most abundant both at local and/or countrywide/regional level (Rolland and Glania 2016, De Barbosa et al. 2017). The regional level data (EAC domain in this research case) can be used to depict both countrywide and regional hydro, solar and wind power resource distribution and complementarity (Zhou et al. 2010). However, it would be difficult to investigate these resources, particularly complementarity and its implication in energy supply balancing, at a local level using the regional average data. This is because renewable technologies complement each other (Zhou et al. 2010), hence a hybrid system that combines an adequate proportion of resources, locally available, provides more security in terms of energy supply (Amador and Dominguez 2005, Rolland and Glania 2016). For this purpose and with the EAC regional power interconnections between countries and their plan for sharing available generational resources (Eastern Africa Power Pool 2011) in mind, a selected study area, denoted here as RUSUM0 falls (cf. Figure 4-1[C]), has been used as an example for the future hydroclimate complementarity and their implications in levelling out imbalances in energy supply. To achieve this, a hypothetical village (as explained in Section 7.6.4) has been used as an example. It is important to note that the climate varies from one location to another. Therefore, no single climate at any particular location is representative of the rest of the EAC region. As a result of this, the power output from any given location, and its implications for energy balance is not representative of the rest of the region. Since the aim of this research is to develop a DSF for achieving reliable, sustainable and climate-resilient energy access in the EAC under different climate scenarios, the systematic approach utilised in calculating the power output from the hydroclimate, their complementarity and implications for an energy balance at Rusumo falls should be seen to be replicable anywhere in the region of the EAC and beyond.

4.3.2 RCM data and RCP selection

As mentioned in Section 3.2, a widely applied and flexible method for capturing important local processes of the climate system, which GCMs cannot reproduce, is through the use of RCMs (Jones et al. 2004). RCMs have been developed to offer an affordable alternative and have the ability to resolve mesoscale processes over a limited region of interest (Chou et al. 2012, Marengo et al. 2012). There are a number of RCMs (McSweeney et al. 2015) available for use in regional climate impact assessment studies. However, it is beyond the scope of this research study to explore all of them in great detail. As stated above, this study data for the EAC domain Figure 4-1(B) has been extracted from CORDEX-AFRICA as shown in Figure 4-1(A). In particular, CORDEX-AFRICA data have been used as they are the only available regional climate data downscaled to the AFRICA domain (Gutowski et al. 2016).

Further reasons for choosing CORDEX-AFRICA are laid in Section 3.3. Furthermore, data for hydroclimate energy resources complementarity, which have been explored at the local scale (cf. Figure 4-1[C]) are extracted from the EAC domain. Both data, at EAC and on a local scale, were used for future climate analyses performed for the scenarios RCP4.5 and 8.5. Future changes (for the period of 2021 to 2100) in temperature, wind speed, solar radiation, and precipitation were assessed against the historical period (1976-2005). The future period 2021-2100 is subdivided into three different time periods, which are: the near future (2021-2050), the middle future (2051-2080) and the long-term future (2071-2100).

Thirty year periods have been adopted following the calculation of the monthly and annual 30-year standard normal, first published in 1989 and updated in 2017 (WMO 2017). This period of thirty years has been used in numbers of studies (e.g.Lenderink et al. 2007, Islam et al. 2009, Li et al. 2010, Dosio 2017). In addition, 30 year time periods closely match the lifespan (20 to 25 years) of wind and solar power infrastructure (Monier and Hestin 2011, Cellura et al. 2012). Even though hydropower plants have a lifespan of over 100 years (Briones Hidrovo et al. 2017), depending on the age of the plant and maintenance schedule, 30 years may correspond with the need for major upgrades (e.g. retrofitting the plan to be used in hybrid with other renewable energy sources).

It should be noted that the IPCC does not provide probability assignments for any of the RCPs (IPCC 2013b). The RCP8.5 is the upper bound of the RCPs and has been designed to support research on impacts and potential policy responses to climate change (Riahi et al. 2011, van Vuuren et al. 2011, Moss et al. 2010). For this reason, the RCP8.5 scenario was chosen to assess the potential changes in hydroclimate in the situation of a future with continued high emissions growth. The remaining three RCPs (that are, RCP6.0, RCP4.5, and RCP2.6) present different pathways of mitigating emissions. According to Thomson et al. (2011), these three RCP scenarios follow more or less a cost-minimizing pathway to reach the target radiative forcing, set measures to limit emissions including but not limited to shifting to electricity from RE, lower emissions energy technologies and the deployment of carbon capture and geologic storage technology. The RCP2.6 aims to keep global-mean temperature rise below 1.5°C relative to the pre-industrial level during the remainder of the 21st-century and one of the key assumptions to achieve this target is the full participation of all countries in the world (van Vuuren et al. 2011). The withdrawal of the United State of America (USA) from the Paris agreement (Chakraborty 2017) broke this key assumption. In addition, Jones et al. (2018) argue that given the continued increases in GHG, achieving RCP2.6 targets is too ambitious. For these reasons, the RCP2.6 was not chosen for this study. This left a choice between RCP4.5 and RCP6.0. RCP4.5was the best choice in this case because together with RCP8.5 already selected, it covered the entire range of radiative forcing resulting from RCP4.5, RCP6.0, and RCP8.5. In brief, the RCP4.5 and RCP8.5 have been chosen for this study based on the reasons provided above.

4.3.3 Observed data for model validation

Climate raw observations data is scarce in the EAC (Funk et al. 2015). Here, the Global Precipitation Climatology Centre (GPCC) version 7 (Schneider et al. 2011), which is a gauge-based, gridded global land surface dataset for the period dated 1901 to the present day has been used for precipitation data. The GPCC data are available from https://www.esrl.noaa.gov/psd/data/gridded/data.gpcc.html. In addition, the Climatic Research Unit (CRU) data sources, have been used for temperature (University of East Anglia 2017). The CRU data are sourced from http://www.cru.uea.ac.uk/data.

The GPCC dataset was used because of its reliability in the East African domain (Endris et al. 2013), and because it has been tested in previous works. For instance, studying the long rains, Yang et al. (2015) show that GPCC anomalies have a slightly smaller magnitude than two satellite gauge datasets from 1979 to the present day. They also show that GPCC was better in reproducing drying conditions in East Africa than the Climate Research Unit (CRU) monthly precipitation datasets (Mitchell and Jones 2005). As per the GPCC dataset, the confidence in the CRU data is that it had been used successfully in a number of East African climatological studies, e.g. Shongwe et al. (2011), Endris et al. (2013), Liebmann et al. (2014) and Rowell et al. (2015).

Data from the European Centre for Medium-Range Weather Forecasts (ECMWF) Interim Re-Analysis (ERA-Interim; Dee et al. 2011) have also been used to validate climate models for wind and solar radiation. The ERA-interim (ERAI) dataset has been used to validate the climate models. The ERAI dataset was used not because of its superior quality to others, but simply because it is the dataset used by CORDEX for model evaluations (Brands et al. 2013). As a consequence, the ERAI datasets are regarded as consistent with models for any given time step and spatial scale (Bett and Thornton 2016). The ERAI datasets have been available from 1979 (Dee et al. 2011), while the CORDEX-AFRICA dataset covers the period from 1950-2005 (CORDEX 2018), therefore 25 years of data (i.e. 1980-2005) are available for use in the model performance evaluation for wind and solar power.

4.3.4 CORDEX-AFRICA RCMs evaluation processes in the context of the EAC

The three-step sequential CORDEX-AFRICA RCMs evaluation procedure has been used in this study:

- Initial evaluation consists of climate model runs for both historical (1976-2005), and future (2021-2100) under both RCP4.5 and 8.5 scenarios (Table 4-1). Models from this list that fulfilled these conditions were selected and constrained to the EAC domain.
- The second step is the evaluation of EAC-RCMs skills to reproduce the EAC climatology, as recommended by Lutz et al. (2016). Taylor diagrams (Taylor 2001) are also used to assess the degree of correspondence between historical EAC-RCMs and observed data. Figure 4-2 illustrates how the Taylor diagram works.

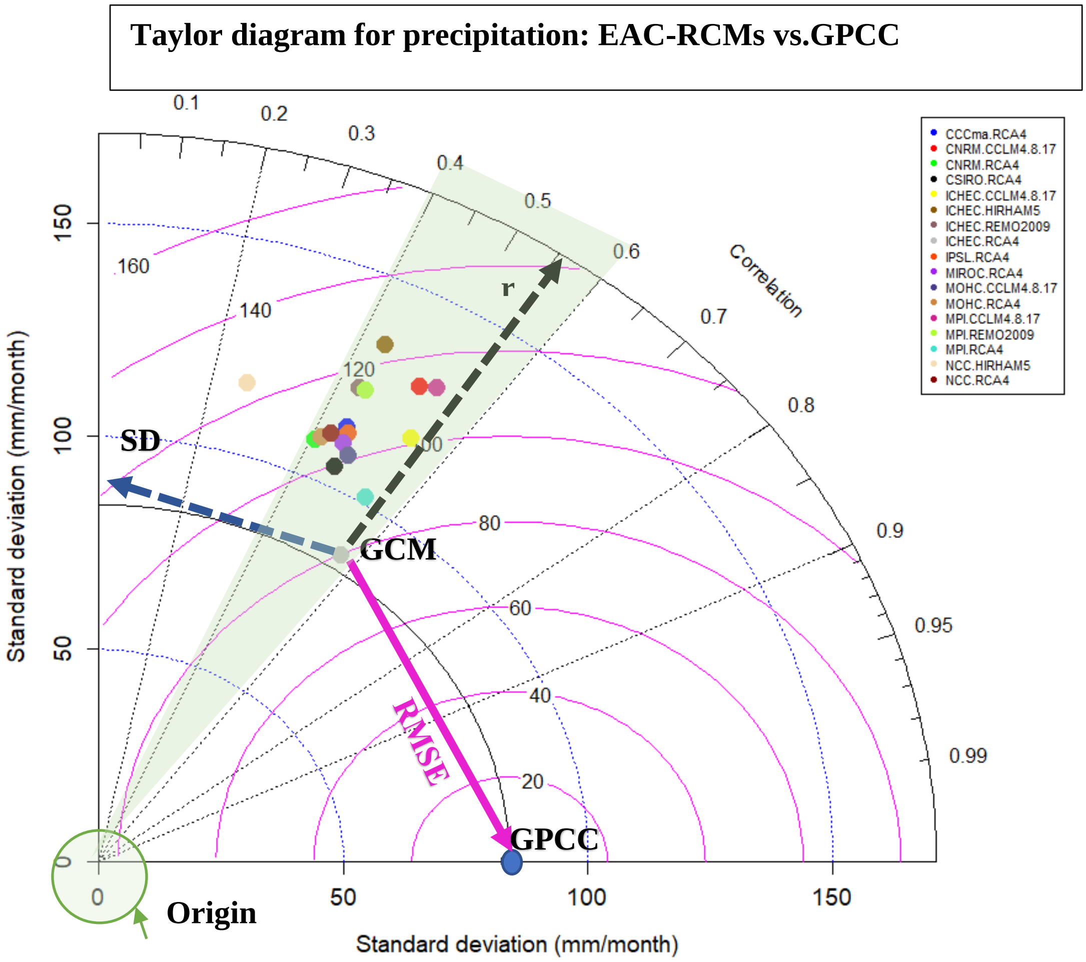

Figure 4-2: An illustrative example of a Taylor diagram.

Taylor diagram shows three statistics: Standard Deviation (SD), Correlation Coefficient (r) and Root-Mean-Square Error (RMSE). The SD can be read from both the x and y axis and is the distance from its origin (0,0, green circle) to the corresponding model value position (e.g. as pointed by the blue dashed line on y axis). The solid black arc line from the reference point (blue dot) shows the correct SD. The distance (pink solid line) from the reference point (GPCC) equals the RMSE. The (r) values (between 0-1) are on the outer black arc line. The black dashed lines from the origin (0,0) to the outer arc are guidelines on how to find a correlation coefficient value of a model. The grey dot labelled GCM is one of the models' positions on a Taylor diagram and the three arrows (in different colours) show the models three statistics. The green triangle shows model positions and their corresponding (r). The triangle shows that most of the models' r lies between 0.4 and 0.6. The top right corner is a legend that helps to match the dots (models) on the diagram with the corresponding model. e.g. the grey dot is ICHEC.RCA4.

The Taylor diagram characterises the statistical relationship between two fields: simulated (EAC_RCMs) and observed (here, GPCC in this diagram). A perfect model under this definition would have an RMSE equal to zero. Such a model would perfectly correlate with the observed data with r value equal to 1 and would have the same SD as the observed field.

The correlation interpretation for this research follows that of Hinkle et al. (1998) correlation interpretation guidance as shown in Table 4-2.

Table 4-2: Correlation coefficient interpretation guideline

Source: Hinkle et al. (1998)

In this example, the ICHEC.RCA4 model has a correlation coefficient (r^2) of about 0.58 (Figure 4-2) and is between moderate and strong correlation (Table 4-2). SD is 96 $mm.month^{-1}$, i.e. the nearest of the GPCC (observed reference), while the RMSE is about 80 $mm.month^{-1}$, i.e. the smallest RMSE compared to the other models (Figure 4-2). Based on the interpretations given above, the ICHEC.RCA4 model has shown a good skill in the reproduction of observed precipitation.

- A final step consists of combining the EAC-RCMs in an MME mean respectively for precipitation, solar radiation, wind speed, and temperature. Räisänen and Palmer (2001), Fowler et al. (2007), Pierce et al. (2009) and Knutti et al. (2010) argue that MME is the most widely used in the climate research community. This step was included as a result of this acceptance in the climate research community as well as the MME advantages in identifying likely trajectories between all physical models (Holtanová et al. 2019).

As an illustration, Figure 4-3 below shows the seasonal cycle of rainfall within the EAC region in the CORDEX, and the MME mean during the period of 2021-2100 under the RCP4.5.

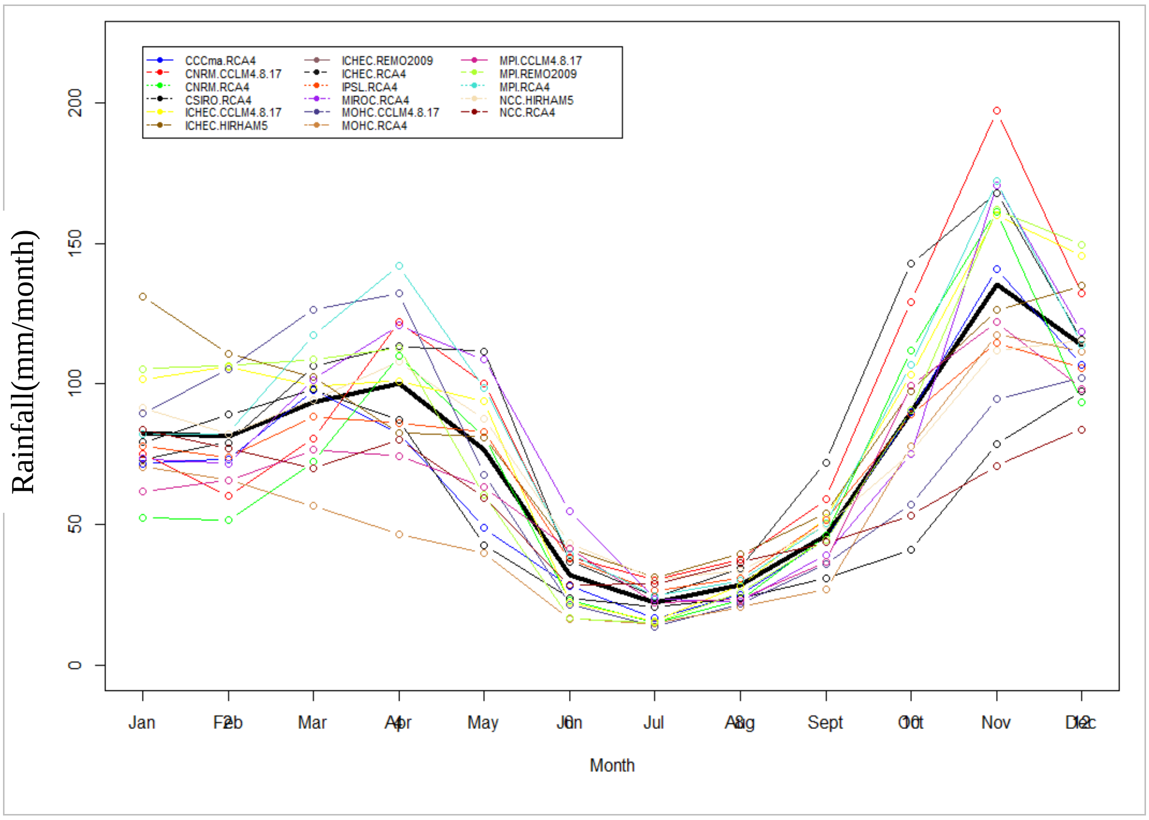

Figure 4-3: MMEM annual cycle of monthly precipitation over the EAC.

The black line indicates the MME (pointed at by arrows) and the rest of the lines in different colours are models. The top left corner shows a legend which gives the names of the models and their corresponding colour line on the figure.

In brief, models with all four variables available with historical runs (1976-2005) and future projections under both RCP4.5 and 8.5 scenarios for the period between 2021 and 2100 which show reasonable skill to faithfully reproduce the observed data, were selected.

4.3.5 Analysis approach for potential future hydroclimate changes

This section explains how we investigated the potential future spatiotemporal changes in hydroclimate patterns in the EAC. The changes are measured between 1976-2005 (the reference period) and 2021- 2100 (the future period) under RCP4.5 and 8.5 scenarios. For both spatial and temporal, future changes have been estimated by taking the difference between the future periods and the baseline period. However, prior to doing this, a data normality test was conducted to decide whether it is better to use a parametric or non-parametric test.

4.3.5.1 Data normality test

A data normality test was conducted to decide whether a parametric or non-parametric test could be used in this research. If data is normally distributed, parametric statistics, based on this assumption could be used (Ghasemi and Zahediasl 2012, Carlo 2013). Kafadar (2003) indicated, that tests for normality calculate the probability that the sample was drawn from a normal population, and the hypotheses to be tested were:

H_0**:** The sample data is not significantly different from a normal population;

H_1: The sample data is significantly different from a normal population.

According to Ghasemi and Zahediasl (2012), the null hypothesis H_0 is that the sample distribution was normal, therefore the alternative hypothesis H_1 could be rejected. If the test is significant, the sample distribution is non-normal, hence the null hypothesis denoted here as H_0 could not be rejected. The following section explores the most common data normality test methods (visual and statistical methods) and draws up a suitable test for this research.

4.3.5.1.1 Visual Methods

According to Field (2009), the data normality distribution test may be assessed through visual inspection such as a frequency distribution (i.e. histogram), boxplot, P-P plot (i.e. probability-probability plot), and Q-Q plot (i.e. quantile-quantile plot). However, one approach on its own is usually unreliable and does not guarantee that the distribution is normal (Altman and Bland 1995, Altman and Bland 1996, Field 2009). Therefore, in order to optimise the capacity for making the best decision, a visual inspection should be used in conjunction with a statistical test, comparing the sample distribution to a normal distribution, to ascertain whether or not the data shows a serious deviation from normality. This research used two of the most common statistical methods which were the normal Q-Q plot and Histogram, in conjunction with the statistical test. There are a number of statistical tests for data normality and the commonly used ones are explored here to justify which best suited this research.

4.3.5.1.2 Statistical methods

This section explores a number of commonly used statistical tests for data normality which include Shapiro-Wilk, Anderson-Darling and Kolmogorov-Smirnov. In this study, we utilised the Shapiro-Wilk test only. The Shapiro-Wilk test, developed by Shapiro and Wilk (1965), is the ratio of two estimates of the population variance (Zadoks 1985). This test has been found to be the most powerful test for normality where *W* is valid for sample sizes greater than 3 and up to 20 (Carlo 2013). However, Royston (1992) and Rayston (1995), extend the Shapiro-Wilk Test, by including a method to allow for unlimited sample sizes. However, Carlo (2013) indicated that the Shapiro-Wilk test may not be as powerful as other tests when identical values, *i.e.* ties, are present in the data. Nevertheless, some researchers (for example Kafadar 2003; Öztuna et al. 2006; Hain and Falk 2010; Ghasemi and Zahediasl 2012) recommended Shapiro-Wilk as the best-preferred test of normality.

Due to the aforementioned statements of support, the Shapiro-Wilk test can be considered as better than other data normality tests such as the Anderson-Darling (AD) and Kolmogorov-Smirnov (KS) tests. The Shapiro-Wilk test is preferred over AD because the latter is severely affected by ties (Stephens 1986). In addition to this, Machiwal and Jha (2012) pointed out that irrespective of how well the data fit the normal distribution, the AD test will often reject the data as non-normally distributed. Furthermore, Carlo (2013) and Öztuna et al. (2006) argued that the Kolmogorov-Smirnov (KS) test has been proven to be less powerful than the other tests in most situations. All in all, the Shapiro-Wilk's method is widely recommended for the normality test because it is generally more sensitive to non-normality and it is the most widely used in the research community for data normality tests (Carlo 2013). Because of this, it was adopted for the data normality test for this research.

In addition, data normality should be assessed with both visual and statistical normality testing. In this respect, Histogram, Q-Q plots, and the Shapiro-Wilk test were adopted for testing data normality for this research. The combination of these three tests helped to make an informed choice of which statistical test to employ. For this research, the parametric statistical test will be used if data are normally distributed and the non-parametric test will be used if the data are no-normally distributed.

4.3.5.2 Hypothesis test and significance testing procedure

This section discusses the hypothesis test and the significance level adopted for this research. The hypothesis test for this section of research was to determine if there is any difference in precipitation, solar irradiance and wind speed between the periods of 1976-2005 and the periods of 2021-2050, 2051-2080 and 2071-2100. The null and alternative hypotheses are formulated as follows: H_O: 1976-2005=2021-2050 OR H_1: 1976-2005≠2021-2050. This formula was repeated for the rest of the periods and each variable under both RCP4.5 and RCP8.5. The significance level for this research was set at α=0.05. To make the hypothesis test, the P-value for the concerned datasets was compared to this significance level. The next section describes the methods employed in chapter five to complete objective three of this research.

4.4 Hydroclimate complementarity and their implication for energy balancing

This section explains how we examined the ability of hydro, wind and solar resources to complement each other under different future climate change scenarios, and its implications for energy supply balancing.

4.4.1 Correlation analysis

For complementarity analysis, it is useful to have some measure of the degree of association between the variables. A number of correlation analysis methods are available, but this research discusses and chooses one from the most widely used which are Pearson linear product-moment, Spearman's rank and Kendall's correlation methods. The Pearson correlation coefficient (r) is an important statistical tool and has been successfully applied in several complementarity studies (Bett and Thornton 2016; Silva et al. 2016; Cantão et al. 2017). Furthermore, as it is based on data covariance and standard deviation, the Pearson correlation coefficient can be easily implemented (Hain and Falk 2010, Carlo 2013). This is because it is a dimensionless measure for the degree of a linear relationship between two variables (Hennemuth et al. 2013), and it is given by:

$$r = \frac{\sum_{i=1}^{n}(x_i - \bar{x})\,(y_i - \bar{y})}{\sqrt{\sum_{i=1}^{n}(x_i - \bar{x})^2}.\sqrt{\sum_{i=0}^{n}(y_i - \bar{y})^2}} \qquad (2)$$

$$Where: \bar{x} = arithmetic\ mean\ of\ x(i)\ ,$$
$$\bar{y} = arthimetic\ mean\ of\ y(i),$$
$$n = sample\ size$$

However, the Pearson product-moment correlation measures the strength of a linear association between two variables, and it is therefore not a desirable measure of association for non-normal multivariate distributions . Previous studies (Rebekić et al. 2015, Hauke and Kossowski 2011, Hamed 2011 and Rana et al. 2014) argue that the most widely used measures of dependence for non-normal multivariate distributions are Spearman's rank correlation and Kendall's τ coefficient. Spearman's rank-order correlation coefficient (ρ_s) is a rank-based version of the Pearson's correlation coefficient, and is mathematically expressed as follows:

$$\rho_s = \frac{\sum_{i=1}^{n}(rank(x_i) - \overline{rank(x)})\,(rank(y_i) - \overline{rank(y)})}{\sqrt{\sum_{i=1}^{n}(rank(x_i) - \overline{rank(x)})^2}\,.\sqrt{\sum_{i=0}^{n}(rank(y_i) - \overline{rank(y)})^2}} \tag{3}$$

Where $rank(x_i)$ and $rank(y_i)$ are the sample of the observations. Kendall's tau correlation coefficient is similar to Spearman's rank-order correlation coefficient (Lumley et al. 2002). It measures the association between two ordinal variables. Its measure is denoted τ, and can be expressed as follows:

$$\tau = \frac{\sum_{i=1}^{n}.\sum_{j=1}^{n} sgn(x_i - x_j)sgn(y_i - y_j)}{n(n-1)} \tag{4}$$

Where:

$$sgn(x_i - x_j) = \begin{cases} 1 & if \ (x_i - x_j) > 0 \\ 0 & if \ (x_i - x_j) = 0 \\ -1 & if \ (x_i - x_j) < 0 \end{cases}$$
$$sgn(y_i - y_i) = \begin{cases} 1 & if \ (y_i - y_j) > 0 \\ 0 & if \ (y_i - y_j) = 0 \\ -1 & if \ (y_i - y_j) < 0 \end{cases} \tag{5}$$

Gibbons (1993) and Chen and Popvich (2002) indicated that the Kendall coefficient quantified the discrepancy between the number of concordant and discordant pairs. In statistics, concordant and discordant are used to describe the relationship between two variables. A pair of observations (e.g. X and Y) is concordant if the subject who is higher on one variable is also higher on the other variable and the pair is discordant if the subject who is higher on one variable is lower on the other variable (Agresti et al. 1987). To illustrate this, two pairs of ranks (x_i, y_i) and (x_j, y_j) are classed as concordant when $x_i < x_j$ and $y_i < y_j$, or $x_i > x_j$ and $y_i > y_j$ or when $(x_i - x_j)(y_i - y_j) > 0$. Similarly, any two pair of ranks (x_i, y_i) and (x_j, y_j) are classed as discordant when: $x_i < x_j$ and $y_i > y_j$, or $x_i > x_j$ and $y_i < y_j$ or when $(x_i - x_j)(y_i - y_j) < 0$. The three correlation coefficients range from -1 to +1, with the absolute values of r, indicating the strength of their relationship for the Pearson correlation coefficients (Hennemuth et al. 2013); and ρ_s and τ indicating the strength of the monotonic relationship between the two variables respectively for the Spearman and Kendall Tau correlation coefficient. Monotonicity means that as the value of one variable increases/decreases, the value of the other variable also increases/decreases. This means that a monotonic relationship is less restrictive than that of relationship (Rebekić et al. 2015, Hauke and Kossowski 2011). Rebekić et al. (2015) highlighted that the most influential factors guiding the choice of which correlation coefficients method to use are data type, presence of outliers, arity of the relationship and the violation of the parametric assumptions.

The decision about which correlation coefficient method is most suitable for this research is based on the result of the data normality test in Section 5.3.2. The correlation coefficient values are interpreted as suggested by Hinkle et al. (1998) presented in Table 4-2 above. This table has been redefined (See Table 4-3) to suit the interpretation of hydroclimate correlation being investigated in this research

Table 4-3: Interpretation of correlation coefficient values

Behaviour	**Correlation Coefficient (CC) Value**	**Interpretation**
Similarity	0.9≤CC≤1.0	Very strong similarity
	0.6≤CC≤0.9	Strong similarity
	0.3≤CC≤0.6	Moderate similarity
	0.0≤CC≤0.3	Weak similarity
	CC=0.0	Negligible relationship
Complementarity	-0.3≤CC≤0.0	Very strong complementarity
	-0.6≤CC≤-0.3	Strong complementarity
	-0.6≤CC≤-0.9	Moderate complementarity
	-0.9≤CC≤-1.0	Weak complementarity

Source: adapted from (Hinkle et al. 1998) and (Canales et al. 2019)

On Table 4-3, the correlation coefficient (CC) value is positive the relationship will be interpreted as similarity and where the CC value is negative, the relationship will be interpreted as complementarity.

4.4.1.1 Hydro, solar and wind power joint variability

This **s**ection starts by describing the bias correction processes and the mathematical equations employed to gauge the power outputs at the local scale. Next, the section explains the methods used to demonstrate the co-variability of the hydro, wind and solar potential power outputs, for the selected case study (a local area). Then, the power outputs are computed without any technological assumptions. This means that there are no adjustments, for example, due to technological efficiency. Finally, the processes by which the power outputs from hydro, wind speed and solar radiation have been calculated are explained.

4.4.1.2 Bias correction methods

Although RCMs are able to describe climate characteristics over regional and local scales, they still feature systematic errors due to the biases inherited from driving the GCMs (Themeßl et al. 2011). Therefore, data from RCMs are regularly bias-corrected before being considered for further use (Fang et al. 2015). There are a number of bias correction methods available today and each correction technique has its own advantages and characteristics (Miao et al. 2016). This study discusses and assesses the widely used bias correction methods such as Distribution Based Scaling (DBS) and Quantile Mapping (QM) and discusses their suitability use for this research. The most suitable method will be chosen.

The DBS approach works well with precipitation and temperature variables (Yang et al. 2010, Rana et al. 2014), making this bias correction approach not suitable for this research. This is because a bias correction approach would need to be able to bias correct four variables: precipitation, temperature, wind speed, and solar radiation. As an alternative, Maraun (2014) indicated that QM is often used for correcting RCMs, and is a feasible approach if the observations are of a similar resolution as the RCMs. However, Maraun (2014) warned that, if the observations were of different resolutions, this mismatch would be reflected in the final results. Therefore, it was decided that this method (QM) also proved unsuitable for use in this particular research. This is because the RCMs and observed data for this research are of different resolutions. The next section explores the delta change bias correction method.

4.4.1.2.1 Delta change method

The Delta change method is based on the assumption that the relative change between a control simulation and a simulation of the future climate can simply be superimposed upon the observed time series, and is mostly used for hydrological impact studies (Björnsson 2012). The Delta change method has been used in many previous studies of the impact of climate on hydropower (Jóhannesson et al. 2007; Ruiter 2012; Xu 2017). However, although the Delta change method proves advantageous in terms of its simplicity for use, it fails to properly handle all of the modelled changes in statistics (Björnsson 2012). With this taken into account, the Delta change method has been used for this research with the exception of k in cross-validation methods in order to ensure that the method processes any changes in statistics correctly.

4.4.1.2.2 Leave *k* out cross-validation

The leave-k-out cross-validation procedure has been used to validate our bias correction. N years of data in each of the corresponding simulated and observed data periods are divided into k blocks (Table 4-4) where each block contained *n* years with non-overlapping subsets. A scaling factor is calculated for each k permutation of K-1 blocks. Those highlighted in blue-grey are permutations of k−1 blocks and those withheld are highlighted in orange. The obtained scaling factors are applied to the simulated data. The cross-validation has been assessed here by computing RMSE between every permutated sample and the observed data. This method has been successfully used in a number of climate-related studies (Piani et al. 2010, Teutschbein and Seibert 2012 and Eden et al. 2012) and has therefore been selected to compute bias correction for this research.

Table 4-4: Visualisation of leave-k-out bias correction cross-validation.

K_1	K_2	K_3	K_4	K_5	K_6
K_1	K_2	K_3	K_4	K_5	K_6
K_1	K_2	K_3	K_4	K_5	K_6
K_1	K_2	K_3	K_4	K_5	K_6
K_1	K_2	K_3	K_4	K_5	K_6
K_1	K_2	K_3	K_4	K_5	K_6

Thirty years of simulated and observed data have been divided into k blocks, each containing 5 years (k=6) with non-overlapping subsets. The best model amongst the 17 models that shows reasonable ability to reproduce precipitation and temperature features has been selected for a renewable resources complementarity study at a local scale. The scaling factor for monthly precipitation, temperature, wind speed and solar radiation for a given year is estimated by using simulated and observed data for all the other years, apart from the 5-year period centred on the year to be estimated. The scaling factor obtained is then applied to the selected model-simulated data, and the Root Mean Square Error (RMSE) is calculated to examine how well the bias-corrected data matches the observed data. To this end, the RMSE of the corrected and uncorrected data are plotted and analysed against each other. Data for the future projected precipitation, wind speed, and solar irradiance are corrected with a multiplier, as indicated in equation (6) while the temperature is corrected with the help of an additive term scaling factor, as in equation (7), based on the difference between the long-term monthly mean observed, and the selected model-simulated temperature control run.

$$P_{csim} = P_{rsim} * \frac{\mu(P_{Obs})}{\mu(P_{hist})} \tag{6}$$

$$T_{csim} = T_{rsim} + [\mu(T_{obs}) - \mu(T_{hist})] \tag{7}$$

P_{csim} and T_{csim} are respectively corrected precipitation and temperature. $P_{hist,}T_{hist}$ are respectively precipitation and temperature corresponding to the model simulated data for 2021-2050, 2051-2080 and 2071-2100. Precipitation P_{Obs}, and temperature T_{obs}, are observed data. $P_{rsim,}$ and T_{rsim} are uncorrected model-simulated data. The procedure in equation (6) was applied to correct the bias for wind speed and solar irradiance.

4.5 Methods for calculating wind, solar and hydropower potential at the local scale

This section explains how we calculated power from wind, solar and hydro in one grid of climate data covering the selected area as shown in Figure 4-1[C].

4.5.1 Wind power

Important factors for determining the available wind power are the mass flow of air $\frac{dm}{dt}$ through a rotor disc of an area where the mass flow rate is a function of the air density ρ and the air velocity U (Miskelly 2016) and is presented as follow:

$$\frac{dm}{dt} = \rho AU \tag{8}$$

The available kinetic energy per unit time (Power), of the airflow, is given by:

$$P_W = \frac{1}{2}\frac{dm}{dt}U^2 = \rho A U^3 \quad (9)$$

The wind power per unit area, P/A or power density is expressed as:

$$\frac{P_W}{A} = \frac{1}{2}\rho U^3 \quad (10)$$

The air density at sea level and standard temperature (15°C) is equal to $1.225 kg\ m^{-3}$ (Miskelly 2016, Silva et al. 2016). Other important parameters to consider in the wind power output calculations are the type of wind turbine and the mechanical and electrical conversion coefficients of the selected wind turbine (Manwell et al. 2010). In addition, other technical characteristics considered are the hub height, hub diameter and swept area, together with the minimum and maximum speeds (Uluyol et al. 2014, Sohoni et al. 2016). To avoid the limitations associated with the choice of a specific wind turbine, previous studies described the wind resource in a more generalized form (Dowling 2013; Fant et al. 2016; Carvalho et al. 2017). The implication of this choice is that there are no adjustments to the power output in respect of these technical characteristics. This study also uses this generalised form of potential wind power (P_W) from the near-surface wind speed according to the equations (11):

$$P_w = \frac{1}{2}\rho U^3 \quad (11)$$

where, P_w is wind power available per unit area (Wm^{-2}), U is wind speed at hub-height (m/s) and ρ = 1.225 $kg\ m^{-3}$ is the air density.

4.5.2 Solar power production

The air temperature (T), and the solar irradiance (RSDS) are variables used to assess solar power generation. Hence, T and RSDS are the main inputs to the solar power calculation. Potential solar power output (P_{pv}) is based on the performance of the PV cells with respect to their nominal power capacity and the actual ambient temperature condition.

For the determination of P_{pv}, the method used by Crook et al. (2011) and followed closely by Panagea et al (2014), Wild et al. (2015) and Bazyomo et al. (2016) is used in this study. To this end, the efficiency of the PV cell $\eta cell$ is defined by:

$$\frac{\eta_{cell}}{\eta_{ref}} = 1 - \beta\left(T_{cell} - T_{ref}\right) + \gamma log_{10} G_{tot} \quad (12)$$

$$\eta_{cell} = [1 - \beta\left(T_{cell} - T_{ref}\right) + \gamma log_{10} G_{tot}\ ]\eta_{ref} \quad (13)$$

where η_{ref} is the reference efficiency of photovoltaic modules estimated by the manufacturer. $T_{cell}\ and\ T_{ref}$ are, respectively, the cell and reference temperatures in which the performance of the PV cell is estimated by the manufacturer. The values of β = 0.0045 and γ = 0.1, based on the work of Parida et al. (2011) and Crook et al. (2011), cell temperature T_{cell} may be expressed as:

$$T_{cell} = C_1 + C_2 T + C_3 G_{tot} \quad (14)$$

T represents the ambient air temperature for the baseline period in °C, coefficients C_1, C_2 and C_3 are coefficients that affect heat transfer from the cell and depend on the details of the module and mounting. Monocrystalline silicon is considered in this research because of the monocrystalline cells' high efficiency. This high efficiency is typically around 26.7 %, which is the highest efficiency confirmed conversion rate out of all commercial PV (Green et al. 2019). For monocrystalline silicon cell properties, these coefficient values are set according to the work of Lasiner and Ang (1990) and are adopted in this study as proposed by Crook et al (2011). Thus: $C1 = -3.75$ °C; $C2 = 1.14$; $C3 = 0.0175\ m^2.W^{-1}$ and a typical value for the reference temperature T_{ref} is 25°C. The final energy power output of a PV system, as proposed by Crook et al. (2011), is assumed to be:

$$P_{pv} = G_{tot}\ \eta_{cell} \quad (15)$$

G_{tot} is the total received solar irradiance at surface and η_{cell} is PV cell efficiency

4.5.3 Hydropower potential production

Hydropower is defined as the generation of electricity from the energy of water (m^3/s) by means of a turbine over a certain head difference (m). The general formula for hydropower (Reynolds 1983) is given as:

$$Hydropower(kW) = \omega(\%) * Q(m^3/s) * g\left({}^{m}/_{s^2}\right) * \Delta H(m) \qquad (16)$$

Where ω is the turbine efficiency in percentage, g is the acceleration of gravity (9.81ms^{-2}), Q represents the water flow rate and ΔH is the falling height (head in m). This study is concerned with complementarity, and therefore the relative hydropower is calculated with no technology assumption considered and can be rewritten: as:

$$Hydropower\ (kW) = Q(m^3/s) * g\left({}^{m}/_{s^2}\right) * \Delta H(m) \qquad (17)$$

The equation (17) indicates that to be able to compute relative potential hydropower, flow rate (Q) and falling height (ΔH) are needed, which are the unknown parameters in the hydropower calculation. The flow rate at the points for this project is computed at an already measured head (ΔH) of 25m (Stadler 2017). Two more random points with heads (ΔH) of 15 and 20 m are considered for later use in the hydropower sensitivity analysis. The hydropower calculation requires river discharge data input, and in the present research, a runoff-rainfall model is required to convert precipitation into the flow. These models can be classified as lumped or distributed models (Devia et al. 2015) and Figure 4-4 (A) and (B) below is an illustrative picture of a lumped and distributed model, respectively.

Figure 4-4: An illustrative picture of lumped and distributed model
Lumped (A) and Distributed (B) hydrological model, ɵ is a parameter assigned to grid cells. Source (Brirhet and Benaabidate 2016).

Lumped models are the most widely used tools for operational applications because they propose simplified catchment scale representations of the transformation of precipitation into river discharge (Coron et al. 2016). In addition, Moradkhani and Sorooshian (2009), Lampert and Wu (2015) indicate that lumped models have the capacity to be easily implemented, as they only require climate and streamflow data inputs. Hence, the Génie Rural à 2 paramètres Mensuel (GR2M) model, taken from the Genie Rural (GR) suite of conceptual hydrological models (Mouelhi et al. 2004, Coron et al. 2016), is used in this study to convert precipitation into the discharge. The GR2M model has been used in a variety of hydrological studies, for example, Andreassian et al. (2006), Huard and Mailhot (2008), Traore (2014), Coron et al. (2016, 2017) and Sidibe et al. (2019).

4.5.3.1 Flow rate (Q) modelling

The GR2M model is here used to convert the selected model precipitation-temperature data into the discharge. The first step in the GR2M rainfall-runoff modelling is to estimate the best parameters that fit the outputs from the model over a given period of observed data. The observed water discharge data available from the Global Runoff Data Centre (GRDC) were used. The period of 1970-1984 was used because it was the longest period-at the point of the study (Rusumo fall hydropower project) without missing values.

The Nash and Sutcliffe (1970) efficiency criteria (NSE) equation (18) is mostly used to assess the hydrological model performance in reproducing the observed discharge:

$$NSE = 1 - \left[\frac{\sum_{i=1}^{n}(Y_i^{obs} - Y_i^{sim})2}{\sum_{i=1}^{n}(Y_i^{obs} - Y^{mean})2}\right] \qquad (18)$$

Here, Y_i^{obs} is the ith observation for the constituent being evaluated, Y_i^{sim} is the ith simulated value for the constituent being evaluated, Y^{mean} is the mean of observed data for the constituent being evaluated and n is the total number of observations. However the NSE criteria has been shown to have mathematical limitations and the Kling–Gupta efficiency criteria (KGE, Gupta et al. 2009), equation (19), was proposed as an alternative to NSE equation (18), as it combined the correlation, bias, ratio of variances or coefficients of variation in a more balanced way (Santos et al. 2018) and was used in this research. The water discharge observed data, collected at point latitude (-2.38^0), were used. This period was divided into two parts: one for calibration (1970-1975), the other for validation (1976-1984). The GR2M model performance is evaluated using the criterion (e.g. Yuemei et al. 2008, Rauf and Ghumman 2018) in Table 4-5 below, and based on the recommended value for the satisfactory GR2M model performance of simulated data KGE>0.5 (Sidibe et al. 2018).

Table 4-5: Criteria for Evaluating the Performance of Hydrological Models and their corresponding Classification

Source: adapted from Yuemei et al. (2008) and Rauf and Ghumman (2018)

4.5.3.2 Calculating Potential evapotranspiration

The potential evapotranspiration (PET) was computed according to the Thornthwaite (1948) function. According to Thornthwaite, this function requires a numeric vector, matrix or time series, of monthly mean temperatures (ºC), together with latitude, which is also a numeric vector with an altitude of the targeted site in degrees. In this research, the observed mean temperature for the Rusumo Falls Project catchment area and the observed discharge both at latitude (-2.38^0) cited above have been used.

4.6 Optimal hybrid combinations of hydro, wind speed and solar power for electrification

This section examines the processes by which the optimal hybrid combinations of hydro, wind speed and solar power for the electrification has been determined for a selected case study area. Near-future data (2021-2050) for hydro, wind and solar power resources in the Rusumo Falls was estimated from the ICHEC-RCA4 under RCP4.5. The near future period was chosen because the renewable energy system technology and the associated financial implications for the 2021-2050 period are assumed to be more similar to that of today than that of the 2051-2080 and 2071-2100 periods because of technology improvement and falling cost (IRENA 2019). In addition, the RCP4.5 was purposely chosen because it is a scenario which was employed to stabilize radiative forcing at 4.5 W /m^2 in the year 2100 without ever exceeding that value, as opposed to RCP8.5 which is "business as usual" (van Vuuren et al. 2011). Therefore, for the purposes of investigating the optimal hybrid combinations of hydro, wind speed and solar power for electrification, the RCP4.5 fits well with the philosophical stance (pioneering for renewable energy) of this research. There are many renewable energy modelling and simulation platforms, but here we used the Hybrid Optimization of Multiple Energy Resources (HOMER). HOMER is the global standard for microgrid and distributed energy systems, designed and used in more than 190 countries with over 150,000 users.

It has also been widely adopted in previous renewable energy system studies including but not limited to the studies conducted by Mitra and Chaudhuri (2006), Setiawan and Nayar (2006), Bekele and Palm (2010), Erdinc and Uzunoglu (2012), Ashourian et al. (2013), Sinha and Chandel (2014), Sen and Bhattacharyya (2014a), Rolland and Glania (2016) and Kim et al. (2017). More details about HOMER is provided in chapter seven. Other hybrid system software tools for computing hybrid renewable energy systems are also available. A detailed review of the analytical capabilities of the most used of these hybrid system software tools is provided in Table 4-6 below.

Table 4-6: Analysis capabilities of the most used hybrid system software tools

Software	Tasks								
	Economic analysis	Technical analysis	PV system	Wind System	Generator set	Storage device	Bio-energy	Hydro energy	Thermal System
HOMER	✓	✓	✓	✓	✓	✓	✓	✓	×
HYBRID2	×	✓	✓	✓	✓	✓	✓	×	✓
iHOGA	✓	✓	✓	✓	✓	✓	✓	✓	×
RETScreen	✓	✓	✓	✓	✓	✓	✓	×	×
HYBRIDS	×	✓	✓	✓	×	✓	×	×	×
SOMES	✓	✓	✓	×	×	✓	×	×	×
RAPRSIM	×	✓	✓	✓	✓	✓	×	×	×
SOLSIM	✓	✓	✓	✓	✓	✓	✓	✓	×
INSEL	✓	✓	✓	✓	✓	✓	×	×	✓
HybSim	✓	✓	✓	×	✓	✓	×	×	×
IPSYS	×	✓	✓	✓	✓	✓	×	✓	×
iGRHYSO	✓	✓	✓	✓	✓	✓	×	✓	×

Source: Sinha and Chandel (2014) and Muthusamy (2018)

The tick (✓) indicates that the software is able to perform the tasks while the cross (×) indicates that the software is not able to perform the tasks. The software acronyms are defined at the beginning of this research in the abbreviations section.

According to Muthusamy (2018), HOMER is the most widely used tool as it is easier and faster to use in evaluation and analysis as there are many possible system configurations available with this tool. As illustrated in Table 4-6, HOMER can also be considered as the best choice for this study, because it gives options for computing the optimal combinations of hydropower, solar and wind energy resources, but, more importantly, it allows for the comparison, analysis, and determination of the Economic Distance Limit to grid (EDL). The HOMER system modelling, simulation processes, and the subsequent analysis are detailed in Section 7.6.

4.7 Chapter summary

The research methodology chapter looked at the tools and processes employed to achieve the aim and objectives of this study. The methods used to achieve each of the objectives have been explained and the corresponding chapters indicated. The link between the research objectives, research questions, and the methods used to answer each of the questions have been shown. The combinations of objectives one, two, three and four help to answer the research questions which are:

A. What are the potential future hydroclimate change scenarios in the EAC?

B. Are the hydroclimate resources complementary to each other for renewable energy generation in the EAC?

C. How can decision-makers in the EAC achieve reliable, affordable and climate-resilient energy access through a complementary renewable energy mix?

Figure 4-5 below provides a summary of this research methodological processes that lead to achieving the aim of this research which is to develop a DSF for achieving reliable, sustainable, and climate-resilient energy access in the EAC under different climate change scenarios.

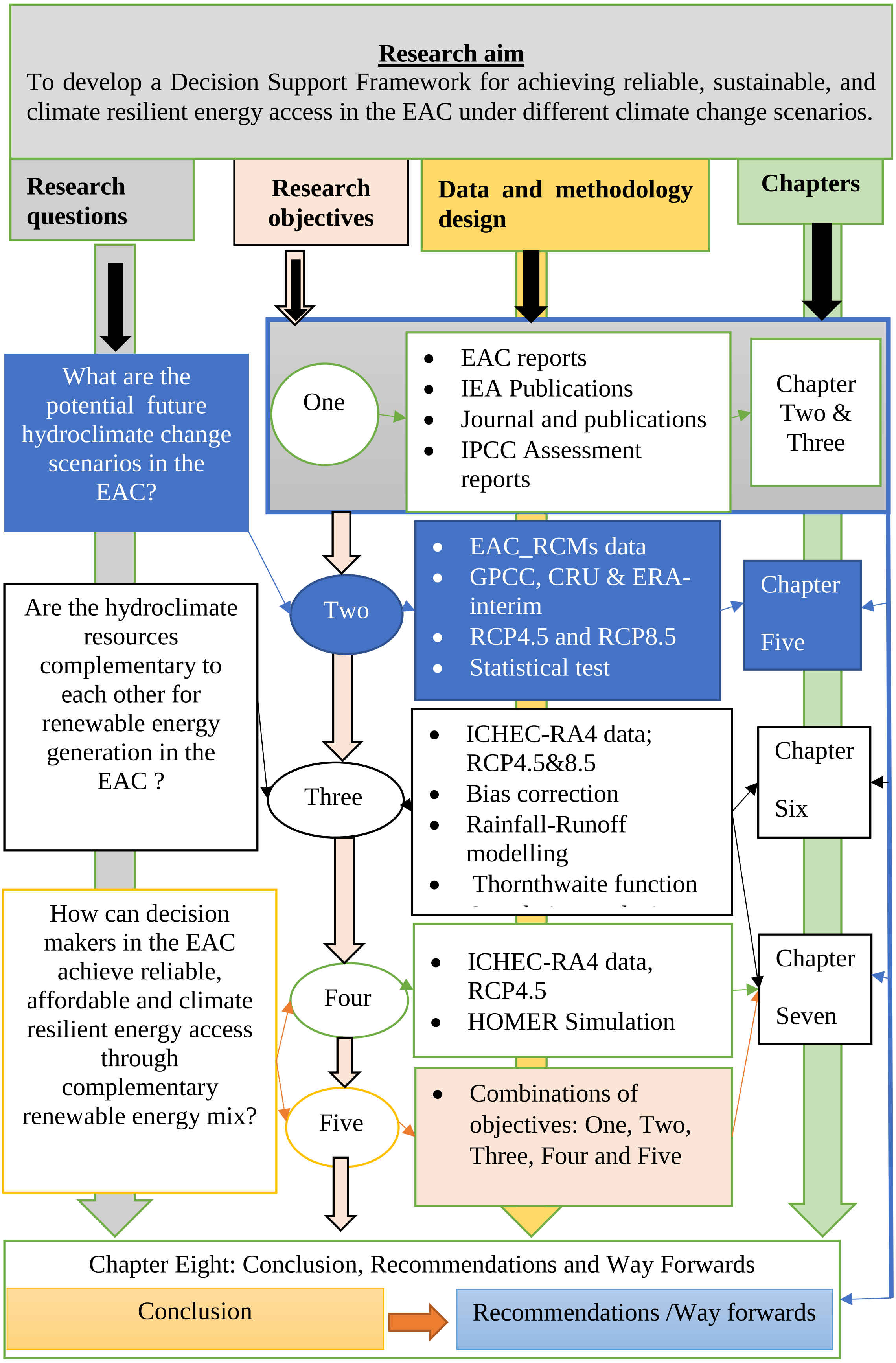

Figure 4-5: Research structure

Chapter 5: Investigating future changes in hydroclimate within the EAC

5.1 Introduction

This chapter investigates the changes in hydroclimate under different climate scenarios (i.e. RCP4.5 and RCP8.5) within the EAC. The change in hydroclimate is necessary information considering the objective two of this study which is to examine the EAC future hydroclimate changes under the RCP4.5 & RCP8.5, and for the period spanning from 2021 to 2100. With regards to future hydroclimate changes, it is important to construct a full picture of possible changes that may occur in both the global and regional climate.

In the case of constructing a full picture of possible hydroclimate changes, advanced climate change modelling, through the use of GCMs and RCMs as driven by a range of RCPs scenarios, are typically used to predict and assess future climate change scenarios (IPCC 2014). Climate change across the EAC has received much attention and many studies have focused on the characteristics of the climate over the EAC, especially rainfall variability patterns (Nicholson 1996, Schreck and Semazzi 2004, Segele et al. 2009, Shongwe et al. 2011, Liebmann et al. 2014, Kent et al. 2015, Rowell et al. 2016, Souverijns et al. 2016). Ongoma et al. (2017) stated that based on the baseline period (1961–1990) and the projection period (2071–2100), the region of East Africa is likely to warm up by 1.7–2.8°C and 2.2–5.4°C under the RCP4.5 and RCP8.5 scenarios, respectively.

A key problem with much of the literature on temperature events across the EAC sub-region is that they usually only focus on one specific country each time. Nevertheless, the findings can be collated for the purposes of contextualising this research. For instance, a study of Uganda undertaken by Nandozi et al. (2012) for the periods of 2070-2100 indicated that the seasons of March-May and September-October are likely to experience future increases in temperature of approximately 0.9℃, whilst in the season spanning June-August, the temperature is expected to decrease by approximately 0.3℃. Liersh et al. (2015) indicated that in Burundi, there is a projected temperature increase within the range of 1.7℃ and 2.9℃ for the period dating 2032-2060. Further to this, a temperature increase of between 3.6℃ and 4.7℃ is expected during the period of 2071-2100. In addition, Wambura et al. (2014) also project an increase in temperature of approximately 0.9℃ by 2050 for Tanzania. Lastly, the Rwandan government (2011) indicated an increase in temperature of up to 2.5% by 2050.

At the time of writing, studies on solar radiation and wind speed remain in the developmental stages with reference to the EAC region as a whole. Furthermore, little is known about the future changes in precipitation, temperature, wind speed and solar radiation across the EAC region in the context of renewable energy generation. Thus, the information provided aims to fill the gaps in the knowledge of this topic. To accomplish this, two questions must be answered:

1. To what extent are CORDEX-AFRICA RCMs able to simulate past hydroclimate patterns over the EAC as a whole?
2. What are the potential spatial-temporal future changes in precipitation, solar irradiance, wind speed and temperature - assuming the RCP4.5 and 8.5 scenarios?

5.2 Data and methodology

The data and methodology used in this chapter are provided in the main research methodology as per Section 4.4. However, for the purposes of readability, they are briefly repeated here**.** Moving forward, the current chapter investigates potential future changes in the hydroclimate over the EAC for the future periods of 2021-2050, 2051-2080 and 2071-2100 which correspond to near, mid and long-term futures respectively. These future changes are measured against the baseline period 1976-2005.

As mentioned in Section 4.3.3, the observed precipitation and temperature data are respectively taken from GPCC and CRU databases. In the absence of observed data for the EAC for wind speed and solar irradiance, ECMWF Re-Analysis Interim data, denoted here as ERAI reanalysis data- obtained from Met Office UK- are used in this research. The ERAI as a dataset shows the results of global climate reanalysis from 1979 to date (Berrisford et al. 2009). The climate model data were extracted from the CORDEX_AFRICA database discussed earlier in the methodology chapter. The data were then constrained to the EAC sub-region domain (*i.e.* for the area -28–42.0E and -12.0–6.0N) as shown in Figure 4-1[B].

The resulting models are termed EAC_RCMs. In order to assess the potential future changes in hydroclimate conditions and give credible answers to the questions mentioned above, a thorough EAC_RCMs evaluation was conducted. This was undertaken in accordance with the research methodology discussed in Section 4.3.4. Before conducting any statistical analysis, the data normality assumption was checked and utilised to determine whether a parametric or non-parametric test was optimal. The methodology for examining data normality is provided in Section 4.3.5.1

5.3 Results and discussions

5.3.1 Model selection and evaluation

5.3.1.1 EAC_RCMs availability

For step one, all CORDEX-Africa_RCMs with available monthly mean values for precipitation, temperature, solar radiation and wind speed data for both historical (1976-

2005) and future (2021-2100) periods under the RCPs 4.5 and 8.5 were selected for consideration. This meant that 17 CORDEX-Africa RCMs out of the 34 available (see table 4-1) fulfilled the conditions laid out. These 17 models are provided in Table 5-1 below:

Table 5-1: List of the 17 CORDEX-AFRICA (GCM-RCMs) used for this study

	RCM	**Driving GCM**	**Short name (GCMs-RCMs)**
1	RCA4	CCCma-CanESM2	CCCma- RCA4
2	CCLM4-8-17	CNRM-CERFACS-CNRM-CM5	CNRM- CCLM4-8-17
3	RCA4	CNRM-CERFACS-CNRM-CM5	CNRM- RCA4
4	RCA4	CSIRO-QCCCE-CSIRO-Mk3-6-0	CSIRO -RCA4
5	CCLM4-8-17	ICHEC-EC-EARTH	ICHEC- CCLM4-8-17
6	HIRHAM5	ICHEC-EC-EARTH	ICHEC- HIRHAM5
7	REMO2009	ICHEC-EC-EARTH	ICHEC- REMO2009
8	RCA4	ICHEC-EC-EARTH	ICHEC- RCA4
9	RCA4	IPSL-IPSL-CM5A-MR	IPSL- RCA4
10	RCA4	MIROC-MIROC5	MIROC- RCA4
11	CCLM4-8-17	MOHC-HadGEM2-ES	MOHC- CCLM4-8-17
12	RCA4	MOHC-HadGEM2-ES	MOHC- RCA4
13	CCLM4-8-17	MPI-M-MPI-ESM-LR	MPI- CCLM4-8-17
14	REMO2009	MPI-M-MPI-ESM-LR	MPI- REMO2009
15	RCA4	MPI-M-MPI-ESM-LR	MPI- RCA4
16	HIRHAM5	NCC-NorESM1-M	NCC- HIRHAM5
17	RCA4	NCC-NorESM1-M	NCC- RCA4

5.3.1.2 EAC_RCMs past-performance approach

With regards to the 17 selected EAC_RCM models presented in Table 5-1, the first set of analyses utilised Taylor diagrams to investigate the degree of correspondence between simulated and observed field data thereby assessing the performance of each model. Taylor diagrams provide "a concise statistical summary of how well patterns match each other in terms of their correlation, their root-mean-square difference and the ratio of their variances" (Taylor 2001). The results for all 17 EAC_RCMs performances presented on Figure 5-1, Figure 5-2, Figure 5-3 and Figure 5-4, represent precipitation, temperature, solar radiation and wind speed respectively.

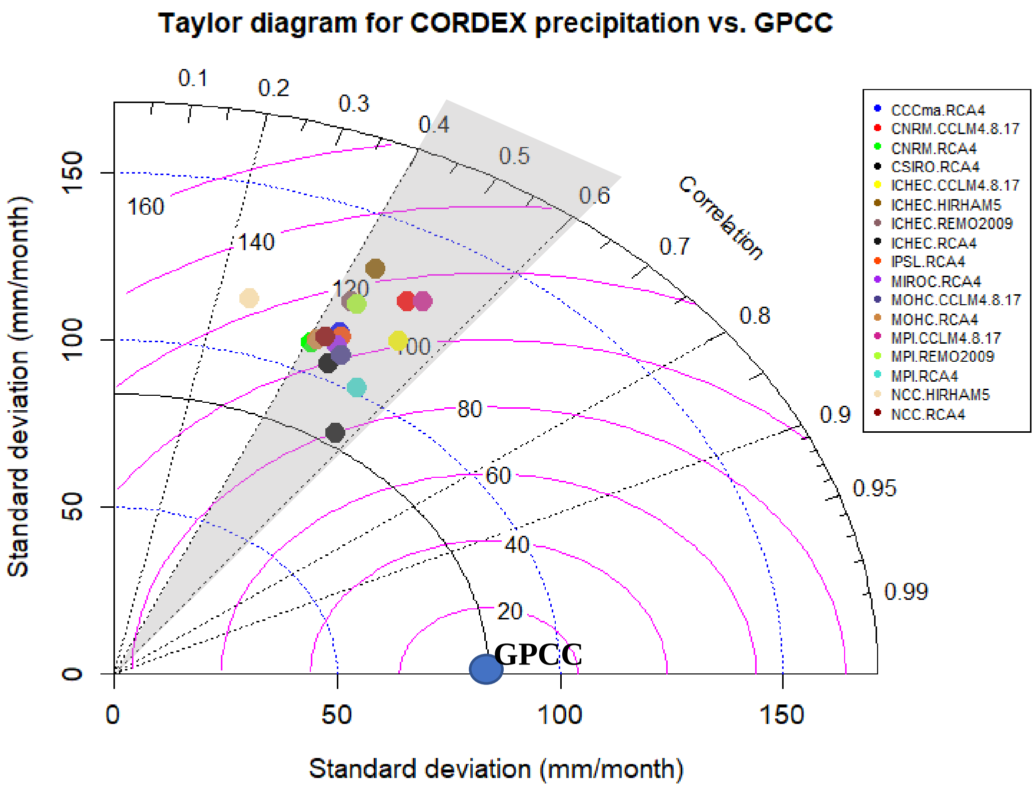

Figure 5-1: Taylor diagram to compare EAC_RCMs simulated and GPCC precipitation
This Taylor diagram displays the statistical patterns of annual mean precipitation simulated by 17 EAC_RCMs, compared with the GPCC precipitation for the same period of 1976-2005. Each model is represented by a different colour on the diagram and is compared to GPCC in blue. Reading and interpreting this diagram should follow the explanations provided in figure 4-2 and the subsequent section. The shaded area shows where most of the models' correlation coefficients lie.

Looking at Figure 5-1 the analyses revealed that most of the models had positive correlation coefficients, lying between 0.4 and 0.6. Only NCC.HIRHAM5 gives a lower positive correlation of r~ 0.3. However, this lower positive correlation is of no real consequence due to the fact that all of the models' correlation coefficients were statistically significant at α=0.05 (P-Value < α). This indicates that despite the sole variance stated, the simulated data remained consistent with the results of the observed data. Models' RMSE varies between 80 and 120 mm/month, except the NCC.HIRHAM5 model which has an RMSE slightly above 120 mm/month. Although the ideal model would have had an RMSE closer to zero, the RMSE alone is not conclusive. In order to draw a conclusion with regards to model performance, the RMSE necessitates interpretation in conjunction with further statistics in accordance with the Taylor diagram. In this regard, the analyses highlighted that on average, most of the models had an SD which varied between 100-135 mm/months. The ICHEC.RCA4 model however, had a relatively small SD of 87.40 mm/months. Interestingly, the SD for the ICHEC.RCA4 model was much closer to the GPCC observed value (83.94 mm/months). Under the statistical relationship explained in Section 4.3.4, the ICHEC.RCA4 is a perfect model compared to the rest of the models. The positive correlation, RMSE and SD between models and observed data indicate that all 17 models are able to reproduce the observed rainfall variability patterns over the EAC.

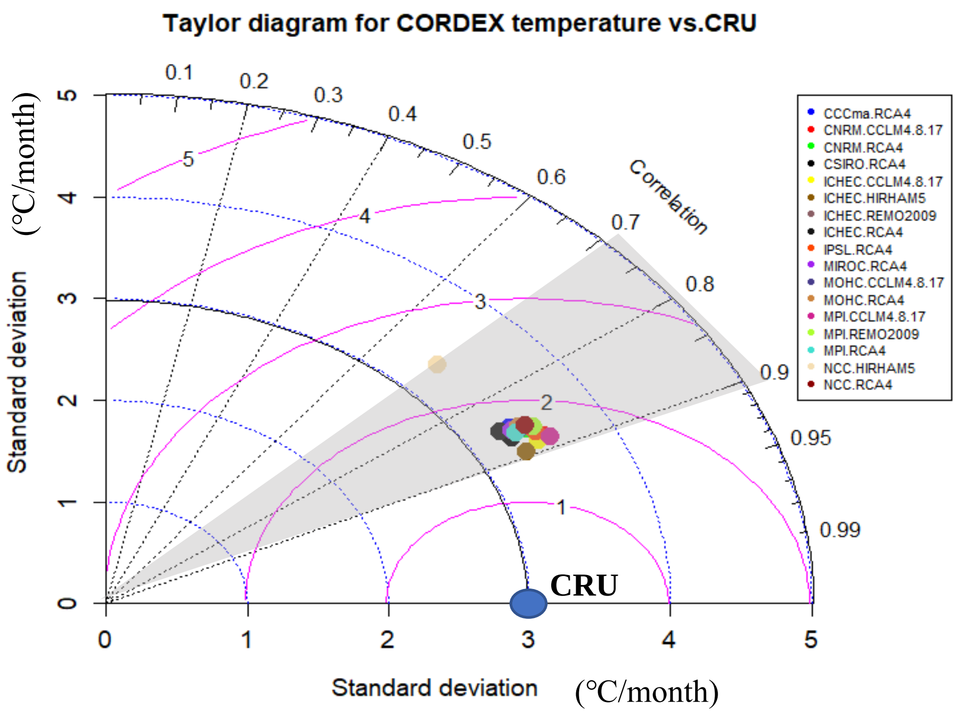

Figure 5-2: Taylor diagram to compare EAC_RCMs simulated and CRU temperature
This Taylor diagram displays the statistical patterns of annual mean temperature simulated by 17 EAC_RCMs, compared with the CRU temperature for the same period of 1976-2005. Each model is represented by a different colour on the diagram and is compared to CRU in blue colour. Reading and interpreting this diagram should follow the explanations provided in figure 4-2 and the subsequent section. The shaded area shows where most of the models' correlation coefficients lie.

The performance of the EAC_RCMs with regards to reproducing the observed temperature across the EAC is displayed in Figure *5-2*. Here, the simulated temperatures have a slightly higher SD (about 3.5°C/month) when compared to the CRU (3°C/month). Figure 5-2 above shows that all of the models have a strong positive correlation (about r >0.7), and that all of the models' correlation coefficients are statistically significant (P-Value <α). The RMSE for all models lies between 1.2°C and 2°C per month. This is with the exception of NCC.HIRHAM5 which has an RMSE of approximately 2.5°C per month. Based on Taylor diagram statistics (as per Section 4.3.4) utilised in conjunction with the positive correlation significance between models and observed data, all of the 17 EAC_RCMs reproduced the observed temperature throughout the EAC.

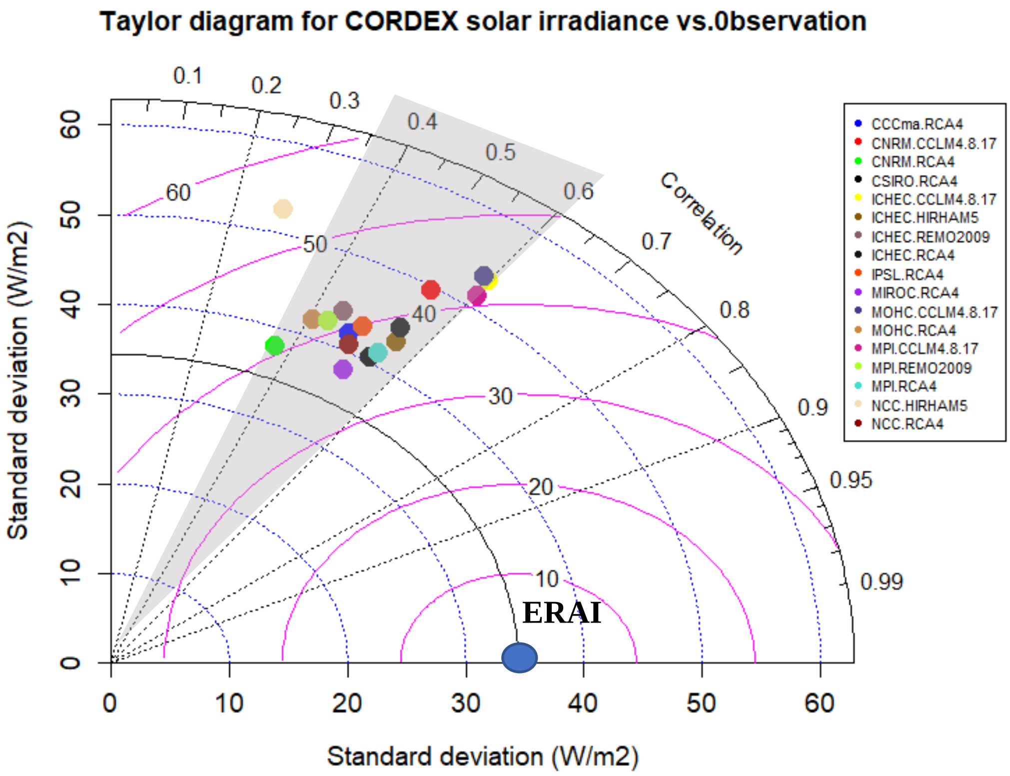

Figure 5-3: Taylor diagram to compare EAC_RCMs simulated and ERAI solar radiation

This Taylor diagram displays the statistical patterns of annual mean solar radiation simulated by 17 EAC_RCMs, compared with the ERAI solar radiation for the same period of 1976-2005. Each model is represented by a different colour on the diagram and is compared to ERAI solar radiation in blue. Reading and interpreting this diagram should follow the explanations provided in Figure 4-2 and the subsequent section. The shaded area shows where most models' correlation coefficients lie.

The ability of the EAC_RCMs to reproduce solar radiation is illustrated in Figure 5-3. The findings show that most models have a positive correlation coefficient between r~0.35 and 0.6. For most models, the SD associated varied between 38 to 53 $W.m^{-2}$ per month, demonstrating high variability in solar radiance patterns when compared to the observed SD 34.46 $W.m^{-2}$/month. The RMSE for each model also varied between 30 and 45 $W.m^{-2}$/month. This is again with the exception of NCC.HIRHAM5, which did not produce results in line with other 16 models for correlation coefficients and RMSE, which are approximately 0.3 and 55 $W.m^{-2}$/month respectively. Despite the fact that there is a clear difference with reference to NCC.HIRHAM5, the results show that all models have a positive correlation coefficient.

With reference to the Taylor diagram statistics (as per Section 4.3.4), all 17 EAC_RCMs have successfully reproduced the observed solar radiation patterns throughout the EAC. The following Figure 5- 4 presents the performances of the EAC_RCMs in reproducing the observed wind speed patterns across the EAC.

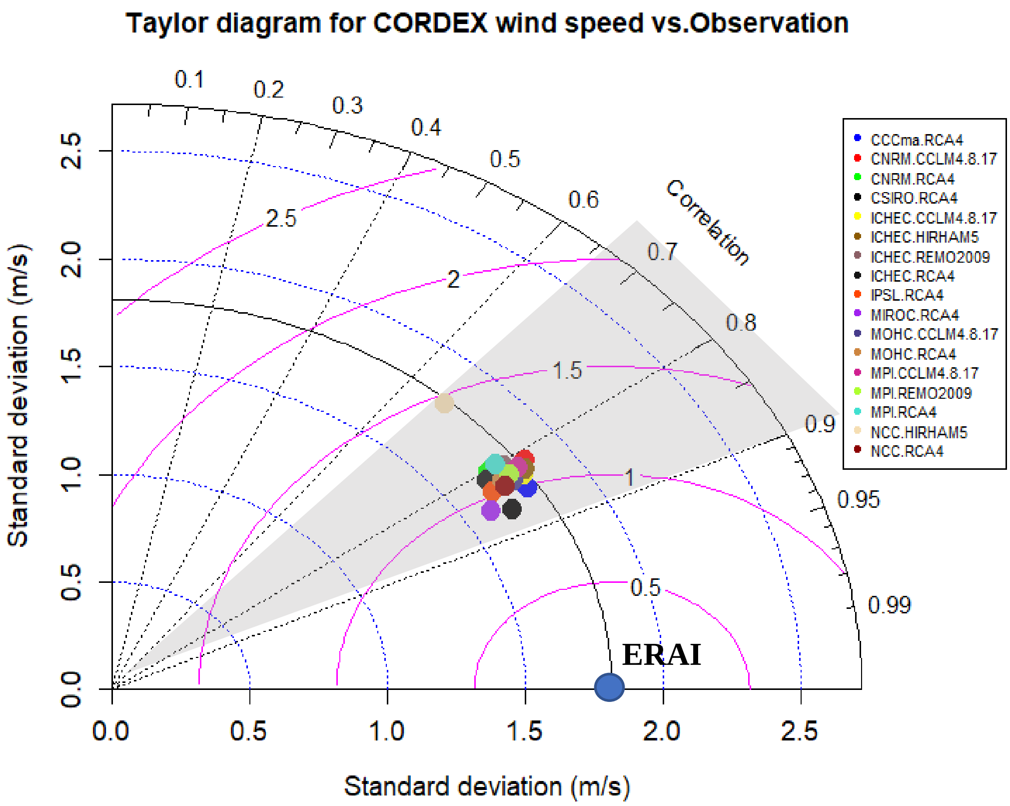

Figure 5-4: Taylor diagram to compare EAC_RCMs simulated and ERAI wind speed
The Taylor diagrams display the statistical patterns of annual mean wind speed simulated by 17 EAC_RCMs, compared with the ERAI wind speed for the same period of 1980-2005. Each model is represented by a different colour on the diagrams and is compared to ERAI. Reading this Taylor diagram should follow the explanations given for Figure 4-2. The shaded area shows where most of the models' correlation coefficients lie.

Figure 5-4 shows that the majority of models have an RMSE of approximately 0.9 and 1.5, showing that there is very little difference between simulated and observed wind speed data. In addition, the models all had a positive and strong correlation coefficient (r>0.7). The models' SD suggested that most of the simulated wind speed displayed SD in close proximation to the black lines. This indicates that the models have an almost identical SD to the observed data. The Taylor diagram statistics between the models and observed data indicate that all the 17 EAC_RCMs are able to reproduce the observed wind speed over the EAC.

In summary, after examining the statistics provided by Taylor diagrams, the evidence from this study suggests that all 17 EAC_RCMs have demonstrated the ability to reproduce the observed data (precipitation, temperature, solar radiation and wind speed). As a result, all models are utilised in order to achieve the aim of this research. The error difference between simulated and observed data will be corrected (cf. bias correction Section 7.3).

5.3.2 Data normality test for hydroclimate

A data normality test was conducted in order to create an informed decision on which statistical test (parametric or non-parametric test) was suitable for this research. Further to this, data Quantile-Quantile (Q-Q) plots, histograms and Shapiro-Wilk tests were also conducted on the hydroclimate under the RCP4.5 and RCP8.5 for the periods between 2021-2100. The results from these tests are shown in figure 5-5 to figure 5-12. The results showed that eight of the figures shared common features, so to avoid repetition of the same information all of the said figures will be analysed and interpreted together. Hence, for the purposes of conciseness the eight-figures 5-5 to figure 5-12 - are presented here as Figure 5-5:12. Where figures have distinctive features, they will be highlighted and further explained (for example Figures 5-7 and 5-8).

5.3.2.1 Precipitation under RCP4.5 and RCP8.5 data normality test

a. Data normality test for Precipitation under RCP4.5

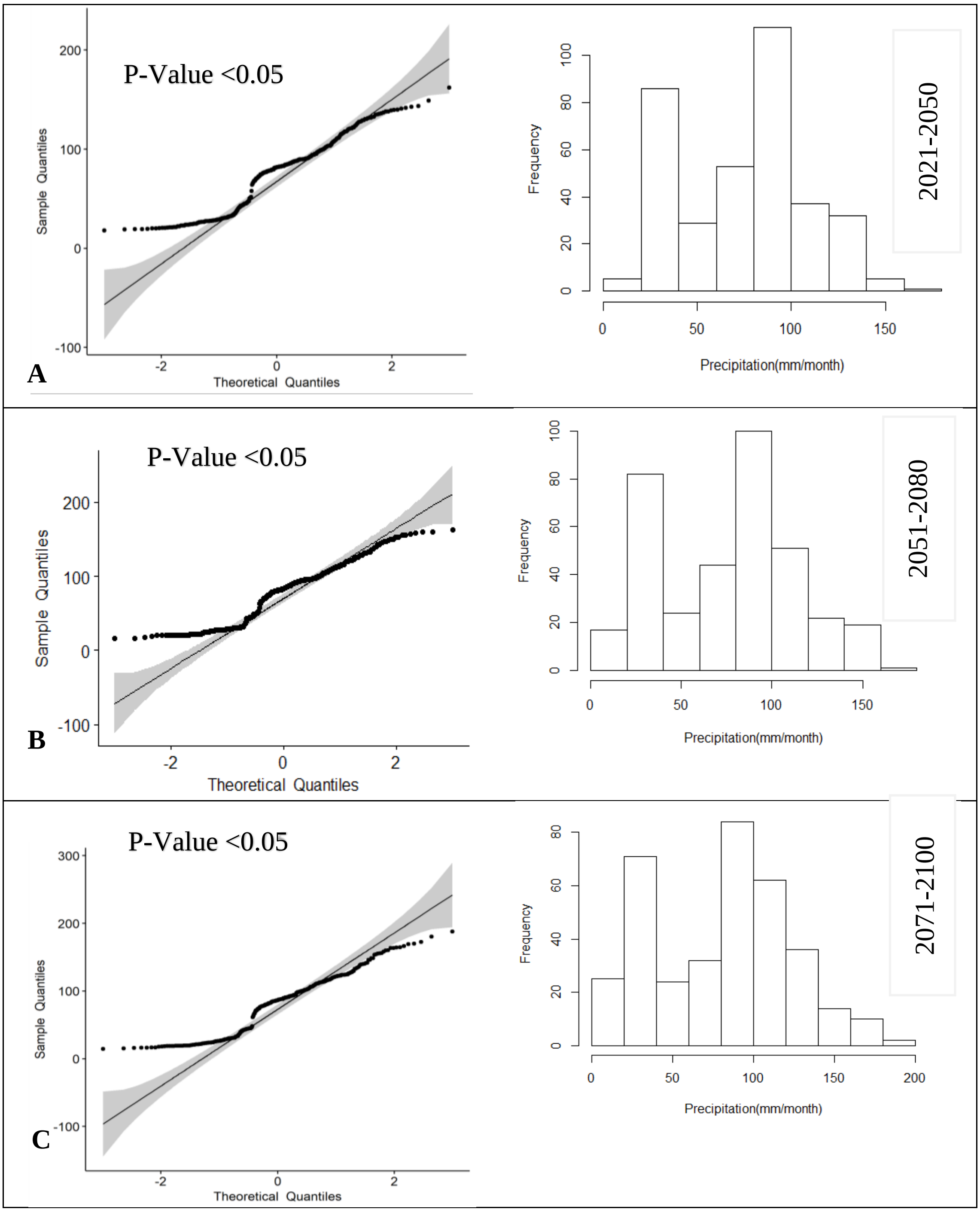

Figure 5-5:Precipitation data normality under RCP4.5
Sub-figures A, B and C are respectively for the periods of 2021-2050, 2051-2080 and 2071-2100. Each of these figures contains Q-Q plots (left column) and histogram plots (right column) for precipitation data under RCP4.5normality examination. Q-Q plot draws the correlation between a given sample and the normal distribution. P-values is the Shapiro-Wilk normality test at α=0.05.

b. Data normality test for precipitation under RCP8.5

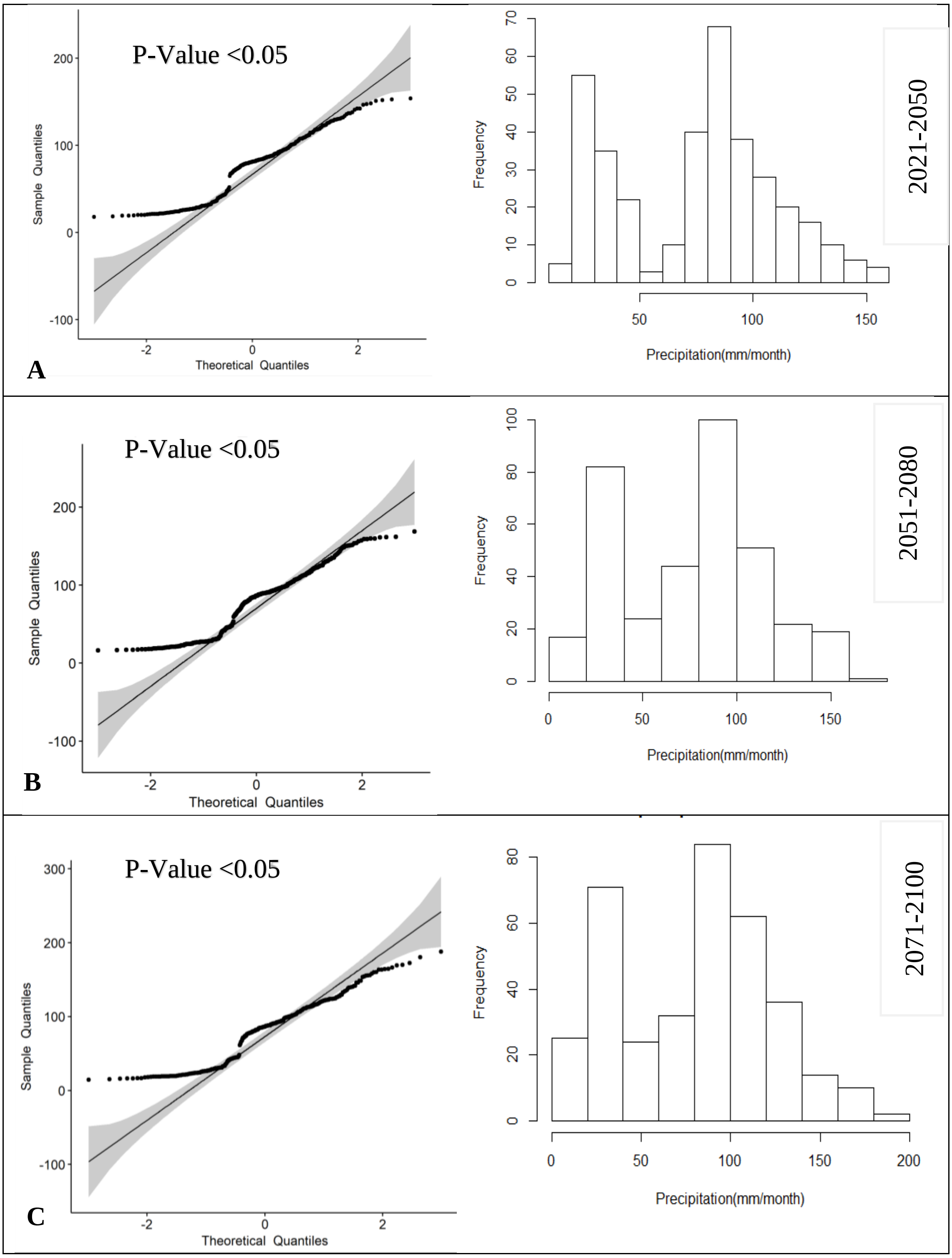

Figure 5-6: Precipitation data normality under RCP8.5
Sub-figures A, B and C are respectively for the periods of 2021-2050, 2051-2080 and 2071-2100. Each of these figures contains Q-Q (left column) and histogram plots (right column) for precipitation data under RCP8.5 normality examination. Q-Q plot draws the correlation between a given sample and the normal distribution. P-values is the Shapiro-Wilk normality test at α=0.05.

5.3.2.2 Temperature under RCP4.5 and RCP8.5 data normality test

a. **Data normality test for temperature under RCP4.5**

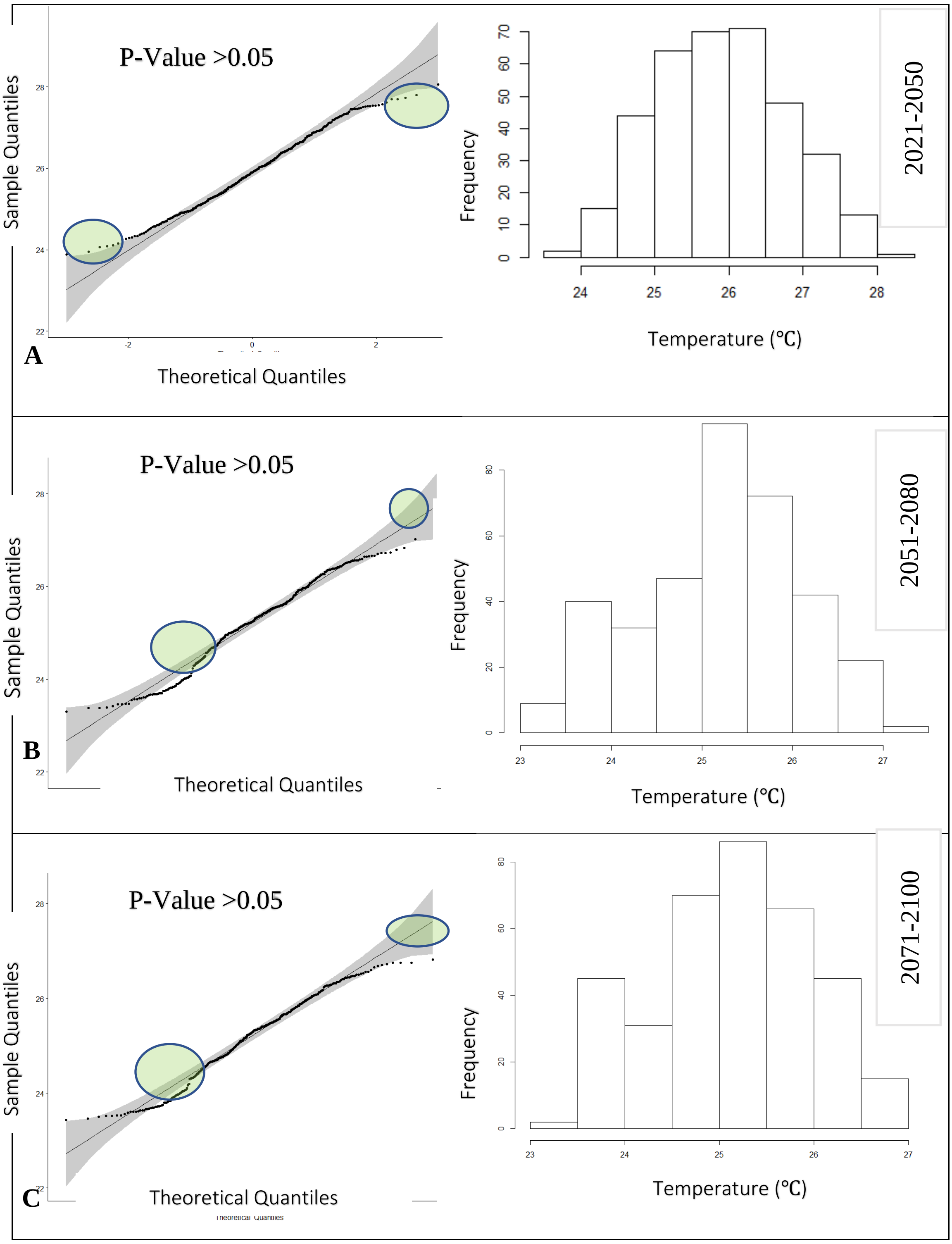

Figure 5-7: Temperature data normality under RCP4.5
Sub-figures A, B and C are respectively for the periods of 2021-2050, 2051-2080 and 2071-2100. Each of these figures contains Q-Q (left column) and histogram plots (right column) for temperature data under RCP4.5 normality examination. Q-Q plot draws the correlation between a given sample and the normal distribution. P-values is the Shapiro-Wilk normality test at α=0.05.

b. Data normality test for temperature under RCP8.5

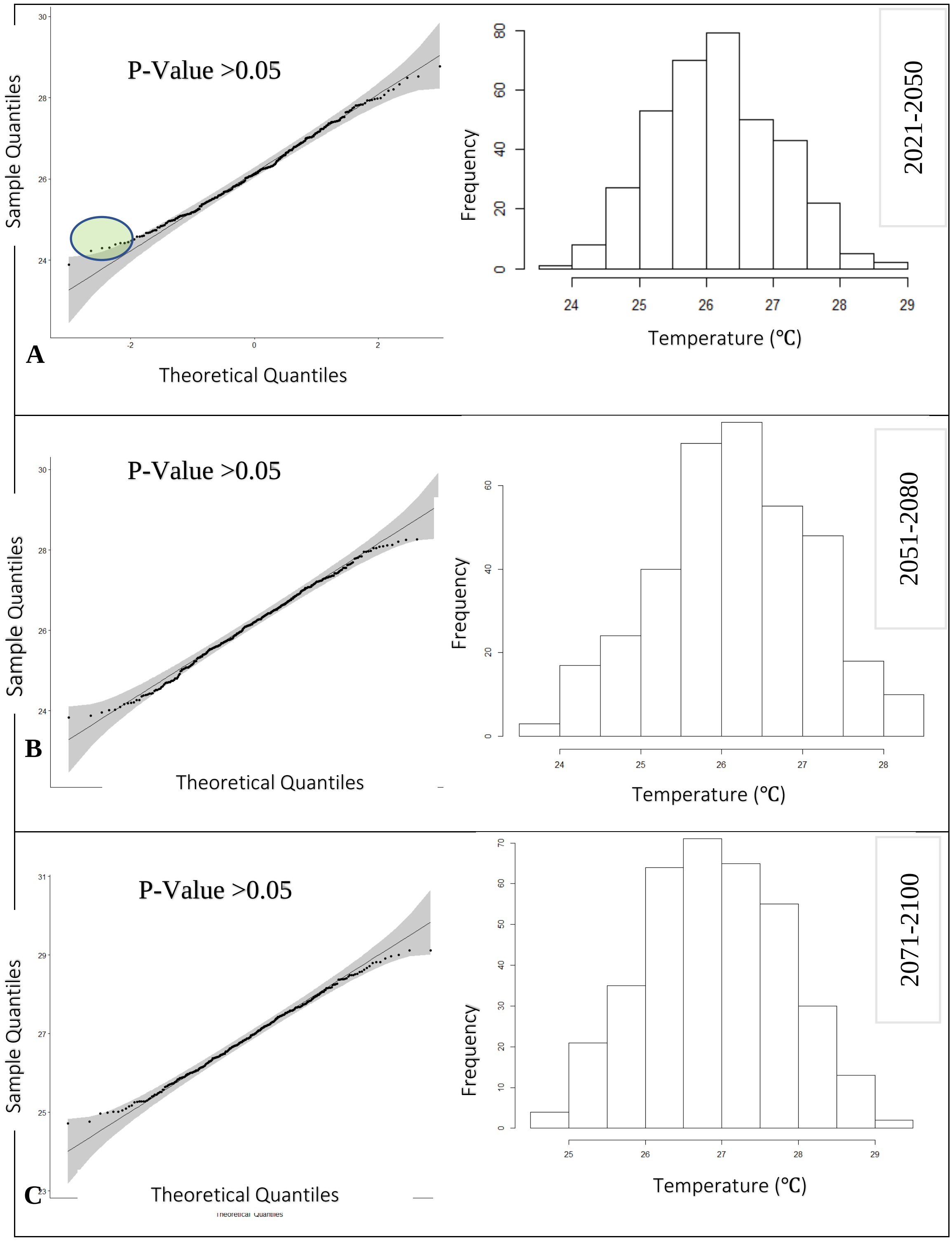

Figure 5-8: Temperature data normality under RCP8.5

Sub-figures A, B and C are respectively for the periods of 2021-2050, 2051-2080 and 2071-2100. Each of these figures contains Q-Q(left column) and histogram plots (right column) for temperature data under RCP8.5 normality examination. Q-Q plot draws the correlation between a given sample and the normal distribution. P-values is the Shapiro-Wilk normality test at α=0.05

5.3.2.3 Wind speed under RCP4.5 and RCP8.5 data normality test

a. Data normality test for wind speed under RCP4.5

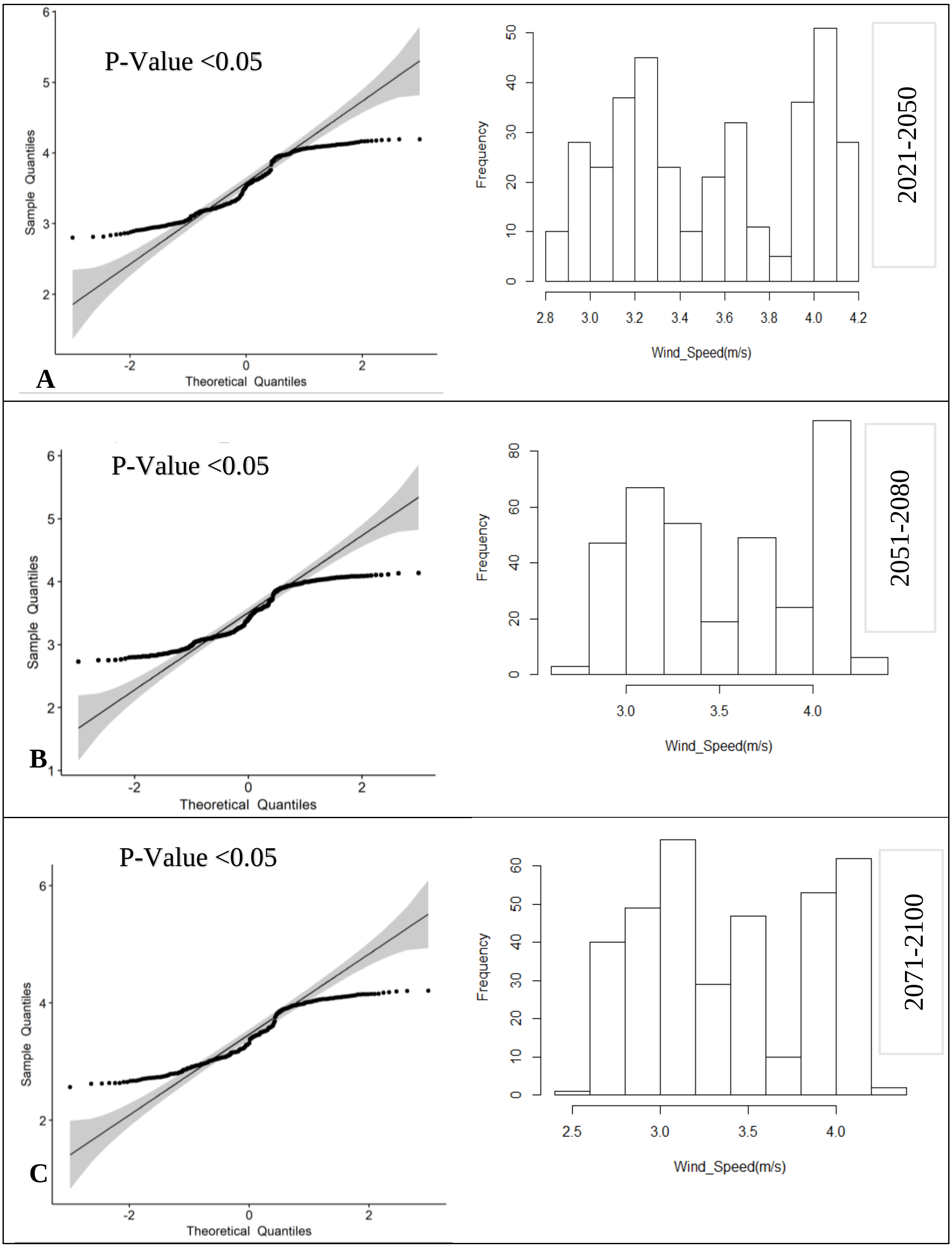

Figure 5-9: Wind speed data normality under RCP4.5

Sub-figures A, B and C are respectively for the periods of 2021-2050, 2051-2080 and 2071-2100. Each of these figures contains Q-Q (left column) and histogram plots (right column) for wind speed data under RCP4.5 normality examination. Q-Q plot draws the correlation between a given sample and the normal distribution. P-values is the Shapiro-Wilk normality test at α=0.05.

b. Data normality test for wind speed under RCP8.5

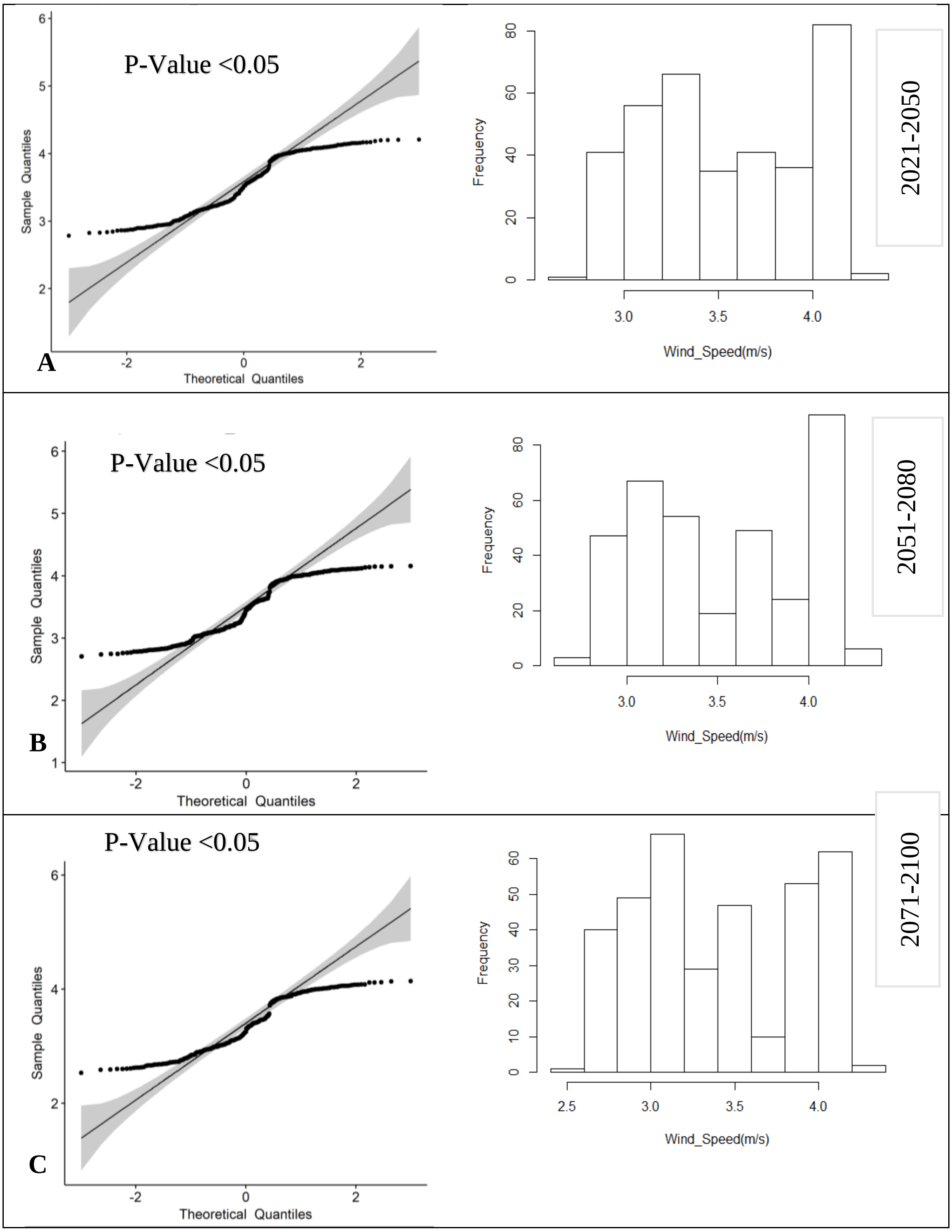

Figure 5-10: Wind speed data normality under RCP8.5

Sub-figures A, B and C are respectively for the periods of 2021-2050, 2051-2080 and 2071-2100. Each of these figures contains Q-Q (left column) and histogram plots (right column) for wind speed data under RCP8.5 normality examination. Q-Q plot draws the correlation between a given sample and the normal distribution. P-values is the Shapiro-Wilk normality test at α=0.05.

5.3.2.4 Solar radiation under RCP4.5 and RCP8.5 data normality test

c. Data normality test for solar radiation under RCP4.5

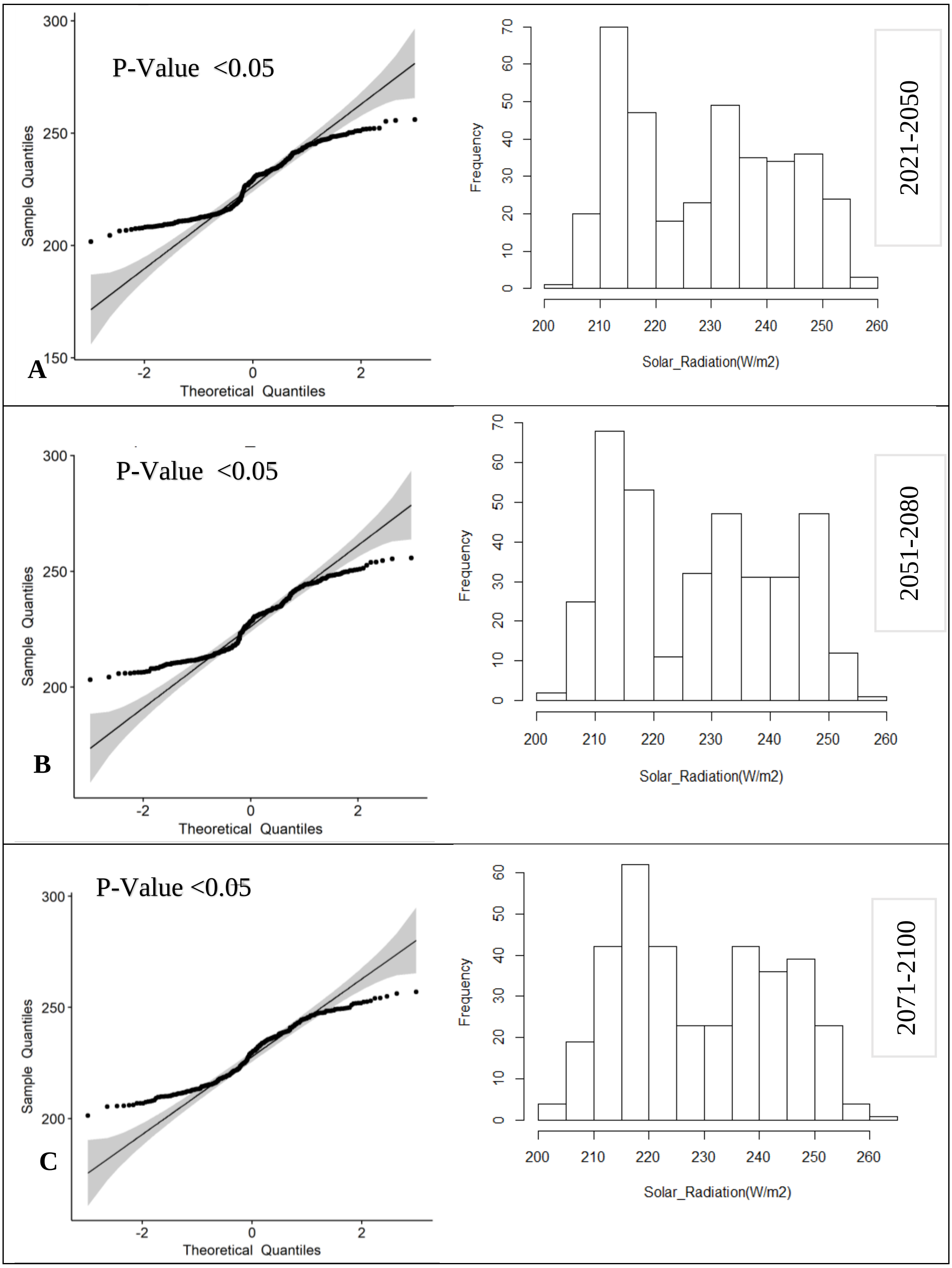

Figure 5-11: Solar radiation data normality under RCP4.5
Sub-figures A, B and C are respectively for the periods of 2021-2050, 2051-2080 and 2071-2100. Each of these figures contains Q-Q (left column) and histogram plots (right column) for solar radiation data under RCP4.5 normality examination. Q-Q plot draws the correlation between a given sample and the normal distribution. P-values is the Shapiro-Wilk normality test at α=0.05.

d. Data normality test for solar radiation under RCP8.5

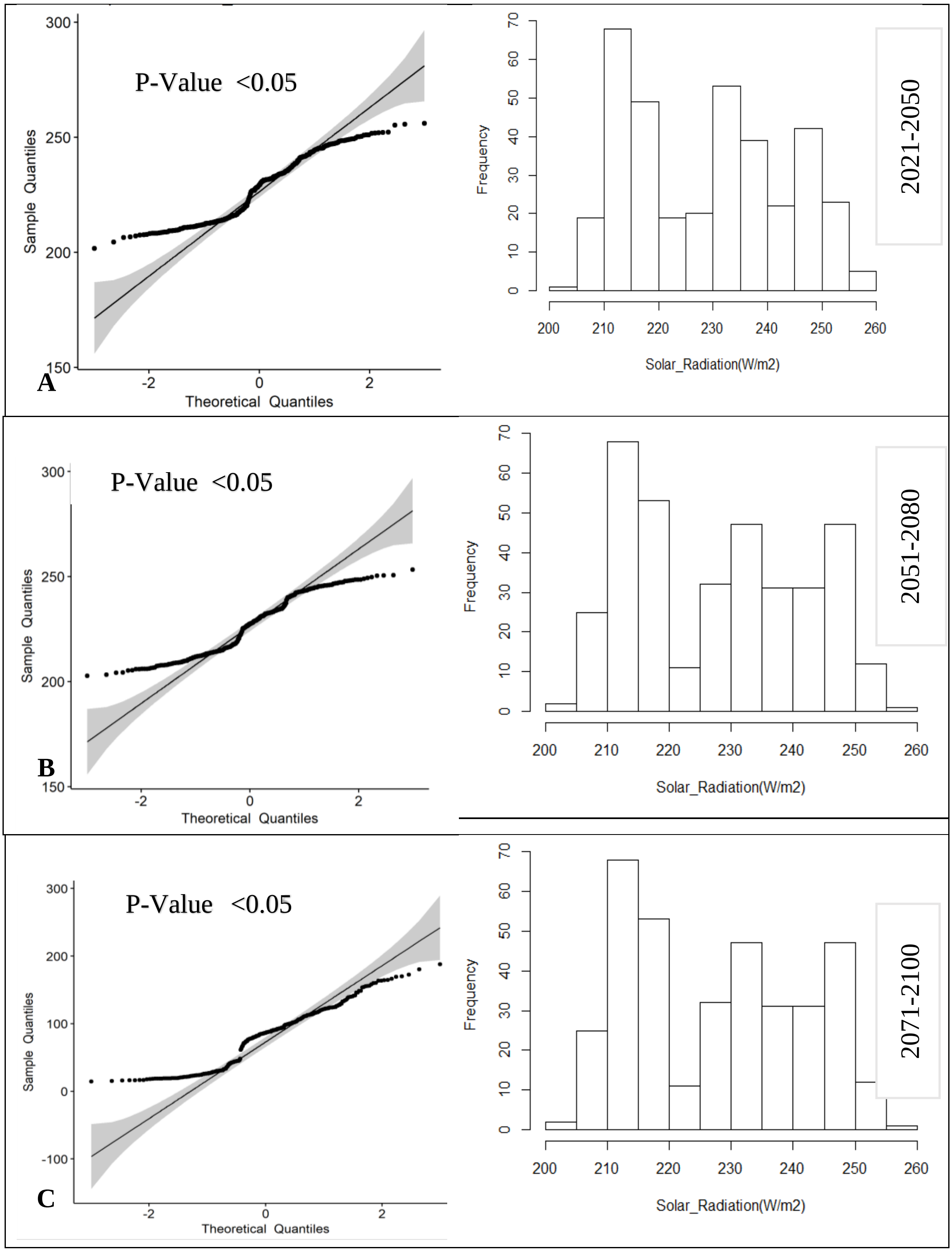

Figure 5-12: Solar radiation data normality under RCP8.5
Sub-figures A, B and C are respectively for the periods of 2021-2050, 2051-2080 and 2071-2100. Each of these figures contains Q-Q (left column) and histogram plots (right column) for solar radiation data under RCP8.5 normality examination. Q-Q plot draws the correlation between a given sample and the normal distribution. P-values is the Shapiro-Wilk normality test at α=0.05.

As previously mentioned, in order to be able to determine data normality distribution, three tests must be conducted. These are Q-Q plots, Histogram and Shapiro-Wilk normality tests. Figures 5-5:12 shows non-normal distributed data. In contrast, for normally distributed data, all data points would fall on the straight line in Q-Q plots and the shape for histograms plots would match congruently with Gaussian distribution. Generally speaking, Gaussian distribution assumes that sampled data values will follow a normal distribution with an equal number of measurements above and below the mean values (Dasgupta and Wahed 2014). A Gaussian distribution in the histogram with an equal number of measurements above (e.g.-1s) and below (e.g. +1s) the mean values is demonstrated in Figure 5-13 below:

Figure 5-13: A Gaussian distribution showing the percentage of values within a certain standard deviation from the mean

Mean (x-) ± standard deviation (s) represent 68.27%, ± 2s represent 95.45%, ± 3s represent 99.73% of all possible values.

Source: (Ditrich 2012)

When looking at Figures 5-5:12, with the exception of Figures 5-7 and 5-8, the figures show that the data drift from the straight line on the Q-Q plots and do not follow a Gaussian distribution in the histograms for the periods of 2021-2100 for precipitation, wind speed and solar radiation under both RCP4.5 and RCP8.5. Figure 5-7 and Figure 5-8, representing temperatures for the periods of 2021-2100 under RCP4.5 and RCP8.5 respectively, show different features. This is because most of the data do fall on the straight line of the QQ plots. The histograms for those two figures also largely align with the Gaussian distribution. The few elements within the two figures that drift from the straight line on the Q-Q plots are highlighted in green circles. For all figures, Figures 5-5:12, data normality was confirmed using a Shapiro-Wilk normality test of the P-values printed on each plot. From this, the figures tested with the exception of Figure 5-7 and Figure 5-8, demonstrated P-values of less than α. This meant that the level of probability with respect to the 2021-2100 data samples being normally distributed was very small under both climate scenarios. The implications of this necessitated the utilisation of a further non-parametric test. Figure 5-7 and Figure 5-8 showed a P-value > α, however, given the fact that the Q-Q plots highlighted some data drift from its straight line coupled with the fact that the requirement for this research is a test that will work for all four hydroclimate variables, a non-parametric test was chosen for use.

5.3.3 Statistical analysis method

The results from the data normality test (as per Section 5.3.2 above) indicated that hydroclimate data considered for this study are no normally distributed. Therefore a non-parametric test was most suitable for examining the significance of changes in hydroclimate variables between the reference period (1976-2005) and future period (2021-2100). More specifically, this research selected the Wilcoxon (1945) signed-rank sum test was selected for this research because it is a popular nonparametric test in terms of comparing outcomes between two independent datasets (Haynes 2013, Dutta and Datta 2016, Neave 2019). Therefore, the statistical hypothesis testing for changes under the RCPs 4.5 and 8.5 are set as follows: H_0: $1976\_2005 = 2021\_2100$; H_1: $1976\_2005 \neq 2021\_2100$. In order to analyse the changes of the variable values between RCPs 4.5 and 8.5, a hypothesis test at significance level $\alpha = 0.05$ was conducted.

5.3.4 Spatiotemporal future changes in hydroclimate over the EAC

The result for this section is divided into two parts: the first part assesses the changes in spatial distribution patterns for the hydroclimate (i.e. precipitation, temperature, solar radiation and wind speed) over the EAC region between the years 2021 and 2100, while the second part investigates both the annual cycle monthly mean and seasonal cycle of hydroclimate changes for the near-term (2021-2051), mid-term (2051-2080) and long-term (2071-2100), under the RCPs 4.5 and 8.5 climate scenarios.

5.3.4.1 Spatiotemporal future changes in precipitation under RCPs 4.5 and 8.5

This section consists of two parts: the first part investigates the precipitation temporal changes for each grid over the region of study and the second part focuses on the annual and seasonal mean precipitation changes. Prior to exploring these changes, the historical seasonal cycle Multimodal Ensemble Mean (MMEM) relative to the observed precipitation, shown in Figure 1-14, has been analysed.

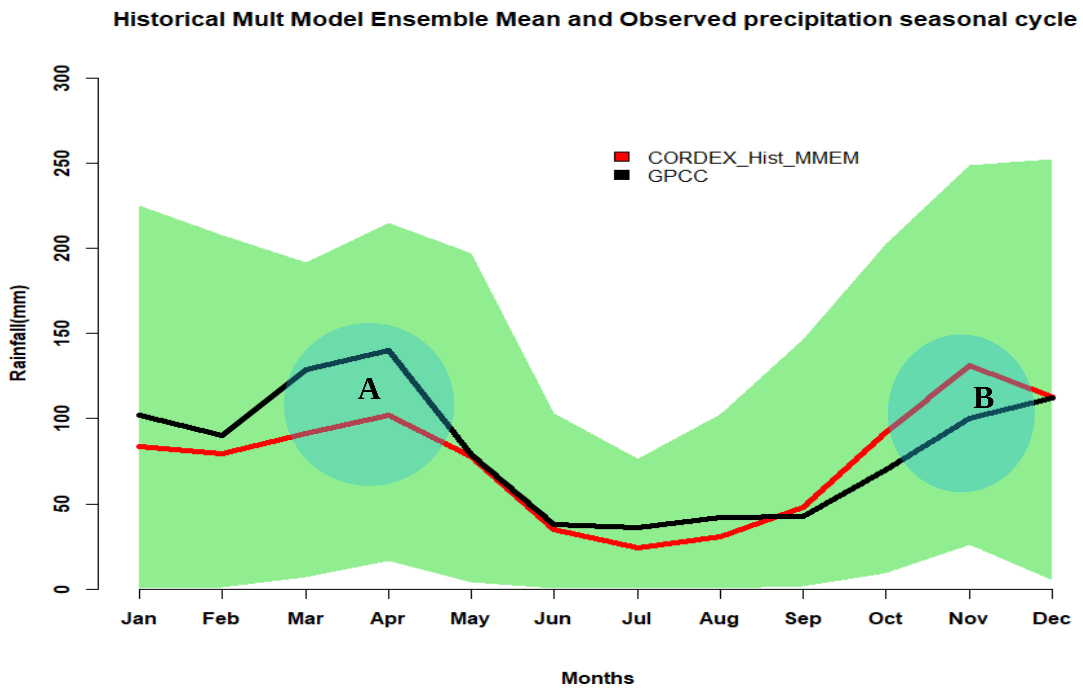

Figure 5-14: MMEM historical and GPCC precipitation cycle
This figure displays the MMEM historical monthly cycle (shown in red), relative to the observed (GPCC) precipitation (shown in black). The green polygon is the MMEM historical precipitation monthly cycle 90th (top) and 10th (bottom) percentile spread. The circles A and B shows the EAC bimodal (March, April and May long rain and September-October and November short rain) precipitation pattern.

Looking at Figure 5-14, it is noticeable that the MMEM underestimates the EAC precipitation during the months of January to May and June to August.

There is also an overestimation for precipitation during the months of September-December. In contrast however, the MMEM captures well the observed precipitation for the months of May and June. Although the MMEM historical runs did not exactly match the observed rainfall patterns, it captured the expected bimodal pattern (i.e. the highlighted A and B circles in Figure 5-14) of rainfall over the EAC region. This is important because the bimodal patterns correspond with the long rainfall. The A circle corresponds with the months of March, April and May [MAM]) and the short rainfall B circle corresponds with the months of October, November and December [OND]). The EAC's long and short rainfall precipitation patterns were highlighted in previous studies of east Africa including Shongwe et al. (2011), Liebmann et al. (2014), and Ongoma et al. (2017). The ability of the MME to simulate the EAC rainfall features increased confidence in the models. The periods where the MME overestimates or underestimates the rainfall patterns is an indication that the MME drifts from the observed patterns. This is something that will be corrected through bias corrections.

5.3.4.1.1 Spatial changes in precipitation over the EAC under RCPs 4.5 and 8.5

This section compares the MMEM simulated precipitation for the periods of 2021-2050, 2051-2080 and 2071-2100 against the baseline period (1976-2005). The results for this section are provided in Figure 5-15 to Figure 5-20. The results from these figures share most of their features with each other, and so, as discussed in other sections, will be analysed and interpreted together. Due to this, Figure 5-15 to Figure 5-20 are denoted as Figure 5-15:20. Each figure has four maps. The first map - labelled A - represents the spatial observed rainfall which serves as the baseline.

It is against this baseline that the projected spatial rainfall B will be measured. Map C represents the changes between the projected data and the baseline. As with any testing, different models will have different results and thus it is expected that some models will project an increase in precipitation whilst others will project a decrease. It is also expected that some models will show no changes. In this regard, Map D shows the percentage of models that are statistically significant (P-Value $<\alpha$, where $\alpha=0.05$) agree on the positive changes (that is, increase) and negative changes (that is, decrease) in precipitation. On the legend, the positive and negative signs (e.g. 100, 50, 0 -50, -100) are used for the purpose of distinguishing the percentages of models that project an increase and decrease respectively. For example, -50 on the legend should be read as 50% of the models over the coloured area in red agree that there is a decrease in precipitation. Zero indicates that the model's agreement is not statistically significant.

Baseline map A has spatial outliers, mostly over Lake Victoria for precipitation and Kenya's highlands for solar radiation. To maintain an easy colour contrast between the baseline and project rainfall, the grids with outliers in the baseline maps [A] have been printed in white. The rest of the maps B, C and D do not have outliers. This colour contrast between the baseline and project rainfall procedure is also applied to solar radiation, wind speed and temperature. As stated above, changes in precipitation under RCP4.5 and RCP8.5 are presented in Figure 5-15: 20.

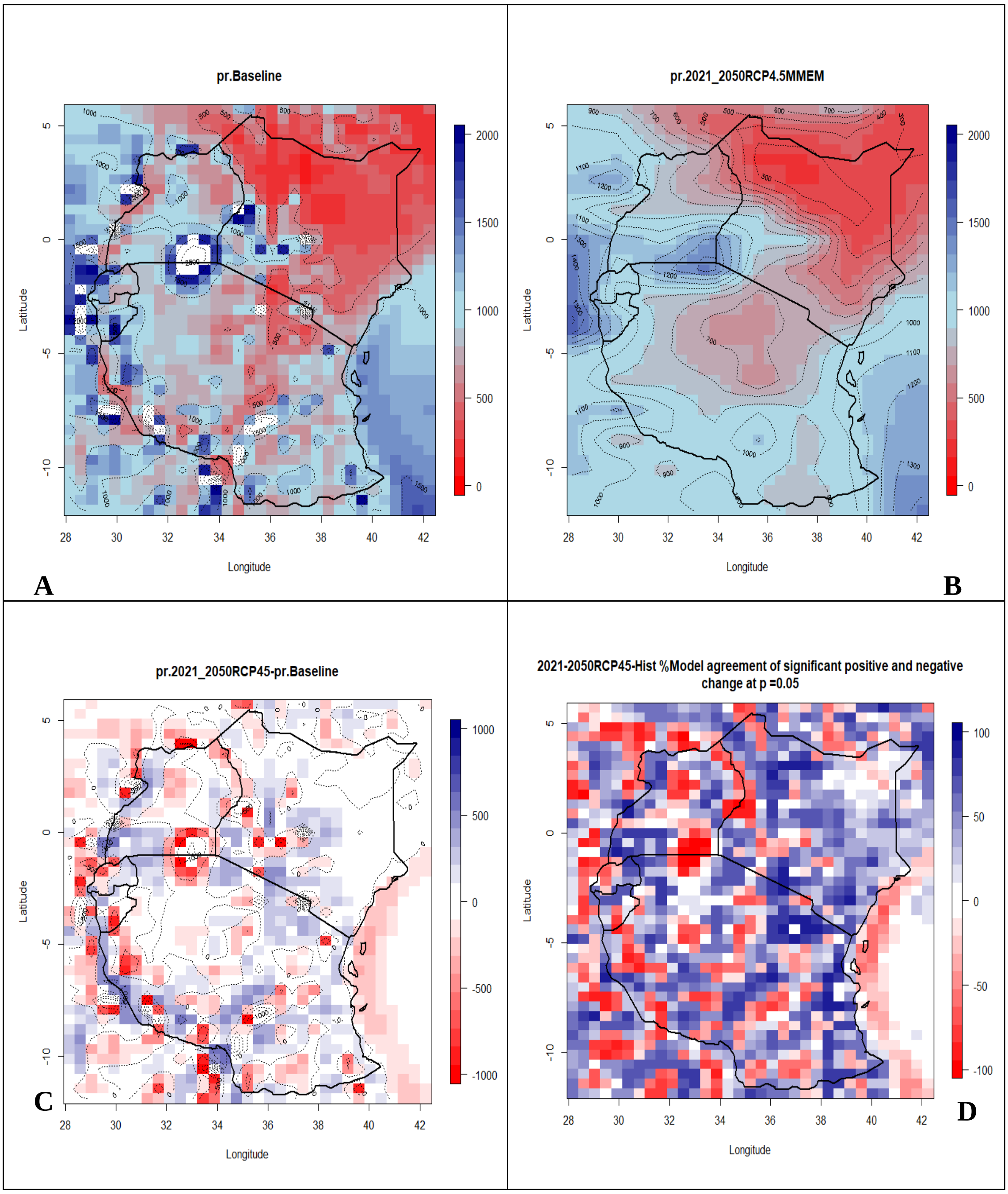

Figure 5-15: Spatial changes in precipitation (mm/month) for the period of 2021-2050 under RCP4.5 over the EAC

Colours should be used to read precipitation distribution for subfigures (A&B) and changes for subfigure (C) while the contours on the maps provide values for spatial variability. Subfigure A [baseline] is historical MMEM, the white colour show grids where there are outliers. Subfigure B is precipitation MMEM under RCP4.5 for 2021-2050 (2050-time horizon). Subfigure C is a map showing changes between the 2050 time horizon and the baseline. The changes are represented by the colour red for fields where precipitation is decreasing (dry conditions), white is where there is no change, and light to dark blue colouring indicates an area where precipitation is increasing (wet conditions). Subfigure D is a map showing the percentage of models that are in agreement on positive changes (blue), negative changes (red) and such agreement is statistically significant at α=0.05. White colour(Subfigure D) indicates that model agreements are statistically insignificant.

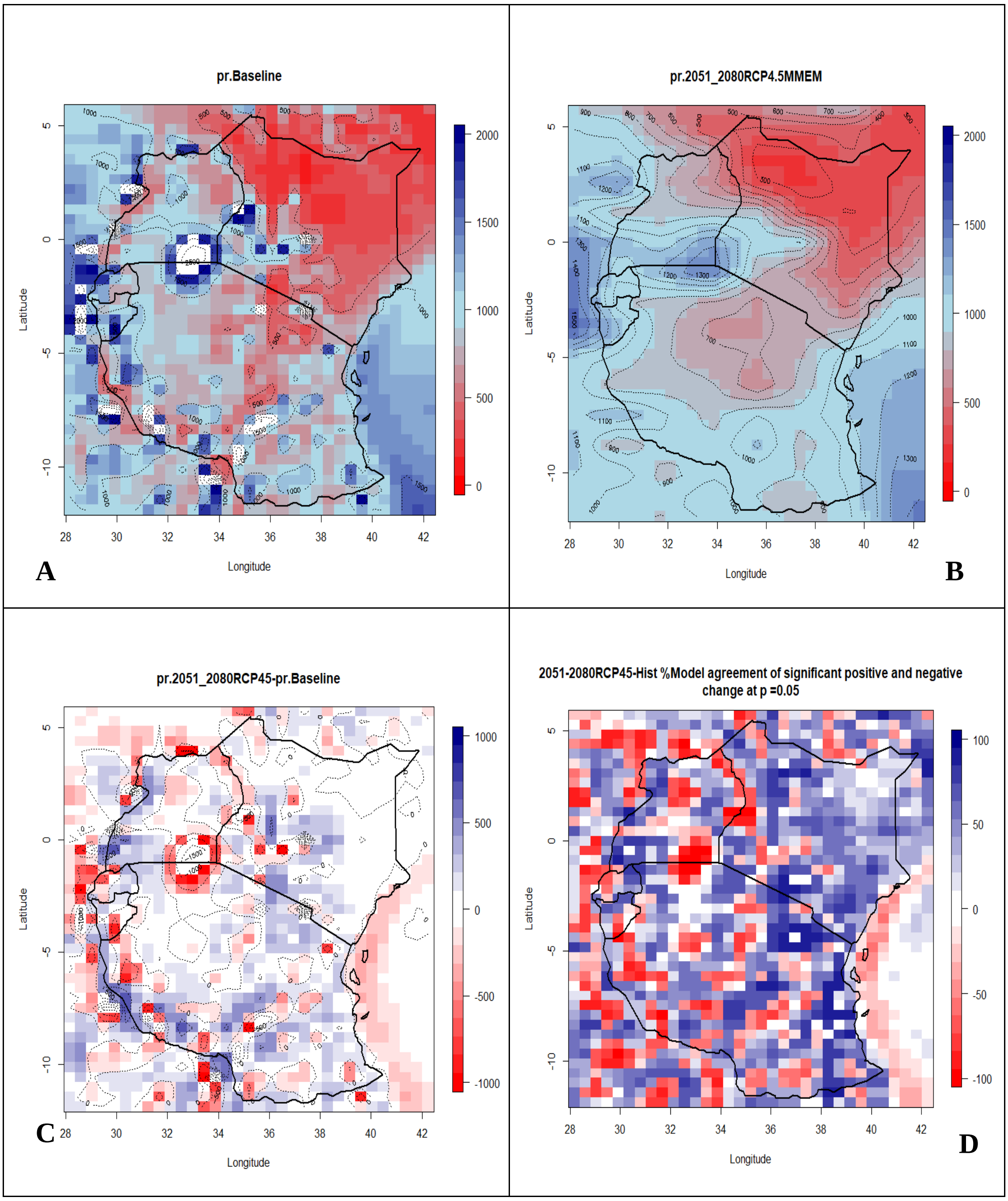

Figure 5-16: Spatial changes in precipitation (mm/month) for the period of 2051-2080 under RCP4.5 over the EAC

Colours should be used to read precipitation distribution for subfigures (A&B) and changes for subfigure (C) while the contours on the maps provide values for spatial variability. Subfigure A [baseline] is historical MMEM, the white colour shows grids where there are outliers. Subfigure B is precipitation MMEM under RCP4.5 for 2051-2080 (2080-time horizon). Subfigure C is a map showing changes between the 2080 time horizon and the baseline. The changes are represented by the colour red for fields where precipitation is decreasing (dry conditions), white where there is no change, and the light to dark blue colours indicate an area where precipitation is increasing (wet conditions). Subfigure D is a map showing the percentage of models that are in agreement on positive changes (blue), negative changes (red) and such agreement is statistically significant at α=0.05. The colour white(subfigure D) indicates that model agreements are statistically insignificant.

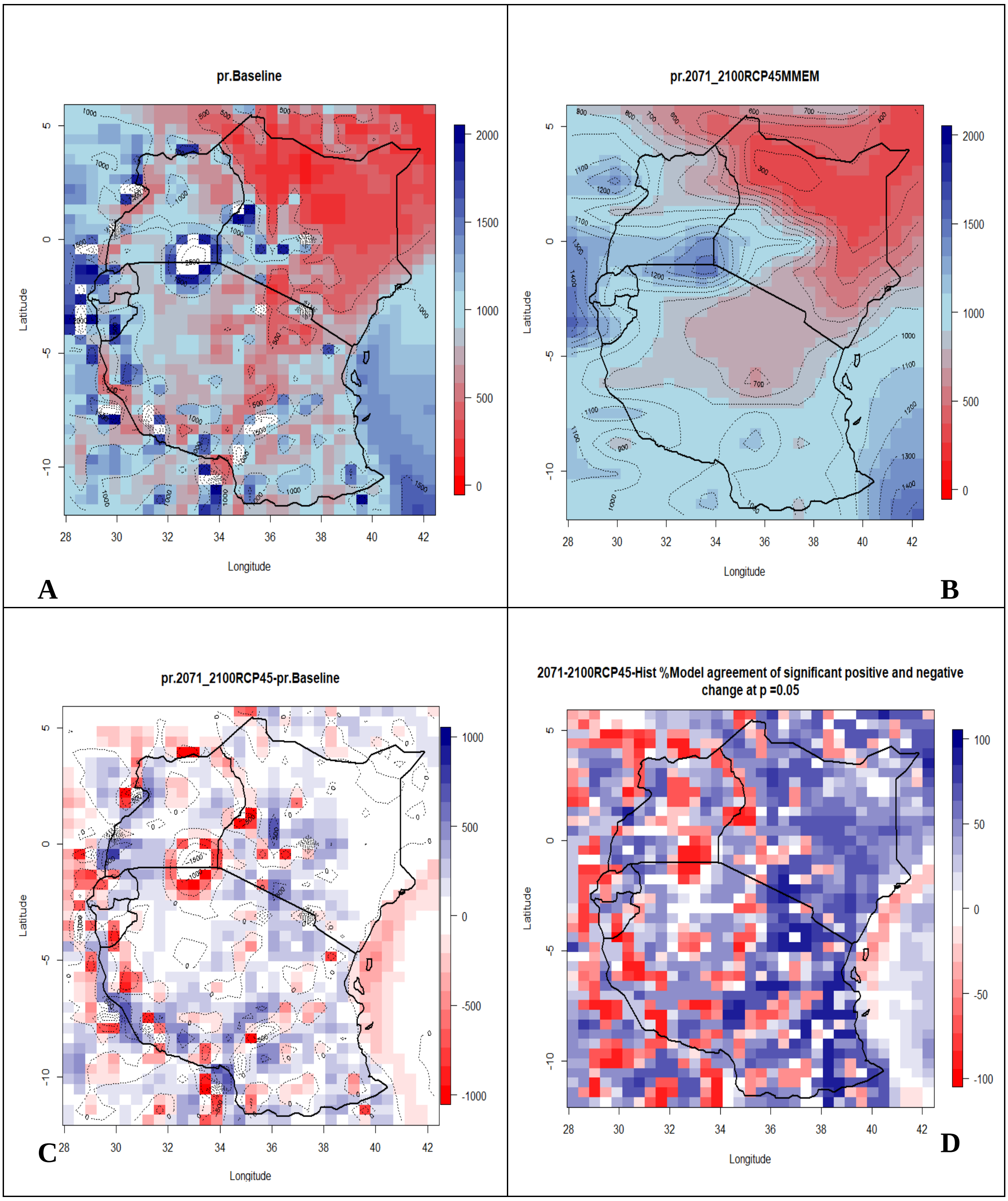

Figure 5-17: Spatial changes in precipitation (mm/month) for the period of 2071-2100 under RCP4.5 over the EAC

Colours should be used to read precipitation distribution for subfigures (A&B) and changes for subfigure (C) while the contours on the maps provide values for spatial variability. Subfigure A [baseline] is historical MMEM, the white colour shows grids where there are outliers. Subfigure B is precipitation MMEM under RCP4.5 for 2071-2100 (2100-time horizon). Subfigure C is a map showing changes between the 2100 time horizon and the baseline. The changes are represented by the colour red for fields where precipitation is decreasing (dry conditions), white where there is no change, and light to dark blue colours indicate an area where precipitation is increasing (wet conditions). Subfigure D is a map showing the percentage of models that are in agreement on positive changes (blue), negative changes (red) and such agreement is statistically significant at α=0.05. The colour white (subfigure D) indicates that model agreements are statistically not significant.

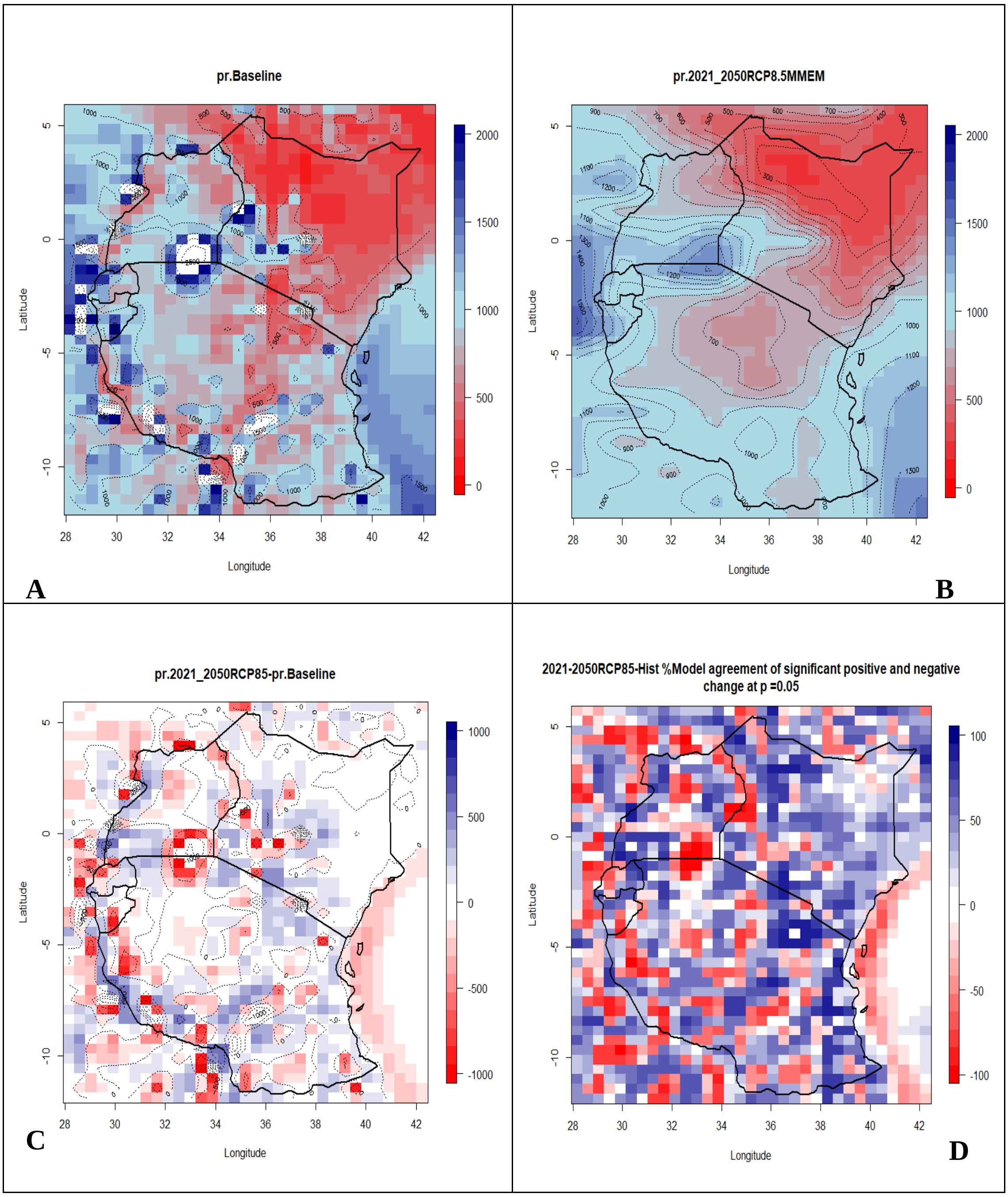

Figure 5-18: Spatial changes in precipitation (mm/month) for the period of 2021-2050 under RCP8.5 over the EAC

Colours should be used to read precipitation distribution for subfigures (A&B) and changes for subfigure (C) while the contours on the maps provide values for spatial variability. Subfigure A [baseline] is historical MMEM, the white colour shows grids where there are outliers. Subfigure B is precipitation MMEM under RCP8.5 for 2021-2050 (2050-time horizon). Subfigure C is a map showing changes between the 2050 time horizon and the baseline. The changes are represented by the colour red for fields where precipitation is decreasing (dry conditions), white where there is no change, and light to dark blue colours indicate an area where precipitation is increasing (wet conditions). Subfigure D is a map showing the percentage of models that are in agreement on positive changes (blue), negative changes (red) and such agreement is statistically significant at α=0.05. The colour white (subfigure D) indicates that model agreements are statistically not significant.

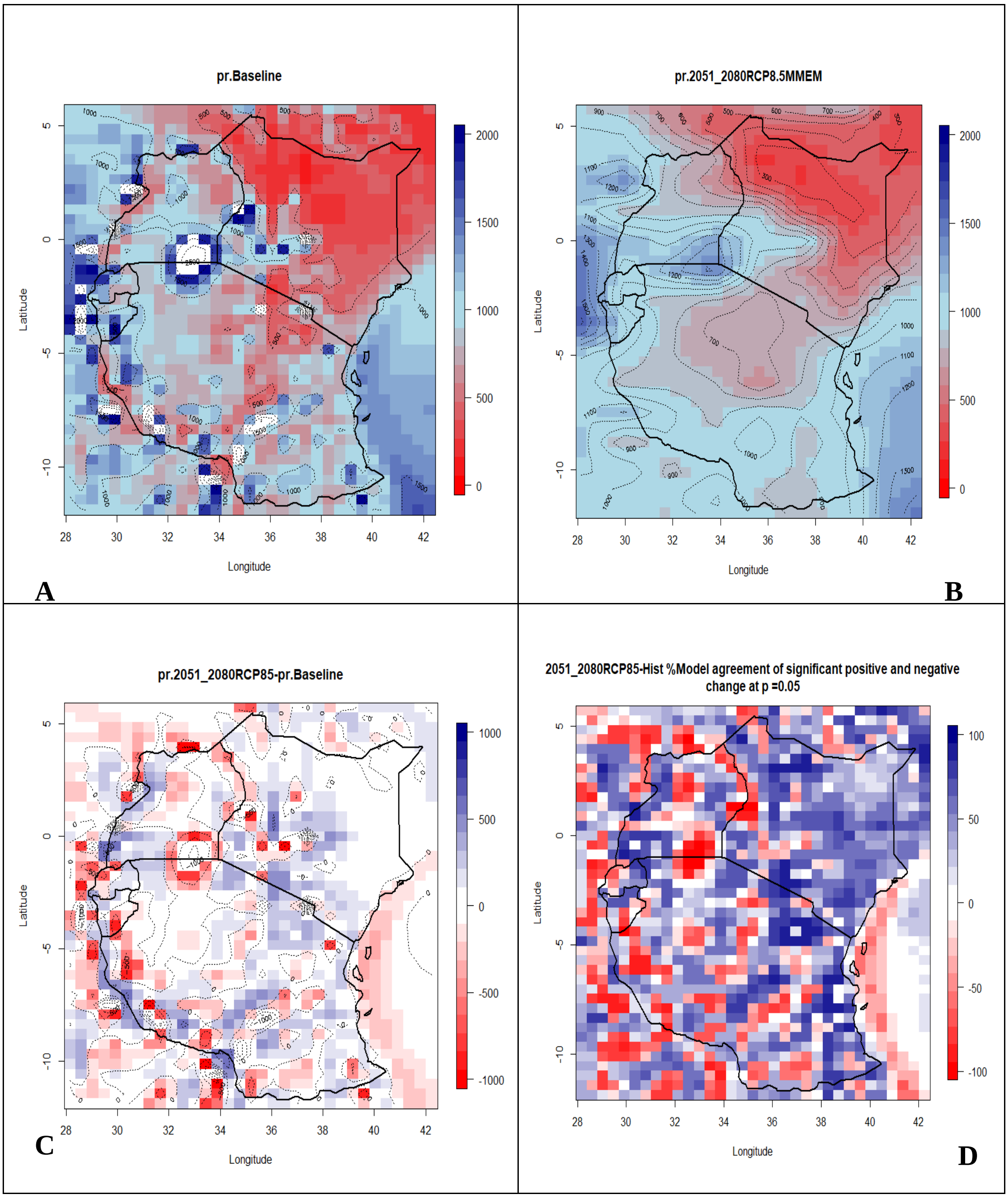

Figure 5-19: Spatial changes in precipitation (mm) for the period of 2051-2080 under RCP8.5 over the EAC

Colours should be used to read precipitation distribution for subfigures (A&B) and changes for subfigure (C) while the contours on the maps provide values for spatial variability. Subfigure A [baseline] is historical MMEM, the white colour shows grids where there are outliers. Subfigure B is precipitation MMEM under RCP8.5 for 2051-2080 (2080-time horizon). Subfigure C is a map showing changes between the 2080 time horizon and the baseline. The changes are represented by the colour red for fields where precipitation is decreasing (dry conditions), white where there is no change, and light to dark blue colours indicate an area where precipitation is increasing (wet conditions). Subfigure D is a map showing the percentage of models that are in agreement on positive changes (blue), negative changes (red) and such agreement is statistically significant at α=0.05. The colour white (subfigure D) indicates that model agreements are statistically not significant.

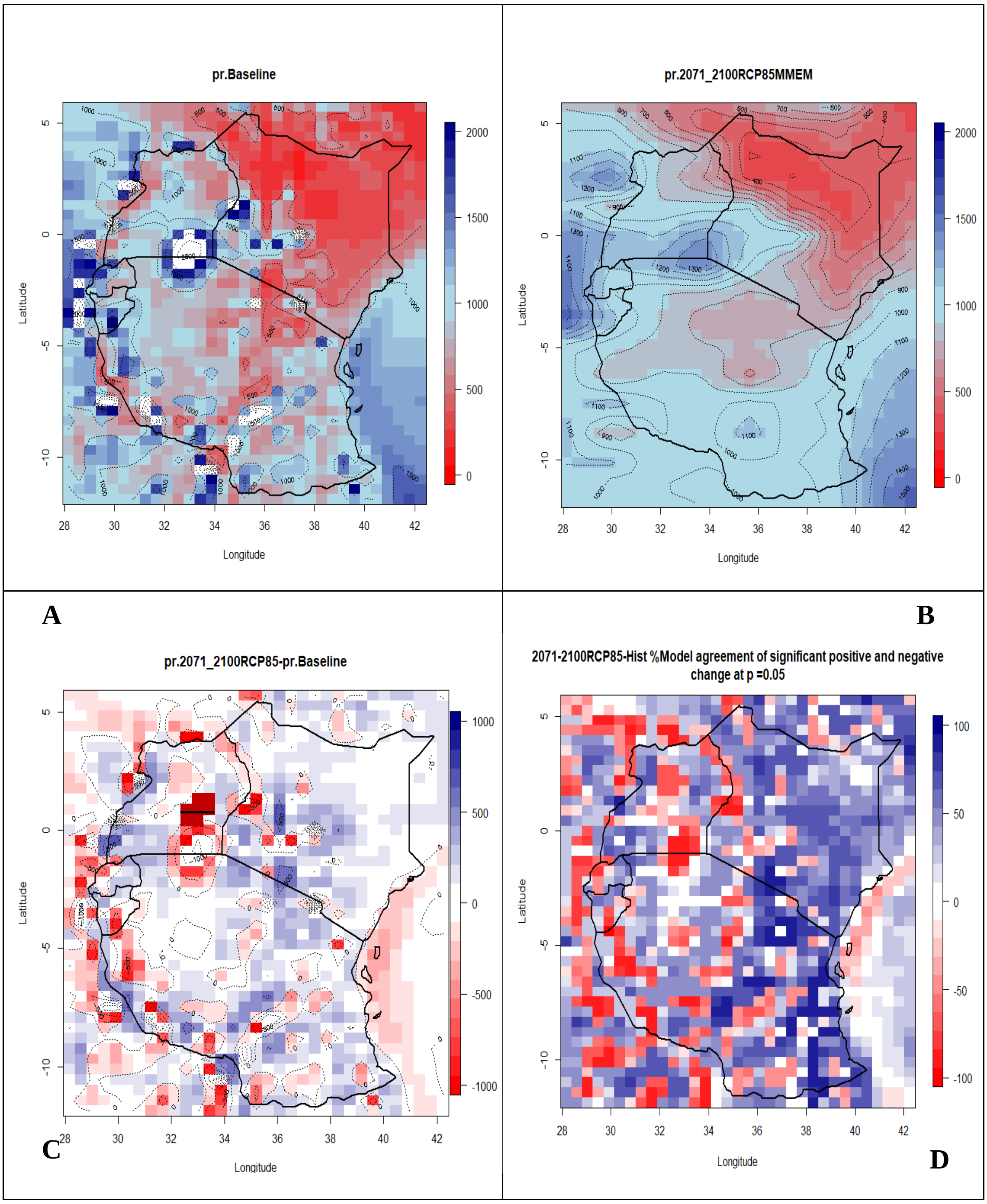

Figure 5-20: Spatial changes in precipitation (mm) for the period of 2071-2100 under RCP8.5 over the EAC

Colours should be used to read precipitation distribution for subfigures (A&B) and changes for subfigure (C) while the contours on the maps provide values for spatial variability. Subfigure A [baseline] is historical MMEM, the white colour shows grids where there are outliers. Subfigure B is precipitation MMEM under RCP8.5 for 2071-2100 (2100-time horizon). Subfigure C is a map showing changes between the 2100 time horizon and the baseline. The changes are represented by the colour red for fields where precipitation is decreasing (dry conditions), white where there is no change, and light to dark blue colours indicate an area where precipitation is increasing (wet conditions). Subfigure D is a map showing the percentage of models that are in agreement on positive changes (blue), negative changes (red) and such agreement is statistically significant at α=0.05. The colour white (subfigure D) indicates that model agreements are statistically not significant.

Statistical testing for the period between 2021-2100 under RCP4.5 indicates that nine out of 12 models predicted a significant increase in precipitation (wet conditions) across the EAC region, whilst 3 of the models predicted a decrease in precipitation (dry conditions). The remaining models predicted no changes (AppendixA1). Under the RCP8.5 scenario, 10 out of 17 models indicated significant wet conditions, 2 models predicted a decrease (dry conditions), while 5 models out of 17 showed no significant changes in precipitation, between the period of 1976-2005 and 2021-2100 (see AppendixA2). Under both RCP4.5 and RCP8.5, all model averages indicated that there would be an increase in precipitation for the period between 2021-2100. This increase in precipitation is consistent with the IPCC (2014) report which indicated that the annual mean rainfall in the EAC is likely to increase in future.

Looking at the individual period shown in Figure 5-15:20 (A and B), it can be seen that a large part of Kenya as well as the central part of Tanzania towards the north-west, generally has less precipitation when compared to the rest of the EAC. Figure 5-15:20 (C) shows that there is no change in rainfall in the north-east of Kenya and the north-west of Tanzania towards Burundi. The western and south-western part of Kenya, towards the north-eastern part of Tanzania, is generally wet with a few pockets of dry areas. Also, no change in spatial rainfall patterns was observed in the central-eastern area of Uganda. It was also observed as generally wet in the west and dry towards central and eastern parts of Uganda. Over Lake Victoria, there are generally substantially dry conditions. This may be due to the outliers in the baseline data over the lake. The western part of Rwanda is dry while the eastern part is generally recorded as being wet. Burundi is wet in the north and north-west while generally displaying no changes in the east towards Tanzania. The central part of Burundi towards the south is shown to be generally dry.

In general, the eastern part of the EAC has low annual precipitation when compared to the rest of the EAC region. These findings were also highlighted by Hoerling et al. (2006) who indicated that the eastern part of East Africa has substantially lower annual precipitation than the rest of the equatorial region. Figures 5-20 (D) shows a complex mixture of the model's agreement on positive and negative changes. This mixture of the model's agreement is due to variation in the topography across the EAC. For instance, mountains act as an obstacle for the flow of air (Tucker and Crook 2005). They are also a source of heat variation (Tucker and Crook 2005). The variation in the topography has been identified by Ogwang et al. (2014) as one of the main causes of precipitation variation the EAC.

5.3.4.1.2 Future annual and seasonal cycle changes in precipitation under RCP4.5 and 8.5

This section assesses the annual and seasonal cycle changes in precipitation under the RCP4.5 and 8.5 scenarios, for the periods 2021-2050, 2051-2080, and 2071-2100.

5.3.4.1.2.1 Potential annual cycle monthly mean changes in precipitation

As per Figure 5-21 (A-B) and detailed in the Appendix (A3), the driest events are much more pronounced in the early years of the dated period 2021-2050 for both RCP4.5 and 8.5 scenarios. The maximum and average decreasing trends of approximately -6.9mm and-2.36mm/per month for the RCP4.5, when the maximum and average decreases under the RCP8.5 are projected to be -4.5mm and -2.16mm per month respectively. The wettest events are much more pronounced at the end of the 2021-2050 period with a maximum increase of about +6.9 mm/month. The average increase is approximately +2.67mm/month under the RCP4.5, while under the RCP8.5, the maximum increase is projected to be about 5.3mm and the average rainfall is approximately 2.55mm per month.

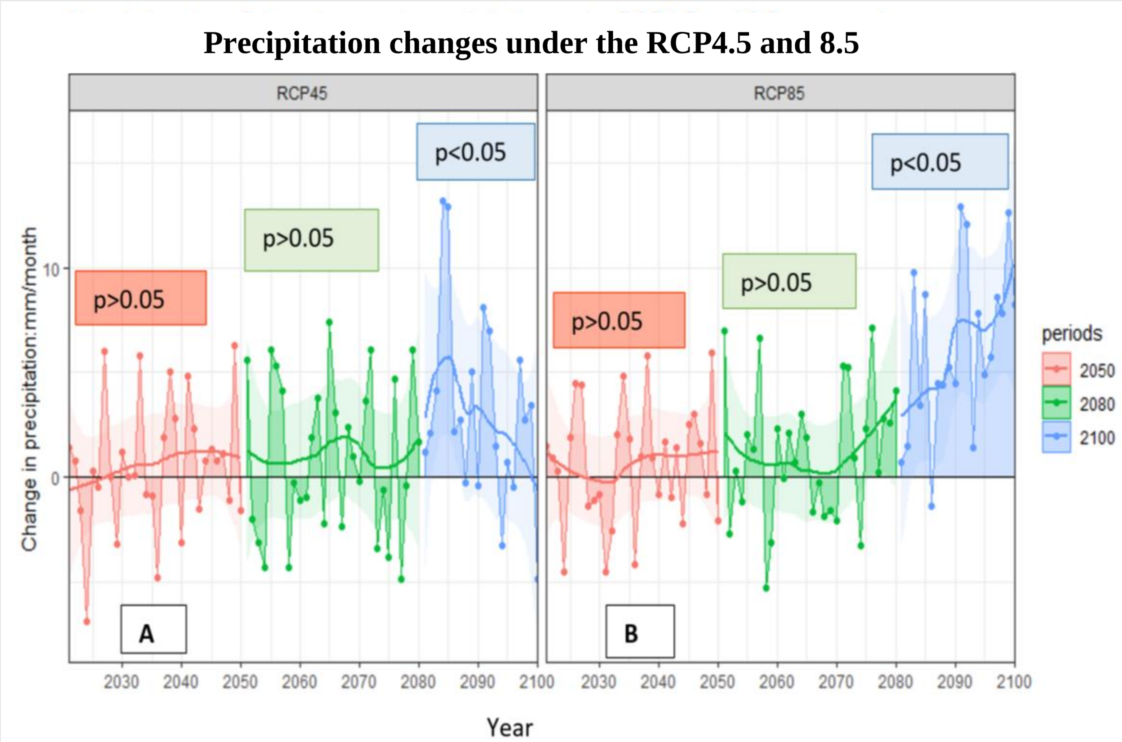

Figure 5-21: Annual cycle of precipitation mean changes under RCP4.5& 8.5
RCP4.5 [A] & RCP8.5[B] show the annual cycle of precipitation mean changes for periods 2021-2050 (2050 time horizon), 2051-2080 (2080 time horizon) and 2071-2100 (2100 time horizon) relative to the period of 1976-2005. Future periods are distinguished by the colour red for 2050, green for the 2080 and blue for the 2100 time-horizons respectively. Positive changes are above the black horizontal line and indicate an increase in precipitation (i.e. wet conditions), while the negative change below the line indicates a decrease in precipitation (i.e. dry conditions). The changing trend for each period under each scenario is summarised by a multimodal mean. P is the P-value (α=0.05) result of the Wilcoxon test between the historical and future periods under both RCP4.5 and RCP8.5 scenarios. The p-values results are coloured to match their respective periods.

For the 2080 time horizon, the number of wet and dry events under the RCP4.5scenario are expected to be about 4.19mm and -2.27mm per month on average. In contrast, under the RCP8.5 scenario, they are expected to be 3.04mm and -2.12mm/per month on average. Thus, it is much wetter under the RCP4.5 than the RCP8.5 for this time horizon. For the 2100 time horizon, the long term future (see Figure 5-21 A&B and detailed in the AppendixA4 (C&F)), dry events are expected to be approximately -1.77mm and -3.27mm per month respectively for the RCP4.5 and 8.5 scenarios. Wet events are estimated at 4.75mm/ month for RCP4.5 and 6.35mm/ month for RCP8.5. The change in rainfall during the long-term future is characterised by wetter and drier events for

RCP4.5 in addition to the wettest and driest for RCP8.5 compared to the previous periods of the near and mid future period. Changes for the 2050 and 2080 time horizons under both RCPs 4.5 and 8.5 is not statistically significant relative to the 1976-2005 period. In contrast however, changes during the period of 2071- 2100 are statistically significant.

5.3.4.1.2.2 Changes in rainfall seasonal cycle under RCPs 4.5 and 8.5

This section explores the potential changes, shown in Figure 5-22 below, in the precipitation seasonal cycles for the periods of 2021-2050, 2051-2080 and 2071-2100.

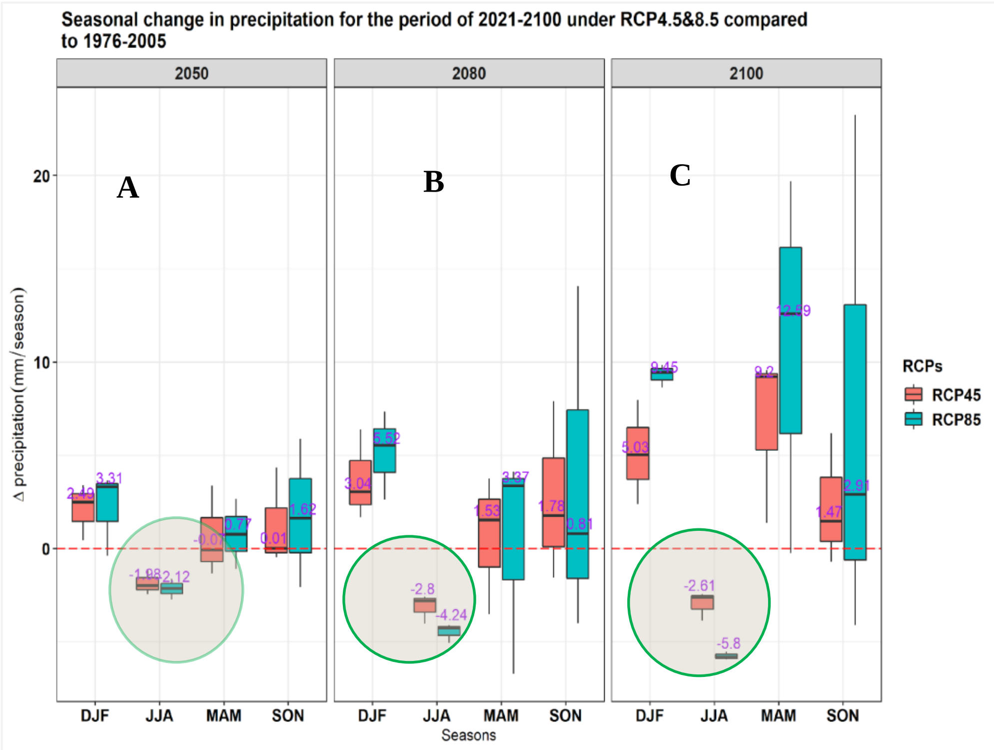

Figure 5-22: Seasonal cycle changes of precipitation under RCP4.5& 8.5
Seasonal cycle changes in rainfall under RCP4.5 are represented in blue and RCP8.5 are represented in red. A, B and C are projected changes respectively for the periods of 2021-2050 (2050 horizon), 2051-2080 (2080 horizon) and 2071-2100 (2100 time horizon). The dashed red line marks the positive and negative values above and below the line respectively. DJF stands for December, January and February, MAM is March April and May, JJA is for June, July and August and SON is for September, October and November. The values (in pink) at each boxplot are the median differences between the RCP4.5 in red and RCP8.5 in blue, relative to 1976-2005. The green circles show dry seasons.

It can be noted from the figures presented that the DJF season is wet under both RCPs and for all periods. Further to this, the DJF season continues to become wetter as time evolves. Although both wet, under RCP8.5 the season is wetter than under RCP4.5 over all time horizons. Also, during the season of DJF, the changes in precipitation difference for the two scenarios are more pronounced at the end of the century. During the period of 2071-2100, the changes in rainfall for the DJF seasons under RCP8.5 are approximately 4.42mm wetter than RCP4.5. In contrast, for the season of MAM, precipitation change is low and tends to be dry under the RCP4.5 scenario.

Under RCP8.5 however, wet conditions are predicted for 2050. During the 2080 horizon, the MAM season is dry under RCP4.5 and wet under RCP8.5. There is a notable difference in rainfall changes under the RCP8.5 and RCP4.5 scenarios for this season, and the variability is much larger under the RCP8.5 scenario. In addition, MAM is wetter during the periods of the 2100-time horizon under both climate scenarios. Under both RCP scenarios and for all the periods, the season of JJA is dry, and as time evolves the season gets drier under RCP8.5 when compared with RCP4.5. This is shown in Figure 5-22 and highlighted in green circles where the value of changes increases negatively. An example of this is evidenced during this season of JJA, where precipitation changes under RCP8.5 are -2.12mm, -4.24mm and -5.8mm per month respectively. The difference in seasonal rainfall cycle changes between the two scenarios, during the season of JJA, is more remarkable during the 2100-time horizon, where the RCP8.5 is -3.13mm per month drier than it is for RCP4.5. With respect to this however, it should be noted that there are more variabilities in the JJA rainfall cycle changes under RCP4.5 than there are under RCP8.5, especially during the 2080 and 2100 time horizons. During the 2050-time horizon, the season of SON is wet under RCP4.5 and is wet with some dry periods under RCP8.5. Further, the season of SON under RCP8.5 has an extensive and considerable rainfall cycle variability when viewed in comparison with the other seasons under both scenarios. The wettest season of all is MAM under RCP8.5. This has an average increase of 12.59mm/month relative to 1976-2005. Overall, the three periods show an increasing trend in precipitation amounts during the seasons of MAM, SON and DJF, while there is a decrease in rainfall during the season of JJA. In addition, these changes in precipitation are more pronounced at the end of the century, than they are in the 2050 and 2080 time-horizons.

In summary, seasonal cycle changes display a continuous increasing trend in the amount of precipitation from the 2050 horizon to the end of this century. The seasons of MAM and SON are the wettest and have large variability in rainfall. Consequently, in the EAC, under both climate scenarios and during the periods of 2021-2100, the seasonal cycle is enhanced as the wet months get wetter and the dry months get drier. JJA is a dry season and becomes drier under the two RCPs, however the rainfall is expected to be higher under RCP8.5 than it is under RCP4.5.

It is very important to note that although the overall changes are showing increasing trends in precipitations, the dry seasons (e.g. JJA) are equally displaying a trend in terms of becoming much drier. This is important to identify because the predicted increase in precipitation is a MMEM trend and has the capacity to mask the dryness in the season of JJA. Hence, the overall predicted increase in precipitation does not contradict the claim that EAC hydropower will be affected by lower levels of rainfall. The seasons of dryness trends will adversely affect the continuous supply of energy from hydropower. This is the reason why complementarity is crucial in smoothing the energy imbalance across the EAC. It also shows what planning needs to take place both for the continuous power supply that will likely be affected by drier dry seasons.

5.3.5 Spatiotemporal future changes in solar radiation under RCPs 4.5 and 8.5

This section investigates the future spatiotemporal changes in solar radiation under the RCP4.5 and RCP8.5 scenarios and is divided into two parts. The first part focuses on the solar radiation changes for each grid over the EAC. The second part examines the changes in solar radiation over the seasonal and annual cycles. Prior to exploring these changes, the MMEM of solar radiation historical seasonal cycles and ERAI observed solar radiation, were compared and analysed. This is shown in Figure 5-23 below.

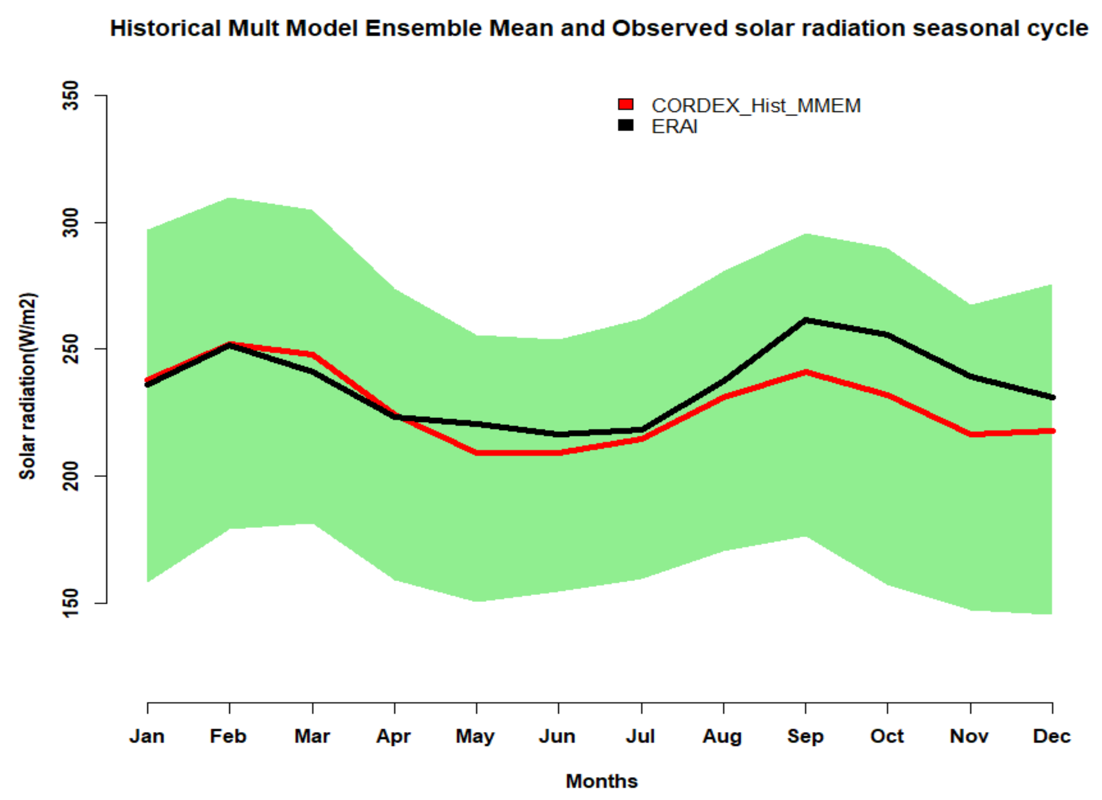

Figure 5-23: MMEM and ERAI (solar radiation) monthly cycle
The MMEM (historical run) is shown in red, and the ERAI (observed) solar radiation monthly cycle is shown by the black line. The green polygon is the MMEM historical solar radiation monthly cycle 90th (top) and 10th (bottom) percentiles.

Figure 5-23 shows that the historical MMEM captures the observed solar radiation for January. It overestimates solar radiation for February and March and underestimates the months of April to December. In general, although the historical MMEM does not exactly fit the observed patterns, its line graph has the same shape and follows the same pattern of change as the observed solar radiation over the region. The discrepancy between the

MMEM and the observed solar radiation patterns will be bias corrected as per Section 7.3.

5.3.5.1 Spatial solar radiation changes over the EAC

Under the RCP4.5scenario, all seventeen EAC_RCM models predicted changes in solar radiation ranging from -5.9W.m^{-2} to +4.57 W.m^{-2}. For each of the seventeen EAC_RCM models, predicted changes and associated statistical significance tests are detailed in Appendix C1. Broadly speaking, the average change between all EAC_RCM models was measured at -2.20 W.m^{-2}. The Wilcoxon statistical test (α=0.05) showed that 15 of the 17 models indicated a significant change in solar radiation spatial distribution patterns. Out of the fifteen, 3 predicted an increase, while 12 predicted a decrease in solar radiation.

Figures 5-24 to Figure 5-29 are maps showing observed (A) and simulated (B) solar radiation regional distributions. Map C illustrates the changes between the observed and simulated solar radiation. As expected, some models projected an increase in solar radiation while others projected a decrease in solar radiation. As a result of this, map D shows the percentage of models that were statistically significant (P-Value <α, where α=0.05) with an agreement on the increase, no changes and a decrease in solar radiation. As already stated, the white colour in the baseline map (A) shows outliers. Due to the fact that the results from the maps share most of the features and, in order to avoid unnecessary repetition, Figures 5-24 to Figure 5-29 are denoted as Figure 5-24:29 and will be analysed together. Further analysis and interpretation will be similar to the previously mentioned process for the discussion of precipitation results as in Section 5.3.4.1.1.

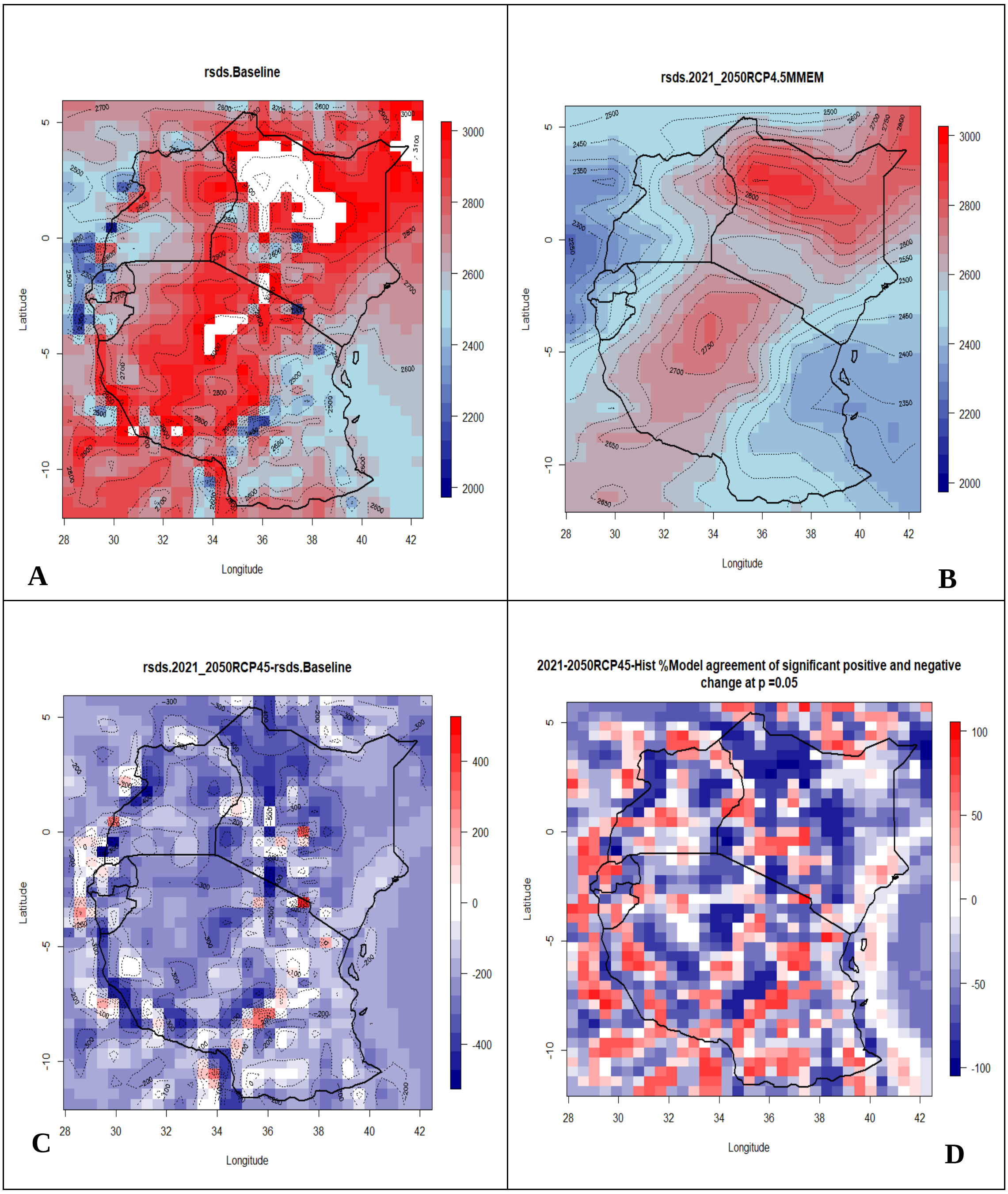

Figure 5-24: Spatial changes in solar radiation (W/m2 per month) for the period of 2021-2050 under RCP4.5 over the EAC

Colours should be used to read precipitation distribution for subfigures (A&B) and changes for subfigure (C) while the contours on the maps provide values for spatial variability. Subfigure A [baseline] is historical MMEM, the white colour shows grids where there are outliers. Subfigure B is solar radiation MMEM under RCP4.5for 2021-2050 (2050-time horizon). Subfigure C is a map showing changes between the 2050 time horizon and the baseline. The changes are represented by a blue colour for fields where solar radiation is decreasing, white colour is where there is no change, and red indicates an area where solar radiation is increasing. Subfigure D is a map showing the percentage of models that are in agreement on positive changes (red), negative changes (blue) and such agreement is statistically significant at α=0.05. White colour (subfigure D) indicates that model agreements are statistically not significant.

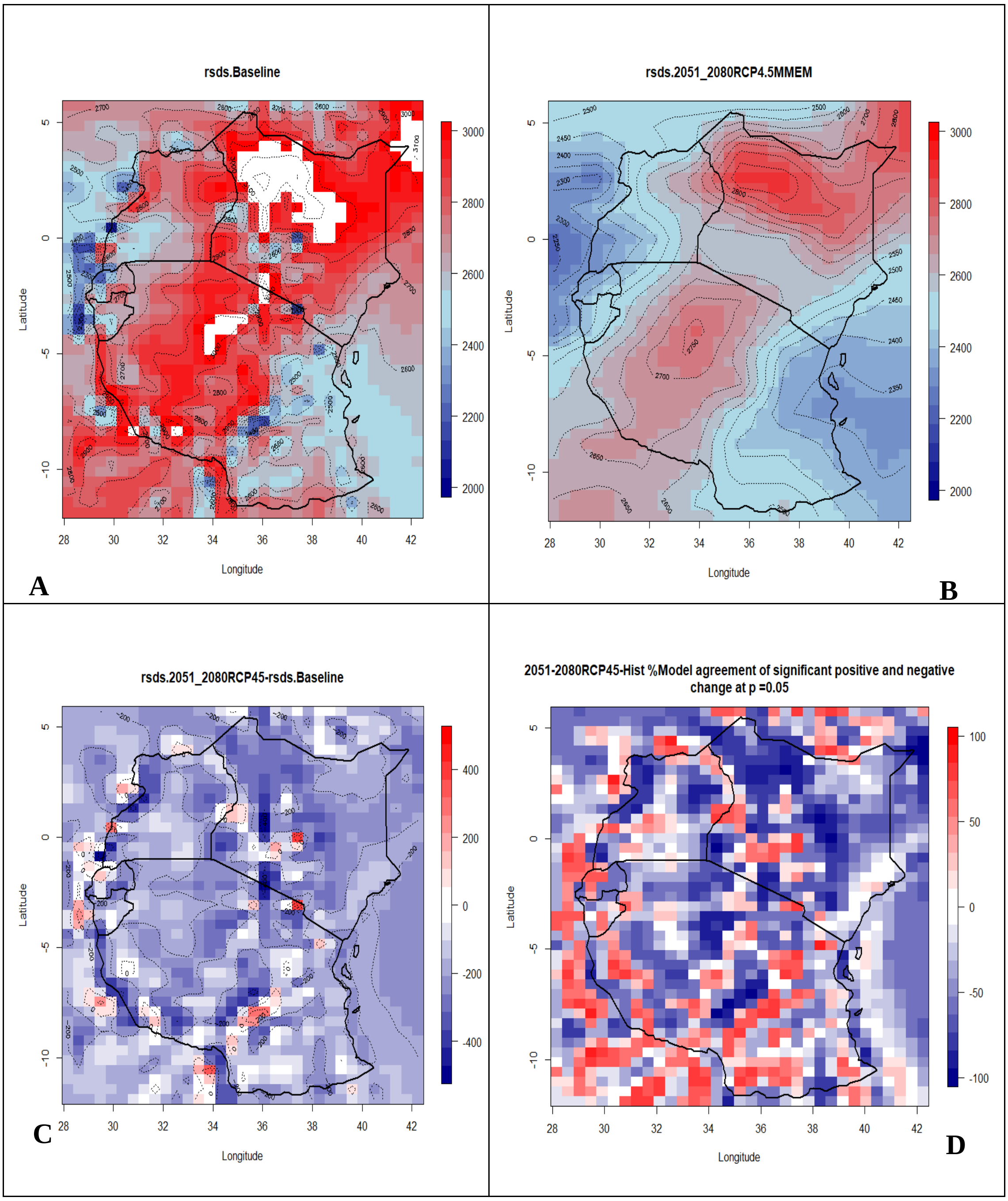

Figure 5-25: Spatial changes in solar radiation (W/m² per month) for the period of 2051-2080 under RCP4.5 over the EAC

Colours should be used to read solar radiation distribution for subfigures (A&B) and changes for subfigure (C) while the contours on the maps provide values for spatial variability. Subfigure A [baseline] is historical MMEM, the white colour shows grids where there are outliers. Subfigure B is solar radiation MMEM under RCP4.5for 2051-2080 (2080-time horizon). Subfigure C is a map showing changes between the 2080 time horizon and the baseline. The changes are represented by a blue colour for fields where solar radiation is decreasing, white colour is where there is no change, and red indicates an area where solar radiation is increasing. Subfigure D is a map showing the percentage of models that are in agreement on positive changes (red), negative changes (blue) and such agreement is statistically significant at α=0.05. White colour (subfigure D) indicates that model agreements are statistically not significant.

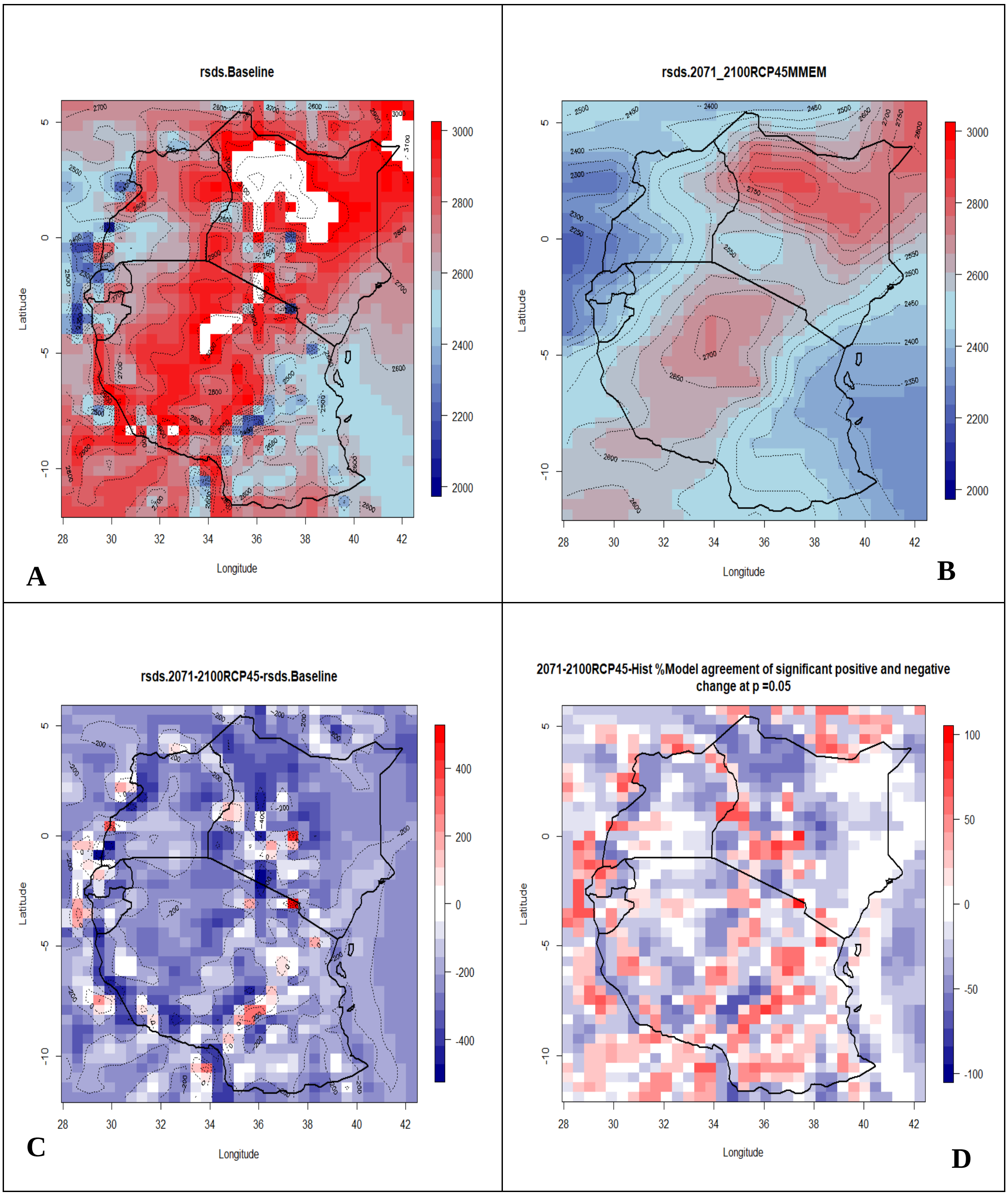

Figure 5-26: Spatial changes in solar radiation (W/m2 per month) for the period of 2071-2100 under RCP4.5 over the EAC

Colours should be used to read solar radiation distribution for subfigures (A&B) and changes for subfigure (C) while the contours on the maps provide values for spatial variability. Subfigure A [baseline] is historical MMEM, the white colour shows grids where there are outliers. Subfigure B is solar radiation MMEM under RCP4.5for 2071-2100 (2100-time horizon). Subfigure C is a map showing changes between the 2100time horizon and the baseline. The changes are represented by a blue colour for fields where solar radiation is decreasing, white colour is where there is no change, and red indicates an area where solar radiation is increasing. Subfigure D is a map showing the percentage of models that are in agreement on positive changes (red), negative changes (blue) and such agreement is statistically significant at α=0.05. White colour (subfigure D) indicates that model agreements are statistically not significant.

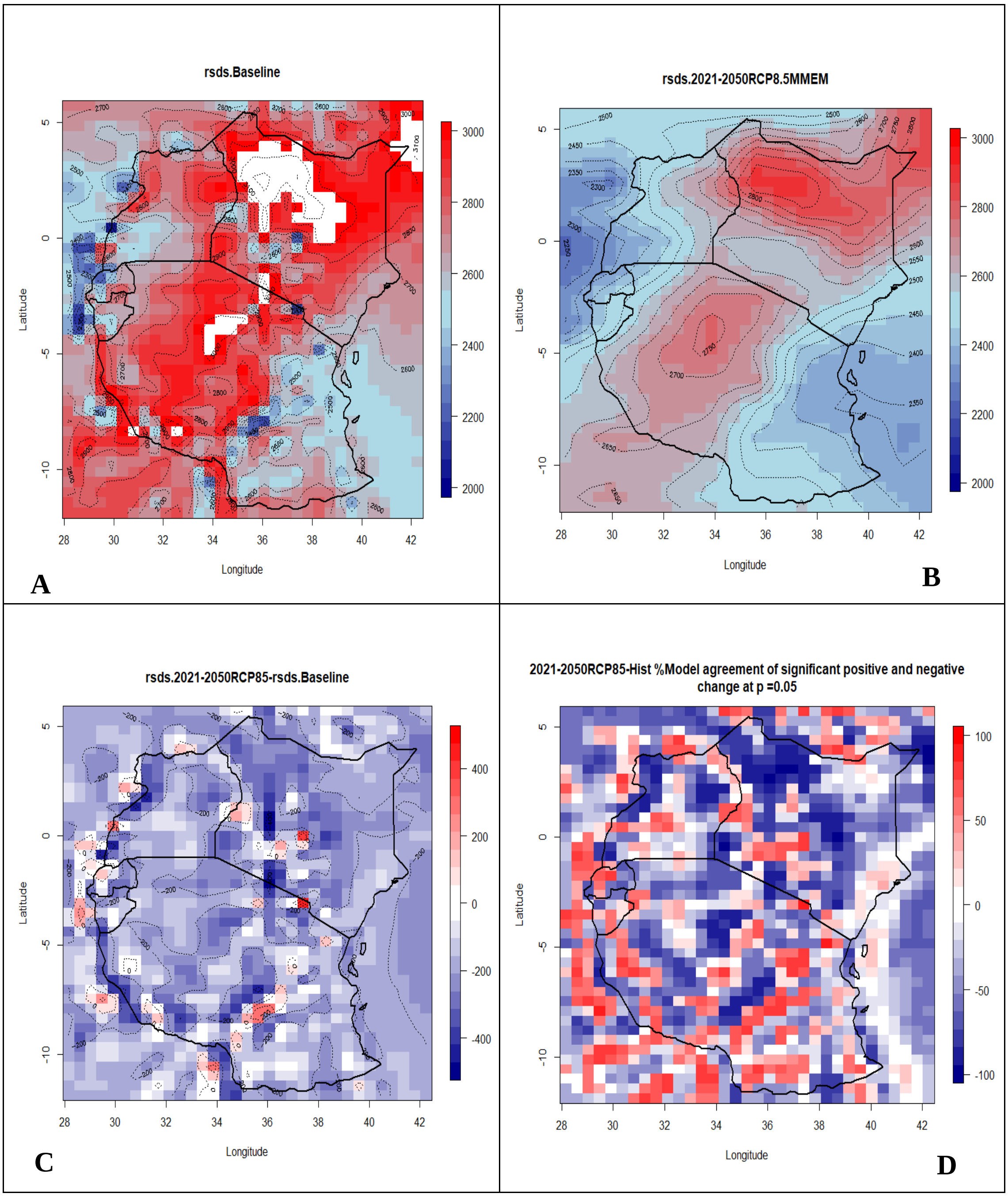

Figure 5-27: Spatial changes in solar radiation (W/m2 per month) for the period of 2021-2050 under RCP8.5 over the EAC

Colours should be used to read solar radiation distribution for subfigures (A&B) and changes for subfigure (C) while the contours on the maps provide values for spatial variability. Subfigure A [baseline] is historical MMEM, the white colour shows grids where there are outliers. Subfigure B is solar radiation MMEM under RCP8.5 for 2021-2050 (2050-time horizon). Subfigure C is a map showing changes between the 2050 time horizon and the baseline. The changes are represented by a blue colour for fields where solar radiation is decreasing, white colour is where there is no change, and red indicates an area where solar radiation is increasing. Subfigure D is a map showing the percentage of models that are in agreement on positive changes (red), negative changes (blue) and such agreement is statistically significant at α=0.05. White colour (subfigure D) indicates that model agreements are statistically not significant.

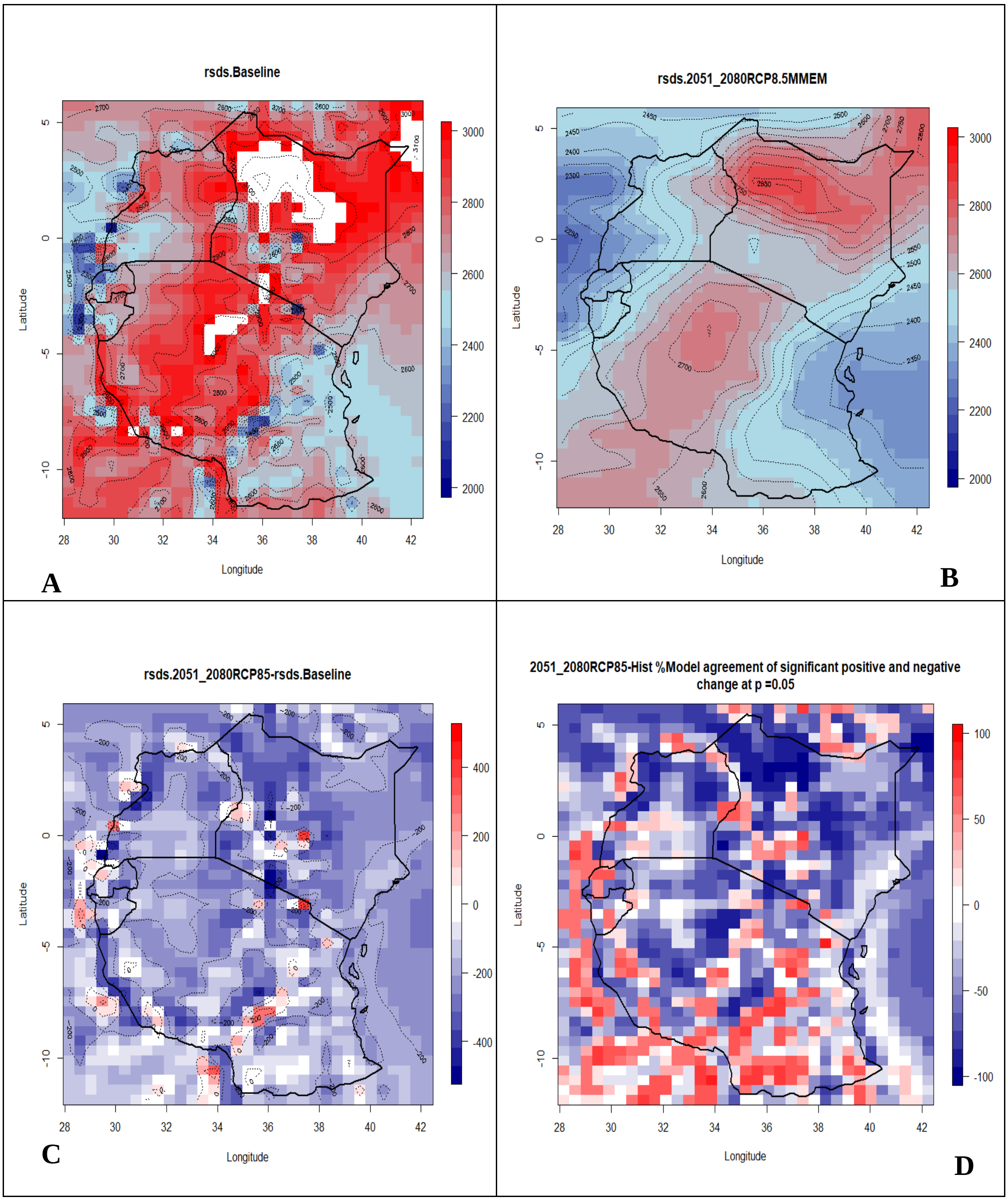

Figure 5-28: Spatial changes in solar radiation (W/m2 per month) for the period of 2051-2080 under RCP8.5 over the EAC

Colours should be used to read solar radiation distribution for subfigures (A&B) and changes for subfigure (C) while the contours on the maps provide values for spatial variability. Subfigure A [baseline] is historical MMEM, the white colour shows grids where there are outliers. Subfigure B is solar radiation MMEM under RCP8.5 for 2051-2080 (2080-time horizon). Subfigure C is a map showing changes between the 2080 time horizon and the baseline. The changes are represented by a blue colour for fields where solar radiation is decreasing, white colour is where there is no change, and red indicates an area where solar radiation is increasing. Subfigure D is a map showing the percentage of models that are in agreement on positive changes (red), negative changes (blue) and such agreement is statistically significant at α=0.05. White colour (subfigure D) indicates that model agreements are statistically not significant.

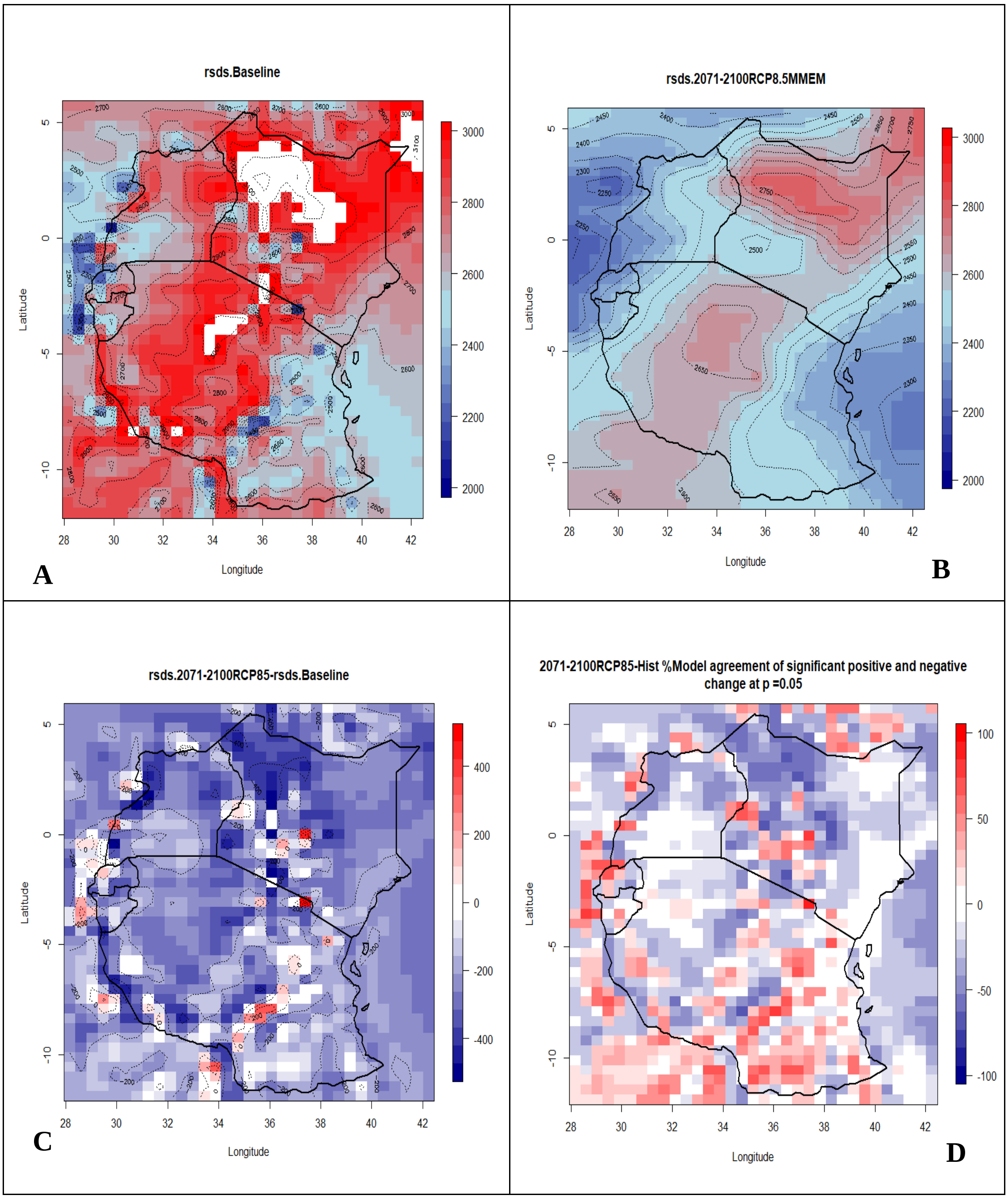

Figure 5-29: Spatial changes in solar radiation (W/m2 per month) for the period of 2071-2100 under RCP8.5 over the EAC

Colours should be used to read solar radiation distribution for subfigures (A&B) and changes for subfigure (C) while the contours on the maps provide values for spatial variability. Subfigure A [baseline] is historical MMEM, the white colour shows grids where there are outliers. Subfigure B is solar radiation MMEM under RCP8.5 for 2071-2100 (2100-time horizon). Subfigure C is a map showing changes between the 2100time horizon and the baseline. The changes are represented by a blue colour for fields where solar radiation is decreasing, white colour is where there is no change, and red indicates an area where solar radiation is increasing. Subfigure D is a map showing the percentage of models that are in agreement on positive changes (red), negative changes (blue) and such agreement is statistically significant at α=0.05. White colour (subfigure D) indicates that model agreements are statistically not significant.

Under the RCP8.5 climate scenario, all EAC_RCM models predicted changes in the spatial distribution of solar irradiance ranging from -7.77 $W.m^{-2}$ to +5.8.5 $W.m^{-2}$. The average change between models was estimated at -3.67W/m2. It should also be noted that under RCP8.5, 15 out of 17 of the models indicated a significant change. Out of the 15 models, 12 indicated a decrease while 3 predicted an increase in solar irradiance. A more detailed breakdown of the changes and the associated significance tests are given in Appendix C1. For the EAC, both the spatiotemporal changes for solar irradiance and the percentage differences in the predictions of the models for the 2021-2100 period under RCP4.5 and 8.5 can be inferred from Figure 5-9. Figures 5-24:29 (A) shows that the observed radiation is high relative to future solar radiation under the RC P4.5 and 8.5 scenarios shown in Figure 5-24:29 (B). The highest observed solar radiation measures at over 3000 $W.m^{-2}$ in both the central and northern part of Kenya, as well as in the central area of Tanzania. From Figures 5-24:29 (A and B), it can be seen that under RCP4.5 and 8.5, solar radiation in most parts of Kenya and the western part of Uganda extending to the south-west of Tanzania forms a belt. This is because these regions have the highest solar irradiance (between 2500 -3000 $W.m^{-2}$) when compared to the rest of the EAC.

The lowest average annual solar radiation in the future under the two-climate scenarios (about 220W/m2) is projected for the western part of Uganda, extending to the south-west of Burundi as well as the eastern part of Tanzania. The projected spatiotemporal changes in solar radiation can be read from Figures 5-24:29(C) under both RCP4.5 and 8.5. For all periods (2021to 2100) and under both climate scenarios, there is a large decrease in the projected solar radiation, as most of the EAC area is dominated by negative change grids (blue colour).

Overall, there is a significant percentage of models that statistically (P-value $<\alpha$) agree on negative changes from the west to the north of Tanzania, extending to Uganda, thus a statistical significance test was required. The statistical significance test indicated that there was no significant difference in the changes in solar between RCP4.5 and 8.5. Although there is a fluctuation in the projected solar irradiance in the EAC, the region will still receive 5kWh on average between the periods of 2021-2100.

5.3.5.2 Future temporal change in solar irradiance under RCP4.5 and 8.5

The previous section assessed the spatial distribution of changes in solar irradiance for the period of 2021-2100 compared to the period of 1976-2005 under RCP4.5 and 8.5. This section assesses the average change over the EAC, in terms of both the seasonal and monthly mean annual cycle of changes in solar irradiance under the RCP4.5 and 8.5 scenarios for the near-future periods of 2021-2050, mid-future periods of 2051-2080 and long-term future periods of 2071-2100.

5.3.5.2.1 The potential monthly mean annual cycle of changes in solar irradiance

The monthly mean annual cycle of change in solar irradiance can be inferred from Figure 5-11 (A, B). From the analysis, it could be suggested that there is a general tendency for decreasing solar irradiance in the near and mid future periods under both RCP4.5 and 8.5. The decrease is more pronounced during the mid-future than it is for the near future and long-term future periods. Under RCP4.5, solar irradiance decreases for the first half of the long-term future and exhibits a tendency to increase for the second half of this period. In contrast, RCP8.5 has a trend of overall negative change.

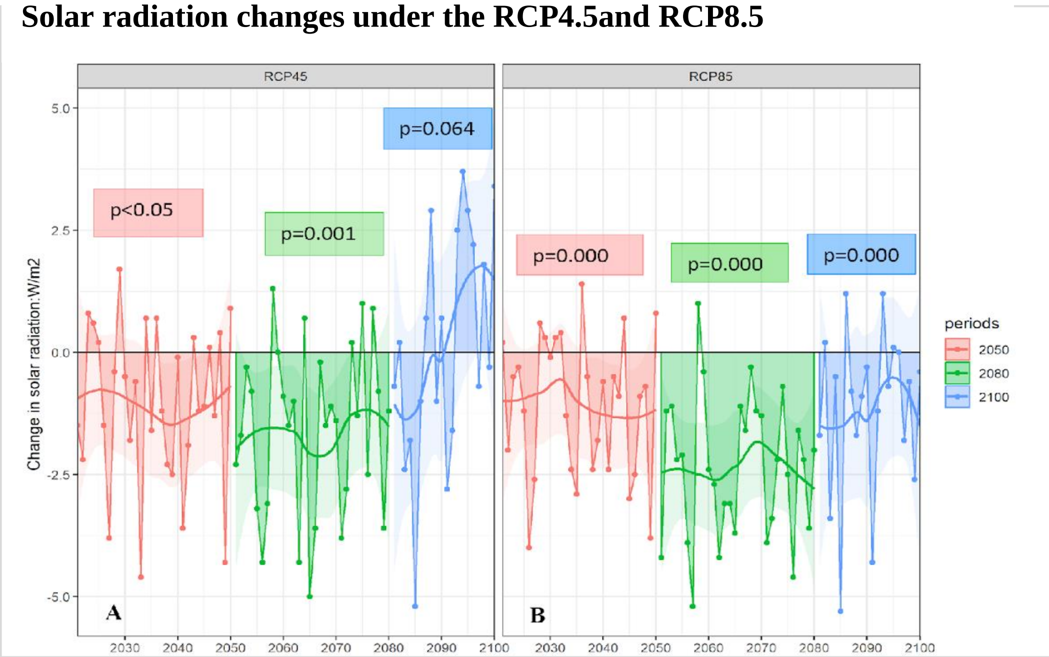

Figure 5-30: Monthly mean annual cycle of solar irradiance changes under RCPs 4.5 & 8.5

RCP4.5[A] & RCP8.5[B] are the monthly mean annual cycle of changes in solar irradiance for periods 2021-2050, 2051-2080 and 2071-2100 respectively, compared to the period of 1976-2005. The periods are distinguished by a red colour for 2050, green for 2080 and blue for the 2100 time-horizons. Above the black horizontal line marks a positive change (i.e. increase in the monthly mean annual cycle of solar irradiance), below the line marks a negative change (i.e. a decrease in the monthly mean annual cycle of irradiance) and the change trend for each period under each scenario is summarised by a multimodal mean. P is the P-value result of the Wilcoxon test between historical and future periods under both RCP4.5 and 8.5. The p-values are coloured to match their respective periods.

Solar radiation changes are much more noticeable in the 2051-2080 period compared to the 2021-2050 and 2071-2100 periods for both scenarios. The near future has a relatively low decrease in solar irradiance under both RCPs 4.5 and 8.5, while the long-term future has a positive trend for the periods of the 2100-time horizon under RCP4.5. Overall, under RCP4.5, a decrease in solar irradiance for the periods of 2021-2050 to the first half of 2071-2100 is expected. An increase is then expected during the second half of 2071-2100. Under RCP8.5, the solar irradiance generally decreases for the 2021-2100 period. The statistical significance test for solar irradiance changes under both RCP4.5 and 8.5 gives a p-value of less than $\alpha=0.05$ (p-value< α) for all periods, except for the period of 2071-2100 under RCP4.5. This result suggests that under both RCPs 8.5 and 4.5 with the exception of 2071-2100 under RCP4.5 where the change was not significant, the EAC expects a decrease in solar irradiance from 2021 to 2100 compared to 1976-2005.

5.3.5.2.2 Seasonal change in solar irradiance across the EAC

The seasonal changes in solar radiation across the EAC under RCPs 4.5 and 8.5 can be inferred from Figure 5-31.

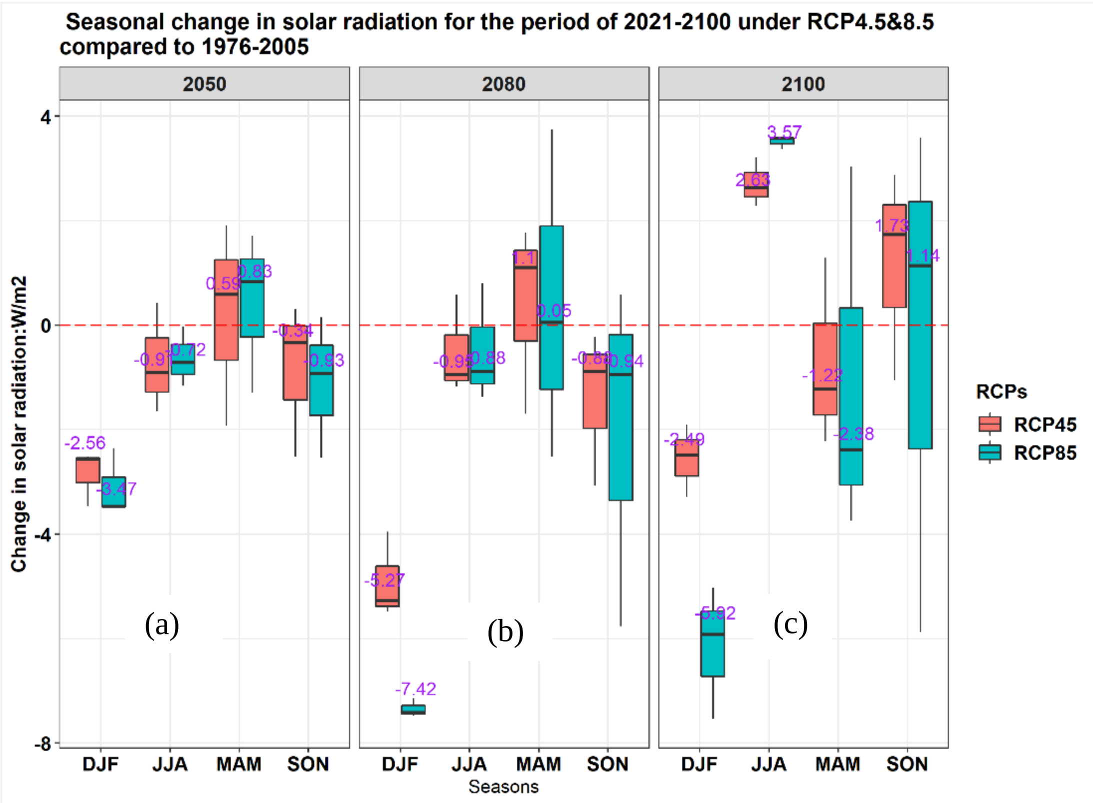

Figure 5-31: Seasonal cycle changes in solar radiation
Boxplots for seasonal cycle changes in solar radiation across the EAC under RCP4.5 and 8.5 are represented by a blue and red colour respectively. (a), (b) and (c) represent respectively changes during the period of near-future (2050-time horizon), mid-future (2080-time horizon) and long-term future (2100 time-horizon). The dashed red line marks positive and negative changes above and below the line respectively. DJF is for December-February, MAM is March-May, JJA is for June -August and SON is for the September- November seasons. The values (in pink) at each boxplot are the median difference between the baseline period (1976-2005) and RCP4.5 (in red) and RCP8.5(in blue).

Looking at Figure 5-31 (a-c), it can be observed that there is a decrease in solar radiation during the DJF cycle under both RCPs 4.5 and 8.5 scenarios, the change being greater in RCP8.5. The difference in the change between the two scenarios is observed during both the mid (e.g., - 7.42 W/m2 for JJA) and long-term future (e.g., -5.92W/m2 for DJF) as can be seen in Figure 5-31 (b) and (c). Correspondingly, there is a greater solar radiation change variability for DJF under RCP8.5 during the period of 2071-2100 compared to the RCP4.5. Figure 5-31 (a)-(c) also indicates that the MAM change in solar radiation increases during the period of 2050 and 2080, whilst there is a pronounced decrease during the periods of the 2100 time-horizon. The variability of change continues to increase as time passes and is more pronounced in the RCP8.5 scenario. JJA is characterised by a solar irradiation decrease under RCP4.5 and 8.5 scenarios during the near and mid future periods, while the long-term future is dominated by an increase in solar radiation under both RCP4.5 and 8.5. In regard to this, the increase is greater in RCP8.5. Moreover, solar radiation change variability is less in the JJA season during 2071-2100 when compared to the previous periods. The change in solar radiation for the SON seasonal patterns are different from those of MAM as previously discussed. Overall, the changes in the solar radiation seasonal cycle tend to decrease for all periods under both RCP4.5 and 8.5. However, solar radiation does show an increase in both the MAM cycle between 2050 and 2080 time horizons and in the JJA and SON seasons during the 2100 period.

In summary, the aim of Section 5.4.3 was to assess the spatiotemporal change in solar irradiance for the period of 2021-2100 when compared to 1976-2005. The analysis has led to the conclusion that the EAC could expect a slight decrease in solar irradiance for both RCP4.5 and 8.5. It is also important to highlight here that the analysis suggests that there is no significant difference in the predicted changes under the two climate scenarios. The assessment of future temporal solar irradiance changes under the two climate scenarios was also conducted for both seasonal and monthly annual cycles of changes in solar irradiance. It was found that there is a significant decrease in solar radiation under both RCPs 4.5 and 8.5 climate scenarios for all periods. This is with the exception of the period of 2071-2100 which showed no significant change in solar irradiance under

RCP4.5. For seasonal cycle changes, solar irradiance generally tended to decrease across 2021-2050, 2051-2080 and 2071-2100 periods. This is with the exception of the season of MAM during the periods of 2050 and 2080 under both RCPs 4.5 and 8.5, in addition to the seasons of JJA and SON during the period of 2100 under RCP8.5. The next section explores the potential spatial and temporal future changes in wind speed under RCPs 4.5 and 8.5.

5.3.6 Spatiotemporal future changes in wind speed under RCPs 4.5 and 8.5

The spatiotemporal future changes of wind speed under RCPs 4.5 and 8.5 are delivered in two parts: the first part investigates the temporal changes for each grid over the region of study, and the second part focuses on the annual and seasonal cycle mean wind speed changes. Prior to exploring these changes, an analysis of the MMEM historical seasonal cycle, relative to the ERAI observed wind speed, as shown in Figure 5-32, has been undertaken.

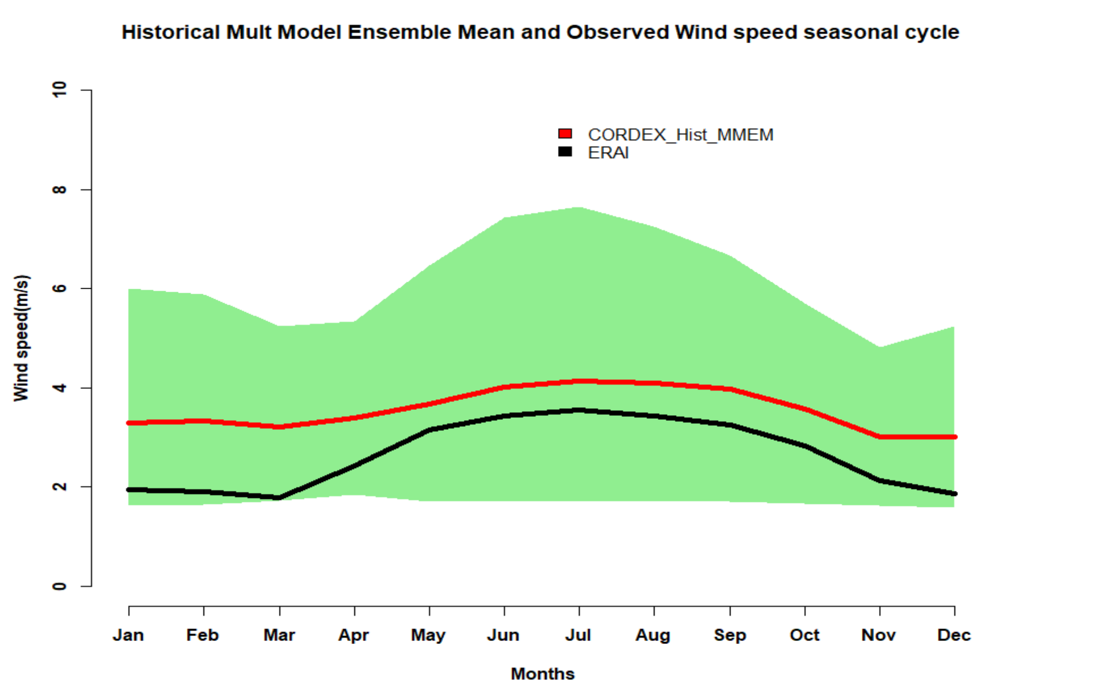

Figure 5-32: MMEM historical and ERAI wind speed monthly cycle
The MMEM (historical run) is shown in red, and the ERAI (observed) temperature monthly cycle is shown with the black line. The green polygon is the MMEM historical temperature monthly cycle 90th (top) and 10th (bottom) percentiles.

It can be observed from Figure 5-32 that the MMEM historical seasonal cycle overestimates the wind speed for all months throughout the year. Wind speed is overestimated more during the months of January to March than in the remainder of the year. Looking at the lines graph for the MMEM historical run and ERAI, it can be seen that as the MMEM historical run increases, the ERAI increases correspondingly. Interestingly, as MMEM historical run decreases, the ERAI also decreases. This means that although the MMEM did not adequately capture the observed wind speed, it has nevertheless produced the expected wind speed patterns in the region.

5.3.6.1 Spatiotemporal wind speed changes under RCP4.5 and 8.5 over the EAC

During 2021-2100 under both RCP4.5 and 8.5 scenarios (Appendix D1 & 2), 6 models out of 17 indicated a significant increase in wind speed, whilst 11 showed no significant changes in the region. It is also worth noting that there was no significant difference in wind changes between the two climate scenarios. The spatiotemporal change in wind speed over the EAC under RCPs 4.5 and 8.5 can be inferred from Figures 5-33 to 5-38. The results from these figures share most features. As a result of this, Figures 5-33 to 5-38 are denoted Figure 5-33: 38. Figure 5-33:38 (A) and (B) are the observed and MMEM wind speed respectively. Figure 5-33:38 (C) are wind speed changes relative to the observed and Figure 5-33:38 (D) are maps showing the percentages of models that significantly agree on positive or negative changes. Further analysis and interpretation will be similar to the process for the discussion of precipitation results as previously discussed in Section 5.3.4.1.

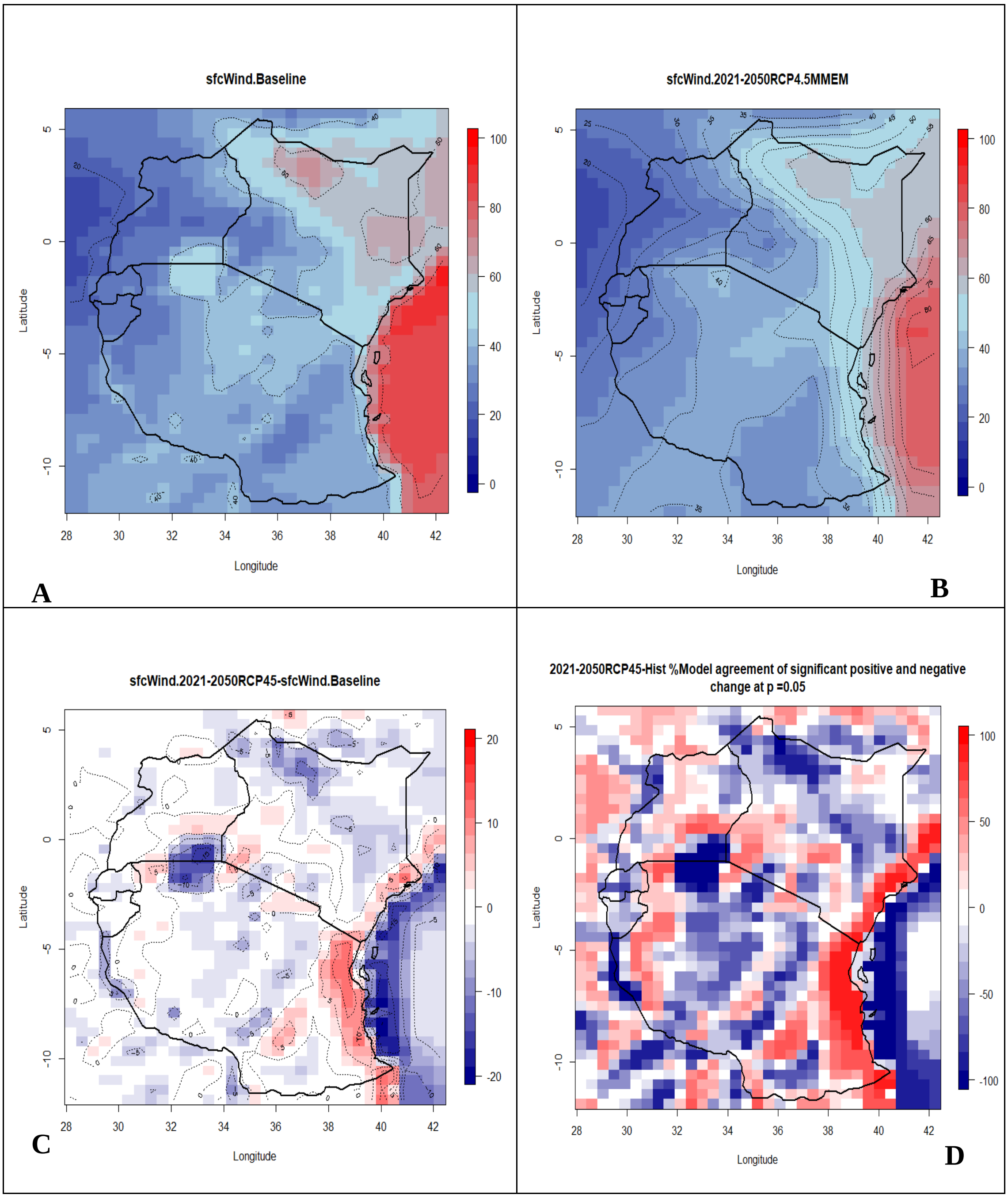

Figure 5-33: Spatial changes in wind speed (m/s) for the period of 2021-2050 under RCP4.5 over the EAC

Colours should be used to read wind speed distribution for subfigures (A&B) and changes for subfigure (C) while the contours on the maps provide values for spatial variability. Subfigure A [baseline] is historical MMEM, the white colour shows grids where there are outliers. Subfigure B is wind speed MMEM under RCP4.5 for 2021-2050 (2050-time horizon). Subfigure C is a map showing changes between the 2050 time horizon and the baseline. The changes are represented by a blue colour for fields where wind speed is decreasing, white colour is where there is no change, and red indicates an area where wind speed is increasing. Subfigure D is a map showing the percentage of models that are in agreement on positive changes (red), negative changes (blue) and such agreement is statistically significant at α=0.05. White colour (subfigure D) indicates that model agreements are statistically not significant

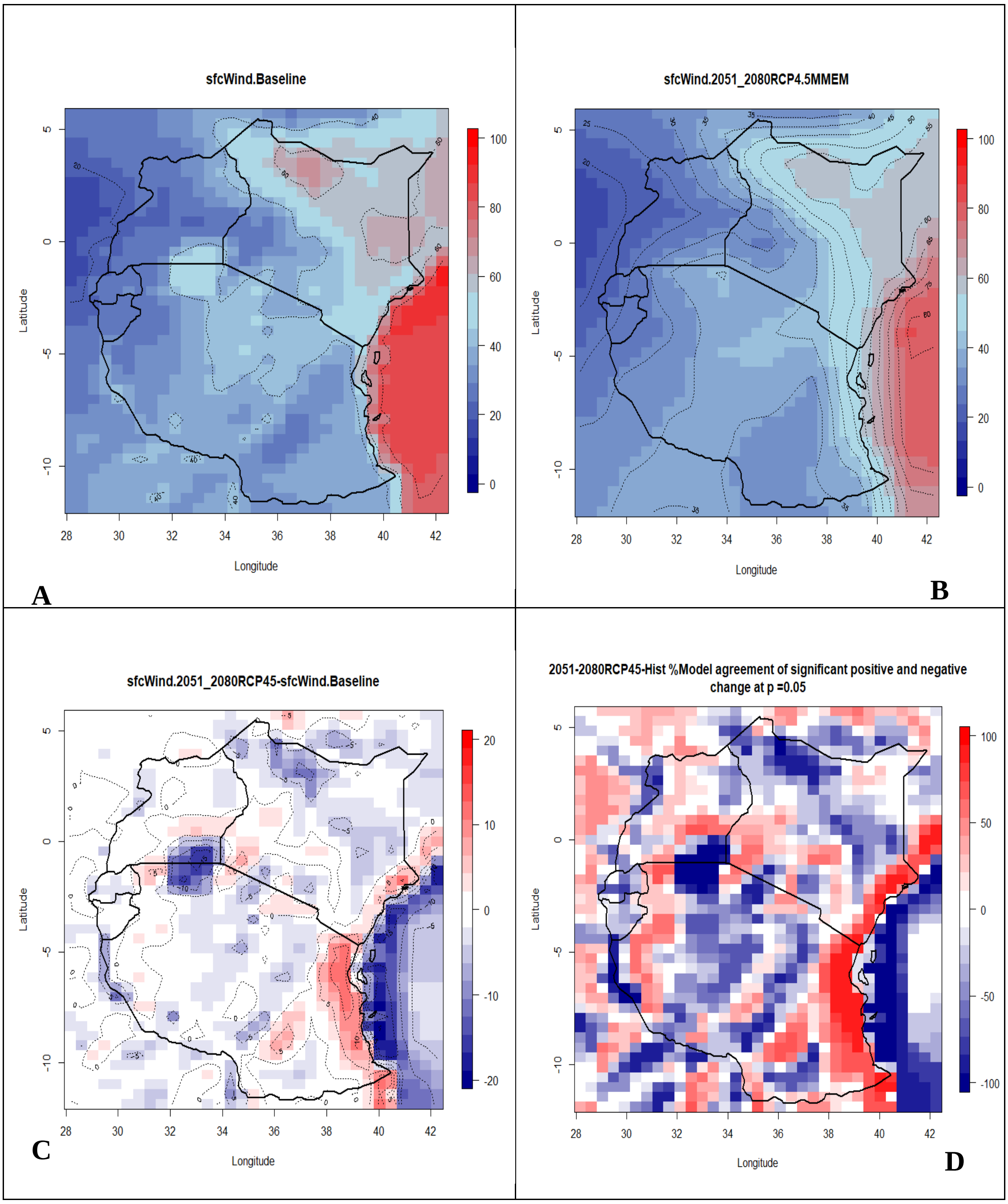

Figure 5-34: Spatial changes in wind speed (m/s) for the period of 2051-2080 under RCP4.5 over the EAC

Colours should be used to read wind speed distribution for subfigures (A&B) and changes for subfigure (C) while the contours on the maps provide values for spatial variability. Subfigure A [baseline] is historical MMEM, the white colour shows grids where there are outliers. Subfigure B is wind speed MMEM under RCP4.5 for 2051-2080 (2080-time horizon). Subfigure C is a map showing changes between the 2080 time horizon and the baseline. The changes are represented by a blue colour for fields where wind speed is decreasing, white colour is where there is no change, and red indicates an area where wind speed is increasing. Subfigure D is a map showing the percentage of models that are in agreement on positive changes (red), negative changes (blue) and such agreement is statistically significant at α=0.05. White colour (subfigure D) indicates that model agreements are statistically not significant.

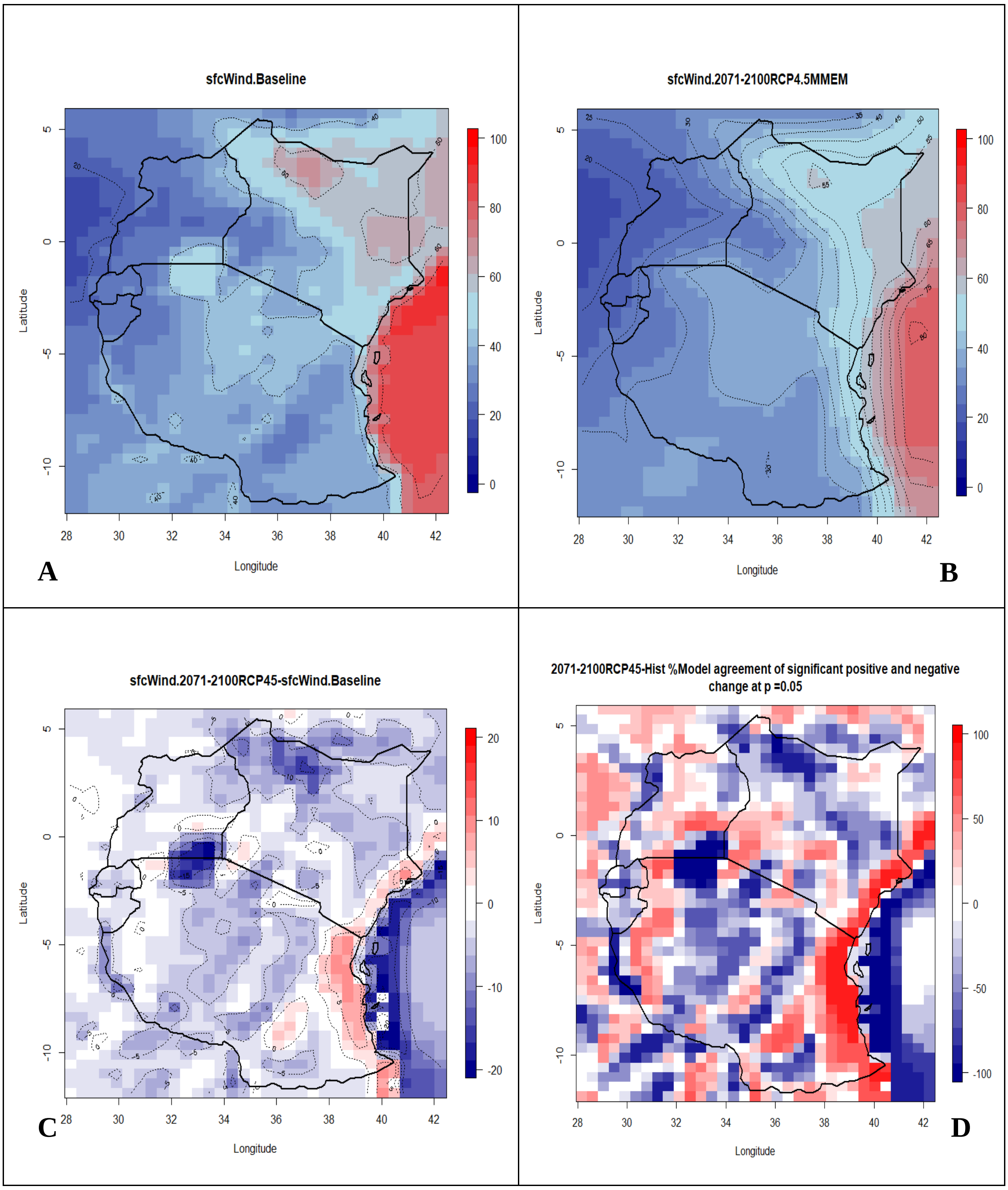

Figure 5-35: Spatial changes in wind speed (m/s) for the period of 2071-2100 under RCP4.5 over the EAC

Colours should be used to read wind speed distribution for subfigures (A&B) and changes for subfigure (C) while the contours on the maps provide values for spatial variability. Subfigure A [baseline] is historical MMEM, the white colour shows grids where there are outliers. Subfigure B is wind speed MMEM under RCP4.5 for 2071-2100 (2100-time horizon). Subfigure C is a map showing changes between the 2100time horizon and the baseline. The changes are represented by a blue colour for fields where wind speed is decreasing, white colour is where there is no change, and red indicates an area where wind speed is increasing. Subfigure D is a map showing the percentage of models that are in agreement on positive changes (red), negative changes (blue) and such agreement is statistically significant at α=0.05. White colour (subfigure D) indicates that model agreements are statistically not significant.

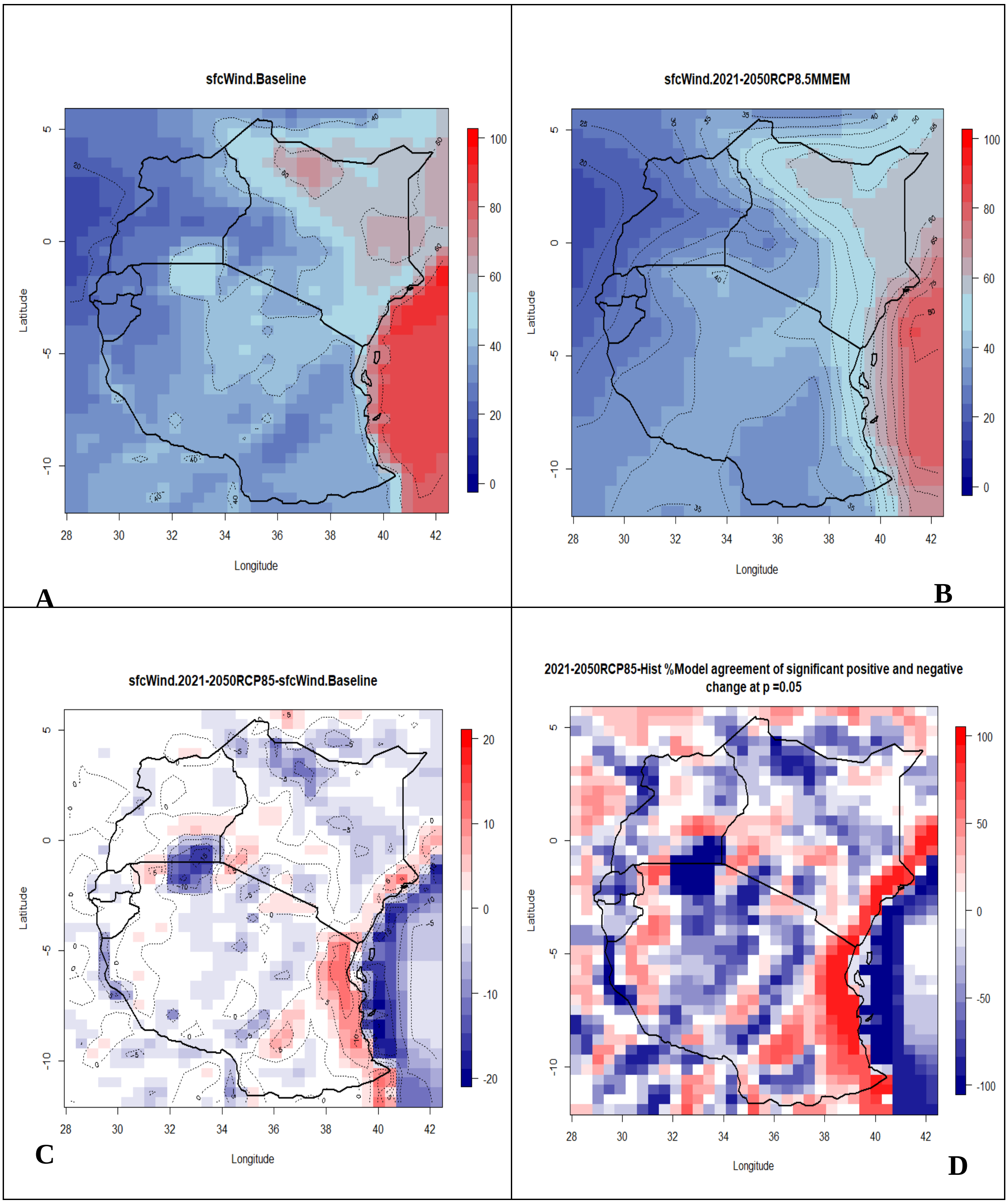

Figure 5-36: Spatial changes in wind speed (m/s) for the period of 2021-2050 under RCP8.5 over the EAC

Colours should be used to read wind speed distribution for subfigures (A&B) and changes for subfigure (C) while the contours on the maps provide values for spatial variability. Subfigure A [baseline] is historical MMEM, the white colour shows grids where there are outliers. Subfigure B is wind speed MMEM under RCP8.5 for 2021-2050 (2050-time horizon). Subfigure C is a map showing changes between the 2050 time horizon and the baseline. The changes are represented by a blue colour for fields where wind speed is decreasing, white colour is where there is no change, and red indicates an area where wind speed is increasing. Subfigure D is a map showing the percentage of models that are in agreement on positive changes (red), negative changes (blue) and such agreement is statistically significant at α=0.05. White colour (subfigure D) indicates that model agreements are statistically not significant.

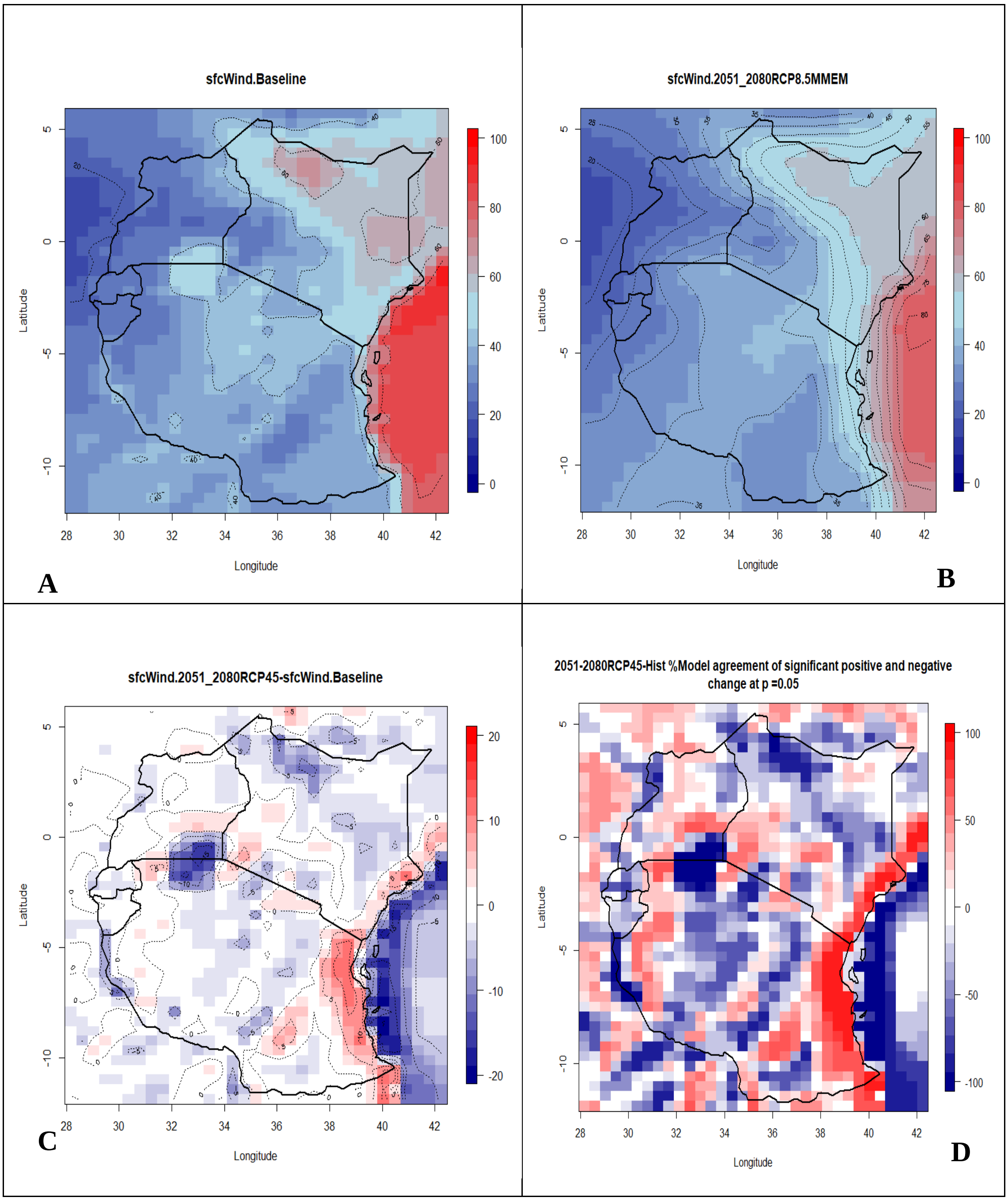

Figure 5-37: Spatial changes in wind speed (m/s) for the period of 2051-2080 under RCP8.5 over the EAC

Colours should be used to read wind speed distribution for subfigures (A&B) and changes for subfigure (C) while the contours on the maps provide values for spatial variability. Subfigure A [baseline] is historical MMEM, the white colour shows grids where there are outliers. Subfigure B is wind speed MMEM under RCP8.5 for 2051-2080 (2080-time horizon). Subfigure C is a map showing changes between the 2080 time horizon and the baseline. The changes are represented by a blue colour for fields where wind speed is decreasing, white colour is where there is no change, and red indicates an area where wind speed is increasing. Subfigure D is a map showing the percentage of models that are in agreement on positive changes (red), negative changes (blue) and such agreement is statistically significant at α=0.05. White colour (subfigure D) indicates that model agreements are statistically not significant.

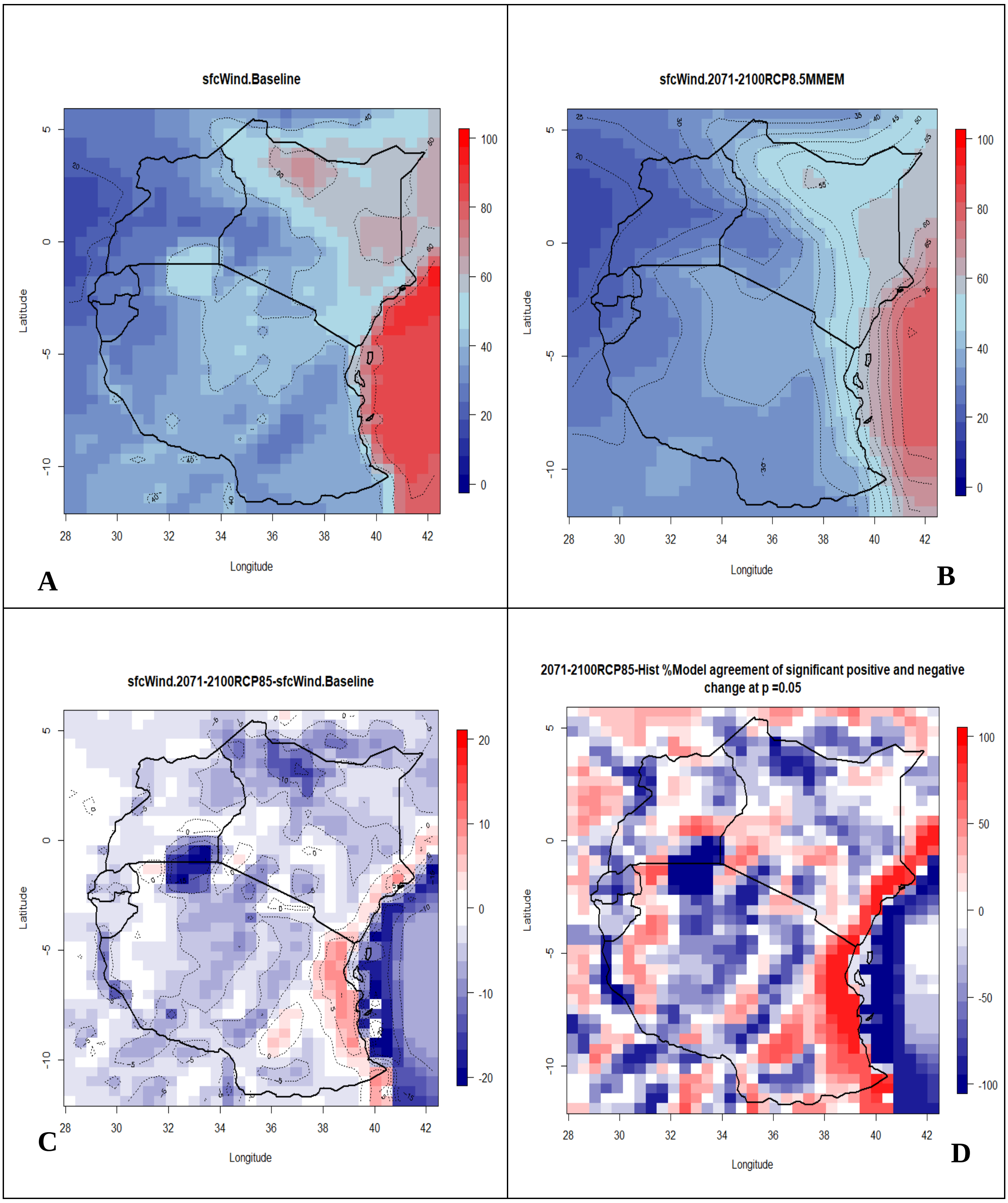

Figure 5-38: Spatial changes in wind speed (m/s) for the period of 2071-2100 under RCP8.5 over the EAC

Colours should be used to read wind speed distribution for subfigures (A&B) and changes for subfigure (C) while the contours on the maps provide values for spatial variability. Subfigure A [baseline] is historical MMEM, the white colour shows grids where there are outliers. Subfigure B is wind speed MMEM under RCP8.5 for 2071-2100 (2100-time horizon). Subfigure C is a map showing changes between the 2100 time horizon and the baseline. The changes are represented by a blue colour for fields where wind speed is decreasing, white colour is where there is no change, and red indicates an area where wind speed is increasing. Subfigure D is a map showing the percentage of models that are in agreement on positive changes (red), negative changes (blue) and such agreement is statistically significant at α=0.05. White colour (subfigure D) indicates that model agreements are statistically not significant.

Looking at the observed wind speed over the EAC region as presented in Figure 5-33:38 (A), wind speed is high in Kenya, with the exception of the western part which extends to Uganda. Further to this, a large part of Uganda and extending to Rwanda and Burundi as well as a large part of north-west Tanzania have a low wind speed compared with the rest of the eastern part of the EAC. This finding concurs with wind speed reports (e.g. REN21-EAC 2016) which indicates that the western region has lower wind speed than the eastern part. Changes across the region under both RCP4.5 and 8.5 scenarios Figure 5-33:38 (C), except during the period of 2071-2100, are dominated by the colour white which indicates that there is no change in wind speed over the region. In addition, there are a few pockets of blue where a negative change in wind speed is projected. This is especially prominent in north-west Kenya. The periods of 2071-2100 are dominated by a general decrease in wind speed across the region. Under the two climate scenarios and during all periods, there is an increase in wind speed on the east coasts of both Kenya and Tanzania shown in Figure 5-33:38 (C). Also, there is a decrease in wind speed in the area around Lake Victoria and under both RCPs 4.5 and 8.5 shown in Figure 5-33:38 (C) indicates that a large number of models are in strong agreement with regards to negative changes in wind speed within the central north-west of Tanzania and central Kenya extending to both the north-west and south-west. To summarise, model agreement on positive change in wind speed can be observed in the west part of Tanzania extending to Uganda, as well as the east coasts of both Tanzania and Kenya.

5.3.6.2 Future temporal change in wind speed under RCPs 4.5 and 8.5

A. Potential annual changes in wind speed

This section assesses the monthly mean annual cycle of wind speed changes for periods 2021-2050, 2051-2080 and 2071-2100 compared to the period of 1976-2005. This includes the analysis of Figure 5-39 (A&B), under both RCP4.5& 8.5 scenarios and wind speed change in the monthly mean annual cycle of wind speed for the periods of the 2050- and 2080-time horizons in which there is a persistent null change in wind speed.

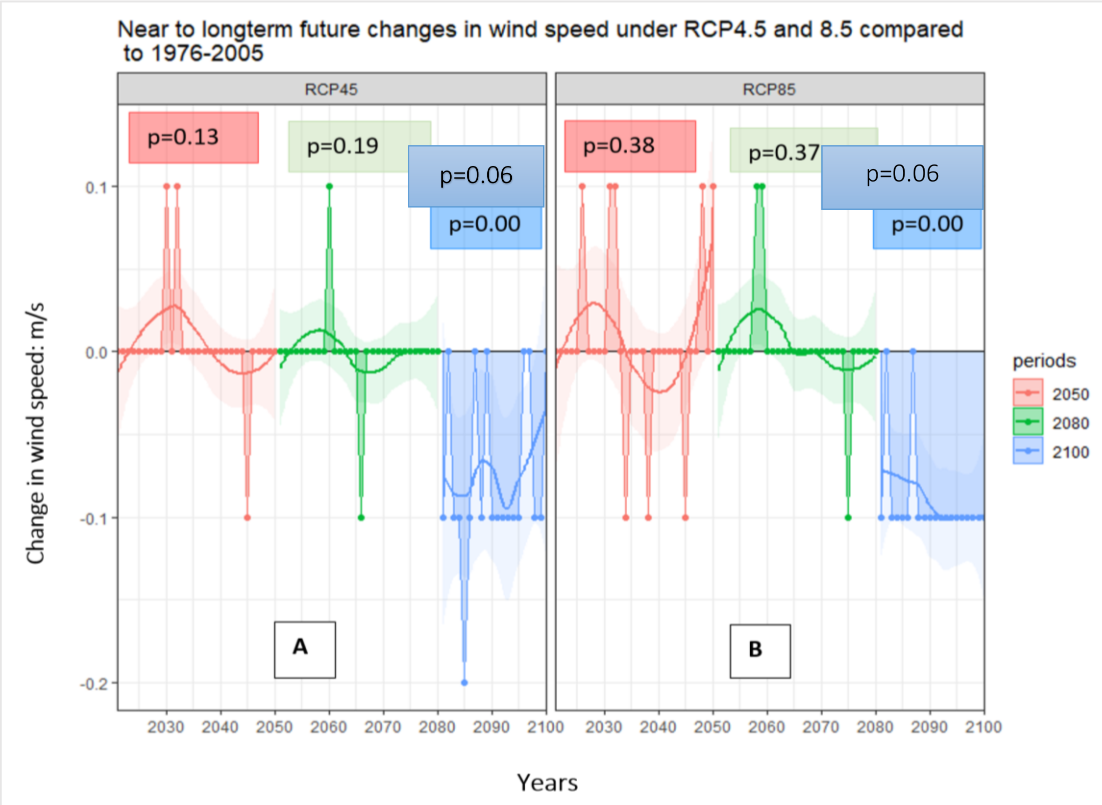

Figure 5-39: Monthly mean annual cycle of wind speed (m/s) changes under RCP4.5& 8.5

RCP4.5[A] & RCP8.5[B] show the monthly mean annual cycle of changes of wind speed for the periods of 2021-2050, 2051-2080 and 2071-2100 compared to the period of 1976-2005. The periods are distinguished by the colour red for 2050, green for 2080 and blue for the 2100 time horizons. Above the black horizontal line marks a positive change (i.e. an increase in wind speed for the monthly mean annual cycle) while negative change (below the line) indicates a decrease in the wind speed for the monthly mean annual cycle. The changing trend for each period under each scenario is summarised by a multimodal mean. P is the P-value, which is the result of the Wilcoxon test between the historical and future periods under both RCP4.5 and 8.5. The p-values are coloured to match their respective periods.

Change in wind speed during the periods between 2021-2100 relative the baseline periods of 1975-2005 is not statistically significant. Therefore, no significant spatiotemporal change in winds speed is expected in the EAC for the period dated up until 2100.

5.3.7 Spatiotemporal future changes in temperature under RCP4.5 and 8.5

This section is divided into two parts: the first part investigates the temporal changes for each grid over the region of study and the second part focuses on the annual and seasonal mean temperature changes. Prior to exploring these changes, the MMEM historical seasonal cycle, relative to the CRU observed temperature is illustrated in Figure 5-40.

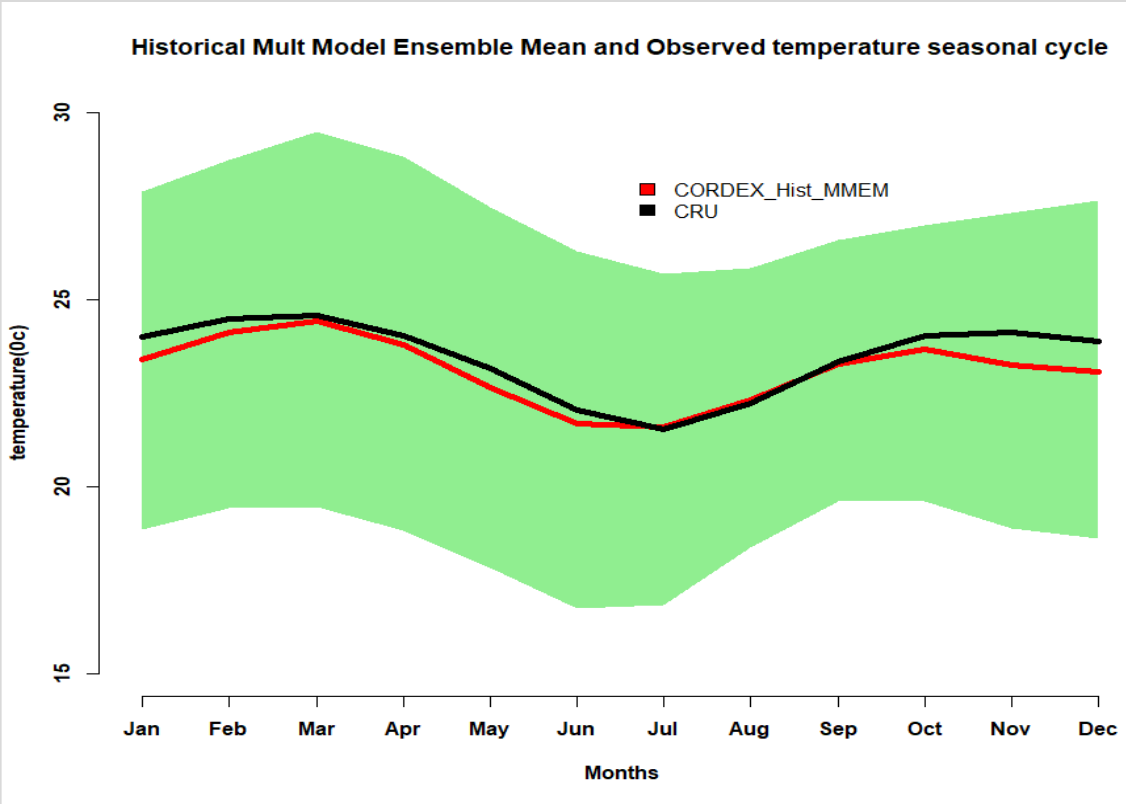

Figure 5-40: MMEM historical and CRU (temperature) monthly cycle
The MMEM (historical run) is shown in red, and the ERAI (observed) temperature monthly cycle is shown on the black line. The green polygon is the MMEM historical temperature monthly cycle 90th (top) and 10th (bottom) percentiles.

Looking at Figure 5-40, it can be noted that the MMEM historical runs slightly underestimate the temperatures during the months of January-June and October-December. In contrast, the MMEM captures well the observed temperatures for the months of July-September. In addition, the line graph for the MMEM historical run and ERAI, follow the same patterns. This is because MMEM historical and ERAI increase and decrease together. This is an indication that the MMEM has simulated the expected temperature patterns over the region.

5.3.7.1 Spatiotemporal temperature changes over the EAC

The results from the 17 models used in this study show that all the models (see Appendix B1-2) project a significant positive increase (at α= 0.05) in temperature between the period of 2021-2100 relative to the 1976-2005 baseline period. The spatiotemporal variability of temperature for the period of 2021-2100 compared to 1976-2005 under the RCP4.5 scenario can be inferred from Figures 5-41 to Figure 5- 46 for precipitation, solar radiation and wind speed. The results shown in the figures for each temperature share many features and due to this, will be analysed collectively. Therefore, Figures 5-41 to Figure 5- 46 are denoted as Figures 5-41:46. Figures 5-41:46 (A) and Figures 5-41:46 (B) denote observed and simulated temperature respectively.

The temperature changes and the model percentage agreement on positive and negative changes are shown in Figures 5-41:46 (C) and Figures 5-41:46 (D) respectively. Further analysis and interpretation will be similar to the aforementioned process for the discussion of precipitation results as given in Section 5.3.4.1.1.

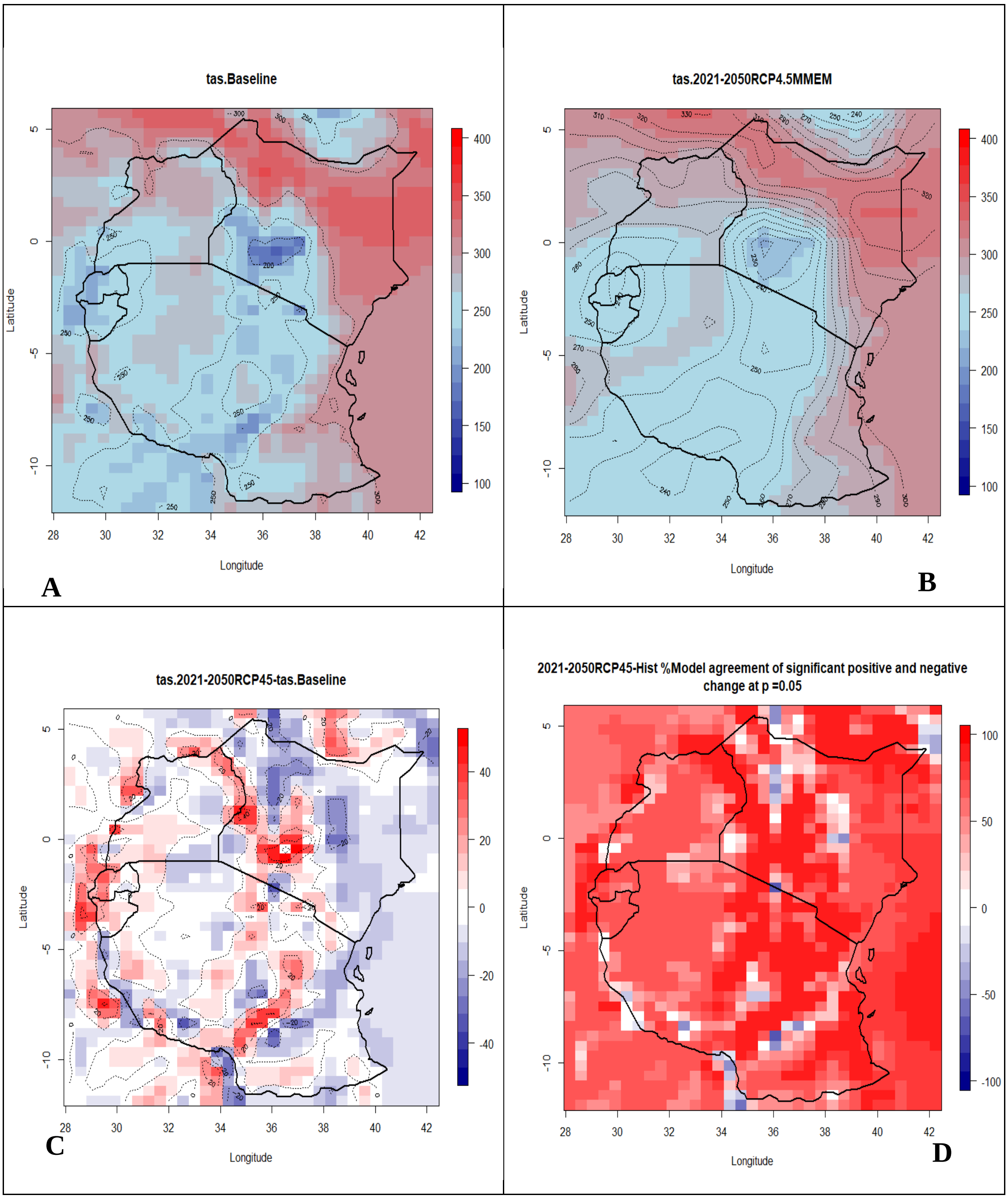

Figure 5-41: Spatial changes in temperature (°C) for the period of 2021-2050 under RCP4.5 over the EAC

Colours should be used to read temperature distribution for subfigures (A&B) and changes for subfigure (C) while the contours on the maps provide values for spatial variability. Subfigure A [baseline] is historical MMEM, the white colour shows grids where there are outliers. Subfigure B is temperature MMEM under RCP4.5 for 2021-2050 (2050-time horizon). Subfigure C is a map showing changes between the 2050 time horizon and the baseline. The changes are represented by a blue colour for fields where temperature is decreasing, white colour is where there is no change, and red indicates an area where temperature is increasing. Subfigure D is a map showing the percentage of models that are in agreement on positive changes (red), negative changes (blue) and such agreement is statistically significant at α=0.05. White colour (subfigure D) indicates that model agreements are statistically not significant.

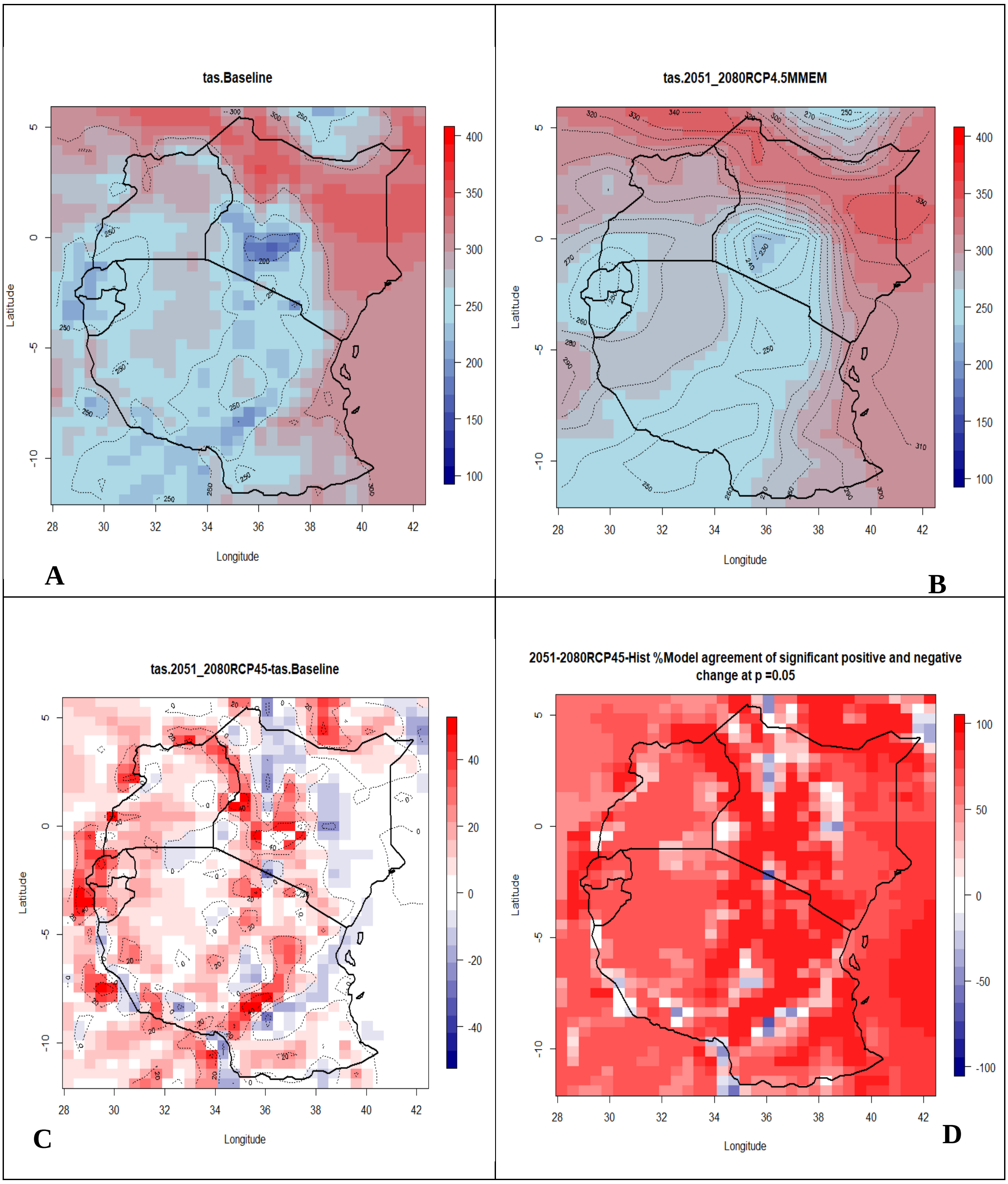

Figure 5-42: Spatial changes in temperature (°C) for the period of 2051-2080 under RCP4.5 over the EAC

Colours should be used to read temperature distribution for subfigures (A&B) and changes for subfigure (C) while the contours on the maps provide values for spatial variability. Subfigure A [baseline] is historical MMEM, the white colour shows grids where there are outliers. Subfigure B is temperature MMEM under RCP4.5 for 2051-2080 (2080-time horizon). Subfigure C is a map showing changes between the 2080 time horizon and the baseline. The changes are represented by a blue colour for fields where temperature is decreasing, white colour is where there is no change, and red indicates an area where temperature is increasing. Subfigure D is a map showing the percentage of models that are in agreement on positive changes (red), negative changes (blue) and such agreement is statistically significant at α=0.05. White colour (subfigure D) indicates that model agreements are statistically not significant.

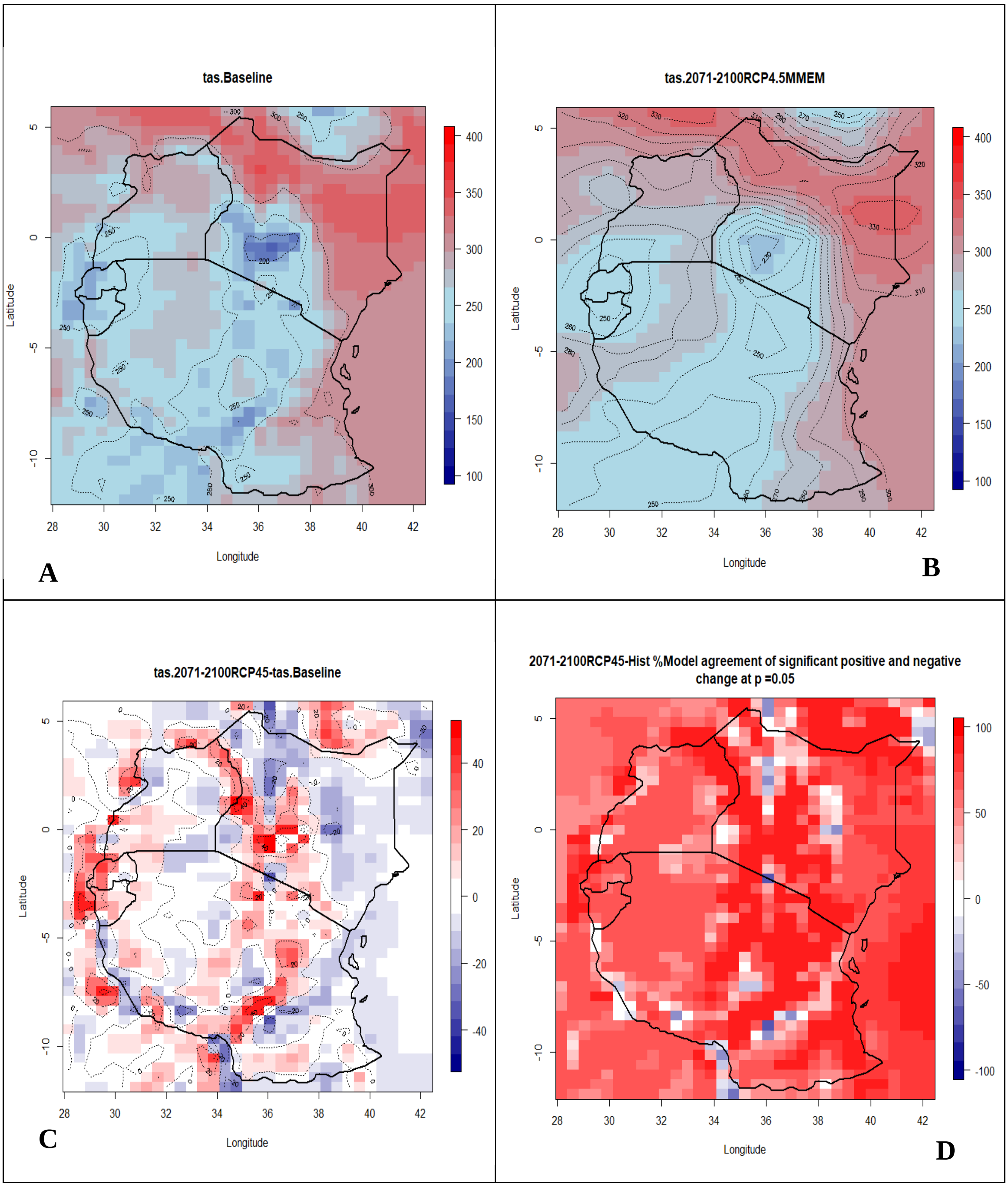

Figure 5-43: Spatial changes in temperature (°C) for the period of 2071-2100 under RCP4.5 over the EAC

Colours should be used to read temperature distribution for subfigures (A&B) and changes for subfigure (C) while the contours on the maps provide values for spatial variability. Subfigure A [baseline] is historical MMEM, the white colour shows grids where there are outliers. Subfigure B is temperature MMEM under RCP4.5 for 2071-2100 (2100-time horizon). Subfigure C is a map showing changes between the 2100time horizon and the baseline. The changes are represented by a blue colour for fields where temperature is decreasing, white colour is where there is no change, and red indicates an area where temperature is increasing. Subfigure D is a map showing the percentage of models that are in agreement on positive changes (red), negative changes (blue) and such agreement is statistically significant at α=0.05. White colour (subfigure D) indicates that model agreements are statistically not significant.

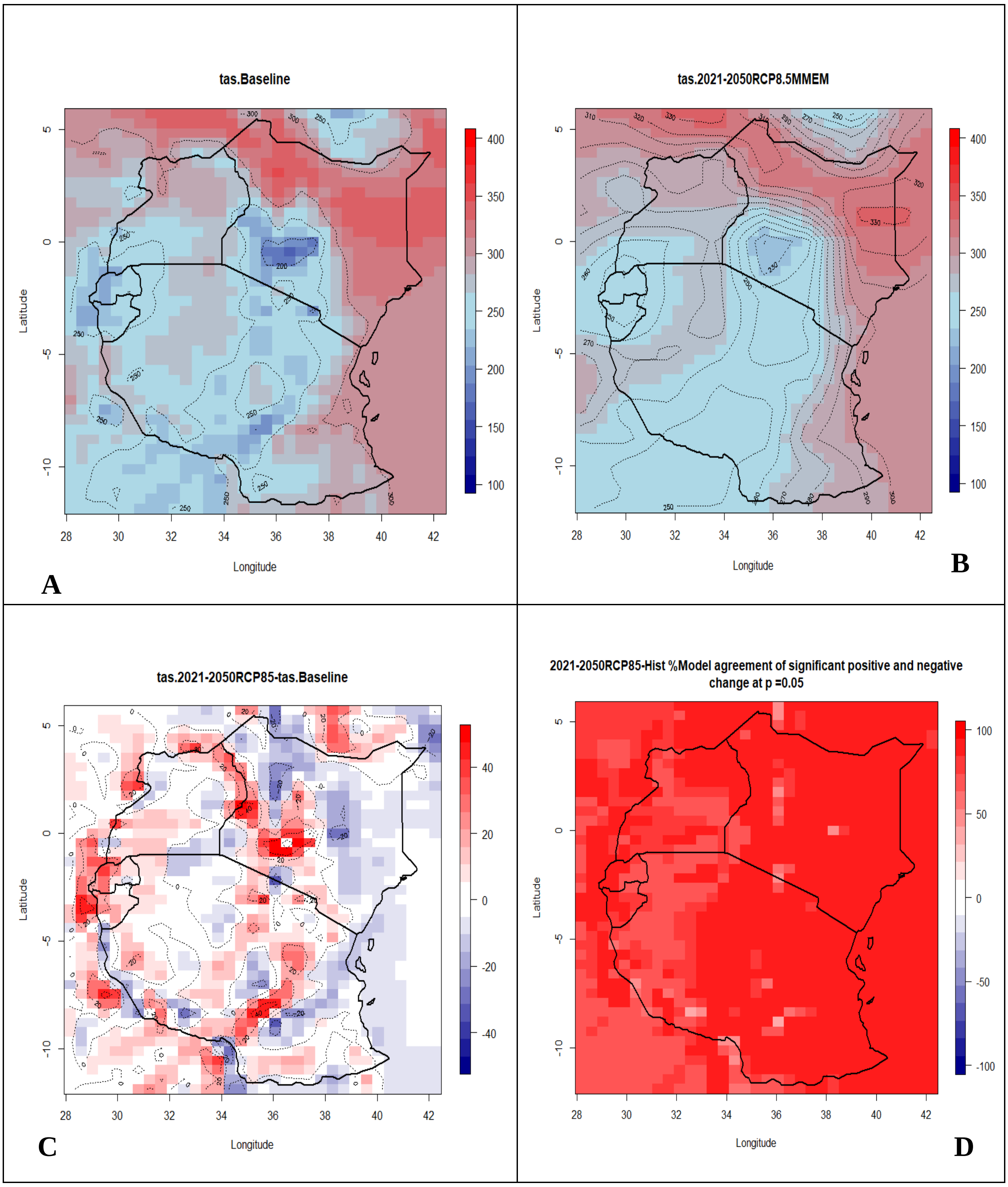

Figure 5-44: Spatial changes in temperature (℃) for the period of 2021-2050 under RCP8.5 over the EAC

Colours should be used to read temperature distribution for subfigures (A&B) and changes for subfigure (C) while the contours on the maps provide values for spatial variability. Subfigure A [baseline] is historical MMEM, the white colour shows grids where there are outliers. Subfigure B is temperature MMEM under RCP8.5 for 2021-2050 (2050-time horizon). Subfigure C is a map showing changes between the 2050 time horizon and the baseline. The changes are represented by a blue colour for fields where temperature is decreasing, white colour is where there is no change, and red indicates an area where temperature is increasing. Subfigure D is a map showing the percentage of models that are in agreement on positive changes (red), negative changes (blue) and such agreement is statistically significant at α=0.05. White colour (subfigure D) indicates that model agreements are statistically not significant.

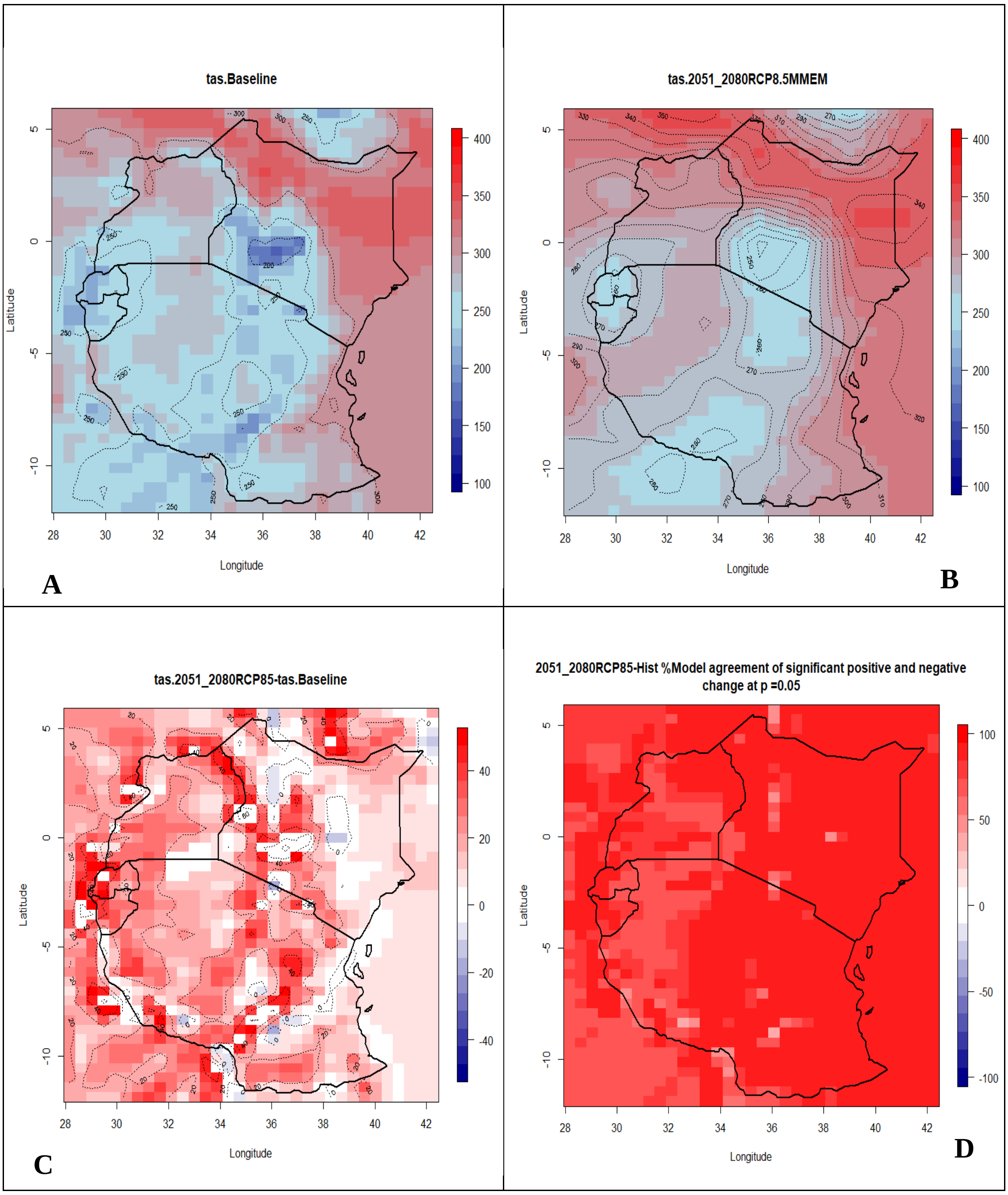

Figure 5-45: Spatial changes in temperature (°C) for the period of 2051-2080 under RCP8.5 over the EAC

Colours should be used to read temperature distribution for subfigures (A&B) and changes for subfigure (C) while the contours on the maps provide values for spatial variability. Subfigure A [baseline] is historical MMEM, the white colour shows grids where there are outliers. Subfigure B is temperature MMEM under RCP8.5 for 2051-2080 (2080-time horizon). Subfigure C is a map showing changes between the 2080 time horizon and the baseline. The changes are represented by a blue colour for fields where temperature is decreasing, white colour is where there is no change, and red indicates an area where temperature is increasing. Subfigure D is a map showing the percentage of models that are in agreement on positive changes (red), negative changes (blue) and such agreement is statistically significant at α=0.05. White colour (subfigure D) indicates that model agreements are statistically not significant.

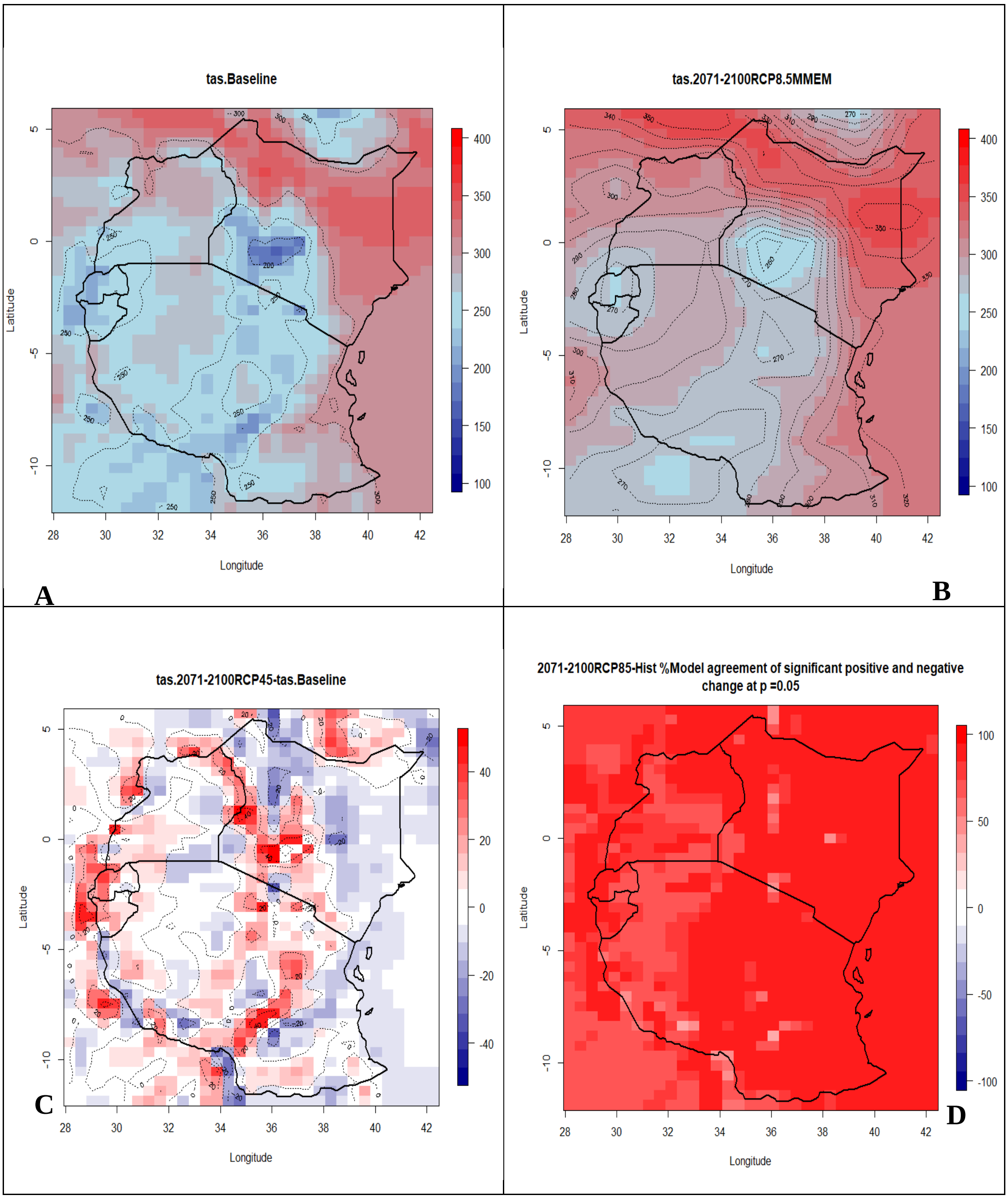

Figure 5-46: Spatial changes in temperature (℃) for the period of 2071-2100 under RCP8.5 over the EAC

Colours should be used to read temperature distribution for subfigures (A&B) and changes for subfigure (C) while the contours on the maps provide values for spatial variability. Subfigure A [baseline] is historical MMEM, the white colour shows grids where there are outliers. Subfigure B is temperature MMEM under RCP8.5 for 2071-2100 (2100-time horizon). Subfigure C is a map showing changes between the 2100time horizon and the baseline. The changes are represented by a blue colour for fields where temperature is decreasing, white colour is where there is no change, and red indicates an area where temperature is increasing. Subfigure D is a map showing the percentage of models that are in agreement on positive changes (red), negative changes (blue) and such agreement is statistically significant at α=0.05. White colour (subfigure D) indicates that model agreements are statistically not significant.

For both RCP4.5 and RCP8.5, Figures 5-41:46 (B) are relative to the observed temperature shown in Figures 5-41:46 (A). It can be seen that the highest annual cumulative monthly temperatures, which exceed 270℃ or 22.5℃ per day and 300℃ or 25℃ per day respectively under RCP4.5 and 8.5 are in the eastern part of Tanzania, extending to the north, the north-west and eastern parts of Kenya, and the north and north-west of Uganda. The relatively high temperature in these regions is explained by the fact that they are mainly within the areas classified as Arid and Semi-arid Land (ASL), as explained by Indeje et al. (2000). In contrast, Rwanda, Burundi, and the central to north-easterly part of Tanzania towards south-west Kenya have low annual cumulative monthly temperatures of approximately 250℃ or 20.8℃/day under RCP4.5 and 270℃ or 22.5℃ per day under RCP8.5. The annual average temperatures, which are about 230℃ or 19.2℃ per day for both RCP4.5 and 8.5, are projected to occur in mountainous areas with a high probability for this occurrence in the south-westerly part of Kenya. This projection aligns with the predictions of Ogwang et al. (2014) who indicated that over East Africa, temperature decreases as elevation increases and vice versa.

The historical annual average temperature spatial distribution over the EAC, as shown in Figure 5-41:46 (A) is comparable to the projected future temperature in that it is slightly lower than for both RCP4.5 and 8.5. From the temporal temperature changes for each grid over the region for the periods of 2021-2050, 2051-2080 and 2071-2100 presented in Figures 5-41:46 (C), it can be seen that the negative changes are more noticeable in the north-east of Kenya and the south-east of Tanzania under both RCP4.5 and 8.5 for both the near future and long-term future periods. This temperature change pattern is also observed in the north-western part of Tanzania extending to central Uganda and then towards the north. Compared to the 2021-2050 and 2071-2100 periods, the period of 2051-2080 has fewer grids indicating negative changes in the aforementioned regions for the same periods under the two climate scenarios. The percentage of agreement of the models for changes in the annual average temperature is presented in Figure 5-41:46 (D). These figures show that the majority of the models agree on a positive change across the region with few grids indicating negative or no change, under the RCP4.5scenario. Under RCP8.5, all models agree on positive changes over the EAC.

Changes in temperature over the region under RCP4.5 range from a minimum of 1.1℃ to a maximum of 2.2℃ and on average, the projected change is approximately 1.59℃ during the period of 2021-2100 when compared to the 1976-2005 period. Under RCP8.5, a minimum charge of about 1.84℃ and a maximum change of 3.4℃ is expected, whilst on average, the change in temperature over the EAC between 2021-2100 compared to 1976-2005 is expected to be approximately 2.58℃. Changes in temperature are higher in RCP8.5 than in RCP4.5 and this has also been highlighted in the future variations of mean rainfall and temperature based on CMIP5 models applied during a study undertaken by Ongoma et al. (2018) for the East African region. In addition, spatiotemporal changes in temperature over the EAC for the periods of 2021-2100 relative to the 1976-2005 baseline are also statistically significant ($p\text{-value}<\alpha=0.05$).

5.3.7.2 Future annual and seasonal cycle changes in temperature under RCPs 4.5 and 8.5

This section assesses the annual and seasonal cyclical changes in temperature under the RCP4.5 and RCP8.5 scenarios for the near, mid and long-term future periods. The results are shown in Figure 5-47 and Figure 5-48 respectively for the annual and seasonal changes.

5.3.7.2.1 The potential changes in annual mean temperature

Figure 5-47 [A] and [B] shows a positive change in the annual mean cycle temperature for all periods (2050-2080 and 2100-time horizons) under both RCP4.5 and RCP8.5. Such change is statistically significant as the p-values in all cases are less than α=0.05. In addition, this figure shows a difference in increase in warming between RCP4.5Figure 5-47 [A] and RCP8.5[B]. This is because it is much warmer in the RCP8.5 than it is in the RCP4.5.

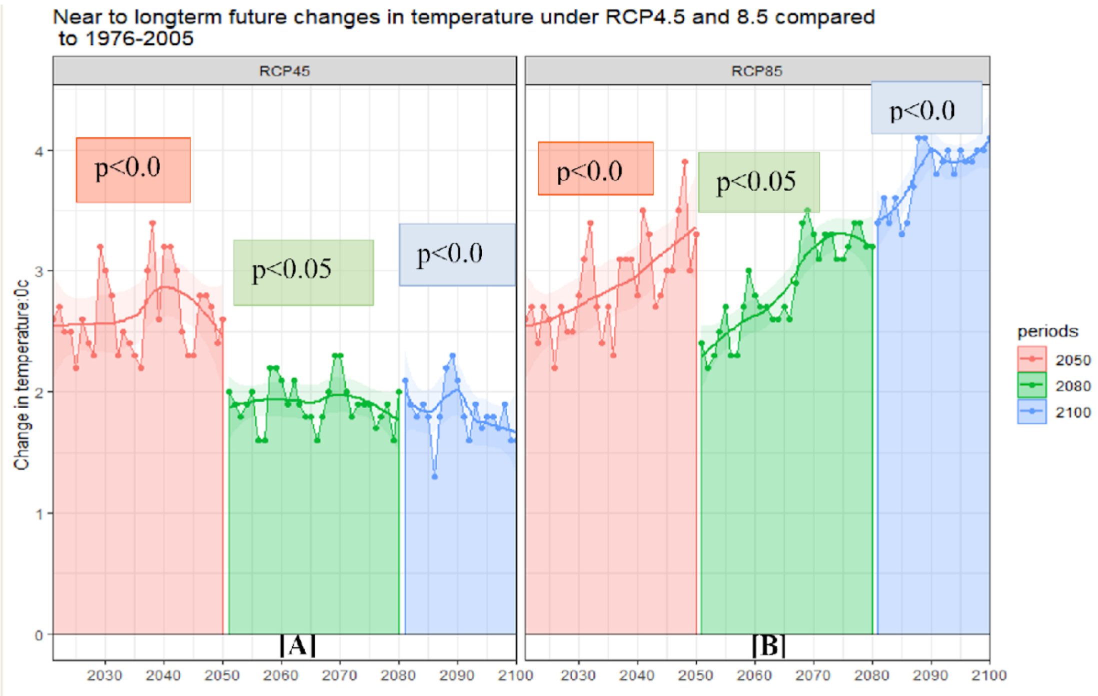

Figure 5-47: Monthly mean annual cycle of temperature changes under RCP4.5 & 8.5

The RCP4.5[A] &RCP8.5[B] are monthly mean annual cycles of temperature changes for periods 2021-2050, 2051-2080 and 2071-2100 compared to the period of 1976-2005. Future periods are distinguished by colour - red for 2050, green for 2080 and blue for the 2100 time horizon periods. Positive changes are shown above the black horizontal line indicating an increase in the monthly mean annual cycle of temperature and warm conditions. Negative changes are shown below the line indicating a decrease in the monthly mean annual cycle of temperature and cool conditions. The changing trend for each period under each scenario is summarised by a multimodal mean. P is the P-value resulting from the Wilcoxon test (α=0.05) for historical and future periods under both RCP4.5 and 8.5. The p-values are coloured to match their respective periods.

Under RCP4.5, Figure 5-47 [A], the temperature is higher during the near future period and decreases over the mid and long-term future. The decrease in warming is due to the emissions stabilisation associated with RCP4.5 (van Vuuren et al. 2011). Figure 5-47 [B] shows that the temperature under RCP8.5 consists of higher warming conditions over the near future period, which fluctuates slightly in the mid future and then rises again over the 2100 period. Relative to the baseline mean, the projected temperature for the period of 2021-2050 (shown in red) increases by roughly 2.6℃ and 2.9℃ under the RCP4.5 and 8.5 climate scenarios respectively.

The average change during the period of 2080 under RCP4.5 as per Figure 5-47 [A-B] (in green), is approximately 1.9℃, or 0.7℃ less than the previous period (2021-2050) under the same climate scenario. Under the RCP8.5, the expected average change is predicted to measure at approximately 2.9℃ or 1℃ more than under RCP4.5.

Temperature changes for the period of 2071-2100 can be inferred from Figure 5-47 [A-B] (shown in blue), where under RCP4.5, the average change in temperature is predicted to be 1.9℃ whilst under RCP8.5, the average change for this period is predicted at approximately 3.6℃, or 1.7℃ higher compared to the change under RCP4.5 .

In summary, this section assessed the potential monthly mean annual cycle of temperature change for 2021-2050, 2051-2080 and 2071-2100 periods, relative to the baseline period of 1976-2005, under RCP4.5 and 8.5. It was found that, under both climate scenarios, the temperature continued to increase for all periods. Notably, under RCP8.5 the results suggested a constant increase in temperature during the 2021-2100 periods. This increase in temperature is consequentially due to the high emission of greenhouse gases associated with RCP8.5. For RCP4.5, it was found that the increase in temperature is high for the period of 2021-2050 and decreased for the periods of 2051-2080 and 2071-2100. This decrease is also due to the reduction of greenhouse gas emissions under the RCP4.5 climate scenario as opposed to RCP8.5.

5.3.7.2.2 Changes in temperature seasonal cycle under RCP4.5 and 8.5

The potential monthly mean annual cycle of temperature change was examined in the previous section. This section investigates the potential changes in the seasonal cycles of temperature for the near, mid, and long-term future periods. The seasonal cycle changes in temperature can be inferred from Figure 5-48 (A-C). It can be seen from Figure 5-48 (A) that for the period of 2021-2050, the highest changes are recorded in JJA while the lowest changes are recorded in the SON seasons under both climate scenarios. The variability of changes under both RCP4.5 and RCP8.5 is high during the period of 2021-2050. Changes in temperature seasonal cycles under RCP8.5 is slightly higher than it is under RCP4.5 in all periods (2021-2100).

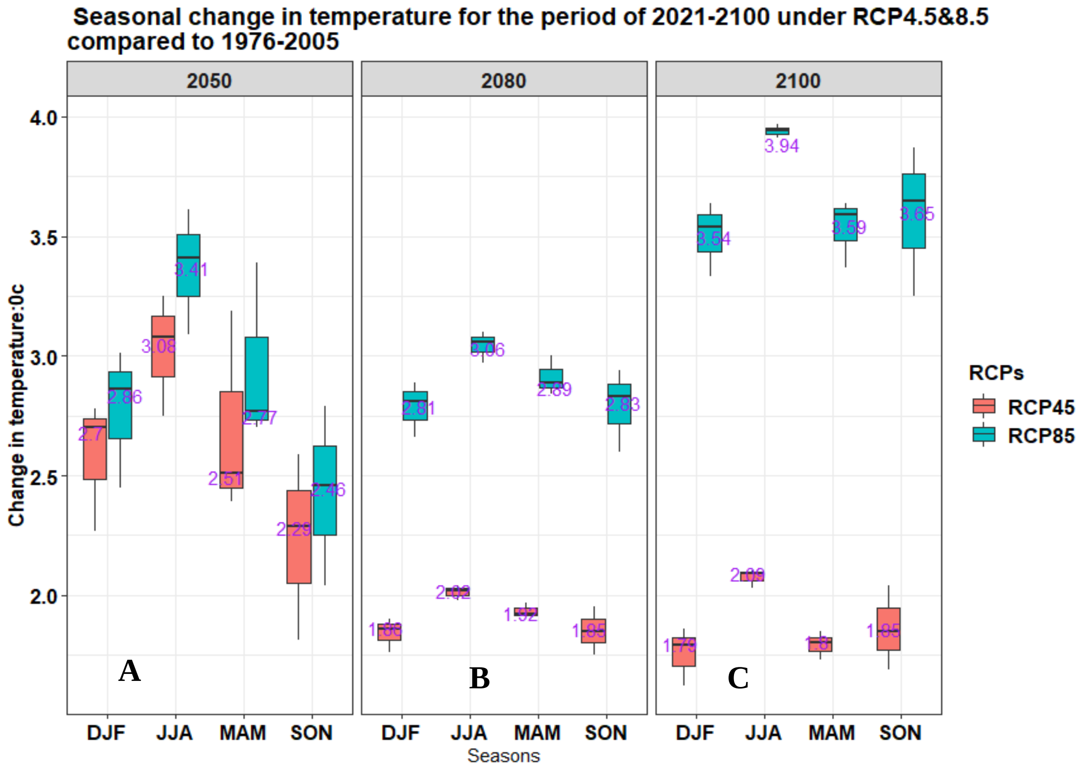

Figure 5-48: Seasonal cycle changes in temperature

Seasonal cycle changes in temperature under RCP4.5are shown in blue and RCP8.5 in red. Subfigures A, B, C are changed during the period of 2021-2050 (2050-time horizon), 2051-2080 (2080-time horizon) and 2071-2100 (2100 time-horizon) respectively. DJF is for December, January and February; MAM is March, April and May, JJA is for June, July and August and SON is for September, October and November seasons. The values (in pink) at each boxplot are the median difference between the baseline period (1976-2005) and RCP4.5in red and the baseline and RCP8.5 in blue

Figure 5-48 (C and B) show that during the periods of the 2080 and 2100 time horizon, the difference in temperature changes between the RCP4.5 and RCP8.5 is relatively high for 2080 but even higher during the later time horizon periods. Seasonal changes in temperature are generally higher during the 2050 time horizon than the 2080 and 2100 time horizon under RCP4.5. The seasonal cycle changes respectively decrease and increase in temperature under the RCP4.5 and 8.5 during the period of 2071-2100. This is due to the difference in the RCPs' assumptions of greenhouse gas concentration in the atmosphere over the forthcoming years (Weyant et al. 2009).

In summary, the aim of section 5.4.4 was to examine the EAC spatiotemporal future changes in temperature under RCP4.5 and RCP8.5 scenarios. For the spatial changes, it was found that 100% of the models indicated that a significant increase in temperature under both RCP4.5 and RCP8.5 is expected over the EAC. On average for all periods, an increase in temperature would be approximately 1.59℃ under RCP4.5, and 2.58℃ under RCP8.5. The potential temporal changes in temperature for the periods of 2021-2050, 2051-2080 and 2071-2100 compared to the baseline period of 1976-2005 under the two climate scenarios were assessed. The results showed that for all periods, the temperature under both climate scenarios is increasing. Notably, under RCP8.5, there is a continuous increase in temperature from the period of 2021-2050 to the period of 2071-2100. This increase in temperature is a consequence of the high emission of greenhouse gases associated with RCP8.5 as opposed to RCP4.5, where the emission is reduced.

5.4 Chapter conclusion

This chapter investigated the potential future changes in precipitation, solar irradiance, wind speed and temperature within the EAC in line with objective two of this research. In achieving this objective, two questions have been answered. The first question referred to the identification of models that were able to reproduce the observed hydroclimate patterns. For this question, the research has shown that 17 CORDEX_Africa models were suitable for this study and thus, they have been used to achieve the aim and objectives of this research.

The second question refers to the investigation of potential spatiotemporal changes in precipitation, solar irradiance, wind speed and temperature under the RCP4.5 and 8.5 climate scenarios. Both research main question 1 which was as What are the potential future hydroclimate change scenarios in the EAC?, and the Objective 2 of this research which was to investigate EAC future hydroclimate changes under different climate scenarios (RCP4.5 and 8.5) for the period spanning from 2021 to 2100, were achieved. Both the seasonal and annual monthly mean cycles of precipitation have been assessed for two climate scenarios. With reference to this, this study has demonstrated that the EAC may not expect a significant change in rainfall during the periods of 2021-2050 and 2051-2080 under both RCP4.5 and 8.5 when compared to the period 1975-2005. However, the findings do suggest that a significant increase in rainfall is projected during the period of 2071-2100. This is consistent with the findings of Ongoma et al. (2017), who indicated an increase in rainfall under RCP4.5 and 8.5 during this period. Concerning the seasonal cycle, this study found that the months of March-May and September-November are shown to have the wettest seasons and largest variability in rainfall. This finding agrees with the current data on East Africa rainfall seasonal cycle i.e. (Shongwe et al. 2011, Liebmann et al. 2014) who argued that March-May and October-December are the seasons with the highest amount of rainfall. Consequently, under both climate scenarios, the study obtained results that demonstrate an enhanced seasonal cycle within the EAC. This means that as the wet months get wetter, the dry months get drier as time moves from the near to the long-term future. These findings add to a growing body of literature which supports the mechanism: ‘‘wet get wetter, dry get drier” as introduced by Held and Soden (2006) and Chou et al. (2009). In keeping with this, June-August is shown to be a dry season which became drier under the two scenarios. Because of this, insight has been gained into the potential increase in evapotranspiration implications, thus reducing the amount of water in the reservoir for hydropower production. However, the rainfall is expected to be higher under RCP8.5 than it is under RCP4.5 which agrees with the findings of Ongoma et al. (2017) for the East African region.

Under the RCP4.5 climate scenario, the 2080 time horizon is projected to be the wettest, followed with a reduction in rainfall due to the stabilization of total emissions before 2100 in the RCP4.5 scenario. In contrast, under RCP8.5, there is a continuous increase in rainfall seasons over the 2021-2100 period. The wet and dry seasons respectively getting wetter and drier will affect the smooth continuous supply of energy from hydropower. Therefore, the projected increase in precipitation is not in contradiction with the claim that shortfalls in rainfall will affect hydropower production over the EAC. The shortfall in hydropower production despite the projected increase in rainfall is in line with Anyah and Semazzi (2006), Lyon and Dewitt (2012), Yang et al. (2014) and Rowell et al. (2015) who argue that the ongoing variability of precipitation in East Africa has led to increases in the intensities of drought and flood events.

This chapter also discussed the spatiotemporal change in solar irradiance over the EAC for the 2021 to 2100 period when compared to the baseline period of 1976-2005. It has been found that the average change for all EAC_RCM models is between -2.20 $W.m^{-2}$ and -3.67$W.m^{-2}$ under both RCP4.5 and 8.5 respectively. For seasonal cycle changes, solar irradiance tended to decrease across all periods of 2021-2050, 2051-2080 and 2071-2100 with the exception of the season of MAM during the periods of the 2050 and 2080 time horizons under RCP4.5, as well as the seasons of JJA and SON during the period of 2100 under RCP8.5. The decrease in solar irradiance in the EAC noted in this research is in line with Wild et al. (2015) which indicated that a large part of the world is expected to experience a decrease in all-sky radiation in the coming decades. According to the REN21 (2016b) report, due to the EAC's geographical position (near the equator), the region is currently has a large amount solar irradiance and this research found that this will continue in the future, at least until the end of this century.

Wind speed is higher in the east part of Kenya than it is in the west extending to Uganda. Also, a large part of Uganda extending south to Burundi, and a large part of north-west Tanzania had low wind speed – less than 4m/s- when compared to the rest of the region. This is in agreement with the current knowledge concerning the geographical distribution of wind in the EAC, as highlighted in the REN21-EAC 2016 report, indicating that wind speeds are relatively low in the regions of Burundi, Rwanda and Uganda. Spatial and temporal changes in wind speed have also been discussed in this chapter. It was found that the EAC, under both RCP4.5 and 8.5 climate scenarios, changes in wind speed for 2021-2050, 2051-2080 and 2071-2100 periods relative to the period of 1976-2005 is insignificant.

The last part of this chapter investigated the future spatiotemporal changes of temperature in the EAC under the RCP4.5 and 8.5 climate scenarios. The findings showed that a significant increase in temperature under both RCP4.5 and 8.5 could be expected. On average for all periods, an increase in temperature of 1.59°C under RCP4.5 and about 2.58°C under RCP8.5 can be expected in the EAC. It was also found that changes in temperature are higher in RCP8.5 than RCP4.5 which is consistent with the study findings on East Africa by Ongoma et al. (2017). The results showed that for all periods, the temperature under both climates scenarios is increasing. Notably, under RCP8.5, there is a continuous increase in temperature from the period of 2021-2050 to the period of 2071-2100. Under RCP4.5, the EAC expects an increase in temperature of about 2.6°C for the period of 2021-2050 and will then see a decrease of about 0.7℃ over the subsequent periods. However, under RCP8.5, the average temperature change is shown to be 2.9℃ for the periods of 2021-2050 and 2051-2080. For the period of 2071-2100, the average temperature is about 3.6℃. This continuous increase in temperature under the RCP8.5 is a consequence of the high emission frequently referred to as “business as usual” (van Vuuren et al. 2011), suggesting a warming scenario if society does not make rigorous measures to cut greenhouse gas emissions as opposed to the RCP4.5 (Thomson et al. 2011), scenario where the emission is being reduced.

Chapter 6: Complementarity of hydro, solar and wind power resources in the EAC

6.1 Introduction

In order to reduce the energy access gap, the EAC requires sustainable and reliable energy sources. With respect to this, renewable energy has been identified as a potential solution (REN21-EAC 2016). It is evidenced that renewable energy resources by nature have both diurnal and seasonal variations which can affect the consistency of energy production (e.g. Jimenez and Lawand 2000, Jóhannesson et al. 2007, Zayas et al. 2015, Bett and Thornton 2016). Therefore, renewable energy plants should, where possible, be designed and implemented in a way that considers a range of resources, all of which complement each other during the diurnal, monthly and annual cycles. Thus, the aim of this chapter is to answer the research question 2 thereby achieving the objective three of this research. Objective three, which is twofold, refers firstly to the assessment of co-variability between hydro, wind speed and solar power resources under the RCPs 4.5 and 8.5 climate scenarios for the periods of 2021-2050, 2051-2080 and 2071-2100. Secondly, it refers to an analysis of the implications of these scenarios for energy supply balancing within the EAC.

The literature review revealed that the EAC's electricity sector is primarily based on hydropower. At more than 50% of the total energy supply, hydropower plays an essential role in terms of its significance as a source of energy production within the region. However, whilst a considerable body of research has been undertaken on hydropower itself, less attention has been paid to the impact of climate change on hydropower development. When hydropower is considered in the context of climate change, the limitations become increasingly apparent. Researchers such as the Worldwatch Institute (World Watch Institute 2010) have highlighted that new investments in hydropower are being implemented with no examination of how climate change will affect them, despite the fact that many existing dams are already plagued by drought-caused power shortages. With regards to this particular study, it is evidenced (cf. Chapter 1:1.2) that all of the EAC countries have experienced drought-caused power shortages to varying extents.

Despite evidence of the impact of climate change on hydroelectricity generation in the region, existing research has failed to explore the potential and complementarity of hydropower production. A failure to explore this in conjunction with other renewable energy sources means a missed opportunity in terms of better informing future renewable energy strategies. Such potential complementarity analysis is critical in informing planning decisions with particular reference to designing future energy systems. Thus, with this in mind, objective three, as addressed in this chapter, will be answered in two parts as a response to the following questions:

1) What is the extent of hydro, wind and solar power resources complementarity in the EAC?
2) How is the observed complementarity, if any, represented in the balancing of potential power output?

6.2 Data and experimental design

Data used for this section originates from the multi-model ensemble which was evaluated in Section 5.3.1. Seventeen models were used for the EAC domain. This is because the data gathered from the seventeen models covered the study reference period (1976-2005), and two Representative Concentration Pathways (RCPs) as required. The two RCPs covered were RCP4.5 (Thomson et al. 2011) and RCP8.5 (Riahi et al. 2011) and the data covered the time period 2021 to 2100. For the purposes of this study, the selected CORDEX-AFRICA models were constrained to the EAC domain (EAC_RCMs). As discussed in Section 4.3.1. The Global Precipitation Climatology Centre (GPCC) version 7 (Schneider et al. 2011), was used as a reference for precipitation estimates in the East

African region because of its accuracy and reliability (Endris et al. 2013; Rowell et al. 2015). In addition, the ERA-interim reanalysis data were used to infer wind speed and solar irradiance, as per Dee et al. (2011) and Berrisford et al. (2009). The ERA-interim reanalysis which is most commonly used for model evaluation in East Africa (Brands et al. 2013), facilitated the comparison with further studies. While ERA-interim data is available from 1979 to present (Dee et al. 2011), the CORDEX-Africa historical data only covered the period dated 1950 to 2005 (CORDEX 2018). Therefore a common period between the two (1976-2005) was selected.

Complementarity studies generally use diverse methodologies, depending on the context and goals of each study. Thus a selection of methodologies with the potential for use in this particular study as was discussed in Section 4.4. were selected. For complementarity analysis, it is useful to be able to measure the degree of association between variables. Therefore, this became a key requirement when selecting the correct approach for this particular study. There are presently a number of methods to measure association. The most widely used are Pearson's linear product-moment, Spearman's rank and Kendall's Tau correlation coefficient methods. The most influential factors guiding the choice of methods to test correlation coefficients is data normality, the presence of outliers, the linearity of the relationship and violation of the parametric assumptions (Rebekić et al. 2015). Further to this, Section 4.3.5.1 of the research methodology chapter illustrated the processes followed when testing data normality, in order to best decide which method to use when testing the extent to which the variables are associated. The following section discusses the results and is organised as follows:

- Testing which correlation coefficient method to use in order to ascertain the data normality for each variable under RCP4.5 and 8.5;
- Assessing the complementarity between precipitation, wind speed, and solar irradiance;

- Establishing hydro, wind and solar potential joint power distribution.

6.3 Results and discussion

6.3.1 Hydroclimate data normality test under RCP4.5 and 8.5

The data normality results as per Section 5.3.2 are confirmed using the Shapiro-Wilk normality test. The results indicate that for all three periods, the hydroclimate data under both climate scenarios are not normally distributed. As previously mentioned, the consequence of having data that shows abnormal distribution dictates the further use of a non-parametric test. In line with this, the Spearman correlation test method was then used to investigate the potential complementarity between the hydro, wind and solar power sources.

6.3.2 Precipitation, wind speed, and solar irradiance complementarity

The most direct way to understand the complementarity relationship between hydroclimate data for the annual cycle monthly mean, is to simply plot the values for each month alongside each other (Figure 6-2) and analyse their monthly and seasonal relationships. The relationship can then be analysed according to the degree of correlation between the variables.

For this study, Figure 6-1 shows the overall magnitude of complementarity between hydroclimate variables. The resulting Spearman correlation (ρ_s) matrix as computed is displayed in Figure 6-1. This figure contains 6 subfigures lettered A to F and are denoted here as Figure 6-1(A-F). For clarity, precipitation, wind speed, and solar radiation are respectively represented by their climatological symbol (pr, sfcWind, and rsds).

RCP4.5 — 2021-2050

pr	0.0061	-0.93***
A	rsds	-0.15**
		sfcWind

RCP8.5 — 2021-2050

pr	-0.041	-0.92***
D	rsds	-0.12**
		sfcWind

RCP4.5 — 2051-2080

pr	0.034	-0.92***
	rsds	-0.10*
B		sfcWind

RCP8.5 — 2051-2080

pr	0.006	-0.92***
	rsds	-0.024
E		sfcWind

RCP4.5 — 2071-2100

pr	-0.21***	-0.92***
	rsds	-0.11**
C		sfcWind

RCP8.5 — 2071-2100

pr	-0.095*	-0.93***
	rsds	-0.033
F		sfcWind

Figure 6-1: Spearman's correlation coefficients for hydroclimate

*A to F are Spearman's correlation coefficients for hydroclimate corresponding to the periods 2021-2050, 2051-2080 and 2071-2100 under RCP4.5(left column) and RCP8.5 (right column). The value of the correlation coefficients and the significance level are marked with asterisks. The asterisk is associated with each significance level and the symbols are as follows: p-values (0.001, 0.01, 0.05) <=> symbols (***, **, *,). The level of significance α=0.05 or below means that the anti/correlation relationship is statistically significant as opposed to the value of α above 0.05.*

Figure 6-1 (A-F) shows that for all of the time periods, precipitation and wind speed have very strong complementarity with an average overall complementarity magnitude (strength of the correlation), ρ_s, above -0.9 for all periods (2021-2050, 2051-2080, 2071-2100), under both RCPs 4.5 and 8.5. Figure 6-1 (C) shows that there is a complementarity between precipitation during the period of 2021-2050 under RCP4.5. However, for the rest of the time periods under both RCP4.5 and RCP8.5, there is no relationship between precipitation and solar radiation in the near to long term future because the observed mixture of complementarities is not statistically significant.

Wind speed and solar radiation have a mixture of complementarities and similarities with their relationship strength ranging from $-0.15 \leq \rho_s \leq 0.11$ for RCP4.5 and 8.5. However, it should be noted that wind speed and solar radiation are complementary during the near future periods under both scenarios while such complementarity is only observed during the mid-future for RCP4.5, as shown in Figure 6-1(B). The complementarity between wind speed and solar radiation shifts to non-complementarity for the period of 2071-2100 under RCP4.5 while exhibiting no relationship under RCP8.5 for the periods of 2051-2080 and 2071-2100. Further examinations were necessary in order to investigate how the observed correlation magnitude is represented in the annual cycle of monthly means for the EAC. Thus, the monthly mean values of precipitation, wind speed, and solar irradiance are plotted against each other as shown in Figure 6-2. It is worth noting at this point, that in the preceding section, it has been shown that under both RCP4.5 and 8.5 for the near, mid and long-term future periods, precipitation and wind speed are anticorrelated (i.e. complementary) at a correlation coefficient ρ_s of above -0.9 (cf.Figure 6-1)

6.3.3 Hydroclimate annual cycle monthly means over the EAC

The EAC precipitation cycle is characterised by high rainfall (Mutai et al. 1998, Indeje et al. 2000, Camberlin et al. 2009) in March to May (MAM), known as the long rainy season. The cycle shows less rainfall from October to December (OND). The latter period is known as the short rainy season and there is no rainfall in June to September (JJAS). Based on this, the precipitation seasonal cycle is projected to remain the same for the period 2071-2100 (Ongoma et al. 2018), and, further to this, Figure 6-2 shows that the relationship between precipitation and wind speed is complementary during the MAM, JJAS and OND seasons.

RCP4.5 **RCP8.5**

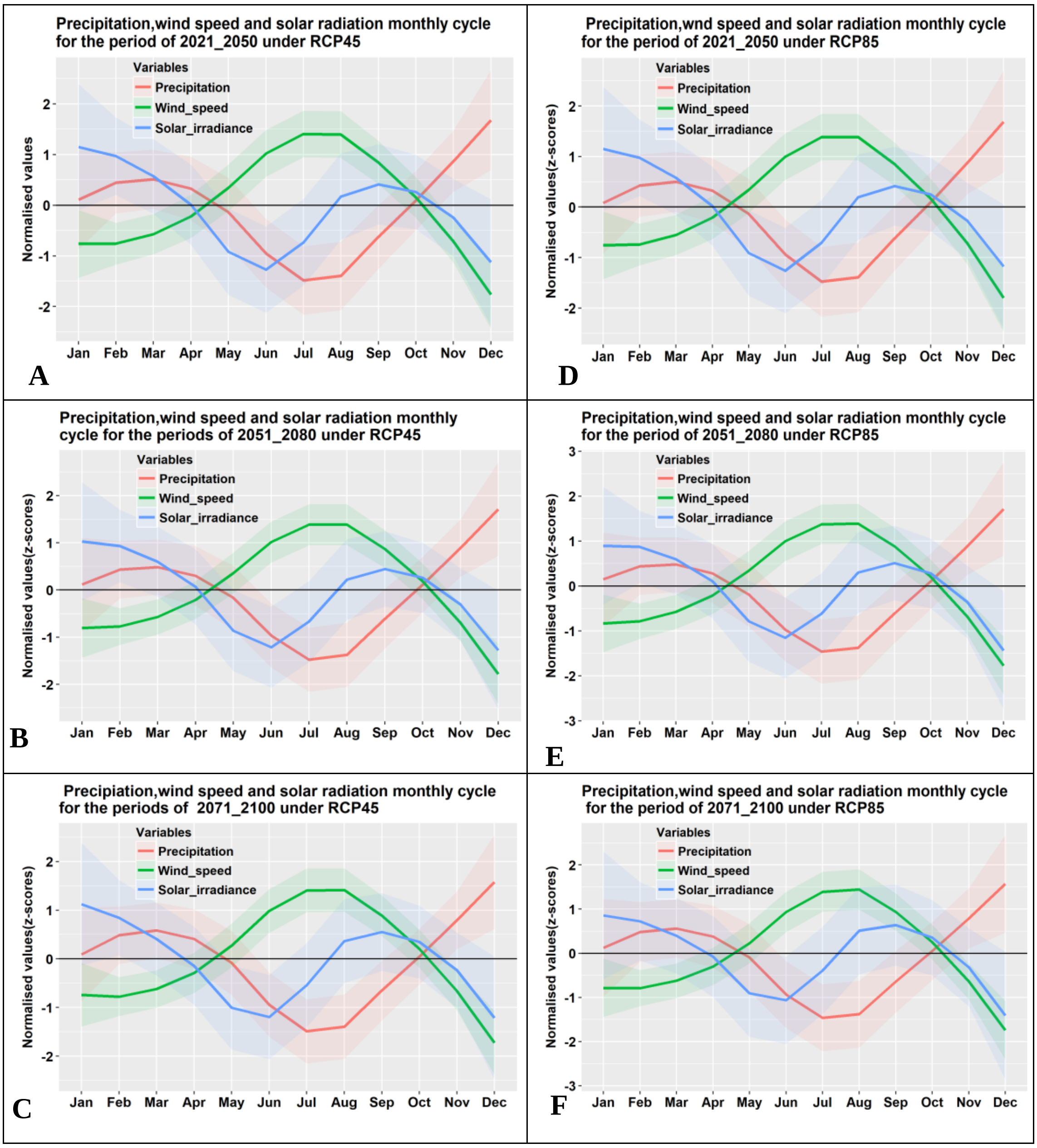

Figure 6-2: Hydroclimate monotonic relationship under RCP4.5 and RCP8.5

A to F are the annual cycle of monthly mean monotonic relationships between hydroclimate under RCP4.5 (right column) and RCP8.5 (left column) scenarios. Data values are adjusted to a notionally common scale using z-score:$z = \frac{x-\mu}{\sigma}$*. The lines and shading indicate the mean and 5th & 95th percentiles of the annual cycle of monthly mean precipitation, wind speed, and solar radiation.*

It is observed that when precipitation starts declining during the dry season, wind speed increases. Also, when precipitation increases during the short rainy season, wind speed also increases. The long rainy season (MAM) is characterised by high precipitation and low wind speed. The month to month relationship shows that for the months of January to March and mid-April, precipitation is at its highest, whereas wind speed is at its lowest as shown in Figure 6-2. As the season cycle draws closer to the dry season (JJAS), this becomes characterised by decreasing precipitation and a subsequent increase of wind speed.

The relationship between solar and precipitation shows no complementarity during the long rainy (MAM) and dry seasons (JJAS). However, it exhibits complementarity during the short rainy season (OND). In contrast, during the two seasons of rain, solar radiation and wind speed are complementary throughout the long rainy season but show no complementarity during the short rain seasons.

On examination of the monthly solar radiation and wind speed relationship, it should be noted for the months of January to June, there is a complementary relationship between the two, whereas for the months of July to December, solar and wind speed have no complementarity. It is also worth noting that under the two scenarios, solar radiation has a mixture of both complementary and non-complementary relationships with wind speed and precipitation. For some of these periods however, the relationships are classed as non-significant as per Spearman's correlation coefficients, detailed in Figure 6-1. The findings also suggest that there is no significant complementarity between precipitation and solar radiation during the near to mid future periods, under both RCP4.5 and 8.5.

In terms of the mid to long-term future periods, the complementarity between wind speed and solar radiation is not significant. Under all climate scenarios for the periods from 2021 to 2100, the monthly mean distribution for solar irradiation **(**see Appendix C 3) is above 200W/m^2, indicating an all-time (i.e. daytime) abundance across the EAC's geographical area. This information is congruent with that of the REN21 (2016) report on solar radiation resources over the East African region. From an energy provision perspective, the complementarity between precipitation, wind speed, and solar radiation indicates that during the dry periods, when hydropower outputs drop, wind power and/or solar power could potentially supplement any energy production deficit. A previous case study conducted in Tanzania (Kainkwa 1998) using precipitation and wind speed station data, yielded some important insights in indicating that the energy requirement necessary could be achieved as a result of the use of hydro and wind power. The findings of this thesis largely confirm Kwainkwa's (1998) research for the EAC as a whole.

Hydro, wind and solar power complementarities are further explored in Section 7.5.1 using a case study. Briefly, however, it was found that the annual cycle of monthly means for precipitation, wind speed and solar irradiance distribution within the EAC displayed a bimodal distribution (that is, rainfall peaks during March to May and October to December seasons). This meant that the data distribution had more than one peak which led to an investigation regarding the relationship between all combinations of two out of the three hydroclimate variables when the third variable had a low, medium and high value. These values were represented by the variable name and were preceded by a cut. Hence, precipitation values are denoted as precip.cut and units are recorded in mm/month. Wind speed values are denoted as wind.cut and units are detailed in m/s. Solar radiation values are represented by solar.cut and the units are recorded as W/m^2.

The investigation aimed to examine whether any two out of the three power sources could produce the required level of power in the event that the third failed. For instance, the investigation examined whether solar and wind have the capacity to fill any deficit in hydropower output caused by reduced rainfall levels during the dry seasons. In order to get the lowest, medium and highest values for the investigation, data for each variable were divided into three groups. The results can be seen in Figure 6-3, Figure 6-4 and Figure 6-5 as per their sub-figures A-F below and are denoted here as Figure 6-3:5.

6.4 Hydroclimate relationship under different availability condition

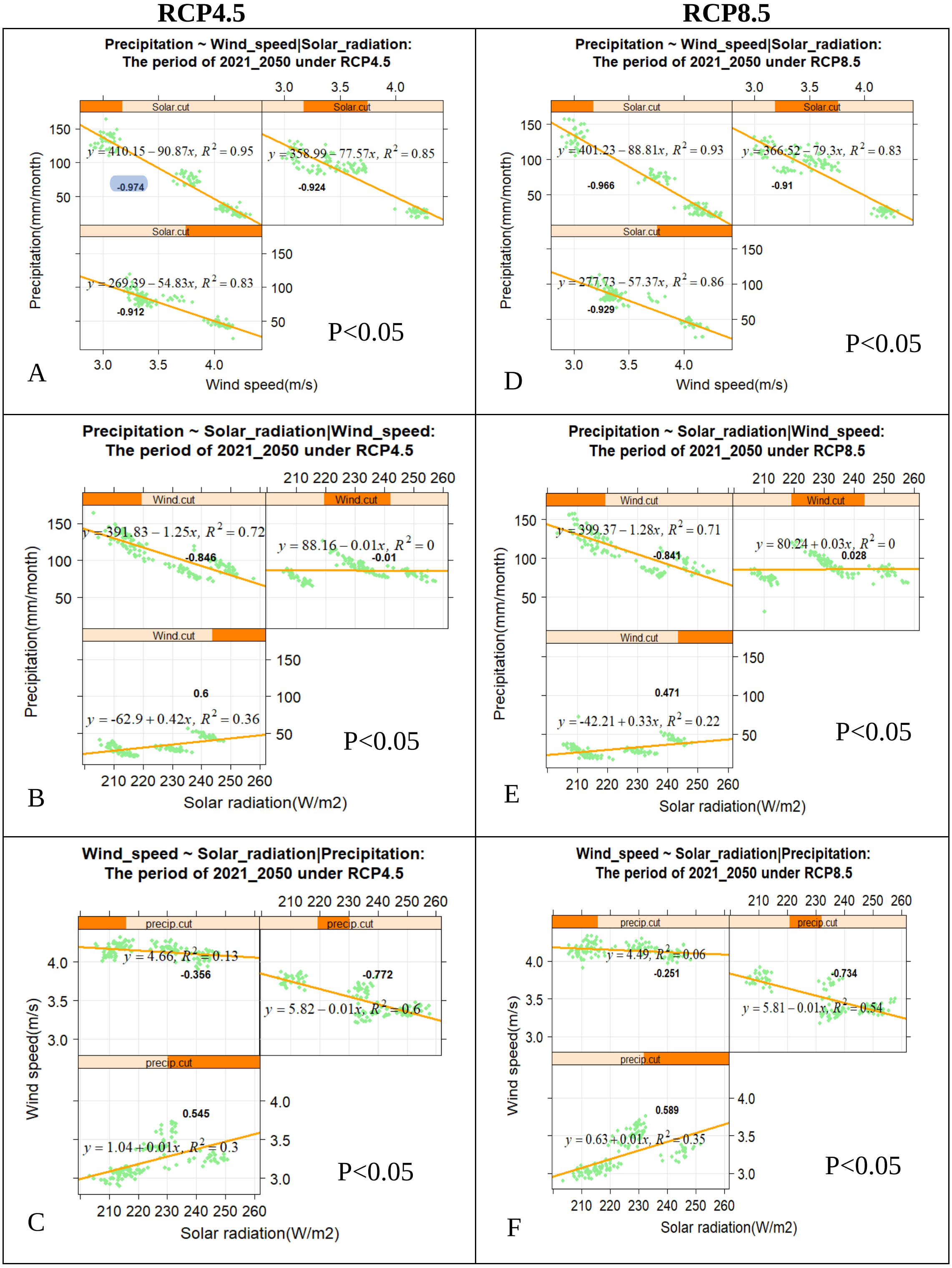

Figure 6-3: Hydroclimate relationship under different availability conditions for 2021-2050

A-F are variations in the monotonic relationship between precipitation, wind speed and solar irradiance when one of the variables is at its minimum, medium and maximum values while the rest of the two variables remain unchanged, for the periods of 2021-2050 under RCP4.5 (right column) and RCP8.5(left column). P and ρ_s are the statistical significance and correlation coefficients for precipitation, wind speed and solar radiation relationships under high, medium and low availability conditions.

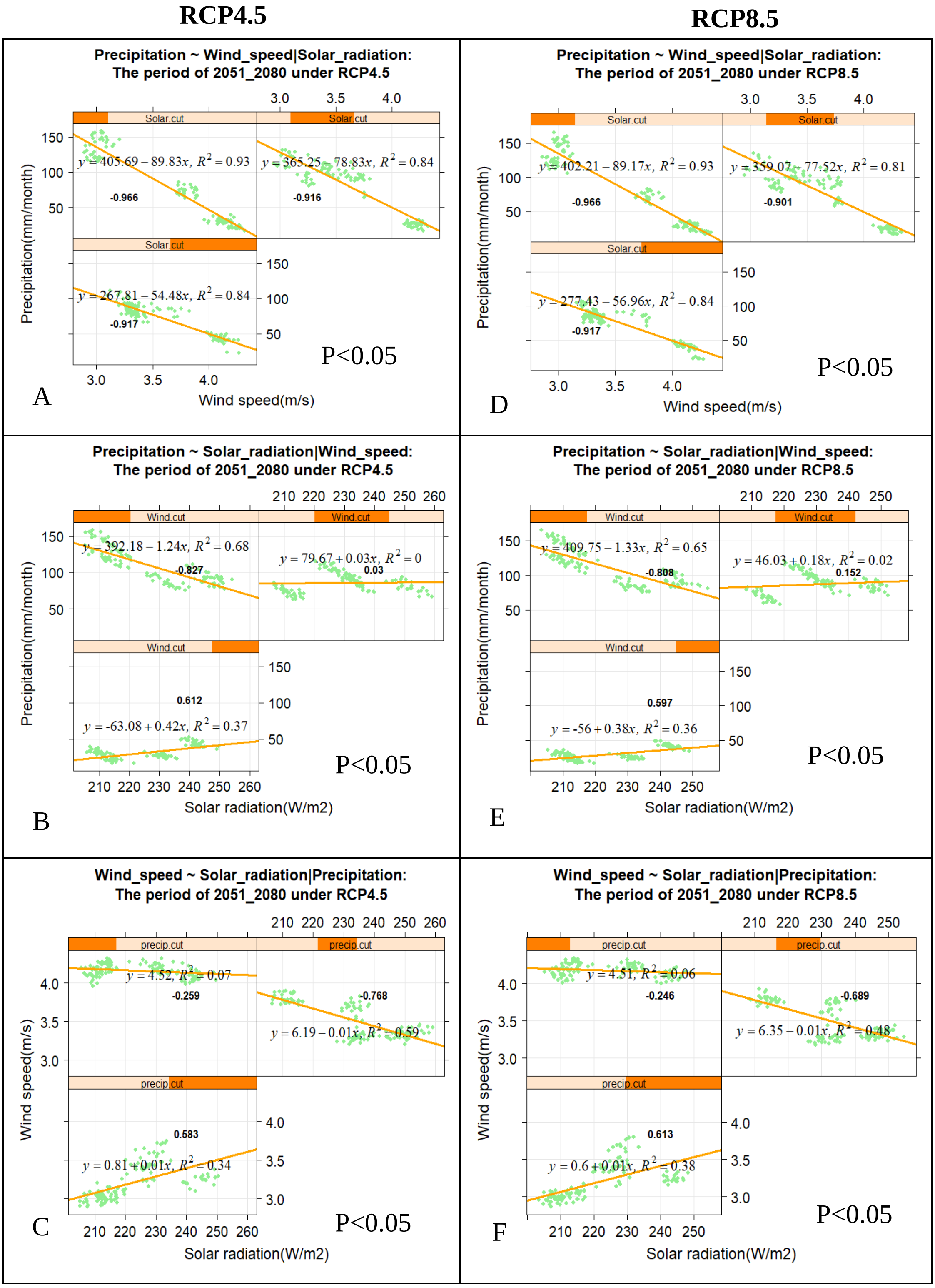

Figure 6-4: Hydroclimate relationship under different availability conditions for 2051-2080

A-F are variations in the monotonic relationship between precipitation, wind speed and solar irradiance when one of the variables is at its minimum, medium and maximum values while the rest of the two variables remain unchanged, for the periods of 2051-2080 under RCP4.5 (right column) and RCP8.5(left column). P and ρ_s are the statistical significance and correlation coefficients for precipitation, wind speed and solar radiation relationships under high, medium and low availability conditions.

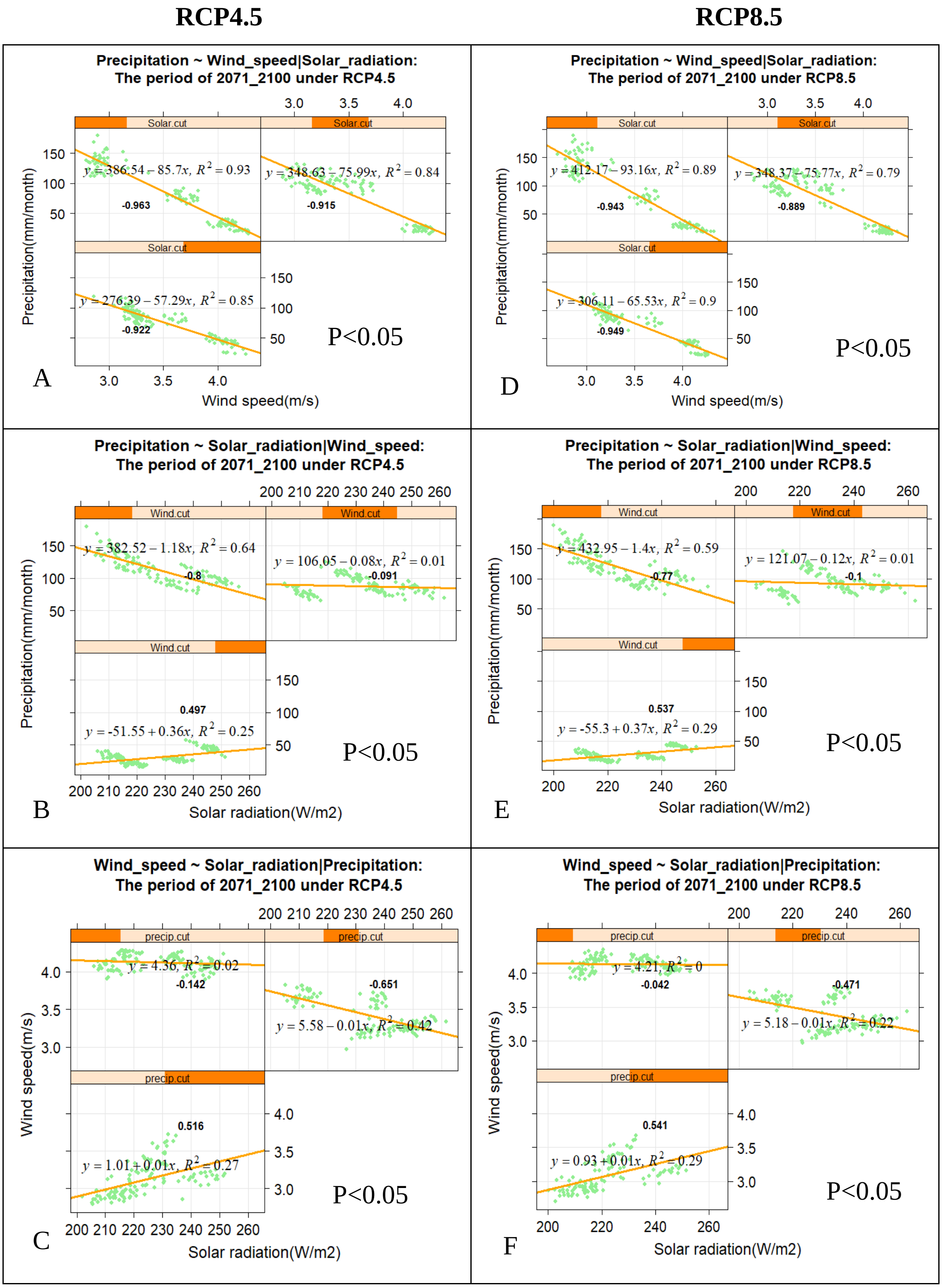

Figure 6-5: 2071-2100 hydroclimate relationship under different availability conditions

A-F are variations in the monotonic relationship between precipitation, wind speed and solar irradiance when one of the variables is at its minimum, medium and maximum values while the rest of the two variables remain unchanged, for the periods of 2071-2100 under RCP4.5 (right column) and RCP8.5(left column). P and ρ_s are the statistical significance and correlation coefficients for precipitation, wind speed and solar radiation relationships under high, medium and low availability conditions.

Looking at the three periods of 2021-2050, 2051-2080 and 2071-2100, the relationships between the sources of power represented by Figure 6-3:5 in sub-figure A-D, show that precipitation and wind speed have an inverse linear relationship when solar irradiance is at the minimum, medium and maximum level for all the periods and RCPs. The negative slope resulting from the relationship between precipitation and wind speed for all periods from 2021 to 2100 under RCP4.5 and 8.5 is an indication that the increase in rainfall per month is associated with a decrease in wind speed. R2, which is the measure of the strength of linear association of rainfall and wind speed, ranged from 0.8 to 0.9. In addition, the strength of the relationship depicted by the correlation coefficient is greater than -0.9 for all periods and scenarios. The relationship between rainfall strength and wind speed is important to highlight. This is because the observed correlation shows evidence that, under the two climate scenarios, the two variables are always complementary, irrespective of the amounts of solar irradiance for the period from 2021 to 2100, hence the negative slope.

Figure 6-3:5, sub-figure B and E show the relationship between precipitation and solar irradiance for minimum, medium and maximum levels of wind speed for the periods 2021-2100 under RCP4.5 and 8.5. The sub-figures (B and E) show that for all periods and RCPs, precipitation and solar radiation had a complementary relationship, with an average slope of approximately -1.5; R2 ranged from 0.77 to 0.84, and a correlation coefficient ≈ -0.8 when wind speed was at a minimum level. When wind speed was at its medium and maximum level, precipitation tended to lose complementarity with solar irradiance. It can, therefore, be concluded that precipitation and solar irradiance has the capacity to complement each other when wind speed is at its lowest level but has little or no complementarity for the periods when wind speed is at medium or maximum levels.

The relationship between solar irradiation and wind speed when precipitation is at its minimum, medium, and maximum values are shown in Figure 6-3:5 in subfigures (C and F). From the data period spanning between 2021 – 2100, it was identified that solar radiation and wind speed tended to have an inverse relationship under the two climate scenarios. This complementarity was more pronounced during the period when precipitation was at a medium level (ρ_s =0.7) and less so when it was at a minimum level (ρ_s=0.025). When precipitation was at its maximum value, wind speed and solar radiation tended to move in the same direction, meaning that the two variables were not complementary. Therefore, an in-depth analysis of the data shows that there is potential complementarity between solar irradiance and wind speed when precipitation is at a minimum or medium level, however there is no complementarity when it is at a higher level.

In summary, this section has assessed the relationships between precipitation, wind speed, and solar irradiance variables, for the period 2021 to 2100, when one variable is set at its minimum, medium and maximum level. The results indicated that under the two climate scenarios, precipitation and wind speed remain complementary irrespective of the amount of solar irradiance. It could also be concluded that precipitation and solar irradiance are complementary when wind speed is at its lowest level but show weak to no complementarity when wind speed is at a medium or maximum level. The study suggests that there is a potential complementarity between solar irradiance and wind speed when precipitation is at its minimum or medium levels. However, there is no complementarity during periods when precipitation is high.

With regards to the context of this research, having two sources of energy in complementarity when the third one is at its lowest value is an indication of the strength of potential complementarity. This is because the deficit in energy from one or more sources can be compensated for by the availability of other sources.

6.5 Hydroclimate spatial variation in correlation for the periods of 2021-2100

This section assesses the complementarity of precipitation, wind speed and solar irradiance on a spatial scale. The results of this assessment are shown in Figure 6-6 (A-F). From the sub-figures A and D, precipitation showed strong complementarity with wind speed in the western regions of the EAC. The area which comprises the Western part of Tanzania towards the eastern part of Burundi and southern area of Rwanda have a correlation coefficient- ρ_s- >-0.7 as indicated by the contour of correlation coefficient values. Other remaining parts of Rwanda, Uganda and Kenya show a mixture of complementarity with a correlation coefficient ranging from 0.3<ρ_s>0.1.

The spatial correlation between solar irradiance and precipitation under RCP4.5 and RCP8.5 for the periods 2021-2050, 2051-2080 and 2071-2100 are shown in Figures (C, F). These show that solar irradiance and precipitation are in complementarity. This is more pronounced in the western part of the EAC which comprises in part of Tanzania, Burundi, Rwanda and Uganda with $\rho_{s>-0.5}$ than it is in Kenya and the eastern part of Tanzania. For wind speed and solar irradiance, the spatial correlation for the periods of 2021-2050, 2051-2080 and 2071-2100, under RCP4.5 and 8.5 Figure 6-6 (A-F), sub-figures (B, E), show that there is generally a strong positive correlation $\rho_{s>0.4}$ across the region. However, the eastern part of Kenya (i.e. the area marked by the whitish colour enclosed between green lines) indicates little or no complementarity between wind speed and solar irradiance.

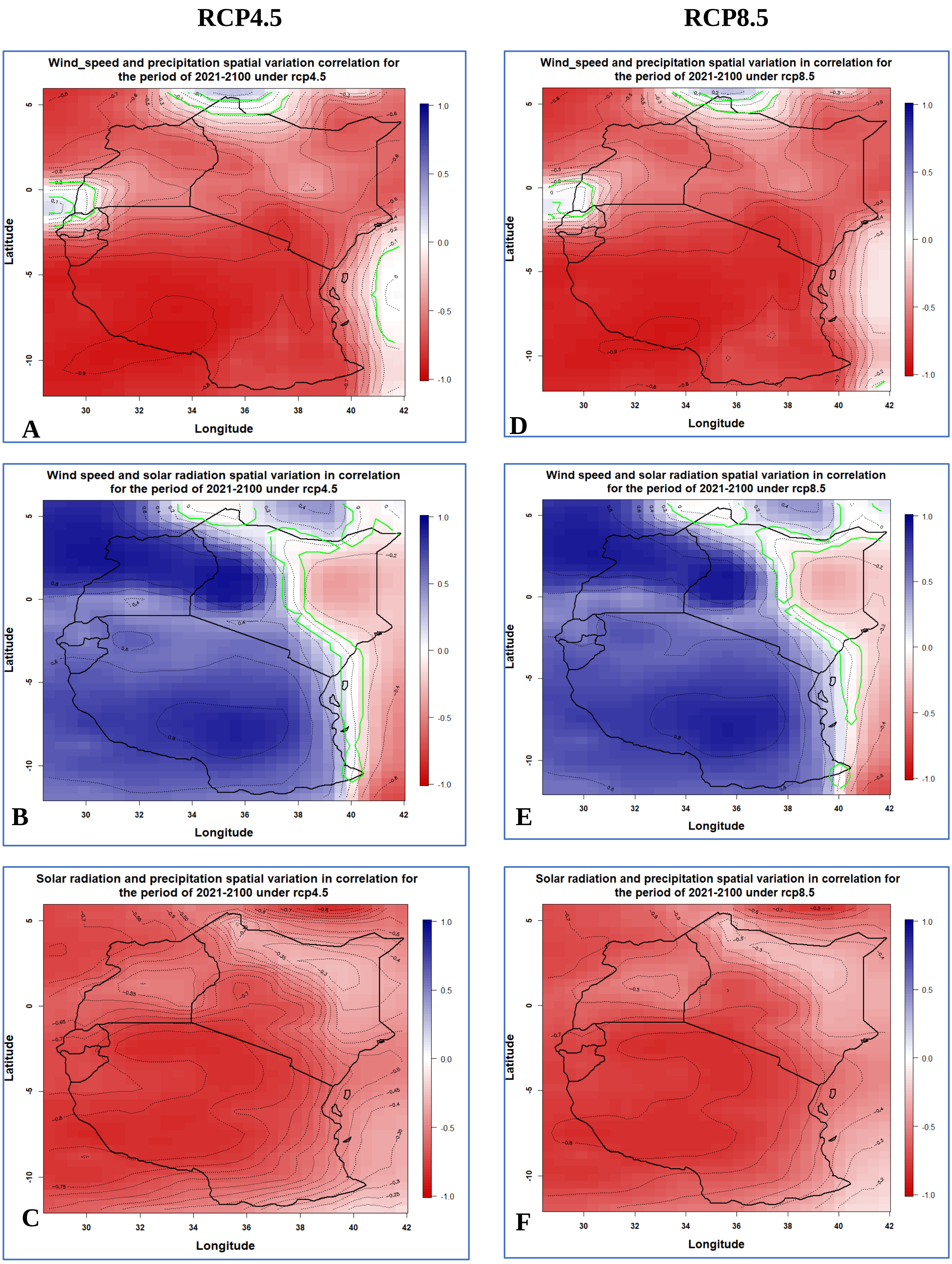

Figure 6-6: Hydroclimate spatial variations in correlation for the periods of 2021-2100
A-F show where precipitation, wind speed and solar irradiance spatial variations are in correlation for the period of 2021-2050 under RCP4.5 (left column) and RCP8.5 (right column). Correlation coefficients range between -1 to +1 and the maps are colour coded: red means anti-correlation, which indicates complementarity; white means no correlation at all, while blue indicates a positive correlation. The green line indicates where the correlation is significant. Spatial correlation values are indicated by contour.

In summary, this section examined the spatial variations in the correlation between precipitation, wind speed, and solar irradiance. It was found that precipitation is complementary (negative correlation) with both solar irradiance and wind speed, being more pronounced in the western region compared to the eastern region of the EAC. These findings are in line with the findings of Camberlin (2018) who indicated that rainfall shifts during the transition seasons, as per the seasonal migration of the ITCZ; leaving room for meridional (north-south direction) low-level winds in both the northern winter and northern summer in East Africa.

This research is in line with Ogwang et al. (2014) who concluded that when the topography (mountains) over the region covering Kenya Tanzania and Uganda is reduced to 25%, the mean rainfall over East Africa is reduced by about 19% while the magnitude of the zonal wind speed (easterlies) increases with the decrease in topographical elevation. Indeje et al. (2000) noted the existence of complex topography over the region of East Africa. This topography influences the aspect of precipitation and wind speed explains the complementarity findings of this research.

The complementarity spatial variability between precipitation and solar radiations can be explained by the fact that the regions of high precipitation are expected to be associated with low solar radiation as a result of stratiform clouds on the mountain escarpment while valleys are often cloud-free (Camberlin 2018).

The key findings are that there is spatial variability in the complementarity of the hydroclimate, meaning that an integrated regional investment in wind, solar and hydropower resources would need to take account of the spatial correlation variability.

6.6 The geographical distribution of hydro, solar and wind power sources for the periods of 2021-2100

The previous section presents the analysis of potential spatiotemporal complementarities between hydro, wind and solar power resources. This section shows how these resources are distributed across the EAC geographical area. Geographical distribution of precipitation, wind speed and solar irradiance for the period 2021 to 2100 under RCP4.5 and 8.5 can be inferred from Figure 6-7.

Visual comparison of the following maps provides a qualitative view of the differences in precipitation, wind speed and solar irradiance geographical distribution patterns across the EAC. Further details of hydroclimate spatial distribution for the near future, mid-future and long-term future periods are provided in Appendix A1, A2, B1, B2, C1, C2, D1 and D2. Figure 6-7 sub-figures (A-F) represents the periods 2021-2100 under both climate scenarios. What is notable is that the western part of the EAC has more precipitation than the eastern part. This is because the eastern part of the EAC is projected to be windier than the western area. In addition, the central part of Tanzania and the north-west of Kenya are projected to have more irradiance than the rest of the region

RCP4.5 **RCP8.5**

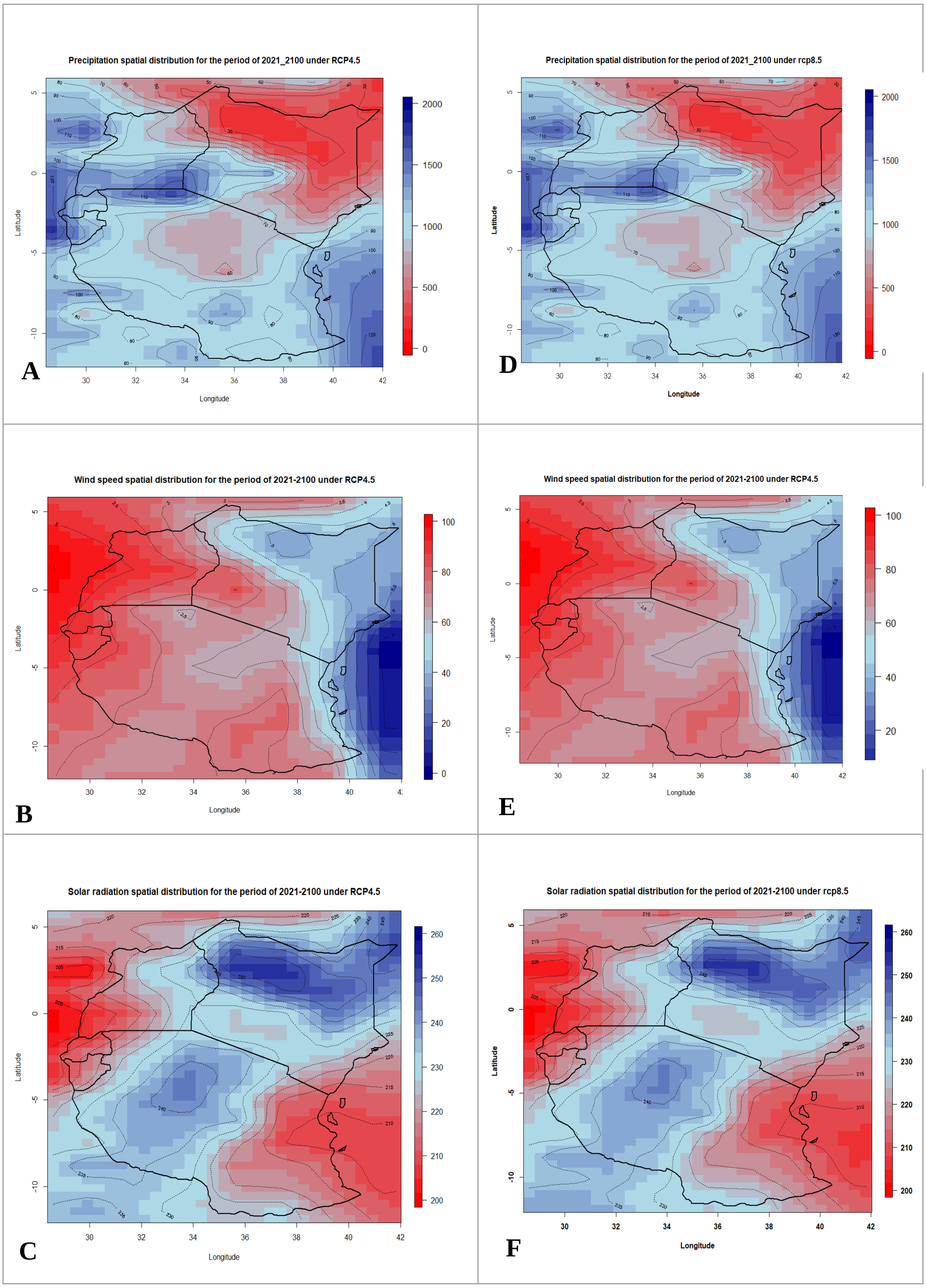

Figure 6-7: 2021-2100 hydroclimate spatial distribution

Maps A to F show the EAC monthly cycle hydroclimate spatial distribution for precipitation (mm), wind speed (m/s), and solar irradiation (W/m^2) for the periods 2021-2100 under RCP4.5 (shown on the left) and RCP8.5 (shown on the right) climate scenarios. The colours show where a variable amount is low (red), medium (light blue) and high (dark blue). The Hydroclimate variations in spatial distribution values are indicated by contours.

It should be noted that the spatiotemporal correlation of hydro, wind and solar energy resources show that precipitation and wind are not only temporally and spatially complementary, but that their level of availability is also based on geographical division. This is evidenced in the west of the EAC, which includes the western parts of Tanzania, Burundi, Rwanda, and Uganda, as these areas experience more rainfall based on their position. The rainfall measured is inclusive of rainfall within the Congo convection zone (Indeje et al. 2000, Camberlin et al. 2009, Ogwang et al. 2014) where convection zones refer to the area where the northeast and southeast winds converge, forcing the warm air to rise into the atmosphere.

This research agrees with the findings of Yang et al. (2014) who indicated that the eastern part of East Africa is drier than the western part. The complementarity between precipitation and wind speed and solar availability throughout the year presents an opportunity for profitable exploitation of the combination of hydro and wind power with solar presently available across the EAC. In addition, the combination of hydro, wind and solar power resources are more likely to provide a smooth supply profile, because a break in the supply of any one of them could be compensated by increasing the supply of one of the others. Hence, at a regional level, hydro and wind speed in conjunction with solar power is more likely to provide a smooth supply profile. At a local level, having alternative sources of renewable energy nearby, such as hydro, wind or solar, could ensure a continuous reliable and efficient electricity supply to satisfy the local need. This could also provide an excellent solution for remote rural electrification where grid extension is either uneconomical or difficult to provide.

6.7 Chapter Summary and Conclusions

This study describes the complementarity of hydro, wind and solar power resources to demonstrate the potential for continuous and reliable renewable power generation over the EAC sub-region. The extent to which one source is complementary to others on a temporal and spatial scale has been demonstrated. The results show that wind speed is complementary to precipitation for the periods of 2021-2050, 2051-2080 and 2071-2100 under RCP4.5 and RCP8.5. The solar irradiance showed a mix of both weak-negative and positive correlation with wind speed and precipitation respectively.

It was shown explicitly that the monthly distribution of precipitation and wind speed indicated that the dry months of JJAS were windier when compared to MAM and OND. In addition, the precipitation and wind speed annual cycle monthly mean meant that distribution was characterised by a bimodal (peaks) delivery. This resulted in further exploration of the co-variability between all combinations of the three variables: wind speed, precipitation, and solar irradiance when one of the three performs at a low, medium or high value. The results indicated that the complementarity between hydro and wind power resources observed in the annual cycle monthly mean holds when the solar radiation is at its maximum, medium, and minimum values.

It was also found that hydropower was always in complementarity with solar power in all the seasons and time periods (2021-2050, 2051-2080, 2071-2100) under the RCP4.5 and 8.5 scenarios. What can clearly be seen from the data is the general pattern of hydro and wind power sources with reference to the fact that their level of availability is geographically dispersed. From this, it could be noted that the Western part of the EAC is projected to have more precipitation than the Eastern part. Due to this, attention should be given to the placement of wind resources in some parts of the EAC, especially the Western parts, where there is a prevailing low wind speed. This recommendation is congruent with the REN21-EAC (2016) report which indicated that Burundi, Rwanda and Uganda have low wind speeds. Notably, the combination of hydro, wind and solar power resources are more likely to provide a smooth energy supply profile because a break in the energy supply of any one of them, could be compensated for by increasing the supply of another.

It can be concluded from the results therefore, that there is a strong potential ability for hydro and wind energy resources to balance each other out across the EAC because the region has well-balanced renewable energy resources. This can enable energy supply which compensates for diurnal, annual, local and regional imbalances.

Chapter 7: Local hydro, wind and solar potential power complementarity

7.1 Introduction

In order to satisfy ever increasing energy needs, countries or regions have to use an energy mix of available resources available locally (ENGIE 2019). In this respect, following on from the precipitation, wind speed and solar radiation state of complementarity at the EAC regional level, as discussed in the last chapter, this chapter aims to examine the degree to which power generated from hydroclimate resources (i.e. precipitation, wind speed and solar radiation) can complement each other at a given location (i.e. a real-world application) to reduce energy supply variability. In order to illustrate this, a hypothetical village, denoted here as the hypothetical village and located within the Rusumo fall study area, has been used as an example and seeks to demonstrate the optimal combinations of future renewable energy generation in a real-world application.

The chapter is divided into two main parts. The first part gives a description of the Rusumo Falls area and justification for the selection of the study area. The part includes generation of climate data (of the study area), bias correction and cross-validation. Then, the potential energy production from wind, solar and hydropower resources in the study area is examined. The second part of this chapter presents the modelling of hydropower complementarity with solar and wind power in a real-world application using available market ready technologies. The renewable energy modelling is carried out using HOMER software and the potential power generation at the Rusumo Falls study area is evaluated. Consequently, it looks at the optimal combination of technologies in a hybrid system to ensure improved energy access and availability. The results and findings of this section will inform the development of the decision support framework in Section 7.7 is provided.

7.2 Description of Rusumo Falls

Rusumo Falls, located at coordinates: 2°22'56.0"S, 30°47'00.0"E, is a joint hydroelectric project between Burundi, Rwanda and Tanzania (Nile Initiative Secretariat, Nile-SEC 2017). Rusumo Falls will provide an additional 26.6 MW to each of the three countries, and strengthen the regional power interconnection between these countries (Nile-SEC 2017). For a project like this, the selection of energy resources available locally is important. This is because it allows testing of the concept of hydroclimate complementarity use based on local resources and tailored to local conditions (Canales et al. 2019). It is for this reason that the Rusumo Falls study area -shown in Figure 4-1[C]- was chosen. Its location at an intersection between the countries Burundi, Rwanda and Tanzania was a key factor. In addition, the location already possessed an existing hydroelectric joint project (the Rusumo Falls project), therefore lending itself to a potential future joint inter-country regional project. In addition, the potential hydro, wind and solar power balancing assessment at the existing location had the potential to provide key information regarding the additional power supply available to compensate for seasonal variations in water flow at the Rusumo fall hydroelectric project. This study consequently utilised the hydropower head (the falling height of water) as already measured and utilised by the existing hydroelectric project. This proved advantageous because it saved time and resources that would otherwise have been used to measure the water falling height at the chosen location.

In order to preserve the physical processes and model internal variability at the chosen study location, data for the ICHEC-RCA4 model were used for the hydroclimate power resources energy balancing assessment. Data from the Rusumo Falls study area has been extracted for the location of one grid (50kmx50km).

7.3 Bias correction and cross-validation

Before computing the potential power output from the ICHEC-RCA4 data, a data bias correction is required because of the model featuring systematic errors which occurred as a result of the biases inherited from driving the GCMs. The delta change bias correction method and leave-k-out cross-validation method have been used to correct and cross-validate bias corrections in the data for precipitation, temperature, wind speed and solar radiation. The bias correction cross-validation results are shown in Figure 7-1, Figure 7-2, Figure 7-3 and Figure 7-4 respectively for precipitation, solar radiation, temperature and wind speed.

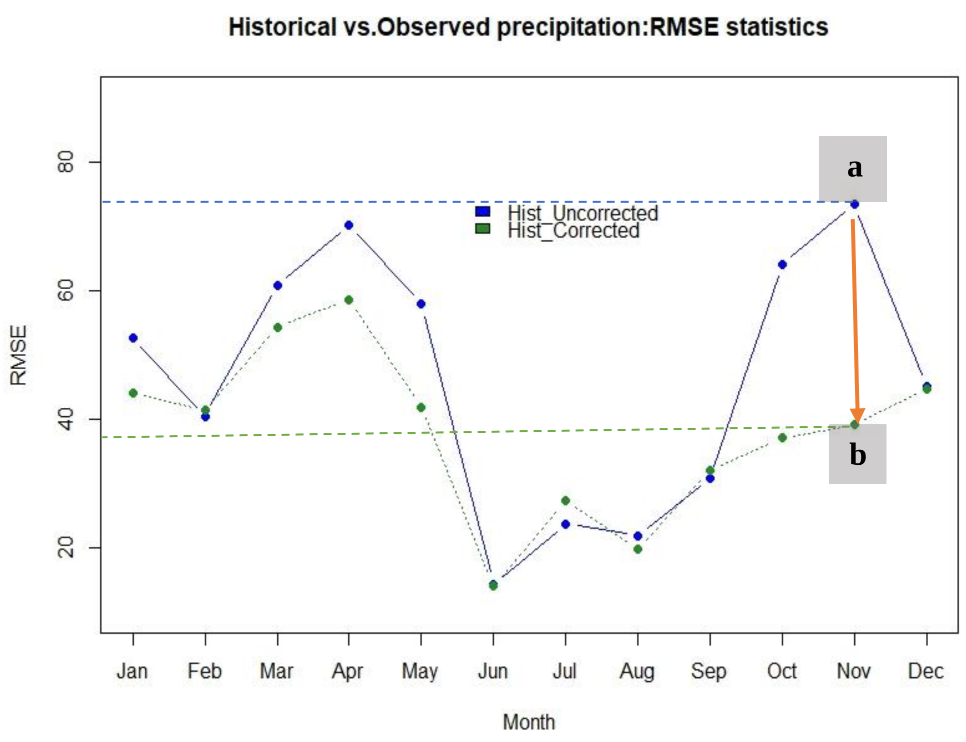

Figure 7-1: Precipitation bias correction and validation

The line plots show calculated RMSE for the uncorrected simulated historical (blue line) and the corrected simulated historical (green line) climate data compared to the observed data. The month of November as selected is an illustrative example where point a is the original value (i.e. before bias correction) and b represents the value of the corresponding month after bias correction. The distance between a and b represents the reduced/added bias. The bias is reduced if the RMSE for corrected simulated data is reduced towards zero. This interpretation is also valid for wind speed, temperature and solar radiation in the subsequent figures.

Figure 7-1 shows that biases have been reduced for the months of January to May, August, and October to December. The bias for July has slightly increased and there are no changes for the months of February, June and September. Although the delta change method did not reduce biases for all of the months, it has reduced the simulated precipitation biases for two of the key features with regards to rainfall seasons across the EAC. These key features are the long rainfall season (March, April and May) and the short rainfall season during October, November and December (Indeje et al. 2000, Schreck and Semazzi 2004, Anyah and Semazzi 2006, Yang et al. 2014b). Figures 7-2 to Figure 7-4 – denoted here as Figure 7-2:4- share similar features. As a result, these figures will be analysed and interpreted together.

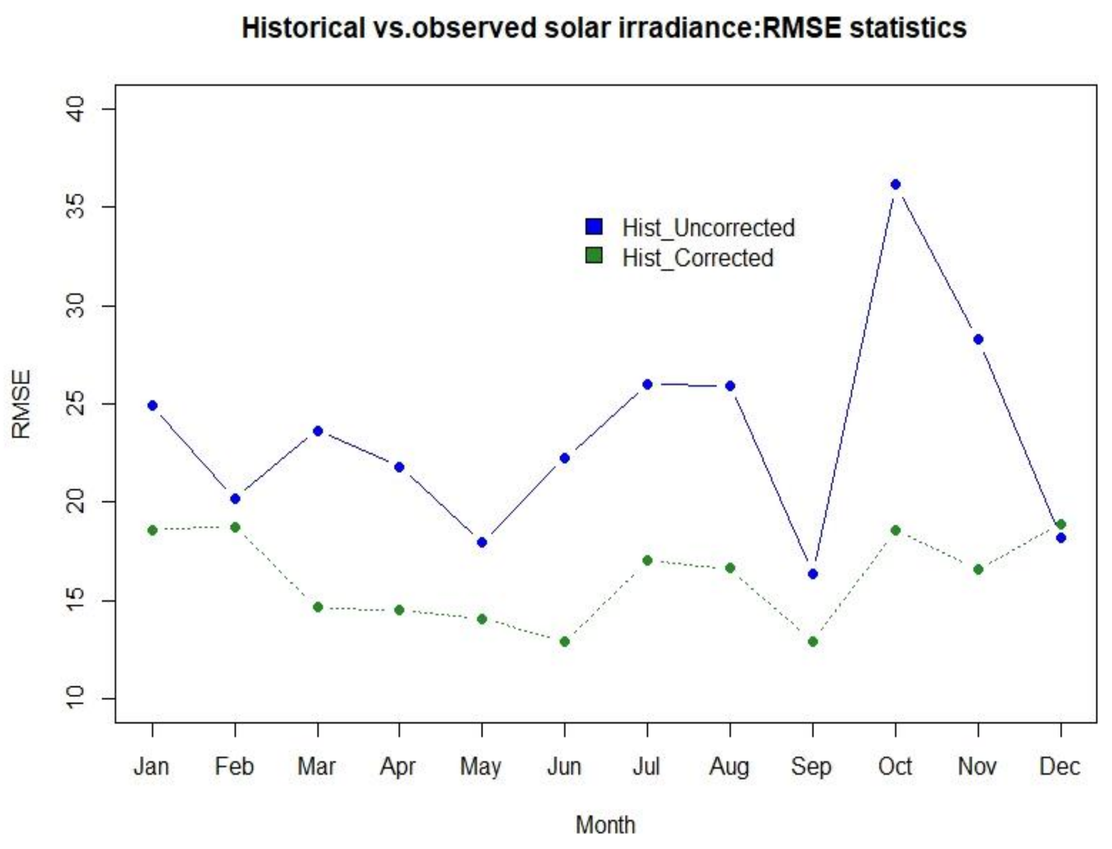

Figure 7-2: Solar radiation bias correction and validation

Line plots are for solar radiation showing a calculated RMSE for the uncorrected simulated historical (blue line) and the corrected simulated historical (green line) climate data compared to the observed data. The bias is reduced if the RMSE between the observed and corrected simulated data is reduced towards zero.

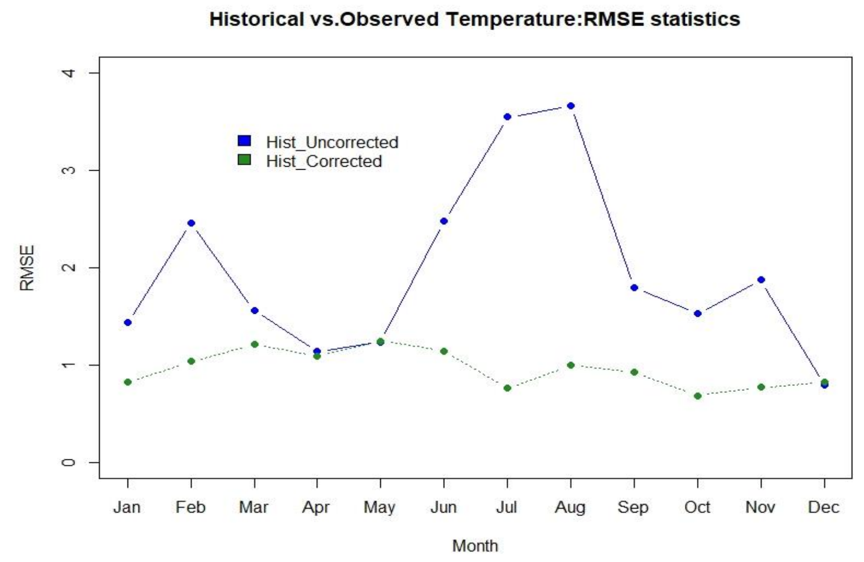

Figure 7-3: Temperature bias correction and validation

Line plots are for temperature showing a calculated RMSE for the uncorrected simulated historical (blue line) and the corrected simulated historical (green line) climate data compared to the observed data. The bias is reduced if the RMSE between the observed and corrected simulated data is reduced towards zero.

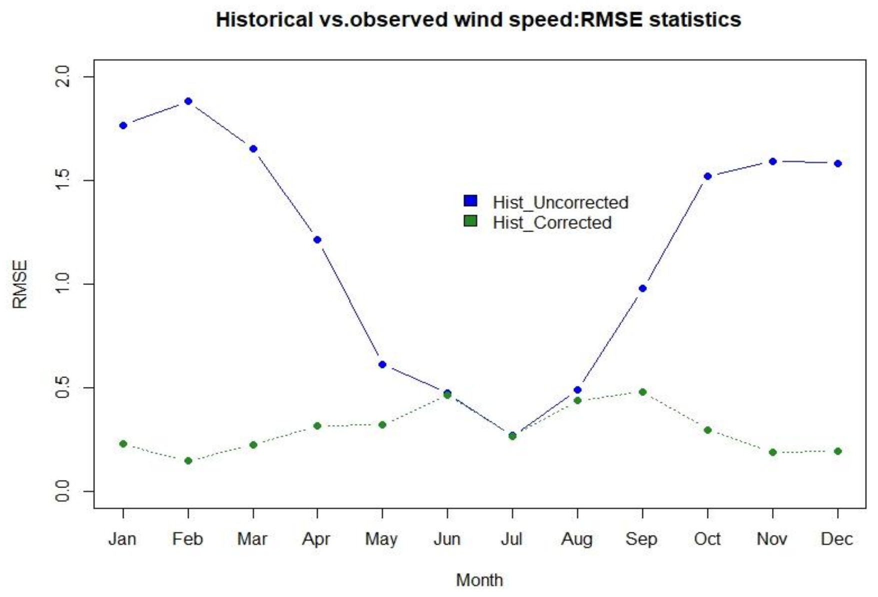

Figure 7-4: Wind speed bias correction and validation

Line plots are for wind speed showing a calculated RMSE for the uncorrected simulated historical (blue line) and the corrected simulated historical (green line) climate data compared to the observed data. The bias is reduced if the RMSE between the observed and corrected simulated data is reduced towards zero.

Figure7-2:4 shows that the original values presented in blue dotted lines have been reduced in most cases. The reductions are represented by the green dotted lines. It is apparent from the observed data that the delta change bias correction method has reduced the ICHEC-RCA4 model data biases in most cases, with the exception of the months of April and May for temperature, and June-July for wind speed. In those months, no change was made. Overall, these results indicate that the delta change bias correction method has reduced the model data biases for most months of the year.

7.4 Potential energy production at the Rusumo Falls study area

This subsection presents and discusses the potential energy production in the Rusumo Falls study area findings. The power outputs from wind speed, solar radiation and precipitation have been obtained using the approach detailed in Section 4.5. The first step of this subsection is to demonstrate how runoff-rainfall modelling was conducted, before preceding to the discussions of the main findings.

7.4.1 Runoff-rainfall modelling

The water discharge for the future period is simulated using the GR2M parameters. The parameters were obtained from GR2M runoff-rainfall modelling as shown in Figure 7-5. The KGE efficiency criteria, shown in equation (19), is used to evaluate the GR2M runoff-rainfall modelling performance. The KGE equation is given as :

$$KGE = 1 - \sqrt{(KGE_{\_r} - 1)^2 + (KGE_{\_\beta} - 1)^2 + (KGE_{\_\alpha} - 1)^2} \qquad \textbf{(19)}$$

Where $KGE_{\_r}$ is the Pearson correlation coefficient between the observed (obs) and the simulated (sim) flows and $KGE_{\_\alpha}$ = sd (sim)/sd(obs), is the ratio between the simulated and observed standard deviations (sd). The $KGE_{\_\alpha}$ evaluates the flow variability error. $KGE_{\_\alpha} > 1$ indicates that the variability in the modelled discharge time series is more than it is in the measured discharge time series, while the opposite case is represented by $KGE_{\_\alpha} < 1$. $KGE_{\_\beta} = mean(sim)/mean(obs)$, is the bias term which evaluates the bias between the simulated and observed flows; $KGE_{_\beta} > 1$indicates an overestimation of the discharge, while the values $KGE_{\_\beta} < 1$ shows an underestimation of the discharge.

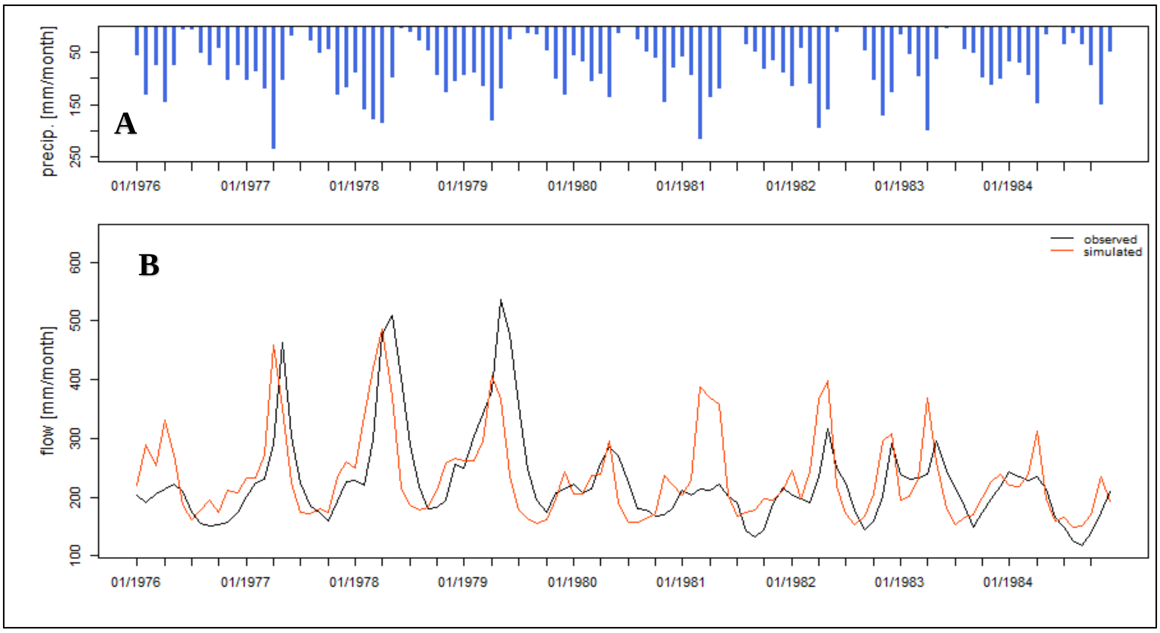

Figure 7-5: GR2M runoff-rainfall modelling performance

Figure 7-5[A] is observed precipitation and Figure 7-5[B] shows the corresponding both observed (black line) and simulated (orange) flows. In the top right corner is the legend showing the observed and simulated flow.

Table 7-1: King-Gupta efficiency criteria

performance criteria	performance criteria	Results
$KGE_{\_r}$	Cor (sim, obs, "pearson")	0.5872
$KGE_{\_\alpha}$	sd (sim) / sd (obs)	0.9392
$KGE_{\_\beta}$	Mean (sim) / mean (obs)	1.0303

Table 7-1 above contains the obtained KGE criteria and $\mathrm{KGE}_{\_\alpha}$ which is equal to 0.9392 indicates that the variability in the modelled discharge time series is lower than in the measured discharge time series. $\mathrm{KGE}_{\_\beta} = 1.0303$ indicates that the discharge is slightly overestimated. It should be noted that good performance, or at least better, results for the model are obtained if the KGE is close to 1 (Nash and Sutcliffe 1970). However, as indicated in the research methodology, the accepted and recommended model performance is an obtained KGE of > 0.5 (e.g., Yuemei et al. 2008, Rauf and Ghumman 2018 and Sidibe et al. 2018). This aligns with the findings of this study as the results in Table 7-1 give a KGE value of 0.581648. The value of greater than 0.5 indicates that the performance of the GR2M is within the recommended performance requirement.

7.5 Discussion of the findings of the Rusumo Falls study area

7.5.1 Monthly and seasonal hydro, wind and solar power joint variability

Figure 7-6 (A&B) shows that hydropower is projected to complement wind power under both RCP8.5 and 4.5. The graph shows that for the months of January to May, hydro and solar power have a positive monotonic linear association, which indicates an anti-complementarity relationship. The latter relationship switches to a negative monotonic linear association, thus a complementarity trend, during the months of May to December.

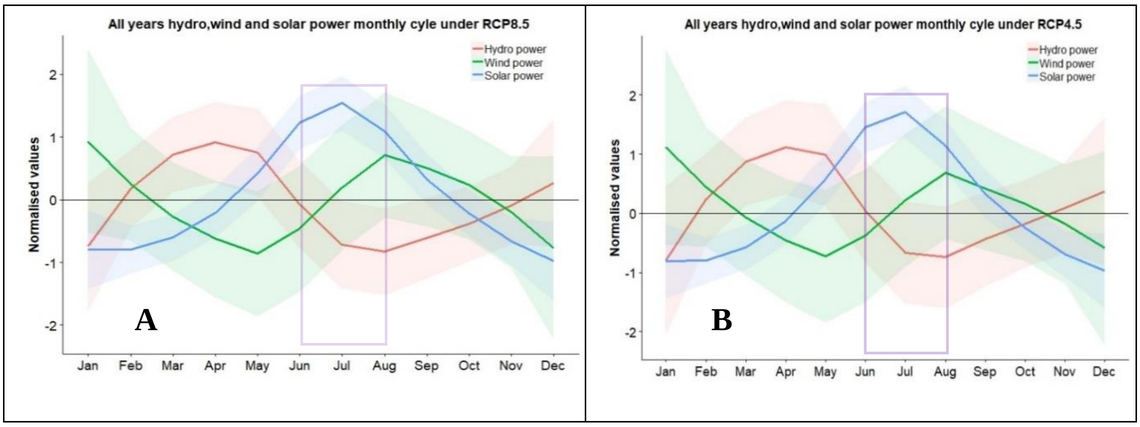

Figure 7-6: Monthly hydro, wind and solar power joint variability

Figure 7.6 shows the normalised value of hydro, wind and solar power of annual monthly cycle joint variability at the case study area for the RCP8.5(A), and RCP4.5(B) and all the periods from 2021 to 2100. The pink boxes highlight the increasing power from wind for the months of JJA.

Figure 7-6 (A&B) displays a complementarity relationship between solar and wind power for the months of January to May and an anti-complementarity relationship between the months of May to December. It can be noted that there is an increase in power generated from the wind during these months which corresponds with the season of JJA. This occurs whilst power from hydro decreases and it can be suggested that this is because the season of JJA is a dry season over the EAC (Schreck and Semazzi 2004, Nandozi et al. 2012, Hamududu and Killingtveit 2016). It can also be observed that, in all months, wind power increases while hydro decreases and vice versa. In brief, hydropower has an invariably complementary relationship with wind power for the period between 2021 to 2100 under both RCP4.5 and 8.5. On the other hand, solar power has a mixed relationship with both hydro and wind power.

In the section that follows, the join variability between the hydro, wind and solar power seasonal cycle will be examined and the strength of such relationships will be determined. These relationships are shown in Figure 7-7, Figure 7-8, and Figure 7-9. These figures share most features and therefore they are grouped as one within this study and discussed together. That being said, the individual figures are also presented for clarity and readability purposes. Within this section, the seasonal cycle for the period between 2021-2100 will be explored followed by an examination of the strength and significance of the relationship.

7.5.2 Hydroclimate potential seasonal power joint variability for the period of 2021 to 2100

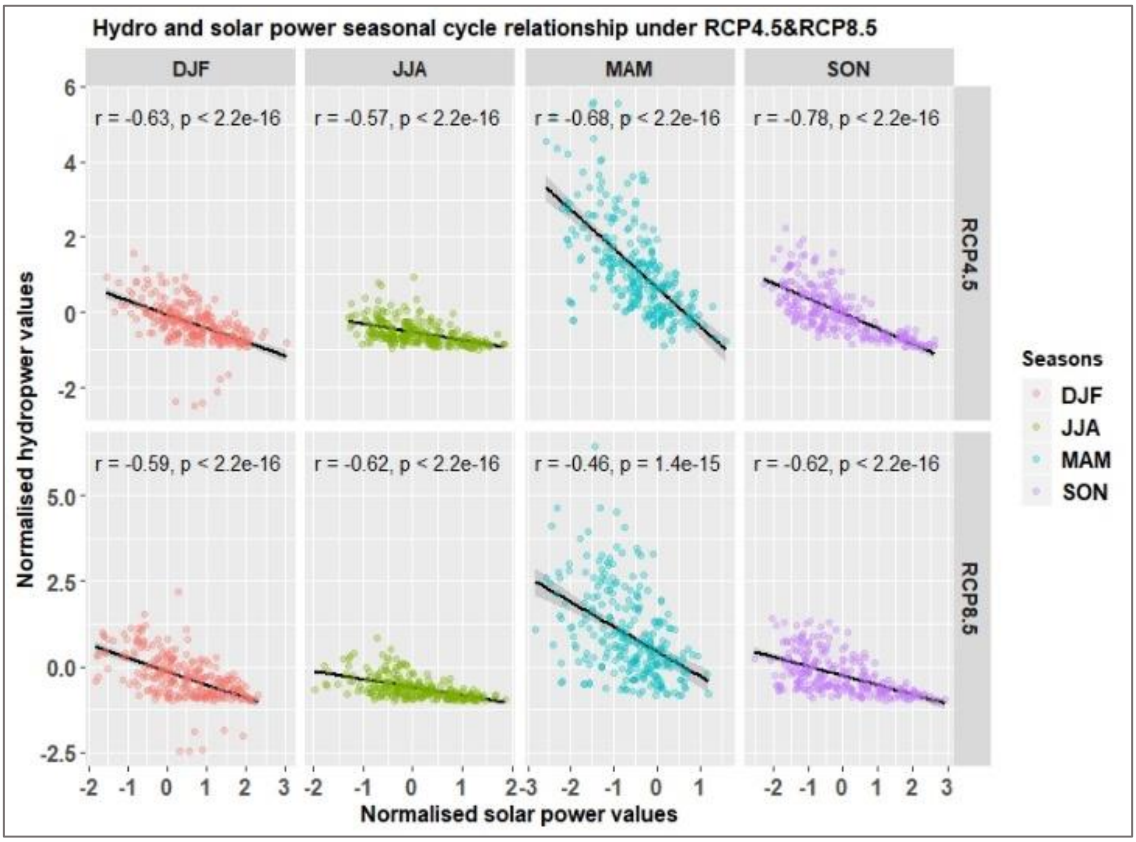

Figure 7-7: Joint variability of hydro and solar seasonal power at Rusumo Falls
This figure shows the seasonal cycle relationship between hydro and solar power sources under the RCP4.5 and 8.5 scenarios for the periods of 2021 to 2100 time. r is the Spearman correlation coefficient denoted ρ_s in the discussion. P is the significance (P-value) of the joint variability at α=0.05. The seasons are DJF-December, January and February; MAM- March, April and May; JJA -June, July and August; and SON-September, October, November.

Based on the time horizons and climate scenarios, the results in Figure 7-7 above indicate that the hydropower seasonal cycle is complementary with solar power. Analysis of the data shows a coefficient of correlation for all seasons ranging from ρ_s= -0.78 to -0.57 for RCP4.5 and ρ_s= -0.62 to -0.46 for RCP8.5. In all cases, for the time horizons and climate scenarios, the p-value is $p < 0.05$ as per Figure 7-7. This indicates that under the two climate scenarios and for the periods between 2021- 2100, the hydropower and solar radiation seasonal cycle relationship is complementary.

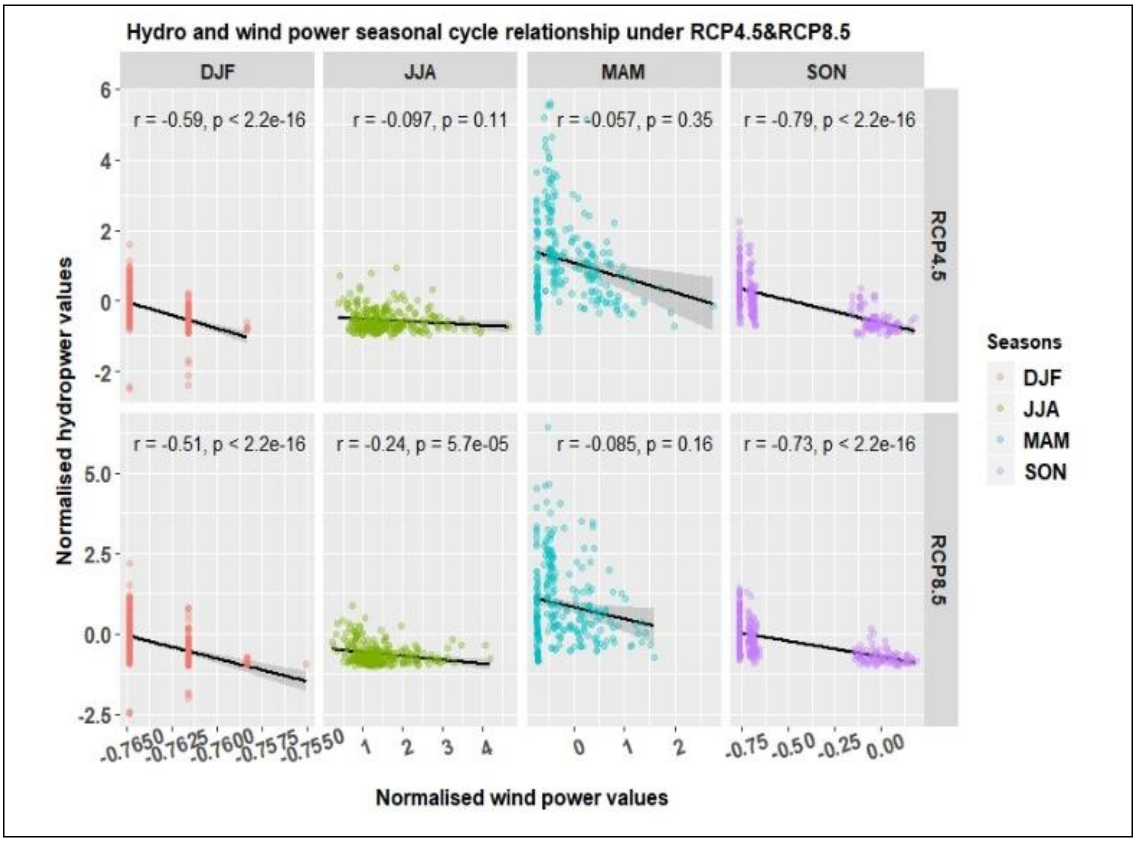

Figure 7-8: Joint variability of hydro and wind seasonal power at Rusumo Falls

This figure shows the seasonal cycle relationship between hydro and wind power sources under the RCP4.5 and 8.5 scenarios for the periods of 2021 to 2100 time. r is the Spearman correlation coefficient denoted ρ_s in the discussion. P is the significance (P-value) of the joint variability at α=0.05. The seasons are DJF-December, January and February; MAM- March, April and May; JJA -June, July and August; SON-September, October, November.

Figure 7-8 above illustrates the seasonal cycle relationship under both climate scenarios. For this figure (7-8), hydro and wind power demonstrate correlation coefficients ranging from -0.057 to -0.79. This is important because this relationship is statistically significant (i.e. the p-value is < 0.05) for the seasons of SON and DJF. However, the relationship is statistically non-significant (i.e. p-value is > 0.05) under the RCP8.5 for the season of MAM and for the seasons of JJA and MAM under the RCP4.5. It should be noted that the season of MAM is a rainy season (Liebmann et al. 2014, Funk et al. 2015) and, as highlighted earlier, the power output from wind for the dry seasons of JJA shows an increasing trend while precipitation shows as decreasing. This means that although the complementarity between hydropower and wind power is not statistically significant during the dry seasons when hydropower is at its low production, the energy from wind power resources can still act as a supplementary source for hydropower during the dry season. This is because the complementarity does not matter if they can both still meet the demand individually (Bett and Thornton 2016). If the hydro and wind power are not complementary and not able to provide a continuous power supply, then a third source of energy to fill the possible deficit in energy supply has to be found.

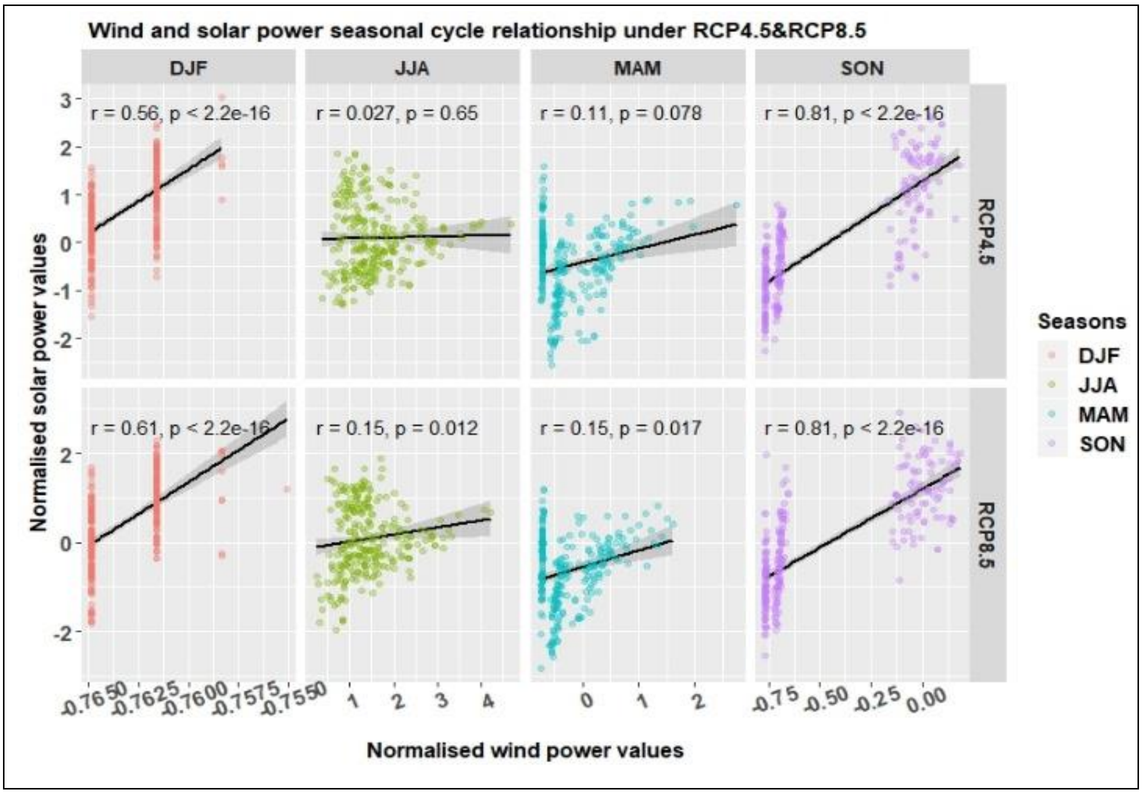

Figure 7-9: Joint variability of wind and solar seasonal power at Rusumo Falls

This figure shows the seasonal cycle relationship of solar and wind power sources under RCP4.5 and 8.5 scenarios for the periods of 2021 to 2100 time. r is the Spearman correlation coefficient shown as ρ_s in the discussion. P is the significance (P-value) of the joint variability at α=0.05. The seasons are DJF-December, January and February; MAM- March, April and May; JJA -June, July and August; SON-September, October, November.

Moving to solar and wind power joint variability, Figure 7-9 above shows that the correlation coefficients for solar and wind power varies from ρ_s: 0,027 to 0.81 for RCP4.5 and 0.012 to 0.81 for RCP8.5. The relationship between solar and wind power is statistically significant (p-value is less than 0.05) for the seasons of SON and DJF, whereas the p-value for the MAM and JJA is not statistically significant (P-value is greater than 0.05). This is an indication that the combination of wind and solar power sources analysed may not be reliable throughout the seasons if the power outputs from the two resources cannot meet the power demand, irrespective of their lack of complementarity status.

In summary, it can be concluded with a high level of certainty that hydropower will remain in complementarity with solar power for all seasons and time periods between the dates 2021-2100, under both RCP4.5 and 8.5 scenarios. If we now turn to the joint variability for both hydro and solar power in conjunction with wind power, the results do not show a consistent complementarity throughout the seasons. Hence, when planning to provide an uninterruptible power supply (i.e. free from blackouts), optimal combinations of the hydro, wind and solar power resources must be taken into consideration.

7.6 Optimal combinations of hydro, wind and solar power resources in a hybrid system for electrification

This section aims to identify the optimal combinations of a hybrid system in order to meet the electricity demand for the hypothetical village. The section, which is split into two parts, considers the power generation technology for electrification and is designed to achieve objectives four and five of this study.

Part one of this section focuses on objective four which is: "to propose optimal hybrid combinations of hydro, wind speed and solar power for electrification of a selected case study area". This part is structured as follows: firstly, it gives the methodology for energy resources hybrid system modelling. Next, it provides the hypothetical village load profile where the term load refers to a demand for electric or thermal energy (Lambert et al. 2005). Finally, it explains data sources, components, assessment and economic modelling.

The second part of this section focuses on answering research question 3 which is: How can decision-makers in the EAC improve energy access in ways which are reliable, affordable and climate-resilient? Objective five of this research, which seeks to develop a systematic pathway for renewable energy implementation in the EAC, helps to answer this question as the overall result of objective five has been produced as a culmination of the analyses undertaken throughout objectives one to four. This includes calculating power outputs from hydro, wind and solar energy sources and requires factors such as the minimum threshold quantity of the river flow (Anderson et al. 2015), wind speed (Miskelly 2016) and solar radiation as well as efficiency and rating of power generation technologies (e.g. Reynolds 1983, Manwell et al. 2010, Wild et al. 2015). These factors can dictate the amount of power output from these renewable energy sources. Therefore, a renewable energy generation system that meets regional electricity demand in a reliable, sustainable and climate-resilient manner, must include the factors mentioned above as key components of the power generation system. IRENA (2017) indicates that the cost efficiency of renewable power generation is improving and that in addition, the associated cost is falling.

Based on future projections, the cost efficiency of renewable power generation technology will continue to fall based on future projections (IRENA 2018). As an illustrative example, the author (IRENA 2018) states that based on project and auction data, the percentage of cost reduction experienced for every doubling of cumulative installed capacity is estimated at 14%, 21% and 35% for offshore wind, onshore wind and solar PV respectively. This suggests that the cost of the technology needed for renewable energy systems and the financial implications of this will differ greatly from today's investment requirements during the middle and long term future. As a consequence, the best combinations based on the near future climate data (2021-2050) for hydro, wind and solar power energy sources from the selected study area are shown in Figure 4-1[C] and were used to simulate energy demand for the hypothetical village. The energy supply for the village was simulated using the application of HOMER PRO software. HOMER PRO was adopted by this study for the reasons described in Section 4.6 and this software is further described in the subsequent section.

7.6.1 HOMER PRO

HOMER PRO is a micropower optimisation software developed by the U.S National Renewable Energy Laboratory (NREL). It repeatedly appears in literature as a preferred tool (e.g., Gilman and Lilienthal 2006, Mitra and Chaudhuri 2006, Asrari et al. 2012, Bekele Beyene 2011, Girma 2013, Chang 2014, Sen and Bhattacharyya 2014, Dharmala 2015, Kim et al. 2017, Muthusamy 2018). The HOMER PRO software is also described as a global standard for micro-grids and the design of distributed energy systems and is used in more than 190 countries by over 150,000 users (Francklyn 2018). The software is designed for micropower systems to measure the behaviour and life-cycle costs of power systems. It facilitates the comparison of power generation technology across a wide range of applications based on the Total Net Present Cost (TNPC) (Gilman and Lilienthal 2006). The TNPC is then used to represent the life cycle cost of a system, such as the costs of initial construction, component replacements, maintenance and other miscellaneous costs (Firincă SD et al. 2015). Overall, the HOMER Pro is used in both developed and developing countries.

Only selected applications of the software in both developed and developing countries are provided because a more detailed review of such applications is beyond the scope of this research. With regards to its utilisation in developed countries, the applications of HOMER PRO includes the findings of Khan and Iqbal (2005) who investigated the feasibility of a hybrid system with hydrogen as an energy carrier in Newfoundland, Canada and conclude that there is a potential solution for stand-alone power generation is to use a hybrid energy system in parallel with some hydrogen energy storage. Previous research by Türkay and Telli (2011) examined the feasibility of combining solar and wind energy with hydrogen as storage with conventional grid-based electricity in order to meet the electricity load of the pilot region in Turkey. Finally, Giatrakos et al. (2009) conducted a study on sustainable energy planning based on a stand-alone hybrid renewable energy system in Karpathos island, Greece.

Selected HOMER Pro applications in developing countries include a feasibility analysis for optimal design and planning of renewable energy-based micro-grid systems for a hypothetical rural community in developing countries (Hafez and Bhattacharya 2012). Hassan et al. (2016) conducted a computer simulation and optimisation of a hybrid power generation system in the rural area of the Muqdadiyah district of Diyala state, Iraq. Other similar studies include Bekele and Palm (2010) who examined the feasibility of a sustainable solar-wind-based hybrid energy system for application in Ethiopia. All of these applications show how HOMER Pro is the preferred tool for multiple renewable energy resource optimisation. Following these successful applications of the HOMER Pro software, this research chose to utilise the software in order to propose optimal hybrid combinations of hydro, wind speed and solar power for electrification of the aforementioned hypothetical village in the selected study area.

7.6.2 How HOMER Pro works

The HOMER Pro performs three principal tasks: simulation, optimisation, and sensitivity analysis (Lambert et al. 2005). The principal tasks performed in the HOMER Pro are shown in Figure 7-10. This figure describes the relationship between the three key principal tasks that have been performed using HOMER Pro. A single optimisation task involves multiple simulations and a single sensitivity analysis consists of multiple optimisations.

Figure 7-10: Conceptual relationship between simulation, optimisation, and sensitivity analysis.
Source: (Francklyn 2018)

In the simulation process, HOMER Pro models the performance of a particular configuration of a hybrid/ micropower system for each hour of the year to determine its practical feasibility and life-cycle cost (Gilman and Lilienthal 2006). In the optimisation process, many different system configurations have been simulated. The unfeasible options are eliminated and the feasible options are ranked according to the TNPC (Lambert et al. 2005, Gilman and Lilienthal 2006). Sensitivity analysis helps assess the effects of uncertainties or changes in the variables over which the designer has no control, such as the average wind speed or the future fuel price (Lambert et al. 2005, Sen and Bhattacharyya 2014b, Francklyn 2018). HOMER Pro works as an optimisation tool that decides whether multiple renewable energy sources can or cannot satisfy the electric load for each of the 8,760 hours in a year based on the TNPC. If these sources are inadequate, HOMER Pro then ensures that other sources such as the generator and grid are incorporated into the configuration system in order to satisfy the demand.

7.6.3 Advantages and Disadvantages of HOMER Pro

Gilman and Lilienthal (2006) argue that HOMER Pro's simulation logic is not as detailed as other time-series simulation software for micropower systems such as HYBRID2 (Green 1996), PV-Design Pro (Fanney 2019), and PV*SOL (Valentin 2013). However, out of all of these models, HOMER Pro is the most flexible in terms of the diversity of its systems. This is because it can model and display modelled results in a wide variety of tables and graphs that help the designer to compare configurations and assess them on their economic and technical merits (Lambert et al. 2005). Moreover, HOMER Pro possesses data for a number of manufacturers' component costs and their sizes specifications? are already built into the program (Farret and Simões 2006, Stiel and Skyllas-Kazacos 2012). Due to this, Belu et al. (2014) argue that HOMER Pro software has all of the features and options necessary to make it a strong option for hybrid optimisation of renewable energy sources.

Other advantages and disadvantages identified by users (e.g. Okedu and Uhunmwangho 2014) indicate that the HOMER Pro runs many combinations efficiently, but will not supplement key values or sizes if they are missed. Consequently, with reference to this study, the HOMER Pro was applied in the optimisation of renewable resources for the hypothetical village and any technical limitations as previously mentioned were taken into consideration.

7.6.4 Hypothetical village data sources and estimated electricity demand

With limited access to load profile data, the load profile for the hypothetical village was built on previous publications and data from the United Nations High Commission for Refugees (UNHCR). Hence, the proxy population data used are from a Refugee Camp (RC) called Mtendeli and the data were provided by the UNHCR. The data are provided in Table 7-2 below and the assumptions in the table are subsequently explained.

The RC is located in the north-west of Tanzania at coordinates: Lat 3°25'17.399" S Lon 30°53'24.212" E. According to the UNHCR (2016), the RC houses a population of 50,000 individuals, accounting for 12109 households (HH).

Table 7-2: Details about the hypothetical village data

Selected particulars	**Details**	**Baseline Electricity demand (kWh/day)**	**Electricity demand (kWh/day)**
Village name	Hypothetical village	-	--------
Country	Extends between Rwanda, Burundi and Tanzania	-	--------
Location	Latitude: -0.99N, -3.0001S	-	--------
	Longitude: 29.99W, 32.0E	-	---------
RC total HH*	12109	-	---------
RC Total* population	50,000	-	----------
Admin divisions*	10 Zones, 93 Villages, 1397 Blocs	-	----------
Estimated number of HH/per zone	$\frac{12109}{10} = 1210.9 \sim 1211$	-	-----------
Hypothetical village HH size	1,211	1.151kWh/day**	1,393.36
RC primary* school	3	5kWh/day***	15
RC secondary* school	2	11kWh/day***	22
RC medical facilities *	2	25kWh/day****	50
Total electricity demand per zone			1,480.36 kWh/day

Source: *(UNHCR 2016); **(Banerjee et al. 2013, IEA 2017); ***(Ugirimbabazi 2015);****(USAID 2011).

The UNHCR indicates that the RC has various services including 2 health facilities, 3 primary schools and 2 secondary schools. The electricity demand for the hypothetical village assessment is based on the above information from the Mtendeli RC. Providing electricity for this large number of the population would require considering a diesel generator in the hybrid system (i.e. Sen and Bhattacharyya 2014b, Kaur and Segal 2017, Halabi et al. 2017, Rousis et al. 2018). Since this section is about proposing an optimal combination of hydro, wind speed and solar power for electrification of the hypothetical village, the number of HH for the hypothetical village is estimated to be equivalent to the HH of one zone within the RC.

It is assumed that all of the 10 zones within the RC have equal HH size, hence one zone measures as: $\frac{12109\text{ HH}}{10\text{ zones}} = 1210.9{\sim}1211$ HH/zone. For context, it should be noted that the population within the considered zone share facilities such as schools and hospitals with other zones. The estimation of the electricity demand for the hypothetical village is based on the International Energy Agency (IEA) energy access definition, which indicates that the average HH with gained access has enough electricity to power four lightbulbs operating at five hours per day per lightbulb, one refrigerator, a fan operating six hours per day, a mobile phone charger and a television operating four hours per day. This equates to an annual electricity consumption of 420 kWh per HH/year based on generally efficient appliances (IEA 2017).

Previously, Banerjee et al. (2013) reported that for universal electrification to be achieved by 2030, there should be a minimum consumption threshold of 420 kWh/HH/year. Since energy efficiency is an integral part of the EAC renewable energy and energy efficiency policy (e.g. Nalule 2016) and the desire to achieve SDGs, it can be assumed that the hypothetical village will use efficient appliances. This will mean that energy consumption will meet the minimum consumption threshold mentioned above. Hence, the 1210.9 HH energy consumption (kWh/day) would measure at $\frac{420\text{kWh}}{365\text{ days}} \times 1211\text{HH} = 1393.36\text{kWh}/$ day. The hypothetical village has 2 health facilities. A study commissioned by the United States Agency for International Development (USAID) in East Africa indicates that a health clinic with high energy requirements consumes between 20 – 30 kWh/day (USAID 2011). Hence, considering that a health clinic consumes on average 25kWh/day [(20kWh/day + 30kWh/day) / 2], the two health clinics located within the hypothetical village are estimated to consume about 50kWh/day (25kWh x 2).

The village also has 3 primary and 2 secondary schools facilities. To understand the level of energy required for the school facilities, assessment is needed on a case by case basis. This is necessary in order to assert the requirement in line with local preferences, needs, and resources (Welland 2017). There are various applications of electricity within schools but the most common applications are lighting (indoor, outdoor and emergency), communications (radio/telephone/email/ fax), water delivery and treatment, computers and ICT, food preparation, and heating and cooling (cf. Jimenez and Lawand 2000, Girma 2013, Practical Action 2014, Welland 2017). Regarding the applications of electricity in each school, the load demand for the hypothetical village is built on power system options for a rural electrification study previously conducted in Rwanda. This study concluded that school facilities in a typical village require 5kwh/day per primary school and 11kwh/day per secondary (Ugirimbabazi 2015).

The school facilities' power consumptions as given by Ugirimbabazi were cross-checked with a previous feasibility study of renewable energy resources for electrification of Mall Island in Ethiopia – a country in the East African region considered to be an African powerhouse with strong overall growth (Brenna et al. 2016). The study concluded that primary schools would need 3.07kWh/day in electricity and secondary schools would need 14.66kWh/day (Mekonnen 2019). As expected, the energy consumptions in the two studies are slightly different (but within the same region). This may be due to the local preferences, needs and resources already mentioned above. Other reasons for the hypothetical village school facilities to build on the school facilities energy consumption in Rwanda is that the Rwandan government has planned to achieve universal energy access by 2024 (USAID 2019), this is six years earlier than its counterparts Tanzania and Burundi who are planning to achieve the 2030 universal energy access target set by United Nations' SDG (cf. UNECA 2018). In addition, Rwanda launched vision 2020 in the year 2000 (KABERUKA 2000), whereby various projects such as Laptop Per Child were initiated by RENCP- Rwanda Education NGO Coordination Platform (Rwagaju and Intwali 2010). Through this project, approximately 250,000 laptops have been distributed to various schools across Rwanda (Buhungiro 2014). Therefore the energy consumption in Rwandan school facilities can serve as a benchmark for developing countries looking to provide sufficient and evolving levels of energy for school facilities. Hence, the 3 primary schools consume on average 5kWh/day x 3 (15kWh/day) and 2 secondary schools consume on average 11 kWh/day x 2, which equates to 22kWh/day. Given the above assumptions, the total hypothetical village electricity demand is therefore 1480.36 kWh/day (1393.36 kWh/day + 15kWh/day + 22kWh/day + 50kWh/day). With this information, either grid or off-grid can be considered as options for the electrification of this village. This depends on which option is economically viable. Within this study, the principal issues and suggestions which have arisen from the two options, as well as a recommendation for which option is best placed, will be discussed.

7.6.5 System modelling

As previously mentioned, data for the hydro, wind and solar radiation power sources are extracted from the ICHEC-RCA4 climate model for an area at coordinates Latitude: -0.99N, -3.0001S and Longitude: 29.99W, 32.0E (cf. Figure 4-1[C]). A hybrid system of photovoltaic (PV), wind turbine, batteries and hydropower technology has been considered. The electricity load for the hypothetical village is Alternating Current (AC). As a result, the wind turbine, the batteries and the PV system are connected to the DC side of the network. The hydro system is connected to its Direct Current (AC) side.

To maintain the energy flow between the AC and DC components and satisfy village demand, a power converter has been provided. Based on the estimated electricity demand of 1480.36 kWh/day as per Table 7-2 for the hypothetical village, the daily and seasonal electricity consumption patterns are also shown in Figure 7-11[A] and Figure 7-11 [B] respectively. The yearly electricity consumption patterns are represented by the Data Map (DMap) shown in Figure 7-11 [C]. These profiles indicate that people consume relatively the same amount of power in all months of the year. More specifically, a considerable amount of power is consumed during the evenings between 5 p.m. and 10 p.m in both the daily and yearly profiles.

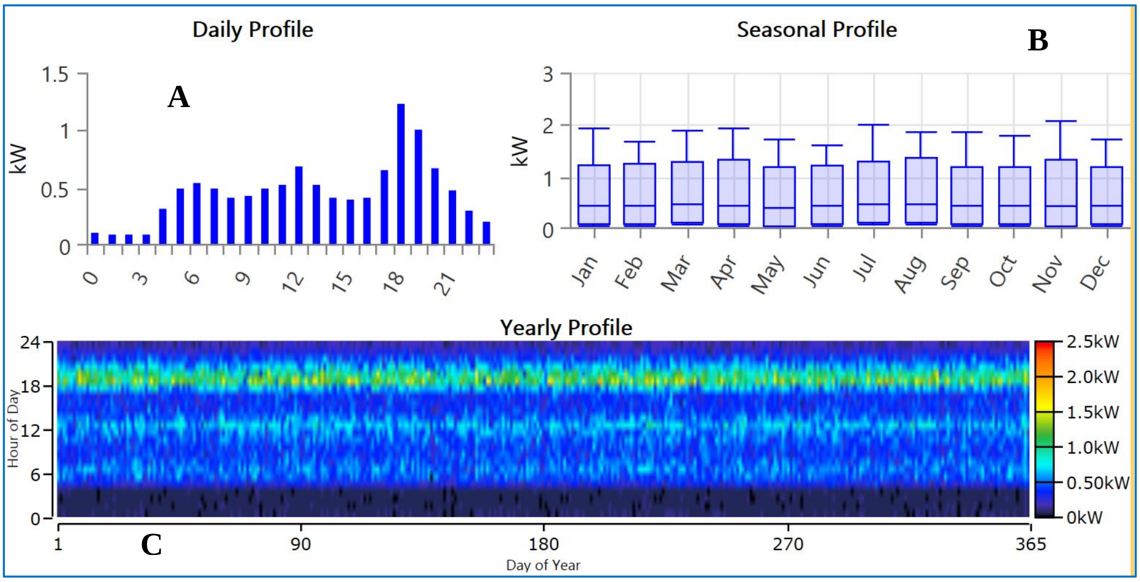

Figure 7-11:Hypothetical village synthetic electricity consumption patterns
Subfigure (A) shows daily consumption throughout the 24 hour cycle and (B) is monthly consumption, while subfigure (C) shows the daily consumption at each hour of the day throughout the year.

Looking at Figure 7-11 [B], the central line in the boxplots shows the overall average monthly electricity consumption patterns, while the top and bottom lines of the boxplots indicate respectively the average monthly maximum and minimum electricity consumptions patterns. With this, the HOMER Pro applies random variability to account for differences in daily electricity consumption behaviours. When the applied random variabilities are aggregated, they become apparent within the monthly energy consumption patterns profile. That is why the seasonal electricity consumption profile shown in Figure 7-11[B] is slightly different from one month to another.

7.6.6 HOMER Pro Components Design

The HOMER Pro components system shown in Figure 7-12 are designed to achieve objective four of this research.

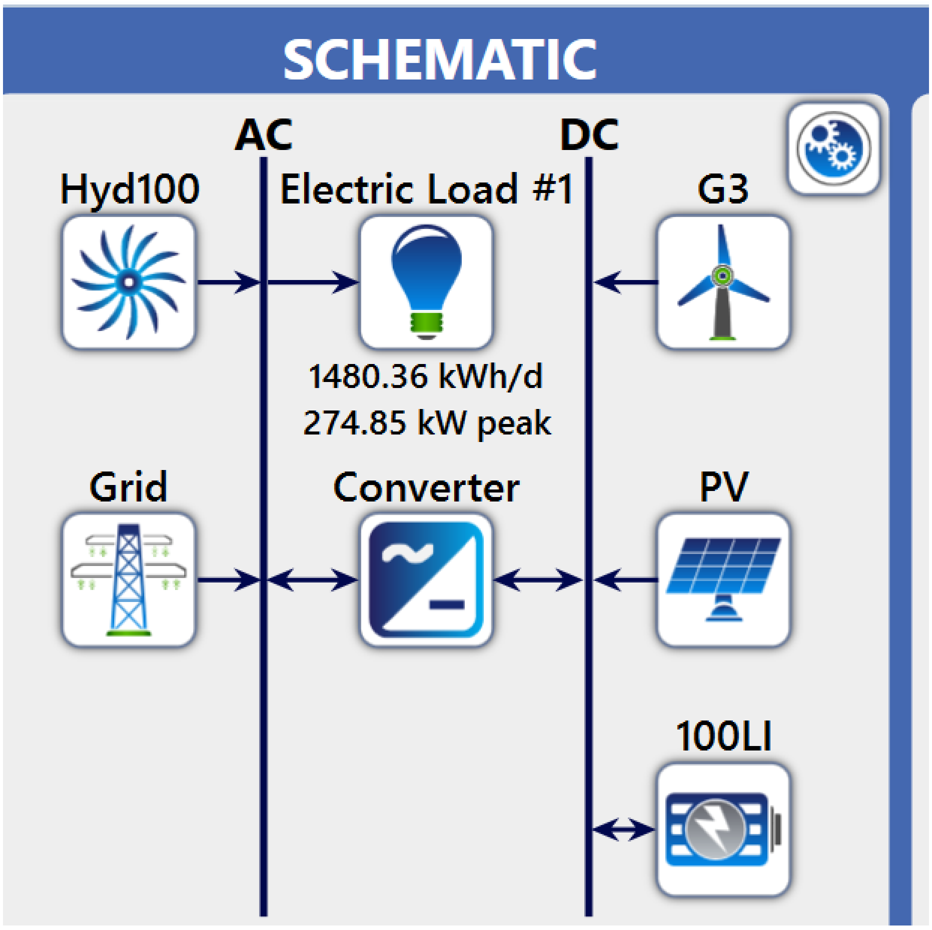

Figure 7-12: Schematic of proposed renewable technologies for the hybrid system

The components of the system are wind power, hydropower and solar PV, and a battery is connected to the DC side to store such electricity. Following previous studies in East

Africa (e.g. Bekele 2011 and Girma 2013), the proposed system is designed with a life span of 25 years and the real interest rate is fixed at 10 %. In addition, the proposed system inflation rate is considered to be 7.8% (AfDB 2018). The cost of connecting the proposed power plant to an existing grid has been evaluated to assess the financial viability of the power plant. As a consequence, a grid-connected component was used in this study for the comparative analysis and determination of the Economic Distance Limit to the grid (EDL). Each component of the hybrid system is described in the following sections, which includes solar PV system, wind turbines, hydro, battery and power converters and the grid.

7.6.6.1 Photovoltaic (PV) system

The PV system is connected in series and a generic flat-plate PV (1kW) has been used to make sure the findings of this study are applicable elsewhere. The costs of the PV system are as shown in Figure 7-13 below.

Figure 7-13: PV system design

The PV capital cost is $2,500.00. The replacement and Operation and Maintenance (O&M) costs are respectively considered to be as 60% and 1% of the capital (Damrongsri et al. 2019). Therefore, the replacement and O&M costs are $1,500.00 and $25.00/year respectively.

For confirmation, the considered PV capital cost was cross-checked with the current market price (e.g. GreenBusinessWatch 2019 and Gov.uk 2019). PV sizing is dependent on the software finding a suitable size for the system. As a consequence of this, the HOMER Pro Optimiser option (highlighted in green, cf. Figure 7-13) was selected. This is because the HOMER Pro Optimiser minimizes user error and finds the optimal sizing much faster than a user-defined size (Lambert et al. 2005). Most of the manufacturers usually offer solar panels with 20-25 years of warranty (Damrongsri et al. 2019). In addition to this, Granata et al. (2014) suggest that a solar panel lifetime is generally 25 years. The number 2 (in red) shown in Figure 7-14 indicates that the PV lifetime gives the option of 20 and 25 years for the HOMER Pro simulation. During the simulation, HOMER Pro will select the number of years that will give the lowest overall life-cycle cost of the PV system.

Studies conducted in both Ethiopia (e.g. Getachew and Getnet 2012) and Rwanda (e.g. Ugirimbabazi 2015) considered a PV array slope angle of 15 degrees and the array azimuth of 0 degrees. Based on this previous research, the PV array slope angle and azimuth as aforementioned are considered in this study. The available solar radiation is given in Figure 7-14 below and as stated elsewhere, the data is sourced from ICHEC-RCA4 model data for the near future (2021-2050) period.

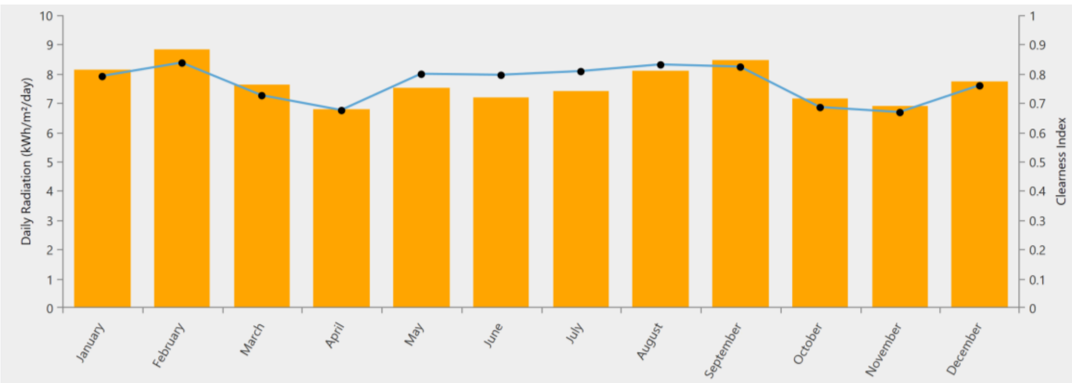

Figure 7-14: Daily solar radiation with clearness index for the period 2021-2050
The yellow bars represent the daily solar radiation and the blue line is clearness index

In previous studies (e.g. Bekele Beyene 2011, Mekonnen 2019) conducted in Ethiopia, a derating factor of 90% was applied to the electric production from each panel. The PV derating factor is a scaling factor that HOMER Pro applies to the PV array power output to account for reduced output in real-world operating conditions compared to the conditions under which the PV panel was rated (Lambert et al. 2005). This means that a derating factor of 90% reduces the PV electric production by 10% to account for the varying effects of real-world operating conditions such as temperature, wiring losses, shading, dust on the panels and ageing (Lambert at al.2006).

7.6.7 Wind turbine

Energy from a wind turbine depends greatly on wind variations (Lydia et al. 2014, Uluyol et al. 2014, Sohoni et al. 2016). A 3 kW wind turbine model was considered and for this wind turbine size and Scirocco (2012) suggests a hub height of 18m. Figure 7-15 below shows the wind power system properties and costs.

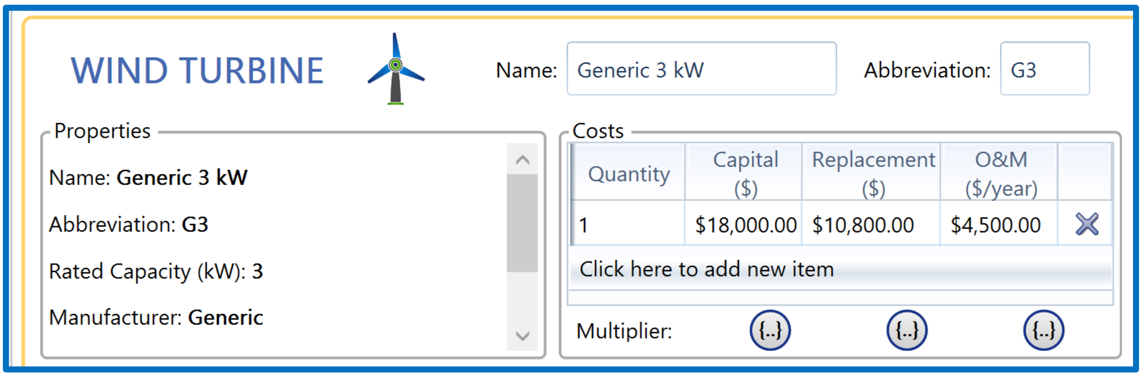

Figure 7-15: Wind system design

The capital cost of one unit is considered to be $18000 USD, the replacement and O&M costs are considered to be 75% and 2.5% of the capital cost respectively (Longe et al. 2017). The wind turbine capital costs and properties assumptions are considered following the analysis of power system options for rural electrification in an Ethiopian study conducted by Bekele (2011). Wind turbine lifespan generally lies between 20 to 25 years (Ziegler et al. 2018), and to allow the simulation program to find a wind turbine lifespan suitable for the designed system both 20 and 25 years were input for the wind turbine lifetime simulation. Figure 7-15 shows that the wind turbine rated capacity is (3kW). The wind turbine rated capacity is explained as the maximum amount of power with which a wind turbine can produce at its rated wind speed. This denotes the wind speed at which the turbine is able to generate electricity at its maximum (Lambert et al. 2005, Scirocco 2012). Wind data from ICHEC-RCA4 model are plotted in Figure 7-16 below.

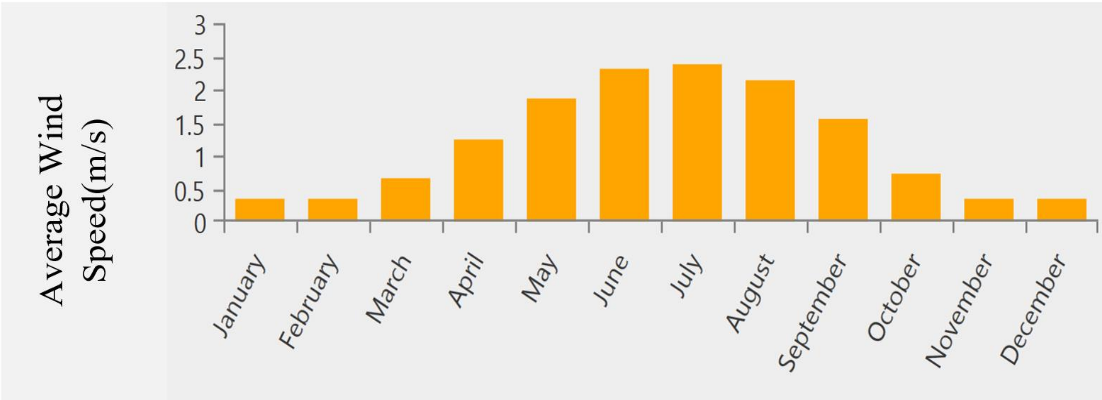

Figure 7-16: Average monthly wind speed for the period of 2021-2050

7.6.8 Hydropower

Figure 7-17 below shows the hydropower design system. The hydropower system is designed for a power output of 100 kW and the turbine is designed for the available net head of 15 metres (Stadler 2017). The heads of 20m and 25m, as well as 5% and 10% of head loss (shaded in yellow), have been added to the simulation for hydropower generation sensitivity analysis.

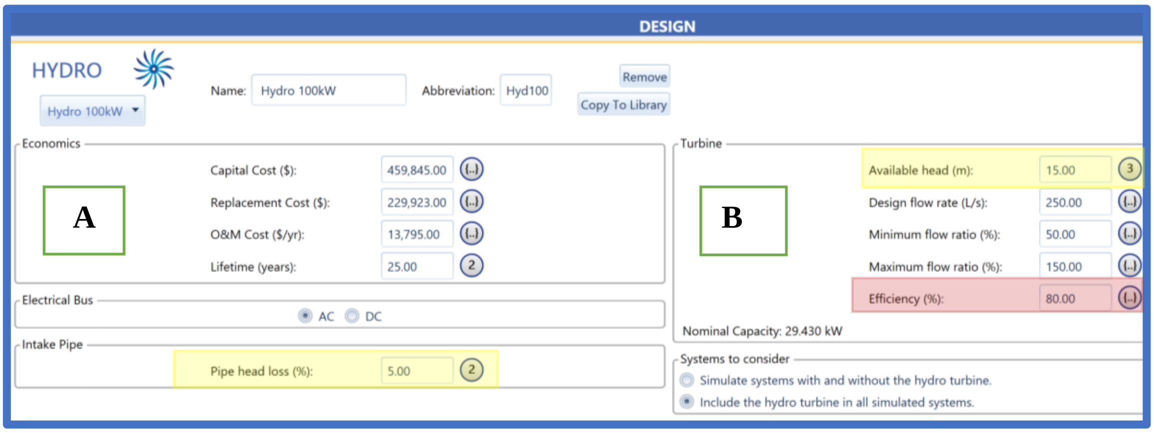

Figure 7-17: Hydropower design
A shows the hydro design economics and B shows the turbine specifications

For this type of water turbine, the economic factors and specifications are shown in Figure 7-17 [A] and [B]. The cost assumptions and specifications for the water turbine are taken from HOMER software database (Homerenergy 2019) as follows. The initial capital cost of this water turbine is $459,845. There is a replacement cost of $229,923 and a maintenance cost of $13,795/year. A 20 and 25 years lifetime for the water turbine were fed into the simulation for the software to find which lifetime is optimal in terms of the water turbine design. The hydropower system economic and turbine specifications were taken from the HOMER Pro database (homerenergy 2019). Figure 7-18 below is a chart showing the river runoff data obtained from the ICHEC-RCA4 model for the near future (2021-2050) at the case study area.

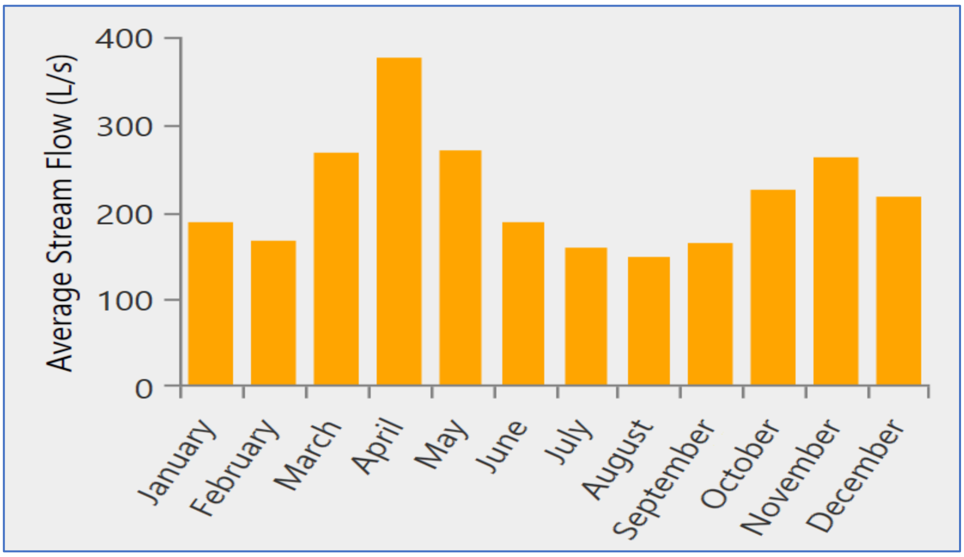

Figure 7-18: Average monthly streamflow for the period of 2021-2050

7.6.9 Battery

An energy storage system is required to reduce the fluctuation, improve the operational efficiency of the hybrid system and provide a reliable energy supply (Miñambres-Marcos et al. 2018). Consequently, the hypothetical village has battery storage that balances the energy production variability due to the intermittent nature of wind and solar energy resources. The details of the battery storage system design are shown in Figure 7-19.

The battery properties are indicated in the section labelled A and the capital, replacement and O&M costs are provided in the section labelled B.

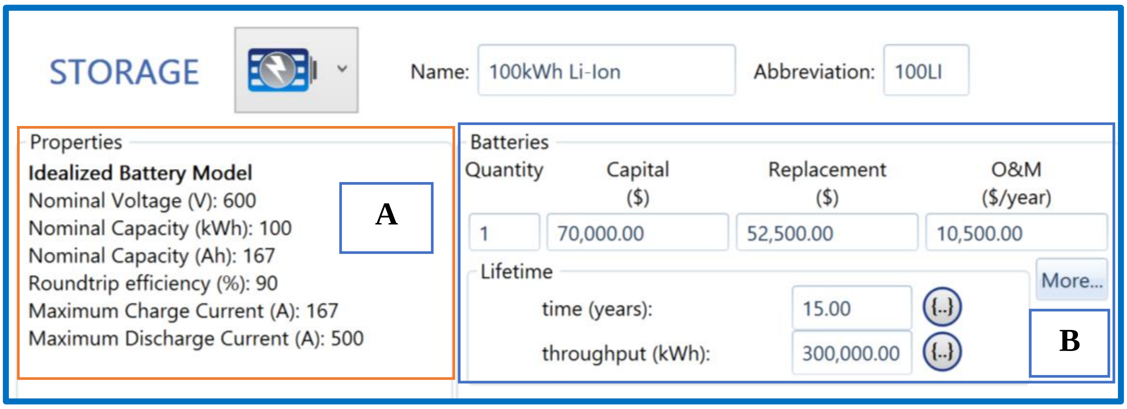

Figure 7-19: Energy Storage System Design

The battery for this system has a nominal voltage of 600 with a 100kWh of storage capacity. The capital cost according to the HOMER Pro database is $70,000.00. The replacement cost is considered to be 75% of the capital cost (Longe et al. 2017) and O&M/year is considered to be 1.5% of the capital cost (Naumann et al. 2015, Damrongsri et al. 2019). This battery capital cost was cross-checked with various other studies and was found to be in line with the costs suggested for Lithium-ion battery (i.e. Luo et al. 2015, Gandarillas and Kelly 2015).

7.6.10 Power converter

The power converters are used to convert the electric energy flow from AC to DC (Asrari et al. 2012). The cost and input for the converter system design are summarised in Table 7-3 below.

Table 7-3: Converter System Design Cost and Input

Converter cost			
Capacity (kW)	Capital($)	Replacement($)	O&M ($/year)
1	$300.00	$300.00	$10.0
Converter Input			
Lifetime (years)		Efficiency (%)	
15		95	

As shown in Table 7-3, the system designed for the hypothetical village has a converter of 1kW capacity. The assumptions made for the installation cost is $300 per 1 kW with a replacement cost of $300 per 1 kW. The O&M is considered as $10 per year (Longe et al. 2017). A lifetime of the battery unit is considered to last 15 years with an efficiency of 95%. The converter capital cost, lifetime and efficiency data were considered based on previous studies (e.g. Getachew and Getnet 2012; Rousis et al. 2018).

7.6.11 Grid Extension

Lambert et al. (2005) indicate that the grid extension tab allows studies such as this one to consider grid extension as an alternative to a stand-alone system. They also place emphasis on the fact that HOMER Pro compares the cost of the grid extension with the cost of each stand-alone system configuration and calculates the break-even grid extension distance (Lambert et al. 2005). The grid extension design is shown in

Figure 7-20 below:

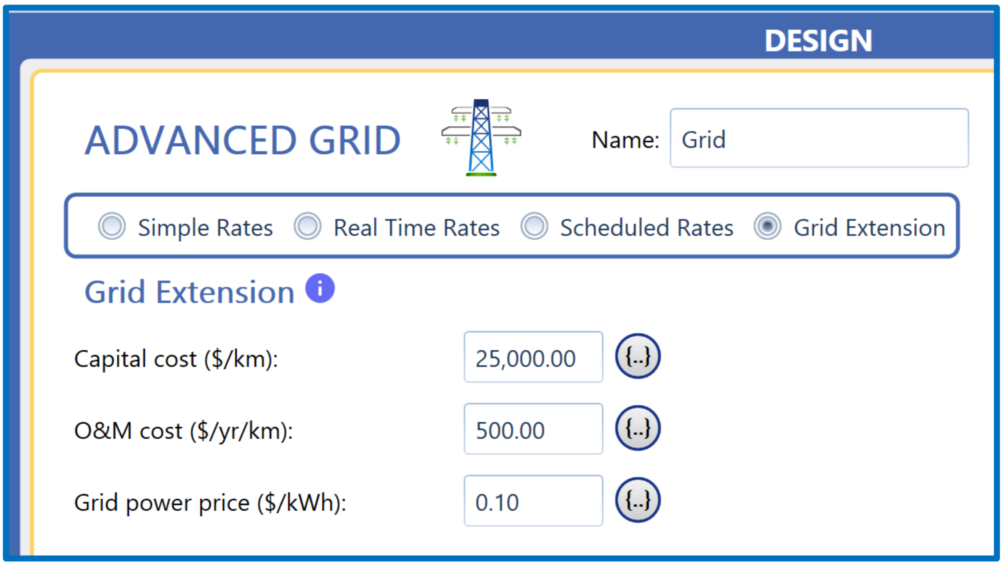

Figure 7-20: Economic cost of grid extension

Concerning the table 7-20 above, the break-even grid extension distance is defined as the distance from the grid at which the total net-present cost of the grid extension is equal to the total net-present cost of the stand-alone system (Lambert et al. 2005, Gilman and Lilienthal 2006). In Sub-Saharan Africa, the average cost of a grid extension is estimated at $20,000/km (Longe et al. 2014). When combined with other electrification components as well as the inflation rate, this price increases to an estimated $25,000/km (Longe et al. 2017). As a result of taking these studies into consideration, the capital cost for the village grid extension is considered to be $25,000.00/km. The O&M is considered to be 20% of the capital cost and the grid price is considered to be $0.10 /kWh (Homerenergy 2019).

7.6.12 HOMER PRO Simulation Input Data

Table 7-4 below shows the parameters that have been loaded into HOMER Pro for optimising and sizing the various components.

Table 7-4: Input data for the system components

System Component	Capital cost [$/kWh]	Replacement cost [$/kW]	O&M cost [$/kW/Year]	Lifetime [years]	Efficiency [%]
PV array	2,500.00	1,500.00	25.00	20;25*	90**
Wind turbine	18,000.00	10,800.00	4,500.00	20;25	45

System Component	Capital cost [$/kWh]	Replacement cost [$/kW]	O&M cost [$/kW/Year]	Lifetime [years]	Efficiency [%]
Hydro 100kW	459,845.00	229,923.00	13,795.00	20; 25	80
100kWh Li-Ion	70,000.00	52,500	10,500.00	15	95
Converter	300	300	0	15	95
Grid Extension	25,000	N/A	500	N/A	N/A

** Two options of lifetime years are given to HOMER; and ** This percentage (%) is based on original power output, not the (%) sunlight conversion into electricity*

7.6.13 Results and discussion

The discussion of the results for this section is divided into two parts as shown in Table 7-5.

Table 7-5: Simulation results

A

Architecture						Cost			
PV (kW)	G3	100LI	Hyd100 (kW)	Converter (kW)	Dispatch	COE ($)	NPC ($)	Operating cost ($/yr)	Initial capital ($)
199		10	29.4	248	CC	$0.447	$4.51M	$142,835	$1.73M
199		10	29.4	248	CC	$0.447	$4.51M	$142,835	$1.73M
199		10	29.4	248	CC	$0.440	$5.08M	$150,102	$1.73M
199		10	29.4	248	CC	$0.440	$5.08M	$150,102	$1.73M
199		10	29.4	248	CC	$0.444	$4.48M	$141,288	$1.73M

Export...

Left Double Click on a particular system to see its detailed Simulation Results.

B

Architecture						Cost			
PV (kW)	G3	100LI	Hyd100 (kW)	Converter (kW)	Dispatch	COE ($)	NPC ($)	Operating cost ($/yr)	Initial capital ($)
199		10	29.4	248	CC	$0.447	$4.51M	$142,835	$1.73M
213	1	10	29.4	246	CC	$0.462	$4.65M	$147,633	$1.78M

Table 7-5[A] shows the first few feasible solutions. Therefore, the list in part [A] of Table 7-5 is not an exhaustive list but gives an indication of the results of the sensitivity analysis performed. Part 2 presented in Table 7-5 (B) has red borders. It shows the optimisation results and gives two of the best cost-effective options for meeting the hypothetical village load. In Table 7-5 (A), HOMER Pro shows a subset of the overall optimisation results by ranking the results. The top-ranked system category shows the results of the configuration of the lowest cost generating systems. The best two solutions are presented in Table 7-5 (B). On analysis of this table, the top row highlighted in green is the best option and presents the optimisation results which are 199 kW of the PV system, 0 wind turbine, 10 batteries, 29.4kW hydro system and 248 kW converter. It should be noted that this research considered combinations of hydro, wind and solar power resources. However, HOMER Pro configured the power generating systems with the least cost, and wind power (highlighted in yellow in Table 7-5[B]) was not part of the system. The cost of the configured system is shown in Table 7-6 and rounded off to the nearest whole number.

Table 7-6: The cost of the configured system

Component	**Capital cost($)**	**Replacement cost($)**	**O&M ($)**	**Salvage ($)**	**Total ($)**
Converter	$74,385	$54,939	$48,177	-$14,963	$162,539
Hydro 100kW	$459,845	$0	$268,040	$0	$727,885
100kWh Li-Ion	$700,000	$387,749	$2,040,174	$105,606	$3,022,316
Flat plate PV	$498,278	$0	$96,816.52	$0	$595,094
System	$1,732,508	$442,688	$2,453,208	-$120,569	$4,507,834

As shown in the above table, there are no replacement costs stated for PV and hydro turbines because their lifetimes are equal to the lifetime of the system, which is 25 years. The system TNPC cost is $4,507,834, thus the Levelized Cost of Energy (LCOE) is $0.45. Gilman and Lilienthal (2006) define LCOE as the average cost per kWh of useful electrical energy produced by the system. For this system, the system operating cost is $142,836. Table 7-7 shows the contribution of each component in meeting the hypothetical village's electricity demand. For the demand to be met, the PV system will provide 71.1% of the supply and the remaining 28.9% will be supplied from hydropower. The scaled monthly average production is shown in Figure 7-21 (A):

Table 7-7: Electricity production of hybrid system components

Production	kWh/Year	%
PV	501,662	71.1
Hydro	203,504	28.9
Total	705,166	100

The simulated shared monthly average electric production between hydropower and photovoltaic is presented in the electrical simulation results given in Figure 7-21 below. As previously mentioned, the best hybrid system is a combination of a photovoltaic, battery inverter and hydropower energy supply.

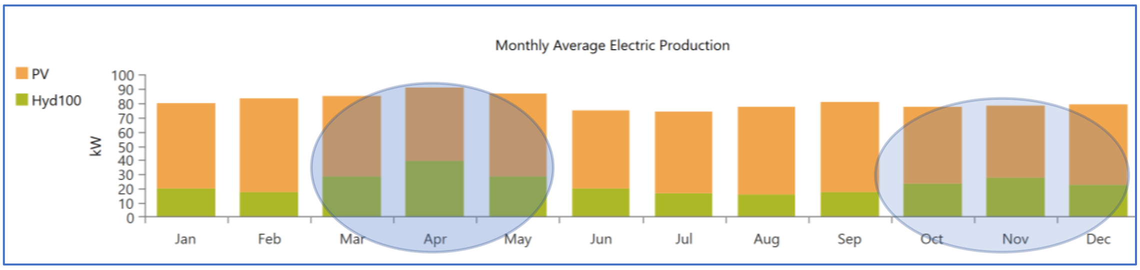

Figure 7-21: Monthly average electricity production for the winning hybrid system
To allow a comparison between the contributing components, the PV and Hydro monthly electricity average electricity production values are scaled and plotted on the y-axis. The highlighted months are rainy seasons.

A closer look at Figure 7-21 above and Figure 7-22 below reveals that hydropower makes a considerable contribution during the months of March to May and October to December which are the East African long and short rainy seasons respectively (Indeje et al. 2000, Hamududu and Killingtveit 2016, Yang et al. 2015b, Camberlin 2018). In addition, Figure 7-21 and Figure 7-22 also show that hydropower contributes less during the months of June, July and August. This is likely to be because these months are considered to be the dry season in East Africa (Indeje et al. 2000, Yang et al. 2015b, Ongoma et al. 2018).

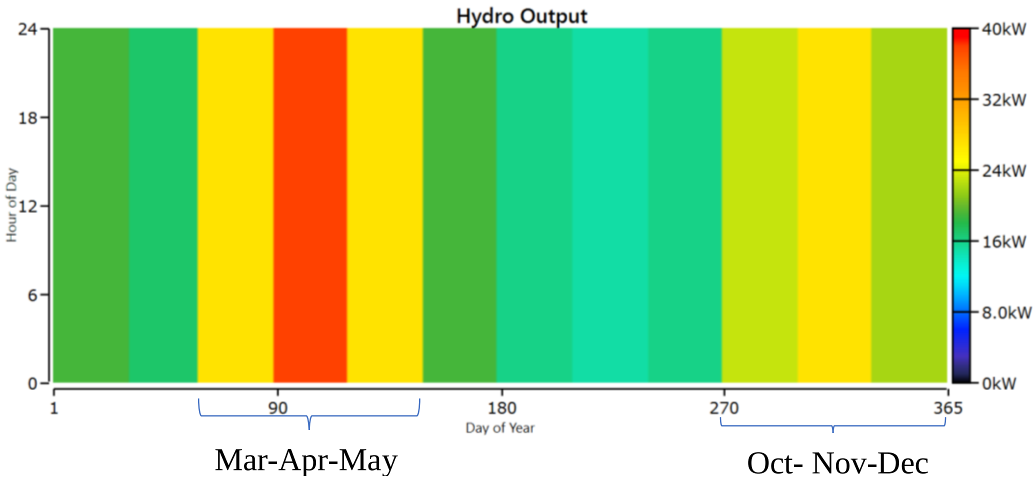

***Figure 7-22: Hydropower* output**
Mar-Apr-May and Oct-Nov-December shows the season when hydro output is high

The increase in hydropower contribution during the rainy seasons and the high contribution of PV during the dry seasons confirm the ability of solar and hydropower resources to complement each other within the selected case study area. As stated previously, wind resources did not contribute for a number of reasons including the low wind speed in the western part of the EAC (REN21-EAC 2016). This study has also highlighted that the western part of the EAC will be characterised by low wind speed during the periods of 2021- 2100.

7.6.13.1 The hybrid standalone system and grid extension options

This section analyses whether a grid extension or a standalone system is the best option for supplying energy to the hypothetical village. Figure 7-23 shows the breakeven grid extension distance. The distance is the length from the grid at which the TNPC of the grid extension is equal to the TNPC of the stand-alone system.

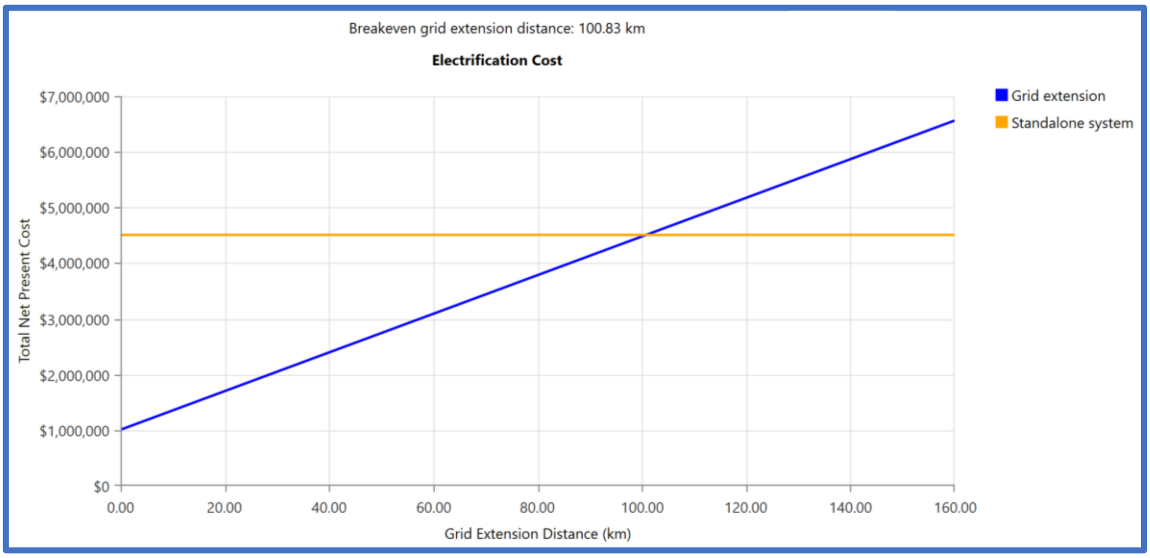

Figure 7-23: Breakeven grid extension distance

Figure 7-23 shows that the system is best delivered through a grid extension providing the existing grid system is not more than 100.83 km away from the hybrid system. Beyond this, a standalone option is more economically viable. Both the designed hybrid system and the village are within the geographic grid distance of 50km x 50km (cf. Figure 4-1[C]) and, as a consequence, the breakeven grid extension distance is beyond the village geographic boundaries. Therefore a grid extension is the best option for supplying electricity to the village.

In summary, the aim of Section 7.6 was to identify the optimal combinations of a hybrid system in order to meet the electricity demand for the hypothetical village. Following the above analysis, a system is proposed where PV provides 71.1% of electricity for the area. The remaining 28.9% of power is to be supplied by hydropower. This research further examined whether a grid extension or standalone system was the best option for supplying electricity to the hypothetical village. The research found that the grid extension is the most economically viable.

7.7 Decision support framework

The aim of this section is to achieve objective five of the research which is as follows: to develop a systematic pathway for renewable energy implementation in the EAC, which will inform the development of a Decision Support Framework (DSF) for renewable energy implementation. The DSF is a tool that will allow policy-makers, investors and energy consultants to, make decisions based on well-informed knowledge of the state of climate change and renewable energy resource provision in the EAC. The DSF will help stakeholders mentioned above to deliver a sustainable and climate resilient energy access, harvested on-site through complementary renewable energy mix. In addition, the DSF provides a step by step of how the energy resources in the EAC can be harnessed to reduce the energy access gap caused by shortfalls in hydropower generation.

The proposed DSF is a result of the combination of methodological approaches employed in objectives one, two, three and four of this research. These objectives were analysed in relation to the existing literature for renewable energy implementation. Figure 7-24 presents the DSF which was developed for renewable energy implementation in the EAC. Resources such as wind, solar, hydro and others are listed. However, it should be noted that this list is by no means exhaustive because there are many other resources available for use which could be added as required. The framework comprises 4 main processes. These are as follows:

- Assessing the load requirement for the household and the availability of resources to meet the load;

-Conducting climate change impact assessments on the identified resources;

-Assessing the complementarity between the identified climate resilient check

-Finally, making investment decisions.

These processes are delivered in 8 steps. Each step and its link to this study are explained as follows:

- **Step1:** (Demand) consists of developing the electrical load assessment business case. In this step, the assessment will determine the electrical load required for an identified number of people at a defined location. This incorporates objective One and Two which demonstrates the need to close the energy access gaps while taking into account climate change factors when developing plans to implement a renewable energy mix. It also provides a business case needed for this step.

An example of an electrical load assessment process has been demonstrated in Section 7.6.4 for the hypothetical village electrical load assessment.

- **Step 2** (Resources assessment) consists of listing the potential resources locally/geographically to meet demand. For this step, RCM data was used to achieve results where hydro, solar and wind power resources were assessed at an EAC regional scale as well as within a case study area (Rusumo hydropower project catchment area). This was undertaken in order to electrify the hypothetical village.
- **Step 3** determines the factors affecting the availability of resources.
- **Step 4** assesses the impact of climate change during the life cycle of the investment.

The methodological processes as per steps 3 and 4 have been demonstrated by studying future hydroclimate changes under different climate scenarios (RCP4.5 & RCP8.5) for the period spanning from 2021 to 2100. This gave an insight into what was expected from the hydro, wind and solar energy sources outputs.

- **Step 5** considers the results from step 4, identifying which of the available resources are more climate-resilient. Within this step, it is then decided whether or not it is worth investing in the previously discussed resources. For instance, there is no point in investing in hydropower alongside a river that is going to disappear at some point during the project life cycle.

Canales et al. (2019) argue that the hybridisation of two or more energy sources within a single power station is one solution for overcoming the mismatch between demand and supply provided by renewable generation. What follows (steps 6 and 7) is an account of complementarity as support for a move to increased hybridisation. These steps are as follows:

- **Step 6** consists of the assessment of complementarity of the energy resources identified in step 5.
- **Step 7** determines whether the complementary resources from step 6 are co-located, not co-located, or a mixture of both. It also assesses whether this matters in context.

For instance, it does not matter if solar and hydropower are not co-located, providing they can both be integrated economically to meet the demand identified in step 1.

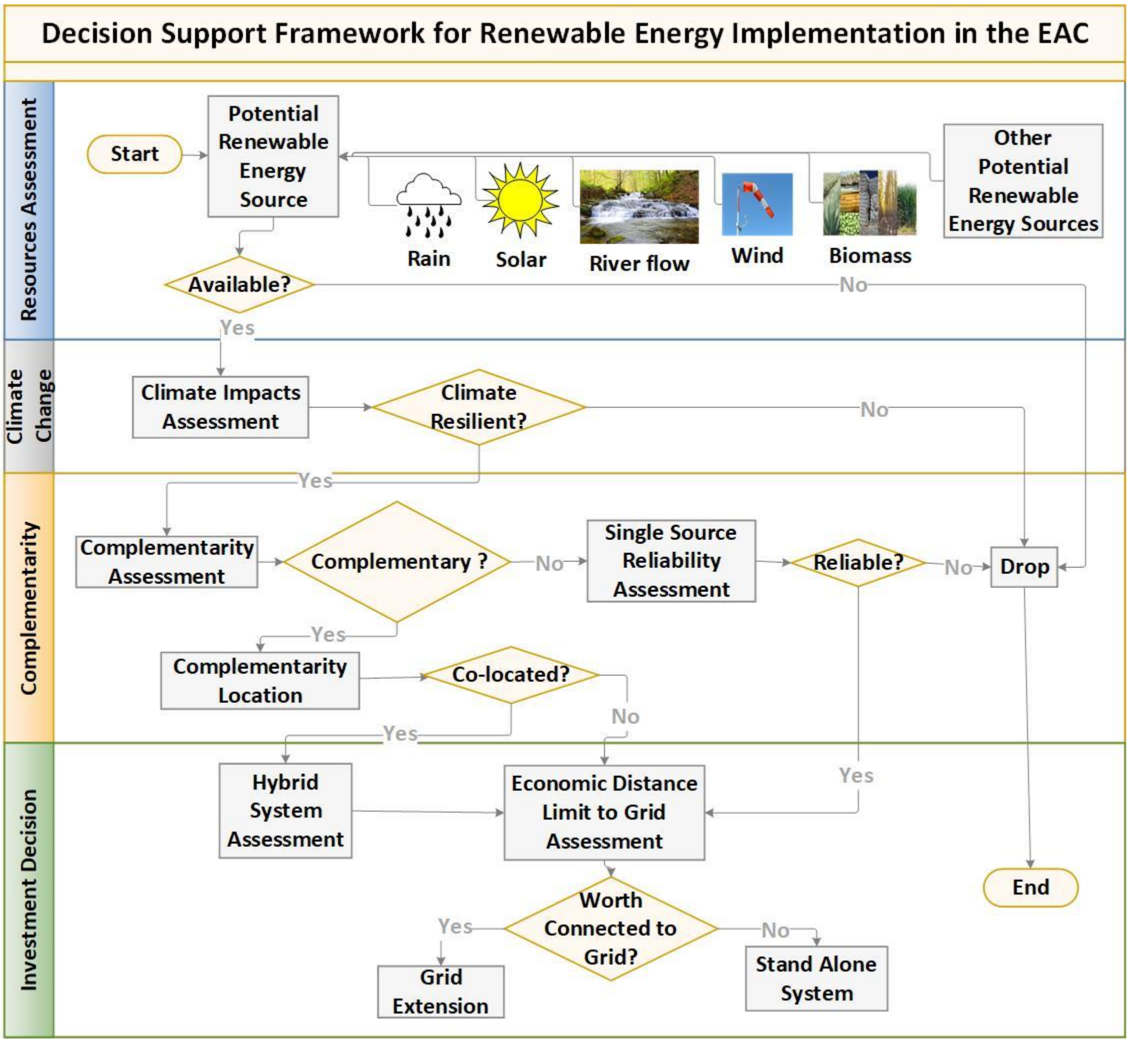

Figure 7-24: Proposed DSF for Renewable Energy Implementation in the EAC

The methodological process for steps 6 and 7 have been informed through a study of the ability of hydro, wind and solar resources to complement each other under different future climate change scenarios during the periods of 2021-2100. It also discusses the implications for energy supply balancing (Objective Three).

- **Step 8** assesses the optimal hybrid system and whether it is economically viable to supply energy through a grid extension or standalone system.

The processes for completing this step have been demonstrated through achieving Objective Four, which is a proposal of optimal hybrid combinations of hydro, wind speed and solar power for electrification of a selected case study area. This step is the last step in the renewable energy implementation decision framework. In brief, the proposed DSF is initiated by an assessment of the electrical load needed to meet the demand. After this, locally/geographically available resources are identified and the factors affecting availability are assessed. The impact of climate is then considered and the viability of the investment determined. The complementarity of the resources is then appraised and the decision to use either a grid extension or standalone energy supply for the complementary power sources is taken.

7.8 Chapter conclusion

To illustrate the implications of hydro, wind and solar power resources complementarity for energy supply balancing in the EAC, a local study area has been selected. The local area referred to is located on the borders of Burundi, Rwanda and Tanzania. The results from the case study indicated that hydropower is always in complementarity with solar power for all seasons during the time periods 2021-2050, 2051-2080, and 2071-2100 under both RCP4.5 and 8.5 scenarios. It has been found however, that the relationship between hydropower and wind power under all RCPs and periods is only statistically significant for the seasons of SON and DFJ as opposed to the periods of MAM and JJA.

In addition, this chapter proposed the optimal hybrid combinations of hydro, wind and solar power for electrification. The electrical demand for a hypothetical village was assessed and used to propose the optimal combinations of the hydro, wind and solar resources, available locally for a hybrid system.

The proposed optimal combination consisted of 28.9% of electricity sourced from hydropower and 71.1% from a solar power system. This research concluded that if an existing grid network is located 100.83 km away or less from the designed system it will be economically sound to connect the system to the national electrical grid network. As previously mentioned, the local study area was conducted at a grid of 50km x 50km, hence the distance of 100.83km goes beyond the geographical boundaries of the village to be connected.

Objective four of this research is to propose a hybrid system with optimal combinations of hydro, wind and solar power for the electrification of a selected case study area, and this was achieved as a result of these findings. Although this study found that wind power resources are not viable in the selected case study area because of low wind speed in the western region, this study showed that in general there is a potential ability of hydropower, solar and wind energy resources to provide a balanced supply within the EAC region. Presently, the region has a well-balanced renewable energy resource, which can work around any local and countrywide imbalances in demand. Therefore, in the EAC, there is currently an extraordinary opportunity to harness the much endowed renewable resources in the region and create a sustainable and reliable energy system at a scale that can drive industrial development and growth.

This chapter also proposed a DSF for energy implementation in the EAC. It gave the steps necessary to identify an economically viable climate-resilient system, using the available local power resources, assessing complementarity, and design a renewable energy hybrid system which can either be connected to an existing grid, positioned as a standalone or a mixture of the two options. This DSF is a tool for renewable energy implementation planners. The proposed DSF helped to achieve objective five of this research, which is to develop a systematic pathway for renewable energy implementation in the EAC

Chapter 8: Conclusion and Recommendations

8.1 Introduction

This chapter presents the key processes, significant findings and conclusion of the research project. It sets out a general discussion of the empirical findings and shows how these finding answer the research questions. The contribution to knowledge achieved through this study from an academic, strategic and policy perspective is highlighted. Finally, this chapter presents the research limitations and recommendations for future research.

8.2 Thesis overview

The aim and five objectives of this research have been achieved through the eight chapters as presented in Figure 8-1**.** This figure shows the framework within which these chapters have been delivered.

Chapter 1 presents the background, problem statement and rationale for this research. The chapter also identifies the aim of the research, the research questions, the objectives and gives an overview of the research methodology.

Chapter 2 and 3 address the first research objective. Through the relevant literature, these two chapters provide the background current level of knowledge and understanding of the status of energy generation and access within the EAC. The renewable energy climate nexus are demonstrated and several issues, such as dependence on hydropower and fossil fuel sources are underlined. The research gaps relating to the understanding of the best mix of renewable energy resources have been identified.

Chapter 4 presents the different research methodologies and methods used to achieve the aim and objectives of this study. It justifies the rationale behind the selection of the approach, data collection and analysis methods that are used in this research. This research is explanatory in nature, therefore, it uses quantitative data for the methods chosen and analysis performed.

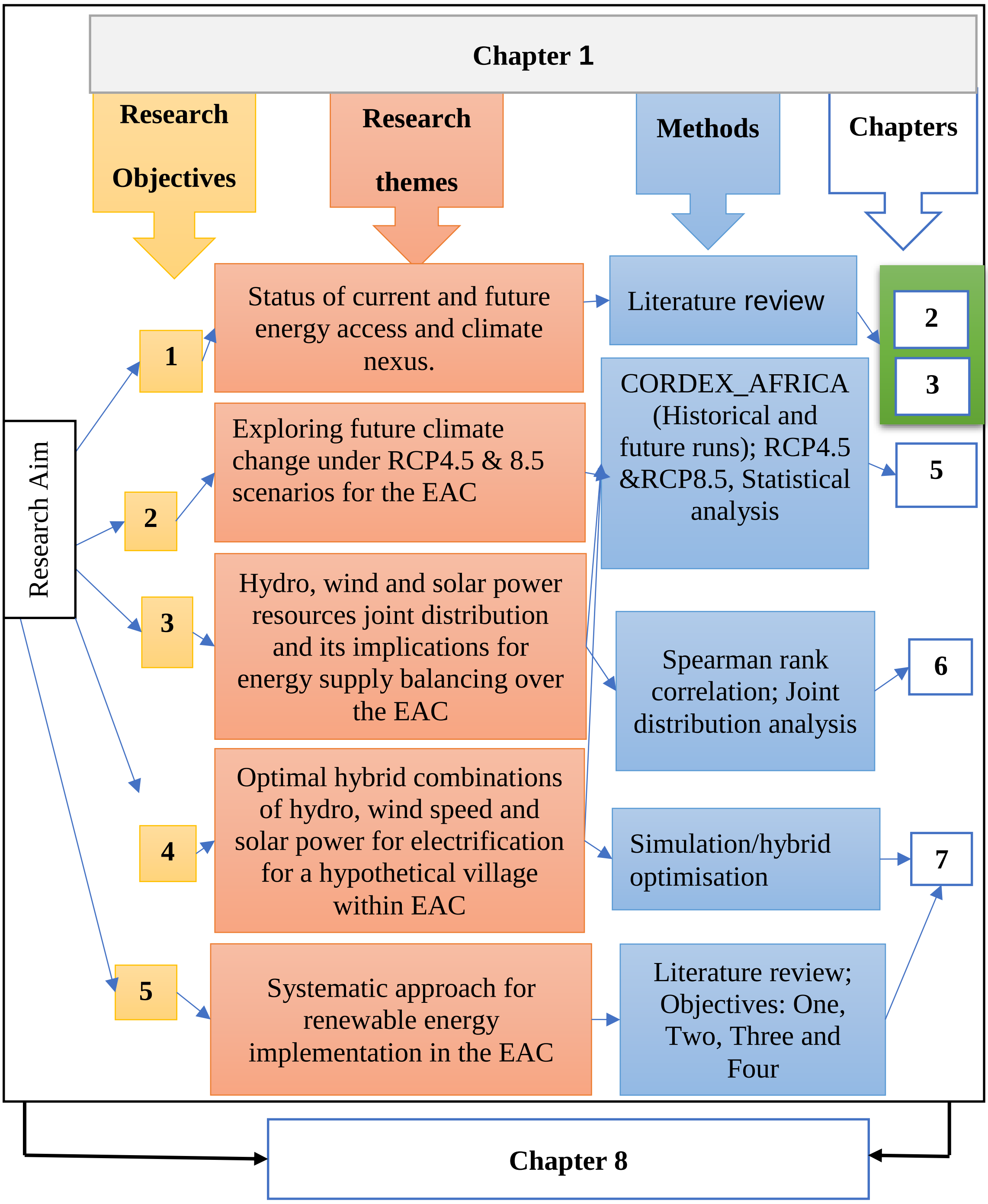

Figure 8-1: Study design

Chapter 5 investigates the potential temporal and spatial future changes in hydroclimate for the EAC under the RCP4.5 and 8.5 climate scenarios by comparing data from the historical 1976-2005 time periods to the future time periods of 2021 to 2100.

Chapter 6 presents the theoretical variability of hydro, wind and solar power resources and the relative complementarity under the RCP4.5 and 8.5 scenarios for the time periods of 2021-2050, 2051-2080 and 2071-2100 and the implications for energy supply balancing are also demonstrated.

Chapter 7 proposes the optimal hybrid combinations of hydro, wind speed and solar power for electrification and develops a systematic pathway for renewable energy implementation in the EAC.

Chapter 8 draws together important findings and highlights the significance of this study. It also provides a general discussion of the empirical findings and shows how these findings answer the research questions and make a contribution to this research project at both academic and strategic policy implementation levels. The research limitations and directions for further research that stem from this study have been presented in this chapter.

8.2.1 Evaluation of the research aim, objectives and research questions

The aim of the study is to develop a DSF for achieving reliable, sustainable, and climate-resilient energy access in the EAC under different climate change scenarios. This was achieved by studying the potential complementarity of hydro, wind and solar power resources in the near future (2021-2050), middle-term future (2051-2080) and long-term future (2071-2100) and the implications for renewable energy supply balancing in the EAC. The purpose was to determine how to achieve a well-balanced renewable energy supply from various sources to smooth the local, regional and countrywide imbalances in energy supply and demand dynamics. The research aim has been met by analysing secondary and primary data, which have been used to effectively achieve the study objectives. The following sections summarise how the results for each objective of this research have been achieved with respect to its specific theme as indicated in

Figure 8-1.

Theme One: The status of current energy access, future renewable energy climate nexus

Objective One, which is "to explore the current status of energy access and future renewable energy implementation plans in the EAC", was answered through a review of the relevant literature, and the analysis and discussion are presented in Chapters 1 and 2. The literature review focusses on the current energy access status and future energy provision for the EAC. Models and theories related to renewable energy and the current state of knowledge of the impact of climate change on renewable energy have been identified and analysed to form the basis for climate and renewable energy modelling. Apart from scientific publications in this area, reports from international organisations that provide development assistance to EAC countries such as the World Bank EAC, IEA and IPCC assessment reports were also used which enabled access to the most up-to-date information.

It was found that the current energy access in the EAC is dominated by traditional biomass (e.g. wood, charcoal and biogas). Traditional biomass is accessed, on average, by 90% of the population, with only 10% having access to modern energy. It has also been established that modern energy generation capacity in the EAC is largely dominated by hydropower and thermal power stations from imported petroleum products. These sources of energy have been identified in the literature, for various reasons, as being neither sustainable nor reliable. Shortfalls of energy generation from hydropower in the EAC have been recorded over the last decade due to a significant reduction in the quantity of water flow to the hydro-electric dams. The lack of water is attributed to a recurring and prolonged drought in the EAC over the last two decades.

The full extent of the deficit in hydropower production is experienced by the local population through the regular power outages in the region, which made hydropower an unreliable source of energy. This has had negative implications on the economies of the EAC countries. It was also shown that the deficits in hydropower production are largely filled by generators that use petroleum products. Therefore this study argues that the reliance on petroleum products to fill the energy production gap in energy provision is not environmentally or economically sustainable for the majority of the poor countries of the EAC. This is because fossil fuels are limited in supply and are a source of greenhouse gas emissions. In addition, petroleum products are subject to price fluctuations that are beyond the control of the EAC governments.

In brief, this research found that the existing modern energy generation capacity in EAC is neither sustainable nor resilient. It has also been established that the rapid growth in energy demand meant that the EAC countries had to find new strategies to supply energy services to its citizens. Consequently, this study suggests that harnessing renewable energy resources offers the EAC a sustainable option to decrease external energy dependence and to supply energy that is viable, sustainable and climate-resilient.

For the EAC to be able to increase energy access in a sustainable way, it is of paramount importance to assess the effects of climate on renewable energy resources and to model a future renewable energy mix that will maximise EAC energy generation. The next section focusses theme two of the research.

Theme Two: Assessing future climate change under RCP4.5 & 8.5 scenarios for the EAC

Objective 2, which is "to investigate EAC future hydroclimate changes under different climate scenarios (RCP4.5 and 8.5) for the period spanning from 2021 to 2100", was fulfilled in Chapter 5. This objective has also helped to answer question 1 of this research which is "What are the potential future hydroclimate change scenarios in the EAC? This question was further divided into the following sub-questions:

1. Which of the available Regional Climate Models (RCMs) will predict reliable patterns of hydroclimate that best resemble the observed patterns in the EAC?
2. What are the potential spatial and temporal future changes in hydroclimate under the RCP4.5 and 8.5 climate scenarios?

For sub-question one, it was found that 17 RCMs were available for the EAC and subsequently used for this research. Sub-question two examined the potential future spatial and temporal changes in precipitation, solar irradiance, wind speed and temperature for the EAC, under the RCP4.5 and 8.5 climate scenarios.

This research has explicitly demonstrated that under the RCP4.5 and 8.5 scenarios, there is a slight difference in the average precipitation for both spatial and temporal fields. It was highlighted that precipitation under RCP4.5 and 8.5, compared to the historical 1976-2005 baseline periods is expected to increase during the future 2071-2100 time periods. This research predicted that the dry seasons will get drier and the wet season wetter from the near to the long-term future (2021 - 2100) and this is more marked under RCP8.5 compared to the RCP4.5.

For the spatial and temporal change in solar irradiance, this study indicated that under both RCPs, the EAC will experience a significant decrease in solar irradiance for the

future periods of 2021-2050, 2051-2080, except 2071-2100 (no change) under RCP4.5, compared to the historical period of 1976-2005. Previous studies (e.g. Gordon 2018) postulated that solar radiation levels in the EAC are high due to its proximity to the equator. In the same vein, and a final note on solar irradiance, solar irradiance in the EAC is on average about 5kWh/day and is constant throughout the year for all periods and under all climate scenarios considered in this study. Solar power resources available in the EAC lend themselves to opportunities for energy generation using solar technologies.
For spatial and temporal changes in wind speed, this research found that under both the RCP4.5 and 8.5 climate scenarios, the EAC should not expect a significant change in wind speed in 2021 to 2100 compared to the 1976-2005 time period, therefore the prediction of energy production from wind speed is that it will remain consistent from now up to the end of this century. It has been noted that the prevailing wind speed for the period of 2021-2100 is relatively low compared to the remaining parts of the EAC. This finding is in line with the previous wind speed availability studies over the EAC conclusion (e.g. REN21-EAC 2016).

Finally, this study found that for the future spatial and temporal changes in temperature in the EAC, for all periods (2021-2100), under both climate scenarios (RCP4.5&8.5) average temperature is projected to increase. It is particularly noteworthy that, under the RCP8.5, there is a continuous increase in average temperature from 2021 to 2100. The research revealed that under RCP4.5, the EAC could expect an increase in temperature of about 2.6℃ for the period of 2021-2050 and will see a drop in changes of about 0.7℃ over the subsequent periods. However, under RCP8.5, the average temperature change is about 2.9℃ for the periods of 2021-2050 and 2051-2080, and 3.6℃ over the periods of 2071-2100. This increase could be explained by the high emission of greenhouse gases associated with RCP8.5 as opposed to the RCP4.5, which is a scenario that stabilizes radiative forcing at 4.5 W/m^2 in the year 2100 without ever exceeding that value

(Thomson et al. 2011). In brief, objective two of this research which was to investigate EAC future hydroclimate changes under different climate scenarios (RCP4.5 and 8.5) for the period spanning from 2021 to 2100, helped to answer research question A of this study.

Theme Three: Hydro, wind and solar power resources joint variability in the EAC under RCP4.5 and 8.5 scenarios and the implications for energy supply balancing

Objective Three, which is "to study the ability of hydro, wind and solar resources to complement each other under different future climate change scenarios during the periods of 2021-2100, and its implications for energy supply balancing", has been addressed in Chapter 6. This chapter investigated the potential complementarity of hydro, wind and solar power resources of the EAC under different climate scenarios and its implications for energy supply balancing. Objective three helped to answer research question 2 which is, "are the hydroclimate resources complementary to each other for renewable energy generation in the EAC?"

This study found that, in the EAC, wind speed is complementary with precipitation for the period from 2021 to 2100 under both the RCP4.5 and 8.5 climate scenarios while solar irradiance has a mix of weak negative (complementarity) and positive (no complementarity) correlation with both wind speed and precipitation. The analysis of the annual cycle of monthly distribution for precipitation and wind speed found that wind speeds are higher in the dry months of June, July and August than in the other months where the precipitation is higher. This suggests that a hybrid strategy with hydropower and wind power generations are complementary. Particular attention has to be made when considering wind power resources because of low wind speed prevalence the western parts of the EAC.

It was also found that the annual cycle of monthly distribution in some months is characterised by precipitation, solar irradiance and wind speed bimodal (high and low peaks) distribution. The relationship between precipitation, wind speed and solar irradiance variables from 2021-2100 was examined, looking at the minimum, medium and maximum value conditions for each power source in turn while keeping the values of the remaining two constant.

The results indicate that under the two climate scenarios (RCP4.5 & 8.5), precipitation and wind speed are always complementary (peaks occurs at different times), irrespective of the solar irradiance. This study also concludes that precipitation and solar irradiance are able to complement each other when wind speed is at its lowest level. However, precipitation and solar irradiance showed little or no complementarity when wind speed is at the medium and maximum values. It should be noted that there is a potential complementarity between solar and wind speed when precipitation availability is at a minimum to a medium level condition. In this research context, having two sources of energy in complementarity when the third one is at its lowest value is an indication that a mixture of these sources can make a well-balanced energy supply. The deficit of energy output from one or two sources can be compensated for by the availability of others. The potential complementarity of hydro, wind and solar power resources was further examined by exploring the implication for energy supply balancing in the EAC. The selected local area, containing the Rusumo hydropower project shared between Burundi, Rwanda and Tanzania, was used as a case study.

The result from the case study indicates that under both RCP4.5 and 8.5 climate scenarios, hydropower is always in complementarity with solar power for all seasons during the periods of 2021-2050, 2051-2080 and 2071-2100. This research found that there is a strong complementarity between hydro and wind power for the seasons of September-

November (SON) and December- January (DJF) compared to the periods of March-May (MAM) and June- August (JJA). However, there is greater power output from wind speed for the months of JJA which correspond to the period of low rainfall in the EAC. A consequence of this study is that under the current EAC renewable energy implementation plans, a mixture of energy supply from renewable sources will remain much more viable in dry seasons due to the much greater capacity of hydro, solar and wind power to balance each other across the region at least till the end of this century.

Theme Four: Optimal hybrid combinations of hydro, wind speed and solar power for electrification of a hypothetical village within the EAC

Objective Four is to "propose optimal hybrid combinations of hydro, wind speed and solar power for electrification of a selected case study area". A local area- Rusumo Falls case study area- was used for hydro, wind and solar power complementarity real-world applications when technology is considered. The case study area is located in the western part of the EAC. In this regard, the electricity demand for a hypothetical village within the Rusumo Falls project catchment area has been assessed and used as a case study. The study in this area found that the optimal combinations for energy balancing consist only of hydro and solar power resources. The case study area has been identified as having a low wind speed (REN21-EAC 2016) and this study also came to the same conclusion for the period between 2021 to 2100. When technology is considered, various factors such as efficiency, costs, the minimum threshold availability of resources - for example, minimum wind speed cut in etc - are factors that dictate technology choices. This explains why the strong potential complementarity between hydro, wind and solar power implications for energy supply balancing eliminated wind power resources from the optimal combinations of hydro, wind speed and solar power.

This study proposed an optimal combination of 29.9% from hydropower and 71.1% of solar power systems. It is noted that optimal combinations of the three resources in other parts of the EAC, for instance in the eastern part, could have reached a different conclusion. Conducting an optional combination at each location of the EAC is outside the scope of this study. This study suggested that it is only economically viable to connect the system to the national grid network if the designed hybrid system is not beyond 100.83km away from the source. Beyond this distance, a standalone system option is more economically viable. These findings demonstrate that objective four was achieved.

Theme Five: A systematic approach for renewable energy implementation in the EAC

Objective Five which is "to develop a systematic pathway for renewable energy implementation in the EAC" was addressed in chapter 8. The proposed decision support framework, shown in Figure 7-24, was developed based on the result of the combinations of the all the preceding chapters of this thesis and analysed in relation to the available literature in the fields of climate change and renewable energy implementation. The proposed DSF is an answer to research question 3, which is, "how can decision-makers in the EAC achieve reliable, affordable and climate-resilient energy access through a? complementary renewable energy mix?"

The DSF is made of four processes which are achieved in four main steps as shown in Figure 7-24 and explained in Section 7.7. This DSF is designed to help renewable energy decision-makers and investors improve access to energy which is both reliable, affordable and climate-resilient. Objective Five was therefore fully achieved by the production of this DSF, which in turn helped to answer the research question 3.

In conclusion, all research questions and objectives formulated to address the aim and objectives of this research have been achieved. Also, the corresponding questions and chapters were explicitly indicated in

Figure 8-1 above. The following section explains the significance of the research results.

8.3 The significance of the findings

The significance of the results that were identified during this research could be summarised as follows:

1. The energy access problem in the EAC cannot be solved with the existing modern energy provision in the EAC as this has been found to be inadequate, variable and unsustainable. Therefore consideration should be given to harnessing renewable energy resources that offer sustainable options for helping the EAC to decrease external energy dependence and supply energy which is viable, sustainable and climate-resilient. The variability of renewable energy resources and their complementarity has not previously been investigated in depth under future climate change scenarios. The findings of this research have laid the foundation that will inform the EAC future energy strategy. In an effort to scale up energy access in a sustainable manner, it is of paramount importance to assess the impact of climate change on renewable energy resources.
2. This research has demonstrated the complementarity of the various renewable sources establishing the appropriate mix of cost-effective solutions for improving energy access. The decision support framework developed in this research provides a systematic approach to decision making that can be used when developing policy, strategies and plans to implement a mix of energy sources to close the access gap.

The research has also provided a methodological framework for achieving the processes laid down in the DSF. There is evidence that all the previous renewable energy implementation plans did not consider aspects of complementarity and long term hydroclimate changes under different climate change scenarios. Therefore this research is very significant for providing a pathway for future planning and implementation of renewable energy at scale in the EAC.

8.4 Contribution to knowledge and its implication for policy and practice

The research provides a number of contributions to knowledge with implications for policy and practice at both an academic and practical level. The research responded to a number of research questions to meet the main aim of this research which is "to develop a Decision Support Framework for achieving reliable, sustainable, and climate-resilient energy access in the EAC under different climate change scenarios." This study asked in particular, "what are the potential future changes in hydroclimate scenarios in the EAC?". "Are the hydroclimate resources complementary to each other for renewable energy generation in the EAC?" and "How can decision makers in the EAC achieve reliable, affordable and climate resilient energy access through a complementary renewable energy mix?" The main contribution of this study to knowledge and the implications for policy and practice are summarised in Figure 8-2 as follows:

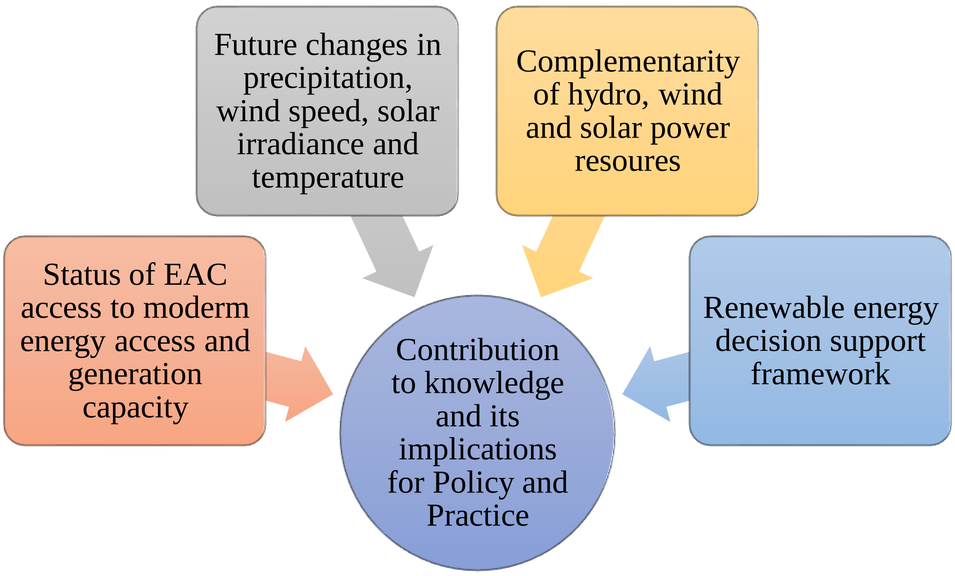

Figure 8-2: Summary of research contribution to knowledge

The first major contribution of the present research is that it provides future projections of precipitation, wind speed, solar irradiance and temperature for the EAC for the near, mid and long term future in relation to a historical baseline. Near-future defines the time periods of 2021-2050, mid-future (2051-2080) and long-term future (2071-2100), and the historical baseline is 1976-2005. These periods have been designed to match the life cycle of renewable energy infrastructure. This information is crucial for renewable energy development as it will allow policy-makers, investors and consultants to design tools, make decisions and act confidently, based on well-informed knowledge of the state of renewable energy resource provision in the EAC. These resources include, but are not limited to, hydro, wind speed and solar irradiance. For example, policymakers could include considerations of climate change in their policy documents, feasibility studies and business cases.

The study responds to the call made by, among others, Kammen et al. (2015), who highlighted that the East African Power Pool Master Plan does not include any analysis of the effects of climate change on the regional power strategy or provide any insight into possible problems associated with climate change conditions. A second important implication of this study derives from the research findings on existing modern energy provision in EAC, which is heavily and unsustainably reliant on hydroelectric power and imported petroleum. The study of the potential complementarity between hydro, wind speed and solar irradiance resources in this research, suggests that harnessing renewable energy resources offers a sustainable option for helping the EAC to decrease external energy dependence and supply energy which is viable, sustainable and climate-resilient to its citizens.

In addition, this study responds, in the context of the EAC, to the call made by the World Watch Institute (2010), notably, "*New African dams are being built with no examination* *of how climate change will affect them, even though many existing dams are already plagued by drought-caused power shortages*." In this respect, the findings of this research suggest that the combination of hydro, wind and solar energy resources should provide a consistent supply of power in spite of the variability of one or other of these resources leading to disruption in the power supply.

The third major contribution of this study stems from the question of how decision-makers in the EAC can improve access to energy which is both reliable, affordable and climate-resilient. Using the Rusumo Falls project area as a case study, this research provides the optimal combinations of hydro, solar and wind power as an illustrative practical example of how the research question 3 can be solved in real life.

The fourth major contribution of this research is the provision of a user-oriented DSF, graphically represented in Figure 7-24, which is designed to serve as a means for policymakers, investors and consultancy to exploit the potential complementarity potential of renewable resources to offset the risks of climate change. The framework provides a process of evaluation while the methodology set out in this research has provided a detailed approach to use when implementing the steps in the decision support framework.

In addition, the findings of this study provide the potential ability of hydro, wind and solar power resources to complement each other under different climate scenarios over the EAC. This information supports the goal of the East African Centre for Renewable Energy and Energy Efficiency (EACREEE 2018) "*to facilitate the creation of an enabling environment for renewable energy and energy efficiency markets and investments, in order to contribute to:*

i.increased access to modern, affordable and reliable energy services

ii. *energy security*

iii. *mitigation of negative effects (e.g. local pollution and GHG emissions)"*

Finally, while the implications of the findings focus on the EAC, the methodology used, and the overall research outcomes have both policy and practical implications for other developing countries looking to strengthen the resilience of their renewable energy infrastructure.

8.5 Research limitation and directions for future research

This section presents some of the research limitations and provides directions for further research that stem from this study. This study focused mainly on hydro, wind and solar power, three of the most exploited renewable energy resources within EAC. This study could be extended to investigate the potential of the other renewable energy options such as biomass, as well as energy from waste processing, wave power and geothermal sources. This research only used regional climate models with a resolution of 50km x 50km. Although this resolution is high enough to provide a good understanding of the renewable energy resources, further research using very high-resolution models would provide an opportunity to identify these renewable energy hot spots at a very small scale. Further research could shed light on the renewable energy complementarity at an individual country level or local scale, rather than at the EAC regional level.

This study provides optimal combinations of hydro, solar and wind power as an illustrative practical example of how decision-makers in the EAC can improve access to energy in a sustainable manner, without targeting a specific group of people. Future research can target specific communities such as off-grid villages and carry out actual energy and site surveys for the purpose of modelling the energy and life cycle cost of the proposed renewable energy supply infrastructure. This study developed a DSF and its application is to be tested in a pilot study.

8.6 Final conclusion

The following are the recommendations for renewable energy implementation in the EAC and elsewhere.

1. Assess the capability of locally available renewable resources to meet the local energy demand.
2. Address the current inefficiencies in the use of locally/regionally available resources and diversify the resources of energy production in the EAC, by utilising the available renewables, including but not limited to hydro, wind and solar.
3. Take account of future climate trends in operations planning for renewable energy systems.
4. Consider the impact of climate change in renewable energy development policies to reduce future risks.
5. Invest more in hybrid energy systems to curtail the inherent intermittent supply associated with a single renewable resource.
6. Focus on assessing the actual reliability and storage capacity of complementary renewable resources at a local, regional and national level in future studies.
7. Offer training to policymakers to increase their awareness of future climate-related risks in their renewable energy development plans.
8. Conduct a study of how to retrofit the existing infrastructure with smart grids to accommodate renewable sources which have intermittent energy generation, modelled on the pioneering work of this study on combining energy sources.

References

Adegoke, Y. (2018) *The Cost of Electricity Shortages in Africa Is More than Just a Problem of Access* [online] available from <https://qz.com/africa/1431213/africas-electricity-shortages-have-health-and-economic-costs/> [12 August 2018]

AfDB (2018) *East Africa Economic Outlook 2018* [online] available from <https://www.afdb.org/fileadmin/uploads/afdb/Documents/Publications/2018AEO/African-Economic-Outlook-2018-East-Africa.pdf>[12 July 2018]

Africa Development Bank (2015) *AfDB Approves Ruzizi III Hydropower Plant Project, Bringing Green Energy to Burundi, DRC and Rwanda* [online] available from <http://www.afdb.org/en/news-and-events/article/afdb-approves-ruzizi-iii-hydropower-plant-project-bringing-green-energy-to-burundi-drc-and-rwanda-15275/> [8 March 2016]

Africa Progress Panel (2015) *Power People Planet - Seizing Africa's Energy and Climate Opportunities: Africa Progress Report 2015*. Switzerland: The Africa Progress Panel

African Development Bank (2018) *Africa Economic Outlook Africa Economic Outlook*. Abidjan: African Development Bank Group

African Energy (2016) *Tanzania Makambako Wind Assessment Tender* [online] available from <https://www.africa-energy.com/article/tanzania-makambako-wind-assessment-tender> [21 November 2016]

Agresti, A., Schollenberger, J., and Wackerly, D. (1987) 'Models for the Probability of Concordance in Cross-Classification Tables'. *Quality and Quantity* 21 (1), 49–57

Alboteanu, I.L., Bulucea, C.A., and Degeratu, S. (2015) 'Estimating Solar Irradiation Absorbed by Photovoltaic Panels with Low Concentration Located in Craiova, Romania'. *Sustainability (Switzerland)* 7 (3), 2644–2661

Altman, D. g. and Bland, J.M. (1996) 'Statistics Notes: Detecting Skewness from

Summary Information'. in *Bmj*. vol. 313 (7066). 1200

Altman, D.G. and Bland, J.M. (1995) 'Statistics Notes: The Normal Distribution'. *Bmj* 310 (6975), 298–298

Amador, J. and Dominguez, J. (2005) 'Application of Geographical Information Systems to Rural Electrification with Renewable Energy Sources'. *Renewable and Sustainable Energy Reviews Energy* 30, 1897–1912

Anderson, D., Moggridge, H., Warren, P., and Shucksmith, J. (2015) 'The Impacts of "run-of-River" Hydropower on the Physical and Ecological Condition of Rivers'. *Water and Environment Journal* 29 (2), 268–276

Anderson, T.R., Hawkins, E., and Jones, P.D. (2016) 'CO2, the Greenhouse Effect and Global Warming: From the Pioneering Work of Arrhenius and Callendar to Today's Earth System Models'. *Endeavour* 40 (3), 178–187

Andreassian, V., Bergström, S., and Chahinian, N. (2006) 'Catalogue of the Models Used in MOPEX 2004 / 2005'. *Large Sample Basin Experiments For4 Hydrological Model Parameterization: Results of the Model Parameter Experiment-MOPEX* [online] 41–94. available from <http://en.scientificcommons.org/43851357>[01 March 2016]

Anyah, R. and Semazzi, F. (2006) 'Variability of East African Rainfall Based on Multiyear RegCM3 Simulations'. *International Journal of Climatology* 27, 357–371

Ashourian, M.H., Cherati, S.M., Mohd Zin, A.A., Niknam, N., Mokhtar, A.S., and Anwari, M. (2013) 'Optimal Green Energy Management for Island Resorts in Malaysia'. *Renewable Energy* 51, 36–45

Asrari, A., Ghasemi, A., and Javidi, M.H. (2012) 'Economic Evaluation of Hybrid Renewable Energy Systems for Rural Electrification in Iran - A Case Study'. *Renewable and Sustainable Energy Reviews* 16 (5), 3123–3130

Ayre, J. (2015) *1st Utility-Scale Solar Energy Project In East Africa Now Online —*

Rwanda's Total Grid Capacity Surges 6% [online] available from <http://cleantechnica.com/2015/02/09/1st-utility-scale-solar-energy-project-east-africa-now-online-rwandas-total-grid-capacity-surges-6/> [7 June 2015]

Banerjee, S.G., Bhatia, M., Azuela, G.E., Jaques, I.S., Ashok, P.E., Bushueva, I., Angelou, N., and Inon, J.G. (2013) 'Global Tracking Framework'. *Sustainable Energy for All, The World Bank.* 3 (Wasshington D.C.), 289

De Barbosa, L.S.N.S., Bogdanov, D., Vainikka, P., and Breyer, C. (2017) 'Hydro, Wind and Solar Power as a Base for a 100% Renewable Energy Supply for South and Central America'. *PLoS ONE* 12 (3), 1–28

Bazyomo, S., Lawin, A., Coulibaly, O., Wisser, D., and Ouedraogo, A. (2016) 'Forecasted Changes in West Africa Photovoltaic Energy Output by 2045'. *Climate* 4 (4), 53

Beilfuss, R. (2012a) 'A Risky Climate for Southern African Hydro'. *International Rivers* (September), 1–60

Beilfuss, R. (2012b) 'A Risky Climate for Southern African Hydro: Assessing Hydrological Risks and Consequences for Zambezi River Basin Dams'. *International Rivers* (September), 1–160

Bekele, B.G. (2011) 'Feasibility Study of Solar-Wind Based Standalone Hybrid System for Application in Ethiopia'. *Proceedings of the World Renewable Energy Congress – Sweden, 8–13 May, 2011, Linköping, Sweden* 57 (0), 826–833

Bekele, G. and Palm, B. (2010) 'Feasibility Study for a Standalone Solar-Wind-Based Hybrid Energy System for Application in Ethiopia'. *Applied Energy* 87 (2), 487–495

Belu, R.G., Chiou, R., Tseng, T.L.B., and Cioca, L.I. (2014) 'Teaching Renewable Energy System Design and Analysis with HOMER'. *ASEE Annual Conference and Exposition, Conference Proceedings*

Berrisford, P., Dee, D., Fielding, K., Fuentes, M., Kallberg, P., Kobayashi, S., and Uppala, S. (2009) 'The ERA-Interim Archive'. *ERA Report Series* 1 (1), 1–16

Bett, P.E. and Thornton, H.E. (2016) 'The Climatological Relationships between Wind and Solar Energy Supply in Britain'. *Renewable Energy* 87, 96–110

Bilgen, S., Kaygusuz, K., and Sari, A. (2004) 'Renewable Energy for a Clean and Sustainable Future'. *Energy Sources* 26 (12), 1119–1129

Björnsson, H. (2012) *Climate Change and Energy Systems* [online] available from <http://books.google.es/books?id=oY-P_7ySepEC>[05 May 2017]

Brands, S., Herrera, S., Fernández, J., and Gutiérrez, J. (2013) 'How Well Do CMIP5 Earth System Models Simulate Present Climate Conditions in Europe and Africa?' *Climate Dynamics* [online] 41, 803–817. available from <http://link.springer.com/10.1007/s00382-013-1742-8%5Cnhttp://link.springer.com/article/10.1007/s00382-013-1742-8> [09 August 2017]

Brenna, M., Foiadelli, F., Longo, M., and Abegaz, T.D. (2016) 'Integration and Optimization of Renewables and Storages for Rural Electrification'. *Sustainability (Switzerland)* 8 (10)

Breslow, P. and Sailor, D. (2002) 'Vulnerability of Wind Power Resources to Climate Change in the Continental United States'. *Renewable Energy* 27 (4), 585–598

Brew-Hammond, A. (2010) 'Energy Access in Africa: Challenges Ahead'. *Energy Policy* [online] 38 (5), 2291–2301. available from <http://dx.doi.org/10.1016/j.enpol.2009.12.016> [02 April 2016]

Briones, H.A., Uche, J., and Martínez-Gracia, A. (2017) 'Accounting for GHG Net Reservoir Emissions of Hydropower in Ecuador'. *Renewable Energy* [online] 112, 209–221. available from <http://dx.doi.org/10.1016/j.renene.2017.05.047>[8 May 2018]

Briones Hidrovo, A., Uche, J., and Martínez-Gracia, A. (2017) 'Accounting for GHG Net Reservoir Emissions of Hydropower in Ecuador'. *Renewable Energy*

Brirhet, H. and Benaabidate, L. (2016) 'Comparison Of Two Hydrological Models (Lumped And Distributed) Over A Pilot Area Of The Issen Watershed In The Souss Basin, Morocco'. *European Scientific Journal, ESJ* 12 (18), 347

Brower, M., Green, D., Hinrichs-rahlwes, R., Sawyer, S., Sander, M., Taylor, R., Giner-reichl, I., Teske, S., Lehmann, H., Alers, M., Hales, D., and Ren 21 (2014) 'Renewables 2014 Global Status Report'. *REN 21 Steering Committee* 216

Buhungiro, E. (2014) *ICT in Rwanda Schools* [online] available from <https://www.newtimes.co.rw/section/read/110664> [18 September 2017]

Bull, D.E., Bull, S.R., Ekmann, J., Sale, M.J., and Schmalzer, D.K. (2007) *Effects of Climate Change on Energy Production and Use in the United States*. Washington, D.C.

Camberlin, P. (2018) *Climate of Eastern Africa* [online] available from <http://climatescience.oxfordre.com/view/10.1093/acrefore/9780190228620.001.0001/acrefore-9780190228620-e-512> [10 July 2019]

Camberlin, P., Moron, V., Okoola, R., Philippon, N., and Gitau, W. (2009) 'Components of Rainy Seasons' Variability in Equatorial East Africa: Onset, Cessation, Rainfall Frequency and Intensity'. *Theoretical and Applied Climatology* 98 (3–4), 237–249

Canales, F.A., Jurasz, J., Beluco, A., and Kies, A. (2019) *Assessing Temporal Complementarity between Three Variable Energy Sources by Means of Correlation and Compromise Programming*. Colombia

Cantão, M.P., Bessa, M.R., Bettega, R., Detzel, D.H.M., and Lima, J.M. (2017) 'Evaluation of Hydro-Wind Complementarity in the Brazilian Territory by Means of Correlation Maps'. *Renewable Energy* 101, 1215–1225

Carlo, M. (2013) *Normality Tests II :* (1954), 1–7

Carty, T. (2017) ‘A Climate in Crisis’. *How Climate Change Is Making Droughty and Humanitarian Disaster Worse in East Africa* (April), 12

Carvalho, D., Rocha, A., Gesteira, M., and Silva Santos, C. (2017) ‘Potential Impacts of Climate Change on European Wind Energy Resource under the CMIP5 Future Climate Projections’. *Renewable Energy* 101, 29–40

Cellura, M., Di Gangi, A., Longo, S., and Orioli, A. (2012) ‘Photovoltaic Electricity Scenario Analysis in Urban Contests: An Italian Case Study’. *Renewable and Sustainable Energy Reviews* [online] 16 (4), 2041–2052. available from <http://dx.doi.org/10.1016/j.rser.2012.01.032> [12 August 2016]

Chakraborty, B. (2017) *Paris Agreement on Climate Change: US Withdraws as Trump Calls It ’Unfair* [online] available from <https://www.foxnews.com/politics/paris-agreement-on-climate-change-us-withdraws-as-trump-calls-it-unfair> [10 July 2019]

Chang, K.H. (2014) ‘A Decision Support System for Planning and Coordination of Hybrid Renewable Energy Systems’. *Decision Support Systems* [online] 64, 4–13. available from <http://dx.doi.org/10.1016/j.dss.2014.04.001> [04 March 2018]

Chen, P.Y. and Popvich, P.M. (2002) *Correlation: Parametric and Nonparametric Measures*. London: Sage Publications

Chou, S.C., Marengo, J.A., Lyra, A.A., Sueiro, G., Pesquero, J.F., Alves, L.M., Kay, G., Betts, R., Chagas, D.J., Gomes, J.L., Bustamante, J.F., and Tavares, P. (2012) ‘Downscaling of South America Present Climate Driven by 4-Member HadCM3 Runs’. *Climate Dynamics* 38 (3–4), 635–653

Cole, M. a., Elliott, R.J.R., and Strobl, E. (2014) ‘Climate Change, Hydro-Dependency, and the African Dam Boom’. *World Development* [online] 60, 84–98. available from <http://www.sciencedirect.com/science/article/pii/S0305750X14000825>

Conway, D., Dalin, C., Landman, W.A., and Osborn, T.J. (2017) ‘Hydropower Plans in

Eastern and Southern Africa Increase Risk of Concurrent Climate-Related Electricity Supply Disruption'. *Nature Energy* [online] 2 (12), 946–953. available from <http://dx.doi.org/10.1038/s41560-017-0037-4> [11 July 2018]

CORDEX (2018) *General Instructions for CORDEX Integrations* [online] available from <https://na-cordex.org/experimental-protocol> [26 February 2018]

Coron, L., Perrin, C., Delaigue, O., Andréassian, V., and Thirel, G. (2016) *AirGR : A Suite of Lumped Hydrological Models in an R-Package*. 18 (2015), 12662

Coron, L., Thirel, G., Delaigue, O., Perrin, C., and Andréassian, V. (2017) 'The Suite of Lumped GR Hydrological Models in an R Package'. *Environmental Modelling and Software* 94, 166–171

COWE, J. (2013) *Climate Change: Biological and Human Aspects*. 2nd edn. Combridge University

Crook, J.A., Jones, L.A., Forster, P.M., and Crook, R. (2011) 'Climate Change Impacts on Future Photovoltaic and Concentrated Solar Power Energy Output'. *Energy & Environmental Science* 4 (9), 3101

Cubasch, U., Wuebbles, D., Chen, D., Facchini, M.C., Frame, D., Mahowald, N., and Winther, J.-G. (2013) 'Introduction'. *Climate Change 2013: The Physical Science Basis. Contribution of Working Group I to the Fifth Assessment Report of the Intergovernmental Panel on Climate Change* 119–158

Cutforth, H.W. and Judiesch, D. (2007) 'Long-Term Changes to Incoming Solar Energy on the Canadian Prairie'. *Agricultural and Forest Meteorology* 145 (3–4), 167–175

Damrongsri, N., Mulayaniparambil, S., Piriyakoontorn, S., and Mikael, F. (2019) *HOMER Components* [online] available from <http://www.esru.strath.ac.uk/EandE/Web_sites/17-18/cumbrae/Homer components.html> [14 May 2019]

Dee, D.P., Uppala, S.M., Simmons, A.J., Berrisford, P., Poli, P., Kobayashi, S., Andrae, U., Balmaseda, M.A., Balsamo, G., Bauer, P., Bechtold, P., Beljaars, A.C.M., van de Berg, L., Bidlot, J., Bormann, N., Delsol, C., Dragani, R., Fuentes, M., Geer, A.J., Haimberger, L., Healy, S.B., Hersbach, H., Hólm, E. V., Isaksen, L., Kållberg, P., Köhler, M., Matricardi, M., Mcnally, A.P., Monge-Sanz, B.M., Morcrette, J.J., Park, B.K., Peubey, C., de Rosnay, P., Tavolato, C., Thépaut, J.N., and Vitart, F. (2011) 'The ERA-Interim Reanalysis: Configuration and Performance of the Data Assimilation System'. *Quarterly Journal of the Royal Meteorological Society* 137 (656), 553–597

Deser, C., Phillips, A.S., Alexander, M.A., and Smoliak, B. V. (2014) 'Projecting North American Climate over the next 50 Years: Uncertainty Due to Internal Variability'. *Journal of Climate* 27 (6), 2271–2296

Devia, G.K., Ganasri, B.P., and Dwarakish, G.S. (2015) 'A Review on Hydrological Models'. *Aquatic Procedia* [online] 4 (December), 1001–1007. available from <http://linkinghub.elsevier.com/retrieve/pii/S2214241X15001273> [09 May 2017]

Dharmala, N. (2015) *A Decentralized Energy Option for Rural Electrification – Using Polygeneration in India*. STOCKHOLM

Dosio, A. (2017) 'Projection of Temperature and Heat Waves for Africa with an Ensemble of CORDEX Regional Climate Models'. *Climate Dynamics* 49 (1–2), 493–519

Dowling, P. (2013) 'The Impact of Climate Change on the European Energy System'. *Energy Policy* [online] 60, 406–417. available from <http://dx.doi.org/10.1016/j.enpol.2013.05.093> [12 May 2017]

Draper, A. (2003) *Hydropower of the Future: New Ways of Turning Water into Energy*. New York: The Rosen

EAC (2011a) *East African Community Change Master Plan*.

EAC (2011b) *4th EAC DEVELOPMENT STRATEGY (2011/12 – 2015/16): Deepening* *and Accelerating Integration*. vol. 2015. Arusha: East Africa Community

EAC secretariat (2015) *East African Community Facts and Figures - 2015*. Arusha: EAC

EAC secretariat (2011) *Eastern Africa: Regional Integration Strategy Paper 2011 - 2015*. (September 2011)

EAPP (2015) *Regional Master Plan 2014* [online] available from <http://eappool.org/cmdownloads/eapp-master-plan-2014-vol-i-main-report/> [26 November 2015]

Eastern Africa Power Pool (2011) *Eastern Africa Power Pool (Eapp) and East African Community (Eac) Regional Power System Master Plan and Grid Code Study*. (May), 1–251

Ebinger, J. and Vergara, W. (2011) *Climate Impact on Energy Systems. Key Issues for Energy Sector Adaptation*. Washington: The World Bank

Ebinger, J., Vergara, W., Ansuategi, A., Boulahya, M.S., John, C., and Ibon, G. (2011a) *Future Risk: Climate Change and Energy Security – Global Challenges and Implications*. 26

Ebinger, J., Vergara, W., and Leino, I. (2011b) *Climate Impacts on Energy Systems : Key Issues for Energy Sector Adaptation* [online] Herndon, VA, USA: World Bank Publications. available from <http://site.ebrary.com/lib/coventry/docDetail.action?docID=10453807&ppg=1> [12 May 2016]

Eden, J.M., Widmann, M., Grawe, D., and Rast, S. (2012) ‘Skill, Correction, and Downscaling of GCM-Simulated Precipitation’. *Journal of Climate* 25 (11), 3970–3984

Edenhofer, O., Pichs-Madruga, R., Sokona, Y., Seyboth, K., Eickemeier, P., Matschoss, P., Hansen, G., Kadner, S., Schlömer, S., Zwickel, T., and Stechow, C. Von (2011) *IPCC, 2011: Summary for Policymakers. In: IPCC Special Report on Renewable*

Energy Sources and Climate Change Mitigation [online] Cambridge: Cambridge University Press. available from <http://srren.ipcc-wg3.de/report> [15 August 2017]

Edwards, N.R., Labriet, M., Loulou, R., Vielle, M., Babonneau, F., Joshi, S.R., Holden, P.B., and Kanudia, A. (2013) 'Worldwide Impacts of Climate Change on Energy for Heating and Cooling'. *Mitigation and Adaptation Strategies for Global Change* [online] 20 (7), 1111–1136. available from <https://link.springer.com/article/10.1007/s11027-013-9522-7> [06 May 2016]

Ellison, L.E. (2012) 'Bats and Wind Energy — A Literature Synthesis and Annotated Bibliography'. *U.S. Geological Survey Open-File Report 2012-1110* 57 pp.

Endris, H.S., Omondi, P., Jain, S., Lennard, C., Hewitson, B., Chang'a, L., Awange, J.L., Dosio, A., Ketiem, P., Nikulin, G., Panitz, H.J., B??chner, M., Stordal, F., and Tazalika, L. (2013) 'Assessment of the Performance of CORDEX Regional Climate Models in Simulating East African Rainfall'. *Journal of Climate* 26 (21), 8453–8475

ENGIE (2019) *The Energy Mix: Towards More Diverse and More Complementary Energies* [online] available from <https://www.engie.com/en/innovation-energy-transition/the-energy-mix/> [9 September 2019]

Environmental and Energy Study Institute (2016) *Fossil Fuel* [online] available from <http://www.eesi.org/topics/fossil-fuels/description> [7 March 2013]

Erdinc, O. and Uzunoglu, M. (2012) 'Optimum Design of Hybrid Renewable Energy Systems: Overview of Different Approaches'. *Renewable and Sustainable Energy Reviews* 16 (3), 1412–1425

Esen, Ö. and Bayrak, M. (2017) 'Does More Energy Consumption Support Economic Growth in Net Energy-Importing Countries?' *Journal of Economics, Finance and Administrative Science* 22 (42), 75–98

European Climate Foundation, World Energy Council, Cambridge Judge Business School, and Cambridge Institute for Sustainability Leadership (2014) *Climate*

Change: Implications for the Energy Sector. [online] 1–16. available from <http://www.cisl.cam.ac.uk/business-action/low-carbon-transformation/ipcc-briefings/pdfs/briefings/IPCC_AR5__Implications_for_Energy__Briefing__WEB_EN.pdf> [11 May 2016]

European Wind Energy Association (2012) 'The Economics of Wind Energy'. *European Journal of Operational Research* 42 (6–7), 714–728

Eyakunze, A. and Salim, A. (2012) *States of East Africa 2012*. Nairobi: Society for International Development

Fang, G.H., Yang, J., Chen, Y.N., and Zammit, C. (2015) 'Comparing Bias Correction Methods in Downscaling Meteorological Variables for a Hydrologic Impact Study in an Arid Area in China'. *Hydrology and Earth System Sciences* 19 (6), 2547–2559

Fanney, H. (2019) *Maui Solar Energy Software Corporation* [online] available from <http://www.mauisolarsoftware.com/> [12 September 2019]

Fant, C., Adam Schlosser, C., and Strzepek, K. (2016) 'The Impact of Climate Change on Wind and Solar Resources in Southern Africa'. *Applied Energy* [online] 161, 556–564. available from <http://dx.doi.org/10.1016/j.apenergy.2015.03.042> [03 March 2018]

Farret, F.A. and Simões, M.G. (2006) *Integration of Alternative Sources of Energy*.

Fer, I., Tietjen, B., Jeltsch, F., and Wolff, C. (2017) 'The Influence of El Niño-Southern Oscillation Regimes on Eastern African Vegetation and Its Future Implications under the RCP8.5 Warming Scenario'. *Biogeosciences* 14 (18), 4355–4374

Fidge, A.; and Martinsen, T. (2006) 'Effects of Climate Change on the Utilization of Solar Cells in the Nordic Region'. *In European Conference on Impacts of Climate Change on Renewable Energy Sources*. held 2006. pp.5-9

Field, A. (2009) *Discovering Statistics Using SPSS : Introducing Statistical Methods Series*. 3rd edn. London: SAGE publications Ltd

Firincă SD, Mircea I, Hiyasat A, and Mircea PM (2015) 'Simulation of the Systems With Renewable Energy Sources Using Homer Software'. *Journal of Sustainable Energy* 6 (2), 60–64

Fischer, E.M. and Knutti, R. (2013) 'Robust Projections of Combined Humidity and Temperature Extremes'. *Nature Climate Change* 3 (2), 126–130

Fowler, H.J., Blenkinsop, S., and Tebaldi, C. (2007) 'Linking Climate Change Modelling to Impacts Studies: Recent Advances in Downscaling Techniques for Hydrological Modelling'. *International Journal of Climatology* 27 (12), 1547–1578

Francklyn, L. (2018) *Microgrid and DER Decisions Simplified* [online] available from <https://microgridnews.com/homer-grid-1-2-release-july2018/> [30 October 2018]

François, B., Borga, M., Creutin, J.D., Hingray, B., Raynaud, D., and Sauterleute, J.F. (2016) 'Complementarity between Solar and Hydro Power: Sensitivity Study to Climate Characteristics in Northern-Italy'. *Renewable Energy* 86, 543–553

Funk, C., Nicholson, S.E., Landsfeld, M., Klotter, D., Peterson, P., and Harrison, L. (2015) 'The Centennial Trends Greater Horn of Africa Precipitation Dataset'. *Scientific Data* 2

Gandarillas, V. and Kelly, N. (2015) *Feasibility of Small Scale Energy Storage Technologies in Rural Areas* [online] available from <http://www.esru.strath.ac.uk/Documents/MSc_2015/Gandarillas.pdf> [20 April 2017]

Getachew, B. and Getnet, T. (2012) 'Feasibility Study of Small Hydro/PV/Wind Hybrid System for off-Grid Rural Electrification in Ethiopia'. *Applied Energy* 97 (5–15)

Gettelman, A. and Rood, R.B. (2016) *Demystifying Climate Models* [online] vol. 2. available from <http://link.springer.com/10.1007/978-3-662-48959-8>[12 April 2016]

Ghasemi, A. and Zahediasl, S. (2012) 'Normality Tests for Statistical Analysis: A Guide for Non-Statisticians'. *International Journal of Endocrinology and Metabolism* 10 (2), 486–489

Giatrakos, G.P., Tsoutsos, T.D., Mouchtaropoulos, P.G., Naxakis, G.D., and Stavrakakis, G. (2009) 'Sustainable Energy Planning Based on a Stand-Alone Hybrid Renewable energy/Hydrogen Power System: Application in Karpathos Island, Greece'. *Renewable Energy* [online] 34 (12), 2562–2570. available from <http://dx.doi.org/10.1016/j.renene.2009.05.019> [14 May 2018]

Gibbons, J.D. (1993) *Nonparametric Measures of Association*. London: Sage Publications

Gilman, P. and Lilienthal, P. (2006) *Micropower System Modeling*. 379–418

Giorgi, F., Jones, C., and Asrar, G.R. (2009) *Addressing Climate Information Needs at the Regional Level: The CORDEX Framework* [online] available from <https://public.wmo.int/en/bulletin/addressing-climate-information-needs-regional-level-cordex-framework> [16 November 2017]

Girma, Z. (2013) 'Hybrid Renewable Energy Design for Rural Electrification in Ethiopia'. *Journal of Energy Technologies and Policy* 3 (13), 38–53

Givati, A., Housh, M., Levi, Y., Paz, D., Carmona, I., and Becker, E. (2017) 'The Advantage of Using International Multimodel Ensemble for Seasonal Precipitation Forecast over Israel'. *Advances in Meteorology* 2017

Global Wind Energy Council (2018) *Global Wind Energy Report: Annual Market Update 2017*. [online] available from <www.gwec.net> [10 August 2019]

Goldemberg, J. (2001) 'Energy and Human Well Being'. *Energy* [online] available from <http://hdr.undp.org/en/reports/global/hdr2001/papers/goldemberg-energy-1.pdf>

Gonçalves-Ageitos, M., Barrera-Escoda, A., Baldasano, J.M., and Cunillera, J. (2015) 'Modelling Wind Resources in Climate Change Scenarios in Complex Terrains'. *Renewable Energy* [online] 76, 670–678. available from

<http://dx.doi.org/10.1016/j.renene.2014.11.066> [07 August 2018]

Gordon, E. (2018) *The Status of Renewable Energy in East Africa*. (August), 30

Gov.uk (2019) *Official Statistics: Solar Photovoltaic (PV) Cost Data* [online] available from <https://www.gov.uk/government/statistics/solar-pv-cost-data> [19 September 2019]

Granata, G., Pagnanelli, F., Moscardini, E., Havlik, T., and Toro, L. (2014) 'Recycling of Photovoltaic Panels by Physical Operations'. *Solar Energy Materials and Solar Cells* [online] 123 (2014), 239–248. available from <http://dx.doi.org/10.1016/j.solmat.2014.01.012> [07 May 2018]

Green, J. (1996) *Hybrid2: The Hybrid System Simulation Model, Version 1.0; User Manual*. (June 1996)

Green, M.A., Hishikawa, Y., Dunlop, E.D., Levi, D.H., Hohl-Ebinger, J., Yoshita, M., and Ho-Baillie, A.W.Y. (2019) 'Solar Cell Efficiency Tables (Version 53)'. *Progress in Photovoltaics: Research and Applications* 27 (1), 3–12

GreenBusinessWatch. (2019) *UK Domestic Solar Panel Costs and Returns 2014 – 2017* [online] available from <https://greenbusinesswatch.co.uk/uk-domestic-solar-panel-costs-and-returns-2010-2017> [19 September 2019]

Gulcu, N., Karaaslan, K., Kandirali, E., and Kocoglu, H. (2006) 'Detection of a Retained Epidural Catheter Fragment'. *Regional Anesthesia and Pain Medicine* 31 (6), 589–590

Gupta, H. V., Kling, H., Yilmaz, K.K., and Martinez, G.F. (2009) 'Decomposition of the Mean Squared Error and NSE Performance Criteria: Implications for Improving Hydrological Modelling'. *Journal of Hydrology* 377 (1–2), 80–91

Gutowski, J.W., Giorgi, F., Timbal, B., Frigon, A., Jacob, D., Kang, H.S., Raghavan, K., Lee, B., Lennard, C., Nikulin, G., O'Rourke, E., Rixen, M., Solman, S., Stephenson, T., and Tangang, F. (2016) 'WCRP COordinated Regional Downscaling

EXperiment (CORDEX): A Diagnostic MIP for CMIP6'. *Geoscientific Model Development* 9 (11), 4087–4095

Hafez, O. and Bhattacharya, K. (2012) 'Optimal Planning and Design of a Renewable Energy Based Supply System for Microgrids'. *Renewable Energy* [online] 45, 7–15. available from <http://dx.doi.org/10.1016/j.renene.2012.01.087> [13 October 2018]

Hafner, M., Tagliapietra, S., and De Strasser, L. (2018) *Energy in Africa: Challenges and Opportunities*.

Hagedorn, R., Doblas-Reyes, F.J., and Palmer, T.N. (2005) 'The Rationale behind the Success of Multi-Model Ensembles in Seasonal Forecasting - I. Basic Concept'. *Tellus, Series A: Dynamic Meteorology and Oceanography* 57 (3), 219–233

Hain, J. and Falk, M. (2010) *Comparison of Common Tests for Normality*. [online] (August), 103. available from <http://www.statistik-mathematik.uni-wuerzburg.de/fileadmin/10040800/user_upload/hain/da_hain_final.pdf> [12 October 2017]

Halabi, L.M., Mekhilef, S., Olatomiwa, L., and Hazelton, J. (2017) 'Performance Analysis of Hybrid PV/Diesel/Battery System Using HOMER: A Case Study Sabah, Malaysia'. *Energy Conversion and Management* [online] 144, 322–339. available from <http://dx.doi.org/10.1016/j.enconman.2017.04.070> [07 October 2018]

Hamed, K.H. (2011) 'The Distribution of Kendall's Tau for Testing the Significance of Cross-Correlation in Persistent Data'. *Hydrological Sciences Journal* 56 (5), 841–853

Hamududu, B.H. and Killingtveit, Å. (2016) 'Hydropower Production in Future Climate Scenarios; the Case for the Zambezi River'. *Energies* 9 (7), 1–18

Harris, M. (2015) *Tanzania Shutting down Hydroelectric Plants amidst Ongoing Drought* [online] available from <https://www.hydroworld.com/articles/2015/10/tanzania-shutting-down-hydroelectric-plants-amidst-ongoing-drought.html> [26 November

2016]

Hassan, Q., Jaszczur, M., and Abdulateef, J. (2016) ‘Optimization of PV/WIND/DIESEL Hybrid Power System in HOMER for Rural Electrification’. *Journal of Physics: Conference Series* 745 (3)

Hauke, J. and Kossowski, T. (2011) ‘Comparison of Values of Pearson’s and Spearman’s Correlation Coefficients on the Same Sets of Data’. *Quaestiones Geographicae* 30 (2), 87–93

Hausfather, Z. (2017) *CLIMATE MODELLING; Analysis: How Well Have Climate Models Projected Global Warming?* [online] available from <https://www.carbonbrief.org/analysis-how-well-have-climate-models-projected-global-warming> [4 July 2018]

Hazeleger, W., Severijns, C., Semmler, T., Ştefănescu, S., Yang, S., Wang, X., Wyser, K., Dutra, E., Baldasano, J.M., Bintanja, R., Bougeault, P., Caballero, R., Ekman, A.M.L., Christensen, J.H., Van Den Hurk, B., Jimenez, P., Jones, C., Kållberg, P., Koenigk, T., McGrath, R., Miranda, P., Van Noije, T., Palmer, T., Parodi, J.A., Schmith, T., Selten, F., Storelvmo, T., Sterl, A., Tapamo, H., Vancoppenolle, M., Viterbo, P., and Willén, U. (2010) ‘EC-Earth: A Seamless Earth-System Prediction Approach in Action’. *Bulletin of the American Meteorological Society* 91 (10), 1357–1363

Hennemuth, B., Bender, S., Bülow, K., Dreier, N., Keup-Thiel, E., Krüger, O., Mudersbach, C., Radermacher, C., and Schoetter, R. (2013) ‘Statistical Methods for the Analysis of Simulated and Observed Climate Data Applied in Projects and Institutions Dealing with Climate Change Impact and Adaptation’. *CSC Report* 13, 135

Hinkle, D.E., Wiersma, W., and Jurs, S.G. (1998) ‘Guideline for Interpreting Correlation Coefficient’. *Applied Statistics for Behavioral Sciences* 105

Holtanová, E., Mendlik, T., Koláček, J., Horová, I., and Mikšovský, J. (2019) 'Similarities within a Multi-Model Ensemble: Functional Data Analysis Framework'. *Geoscientific Model Development* 12 (2), 735–747

homerenergy (2019) *Logarithmic Profile*. 2–3

Huard, D. and Mailhot, A. (2008) 'Calibration of Hydrological Model GR2M Using Bayesian Uncertainty Analysis'. *Water Resources Research* 44 (2), 1–19

Hulme, M., Doherty, R., Ngara, T., New, M., and Lister, D. (2001) 'African Climate Change: 1900-2100'. *Climate Research* 17 (2 SPECIAL 8), 145–168

IEA (2019) *Sustainable Development Goal 7: Ensure Access to Affordable, Reliable, Sustainable and Modern Energy for All* [online] available from <https://www.iea.org/sdg/electricity/> [20 February 2019]

IEA (2017) *WEO Energy Access Outlook 2017, Methodology for Energy Access Analysis*. 1–9

IEA (2014) *Africa Energy Outlook*. 1–237

Indeje, M., Semazzi, F.H.M., and Ogallo, L.J. (2000) 'ENSO Signals in East African Rainfall Seasons'. *International Journal of Climatology* 20 (1), 19–46

International Renewable Energy Agency (IRENA) (2015) *Africa 2030: Roadmap for a Renewable Energy Future, REmap 2030 Programme*.

IPCC (2014) *Climate Change 2014: Synthesis Report. Contribution of Working Groups I, II and III to the Fifth Assessment Report of the Intergovernmental Panel on Climate Change*. Switzerland,: Intergovernmental Panel on Climate Change

IPCC (2013a) *IPCC Factsheet : What Is the IPCC ?* 1–2

IPCC (2013b) 'Climate Change 2013: The Physical Science Basis. Contribution of Working Group I to the Fifth Assessment Report of the Intergovernmental Panel on Climate Change'. *Intergovernmental Panel on Climate Change, Working Group I Contribution to the IPCC Fifth Assessment Report (AR5)(Cambridge Univ Press,* *New York)* 1535

IPCC (2008) *Climate Change 2007 Synthesis Report*.

IPCC (2007) *Climate Change 2007: Impacts, Adaptation and Vulnerability: Contribution of Working Group II to the Fourth Assessment Report of the Intergovernmental Panel*. Cambridge: Cambridge University Press

IPCC (2001) 'Physical Climate Processes and Feedbacks'. *Climate Change 2001: The Scientific Bases. Contribution of Working Group I to the Third Assessment Report of the Intergovernmental Panel on Climate Change* [online] 881. available from <https://www.ipcc.ch/ipccreports/tar/wg1/pdf/TAR-07.PDF>

IPPC (1992) '1992 IPCC Supplement'. *IPCC First Assessment Report* [online] 48 (9), 1334–1334. available from <https://academic.oup.com/cid/article-lookup/doi/10.1086/599017> [31 October 2016]

IRENA (2019) *Data, Research and Resources on Renewable Energy Costs* [online] available from <https://www.irena.org/costs> [20 January 2019]

IRENA (2018) *Renewable Power Generation Costs in 2017* [online] available from <https://www.irena.org/-/media/Files/IRENA/Agency/Publication/2018/Jan/IRENA_2017_Power_Costs_2018.pdf> [04 May 2018]

IRENA (2017) *Synergies Between Renewable Energy and Energy Efficiency* [online] available from <http://www.irena.org/remap> [04 May 2018]

IRENA (2016) *Renewables Readdiness Assessment - United Republic of Tanzania* [online] available from <http://www.irena.org/Menu/index.aspx?PriMenuID=13&mnu=Pri>[04 May 2018]

IRENA (2014) *A Renewable Energy Roadmap*. (June)

Islam, S.U., Rehman, N., and Sheikh, M.M. (2009) 'Future Change in the Frequency of Warm and Cold Spells over Pakistan Simulated by the PRECIS Regional Climate

Model’. *Climatic Change* 94 (1–2), 35–45

Jäger-Waldau, A. (2013) *PV Status Report 2013*.

Jakob Themeßl, M., Gobiet, A., and Leuprecht, A. (2011) ‘Empirical-Statistical Downscaling and Error Correction of Daily Precipitation from Regional Climate Models’. *International Journal of Climatology* 31 (10), 1530–1544

Jerez, S., Tobin, I., Vautard, R., Montávez, J.P., López-Romero, J.M., Thais, F., Bartok, B., Christensen, O.B., Colette, A., Déqué, M., Nikulin, G., Kotlarski, S., van Meijgaard, E., Teichmann, C., and Wild, M. (2015) ‘The Impact of Climate Change on Photovoltaic Power Generation in Europe’. *Nature Communications* [online] 6, 10014. available from <http://www.nature.com/doifinder/10.1038/ncomms10014> [28 November 2018]

Jimenez, A.C. and Lawand, T. (2000) *Renewable Energy for Rural Schools*.

Jjunju, E. and Killingtveit, A. (2015) ‘Modelling Climate Change Impacts on Hydropower in East Africa Modelling Climate Change Impacts on Hydropower in East Africa’. *International Journal on Hydropower and Dams* (January 2015)

Jóhannesson, T., Aðalgeirsdóttir, G., Björnsson, H., and Crochet, P. (2007) *Effect of Climate Change on Hydrology and Hydro-Resources in Iceland* [online] available from <http://www.raunvis.hi.is/~sg/CE_report.pdf> [20 May 2017]

Jones, A., Haywood, J.M., and Jones, C.D. (2018) ‘Can Reducing Black Carbon and Methane below RCP2.6 Levels Keep Global Warming below 1.5 °C?’ *Atmospheric Science Letters* 19 (6), 1–5

Jones, R., Noguer, M., Hassell, D., Hudson, D., Wilson, S., Jenkins, G., Mitchell, J., Taylor, R., Office, M., and Centre, H. (2004) ‘Generating High Resolution Climate Change Scenarios Using Precis’. *Office* 40

KABERUKA, D. (2000) *Republic of Rwanda Ministry of Finance and Economic Planning*. (July), 1–31

Kafadar, K. (2003) 'Testing for Normality'. *Journal of the American Statistical Association* 98 (463), 765–765

Kainkwa, R.R. (1998) *Wind Energy as an Alternative Source to Alleviate the Shortage of Electricity That Prevails during the Dry Season] a Case Study of Tanzania*. 56–63

Kammen, D.M., Jacome, V., and Avila, N. (2015) *A Clean Energy Vision for East Africa : Planning for Sustainability , Reducing Climate Risks and Increasing Energy Access*. (March), 1–28

Karekezi, S., Kimani, J., Onguru, O., and Kithyoma, W. (2009) 'Large Scale Hydropower, Renewable Energy and Adaptation to Climate Change: Climate Change and Energy Security in East and Horn of Africa'. *Occasional Paper, Heinrich Böll Stiftung* [online] (No. 33), 105. available from <http://scholar.google.com/scholar?hl=en&btnG=Search&q=intitle:Large+Scale+Hydropower,+Renewable+Energy+and+Adaptation+to+Climate+Change:+Climate+Change+and+Energy+Security+in+East+and+Horn+of+Africa#0> [01 April 2016]

Karekezi, S. and Kithyoma, W. (2005) *Sustainable Energy in Africa: Cogeneration and Geothermal in the East and Horn of Africa - Status and Prospects* [online] Nairobi. available from <http://www.afrepren.org/published_volumes_main.htm#Sustainable_Energy_in_Africa> [01 April 2016]

Karekezi, S. and Kithyoma, W. (2003) 'Renewable Energy Development'. *Workshop on African Energy Experts on Operationalizing the NEPAD Energy Initiative, June* 2–4

Kaur, T. and Segal, R. (2017) 'Designing Rural Electrification Solutions Considering Hybrid Energy Systems for Papua New Guinea'. *Energy Procedia* 110 (December 2016), 1–7

Kaygusuz, K. (2007) 'Energy for Sustainable Development: Key Issues and Challenges'. *Energy Sources, Part B: Economics, Planning and Policy* 2 (1), 73–83

Kazoora, G.C. (2014) *Promoting Energy Efficiency in Sub-Saharan Africa*. [online] April. available from <https://warwick.ac.uk/fac/sci/eng/elith/publications/proceedings/eebea-elith_kazoora.pdf>[04 August 2016]

Kemenes, A., Forsberg, B.R., and Melack, J.M. (2007) 'Methane Release below a Tropical Hydroelectric Dam'. *Geophysical Research Letters* 34 (12)

Kent, C., Chadwick, R., and Rowell, D.P. (2015) 'Understanding Uncertainties in Future Projections of Seasonal Tropical Precipitation'. *Journal of Climate* 28 (11), 4390–4413

Khan, M.J. and Iqbal, M.T. (2005) 'Pre-Feasibility Study of Stand-Alone Hybrid Energy Systems for Applications in Newfoundland'. *Renewable Energy* 30 (6), 835–854

Kibati, M. (2015) *Viewing Lake Turkana Wind Power through Vision 2030 Lens* [online] available from <http://www.standardmedia.co.ke/business/article/2000168872/viewing-lake-turkana-wind-power-through-vision-2030-lens> [19 July 2015]

Kim, H., Bae, J., Baek, S., Nam, D., Cho, H., and Chang, H.J. (2017) 'Comparative Analysis between the Government Micro-Grid Plan and Computer Simulation Results Based on Real Data: The Practical Case for a South Korean Island'. *Sustainability (Switzerland)* 9 (2)

Kinuthia, P.N. (2014) *Energy Business Opportunities in the East African Community*. held 2014

Knutti, R., Furrer, R., Tebaldi, C., Cermak, J., and Meehl, G.A. (2010) 'Challenges in Combining Projections from Multiple Climate Models'. *Journal of Climate* 23 (10), 2739–2758

Kollikho, P. (2013) *Inside Stories on Climate Compatible Development Harnessing Geothermal Energy : The Case of Kenya*. (January)

Lafaysse, M., Hingray, B., Mezghani, A., Gailhard, J., and Terray, L. (2014) 'Internal Variability and Model Uncertainty Components'. *Water Resources Research* 3317–3341

Lambert, T., Gilman, P., and Lilienthal, P. (2005) 'Micro Power System Modelling'. *Integration of Alternative Sources of Energy* 379–418

Lampert, D.J. and Wu, M. (2015) 'Development of an Open-Source Software Package for Watershed Modeling with the Hydrological Simulation Program in Fortran'. *Environmental Modelling and Software* 68, 166–174

Lenderink, G., Buishand, A., and Van Deursen, W. (2007) 'Estimates of Future Discharges of the River Rhine Using Two Scenario Methodologies: Direct versus Delta Approach'. *Hydrology and Earth System Sciences* 11 (3), 1145–1159

Li, H., Sheffield, J., and Wood, E.F. (2010) 'Bias Correction of Monthly Precipitation and Temperature Fields from Intergovernmental Panel on Climate Change AR4 Models Using Equidistant Quantile Matching'. *Journal of Geophysical Research Atmospheres* 115 (10)

Liebmann, B., Hoerling, M.P., Funk, C., Bladé, I., Dole, R.M., Allured, D., Quan, X., Pegion, P., and Eischeid, J.K. (2014) 'Understanding Recent Eastern Horn of Africa Rainfall Variability and Change'. *Journal of Climate* 27 (23), 8630–8645

Liu, B.Y.H. and Jordan, R.C. (1960) 'The Interrelationship and Characteristic Distribution of Direct, Diffuse and Total Solar Radiation'. *Solar Energy* 4 (3), 1–19

Liu, H., Masera, D., and Esser, L. (2013) *World Small Hydropower Development Report 2013*. 1–3

Longe, O., Rao, N., Omowole, F., Oluwalami, A., and Oni, O. (2017) 'A Case Study on Off-Grid Microgrid for Universal Electricity Access in the Eastern Cape of South

Africa'. *International Journal of Energy Engineering* 7 (2), 55–63

Longe, O.M., Ouahada, K., Ferreira, H.C., and Chinnappen, S. (2014) 'Renewable Energy Sources Microgrid Design for Rural Area in South Africa'. *IEEE ISGT-America* 1–5

Lumley, T., Diehr, P., Emerson, S., and Chen, L. (2002) *THE IMPORTANCE OF THE NORMALITY ASSUMPTION IN LARGE PUBLIC HEALT*. 23:151-69

Luo, X., Wang, J., Dooner, M., and Clarke, J. (2015) 'Overview of Current Development in Electrical Energy Storage Technologies and the Application Potential in Power System Operation'. *Applied Energy* 137, 511–536

Lupo, A. and Kininmonth, W. (2013) 'Global Climate Models and Their Limitations'. *Climate Change Reconsidered II: Physical Science.* 7–148

Lutz, A.F., ter Maat, H.W., Biemans, H., Shrestha, A.B., Wester, P., and Immerzeel, W.W. (2016) 'Selecting Representative Climate Models for Climate Change Impact Studies: An Advanced Envelope-Based Selection Approach'. *International Journal of Climatology* 36 (12), 3988–4005

Lydia, M., Kumar, S.S., Selvakumar, A.I., and Prem Kumar, G.E. (2014) 'A Comprehensive Review on Wind Turbine Power Curve Modeling Techniques'. *Renewable and Sustainable Energy Reviews* [online] 30, 452–460. available from <http://dx.doi.org/10.1016/j.rser.2013.10.030> [04 August 2018]

Lyon, B. and Dewitt, D.G. (2012) 'A Recent and Abrupt Decline in the East African Long Rains'. *Geophysical Research Letters* 39 (2), 1–5

Macgill, I. and Ho, A.W.Y. (2009) 'Wind Energy Converters'. *Renewable Energy* 1–59

Machiwal, D. and Jha, M.K. (2012) *Hydrologic Time Series Analysis: Theory and Practice*. New Delhi: Springer

Manwell, J.F., McGowan, J.G., and Rogers, A.L. (2010) *Wind Energy Explained: Theory, Design and Application*. London: John Wiley & Sons

Maraun, D. (2014) '12/9/2014 AMS Journals Online - Bias Correction, Quantile Mapping, and Downscaling: Revisiting the Inflation Issue'. *Journal of Climate* [online] 26 (2013), 2013–2014. available from <http://journals.ametsoc.org/doi/10.1175/JCLI-D-12-00821.1> [17 March 2016]

Marengo J., Alves, L.M., Valverde, M., and C., J.A.J. (2009) 'Future Change of Temperature and Precipitation Extremes in South America as Derivered from the PRECIS Regional Climate Modeling System'. in *International Journal of Climatology*. 1–15

McGregor, G.R. and Ebi, K. (2018) 'El Niño Southern Oscillation (ENSO) and Health: An Overview for Climate and Health Researchers'. *Atmosphere* 9 (7)

McLamb, E. (2011) *Fossil Fuels vs. Renewable Energy Resources* [online] available from <http://www.ecology.com/2011/09/06/fossil-fuels-renewable-energy-resources/> [7 March 2016]

McSweeney, C., Buontempo, C., Mathison, C., Jones, R., Williams, K., and Wang, C. (2015) 'An Ensemble Climate Projection for Africa'. *Climate Dynamics* 44 (7–8), 2097–2118

McVeigh C., J. and Mordue G., J. (1999) *Energy Demand and Planning*. London: Routledge

Mdone, E., Klemm, J., and Greenstein, G. (2017) *AN EVALUATION OF DAMS UNDER THE PROGRAMME Right Priorities for Africa ' s Power Sector*. Abidjan

Meehl, G.A., Stocker, T.F., Collins, W.D., Friedlingstein, P., Gaye, A.T., Gregory, J.M., Kitoh, A., Knutti, R., Murphy, J.M., Noda, A., Raper, S.C.B., Watterson, I.G., Weaver, A.J., and Zhao, Z.-C. (2007) '2007: Global Climate Projections'. *Climate Change 2007: Contribution of Working Group I to the Fourth Assessment Report of the Intergovernmental Panel on Climate Change* [online] 747–846. available from <http://www.ipcc.ch/pdf/assessment-report/ar4/wg1/ar4-wg1-chapter10.pdf> [14

April 2016]

Mekonnen, A. (2019) *Feasibility Study of Renewable Energy Resources for Electrification of Small Island*. (February)

Miao, C., Su, L., Sun, Q., and Duan, Q. (2016) 'A Nonstationary Bias-Correction Technique to Remove Bias in GCM Simulations'. *Journal of Geophysical Research* 121 (10), 5718–5735

Milly, P.C.D., Dunne, K.A., and Vecchia, A. V. (2005) 'Global Pattern of Trends in Streamflow and Water Availability in a Changing Climate'. *Nature* 438 (7066), 347–350

Miñambres-Marcos, V.M., Barrero-González, F., and Isabel Milanés-Montero, M. (2018) 'A Grid Connected Photovoltaic Inverter with Battery-Supercapacitor Hybrid Energy Storage Víctor'. *Sensors* 17 (2), 822–828

Ministry of Energy and Mineral Development (2007) *The Renewable Energy Policy for Uganda*. [online] 128. available from <RENEWABLE ENERGY POLIC9-11-07.pdf> [15 April 2016]

Miskelly, A. (2016) *Wind Energy* [online] available from <http://energy.anero.id.au/wind-energy>

Mitchell, T.D. and Jones, P.D. (2005) 'An Improved Method of Constructing a Database of Monthly Climate Observations and Associated High-Resolution Grids'. *International Journal of Climatology* 25 (6), 693–712

Mitra, I. and Chaudhuri, S.P.G. (2006) 'Remote Village Electrification Plan through Renewable Energy in the Islands of Indian Sundarbans'. *INTERNATIONAL SOLAR ENERGY SOCIETY UK SECTION Renewable Energy in Maritime Island Climates REMIC2* [online] 315–320. available from <http://www.homerenergy.com/webcast-downloads/ises-remic2-v2.pdf> [04 May 2016]

Monier, V. and Hestin, M. (2011) *European Commission DG ENV A Project under the*

Framework Contract STUDY ON PHOTOVOLTAIC PANELS SUPPLEMENTING THE IMPACT ASSESSMENT FOR A RECAST OF THE WEEE DIRECTIVE. (April)

Moradkhani, H. and Sorooshian, S. (2009) *General Review of Rainfall-Runoff Modeling: Model Calibration, Data Assimilation, and Uncertainty Analysis*. Berlin: Springer

Moss, R.H., Edmonds, J.A., Hibbard, K.A., Manning, M.R., Rose, S.K., Van Vuuren, D.P., Carter, T.R., Emori, S., Kainuma, M., Kram, T., Meehl, G.A., Mitchell, J.F.B., Nakicenovic, N., Riahi, K., Smith, S.J., Stouffer, R.J., Thomson, A.M., Weyant, J.P., and Wilbanks, T.J. (2010) 'The next Generation of Scenarios for Climate Change Research and Assessment'. *Nature* 463 (7282), 747–756

Mouelhi, S., Aux, D.E.S.E., and Des, E.T. (2004) 'Vers Une Chaîne Cohérente de Modèles Pluie-Débit Aux Pas de Temps Pluriannue, Annuel, Mensuel et Journalier'. *Hydrologie. ENGREF (AgroParisTech)*

Mutai, C.C., Ward, M.N., and Colman, A.W. (1998) 'Towards the Prediction of the East Africa Short Rains Based on Sea-surface Temperature–Atmosphere Coupling'. *International Journal of Climatology* 18 (9), 975–997

Muthusamy, S. (2018) *Software Tools for Analyzing the Integration of Various Renewable Energy Systems*. 2 (August), 135–140

Nalule, V.R. (2016) *Energy in the East African Community: The Role of the Energy Charter Treaty*.

Nandozi, C.S., Omondi, P., Komutunga, E., Aribo, L., Isubikalu, P., and Tenywa, M.M. (2012) 'Regional Climate Model Performance and Prediction of Seasonal Rainfall and Surface Temperature of Uganda'. *African Crop Science Journal* 20 (s2), 213–225

NAPE (2014) *Social Consequences of the Bujagali Hydropower Project* [online] available from <https://www.internationalrivers.org/files/attached-files/bujagali_unsettlingbusiness_1.pdf> [15 April 2016]

Nash, J.. and Sutcliffe, J.. (1970) *River Flow Forecasting through Conceptual Models Part I — A Discussion of Principles*. 10 (3), Pages 282-290

National Wind Coordinating Commitee (2010) *Birds , Bats , and Their Habitats :* [online] 1–8. available from <http://www.nationalwind.org/assets/archive/Wind_Turbine_Interactions_with_Birds_and_Bats_-_A_Summary_of_Research_Results_and_Remaining_Questions__2004_.pdf> [03 March 2017]

Naumann, M., Karl, R.C., Truong, C.N., Jossen, A., and Hesse, H.C. (2015) 'Lithium-Ion Battery Cost Analysis in PV-Household Application'. *Energy Procedia* [online] 73, 37–47. available from <http://dx.doi.org/10.1016/j.egypro.2015.07.555> [12 April 2016]

Niang, I., Ruppel, O.C., Abdrabo, M.A., Essel, A., Lennard, C., Padgham, J. and Urquhart, P. (2014) Africa. In: Barros, V.R., Field, C.B., Dokken, D.J., Mastrandrea, M.D., Mach, K.J., Bilir, T.E., Chatterjee, M., Ebi, K.L., Estrada, Y.O., Genova, R.C., Gi, E. (2014) *Climate Change 2014: Impacts, Adaptation, and Vulnerability. Part B: Regional Aspects. Contribution of Working Group II to the Fifth Assessment Report of the Intergovernmental Panel on Climate Change*. Cambridge: Cambridge University Press

Nicholson, S.E. (1996) 'A Review of Climate Dynamics and Climate Variability in Eastern Africa'. *The Limnology, Climatology and Paleoclimatology of the East African Lakes* 25–56

Nicholson, S.E. and Kim, J. (1997) 'The Relationship of the El Nino-Southern Oscillation to African Rainfall'. *International Journal of Climatology* 17 (2), 117–135

Niedzielski, T. (2015) *Learn More about Southern Oscillation TROPICAL METEOROLOGY AND CLIMATE | Tropical Climates TROPICAL*

METEOROLOGY & CLI- MATE | El Niño and the Southern Os- Cillation.

Nikulin, G., Jones, C., Giorgi, F., Asrar, G., Büchner, M., Cerezo-Mota, R., Christensen, O.B., Déqué, M., Fernandez, J., Hänsler, A., van Meijgaard, E., Samuelsson, P., Sylla, M.B., and Sushama, L. (2012) 'Precipitation Climatology in an Ensemble of CORDEX-Africa Regional Climate Simulations'. *Journal of Climate* 25 (18), 6057–6078

Nile-SEC (2017) *Construction of Rusumo Falls Hydroelectric Project* [online] available from <https://www.nilebasin.org/new-and-events/133-construction-of-rusumo-falls-hydroelectric-project-to-start-30-march-2017> [10 March 2018]

NOAA (2018) *What Are El Niño and La Niña?* [online] available from <https://oceanservice.noaa.gov/facts/ninonina.html> [4 March 2019]

Ogwang, B.A., Chen, H., Li, X., and Gao, C. (2014) 'The Influence of Topography on East African October to December Climate: Sensitivity Experiments with RegCM4'. *Advances in Meteorology* 2014

Okedu, K.E. and Uhunmwangho, R. (2014) 'Optimization of Renewable Energy Efficiency Using HOMER'. *International Journal of Renewable Energy Research* 4 (2), 421–427

Oketch, M. and Ngware, M.W. (2015) *Urbanization and Education in East Africa*. Nairobi: The Africa Population and Health Research Center

Ongoma, V., Chena, H., and Gaoa, C. (2018) 'Projected Changes in Mean Rainfall and Temperature over East Africa Based on CMIP5 Models'. *International Journal of Climatology* 38 (3), 1375–1392

Ongoma, V., Haishan, C., and Chujie, G. (2017) 'Projected Changes in Mean Rainfall and Temperature over East Africa Based on CMIP5 Models'. *Int. J. Climatol.* (October)

Othieno, H. and Awange, J. (2016) *Energy Resources in East Africa* [online] available from <http://link.springer.com/10.1007/978-3-319-25187-5_2> [14 September 2017]

Owusu, P.A. and Asumadu-Sarkodie, S. (2016) 'A Review of Renewable Energy Sources, Sustainability Issues and Climate Change Mitigation'. *Cogent Engineering* [online] 3 (1), 1–14. available from <http://dx.doi.org/10.1080/23311916.2016.1167990> [17 April 2017]

Öztuna, D., Elhan, A.H., and Tüccar, E. (2006) 'Investigation of Four Different Normality Tests in Terms of Type 1 Error Rate and Power under Different Distributions'. *Turkish Journal of Medical Sciences* 36 (3), 171–176

Parida, B., Iniyan, S., and Goic, R. (2011) 'A Review of Solar Photovoltaic Technologies'. *Renewable and Sustainable Energy Reviews* [online] 15 (3), 1625–1636. available from <http://dx.doi.org/10.1016/j.rser.2010.11.032> [15 May 2016]

Pašičko, R., Branković, Č., and Šimić, Z. (2012) 'Assessment of Climate Change Impacts on Energy Generation from Renewable Sources in Croatia'. *Renewable Energy* 46, 224–231

Pereira de Lucena, A.F., Szklo, A.S., Schaeffer, R., and Dutra, R.M. (2010) 'The Vulnerability of Wind Power to Climate Change in Brazil'. *Renewable Energy* [online] 35 (5), 904–912. available from <http://dx.doi.org/10.1016/j.renene.2009.10.022>[15 May 2016]

Philipps, S. (2018) *Photovoltaics Report, Updated: 27 August 2018* [online] available from <https://www.ise.fraunhofer.de/content/dam/ise/de/documents/publications/studies/Photovoltaics-Report.pdf> [12 February 2019]

Phillips, N.A. (1956) 'The General Circulation of the Atmosphere: A Numerical Experiment'. *Quarterly Journal of the Royal Meteorological Society* [online] 82 (352), 123–154. available from <https://doi.org/10.1002/qj.49708235202> [12 April

2017]

Piani, C., Haerter, J.O., and Coppola, E. (2010) 'Statistical Bias Correction for Daily Precipitation in Regional Climate Models over Europe'. *Theoretical and Applied Climatology* 99 (1–2), 187–192

Pierce, D.W., Barnett, T.P., Santer, B.D., and Gleckler, P.J. (2009) 'Selecting Global Climate Models for Regional Climate Change Studies'. *Proceedings of the National Academy of Sciences* [online] 106 (21), 8441–8446. available from <http://www.pnas.org/content/106/21/8441.abstract%5Cnhttp://www.pnas.org/content/106/21/8441.full.pdf%5Cnhttp://www.pnas.org/cgi/doi/10.1073/pnas.0900094106> [14 June 2017]

Pisupati, S. (2019) *Energy Conservation and Environmental Protection:Global Energy Consumption* [online] available from <https://www.e-education.psu.edu/egee102/node/1925> [14 June 2019]

Practical Action (2014) *Poor People's Energy Outlook: Key Messages on Energy for Poverty Alleviation*.

Pryor, S.C. and Barthelmie, R.J. (2010) 'Climate Change Impacts on Wind Energy: A Review'. *Renewable and Sustainable Energy Reviews* 14 (1), 430–437

Rahmstorf, S., Foster, G., and Cazenave, A. (2012) 'Comparing Climate Projections to Observations up to 2011'. *Environmental Research Letters* 7 (4)

Räisänen, J. (2007) 'How Reliable Are Climate Models?' *Tellus, Series A: Dynamic Meteorology and Oceanography* 59 (1), 2–29

Räisänen, J. and Palmer, T.N. (2001) 'A Probability and Decision-Model Analysis of a Multimodel Ensemble of Climate Change Simulations'. *Journal of Climate* 14 (15), 3212–3226

Rana, A., Foster, K., Bosshard, T., Olsson, J., and Bengtsson, L. (2014) 'Impact of Climate Change on Rainfall over Mumbai Using Distribution-Based Scaling of

Global Climate Model Projections'. *Journal of Hydrology: Regional Studies* 1, 107–128

Rashid, M.M., Beecham, S., and Chowdhury, R.K. (2015) 'Statistical Downscaling of CMIP5 Outputs for Projecting Future Changes in Rainfall in the Onkaparinga Catchment.' *The Science of the Total Environment* 530–531 (2015), 171–82

Rauf, A. ur and Ghumman, A.R. (2018) 'Impact Assessment of Rainfall-Runoffsimulations on the Flow Duration Curve of the Upper Indus River-a Comparison of Data-Driven and Hydrologic Models'. *Water (Switzerland)* 10 (7)

Rayston, P. (1995) 'Remark as R94: A Remarkon Algorithmas 181: The W-Test for Normality'. *Journal of the Royal Statistical Society.Series C(Applied Stattistics)* 44 (4), 547–551

Rebekić, A., Lončarić, Z., Petrović, S., and Marić, S. (2015) 'Pearson's or Spearman's Correlation Coefficient – Which One to Use ?' *Poljoprivreda* 21 (2), 47–54

REN21-EAC (2016) *RENEWABLE ENERGY AND ENERGY EFFICIENCY REGIONAL EAC RENEWABLE ENERGY STATUS REPORT*. (May), 2–4

REN21 (2016a) *REN21-East Africa 2016*.

REN21 (2016b) *EAC Renewable Energy and Energy Efficiency Regional Status Report*. Paris

REN21 (2015) *RENEWABLES 2014 GLOBAL STATUS REPORT* [online] available from <http://www.ren21.net/Portals/0/documents/Resources/GSR/2014/GSR2014_full report_low res.pdf> [13 May 2016]

Republic of Kenya (2011) 'SREP Investment Plan for Kenya'. *Scaling-up Renewable Energy Program. Investment Plan for Kenya.* 1–66

Reynolds, T. (1983) *STRONGER THAN A HUNDRED MEN: A History of the Vertical Water Wheel*. London: Johns Hopins Press

Riahi, K., Rao, S., Krey, V., Cho, C., Chirkov, V., Fischer, G., Kindermann, G., Nakicenovic, N., and Rafaj, P. (2011) 'RCP 8.5-A Scenario of Comparatively High Greenhouse Gas Emissions'. *Climatic Change* 109 (1), 33–57

Rolland, S. and Glania, G. (2016) 'For Rural Electrification : Hybrid Mini-Grids for Rural Electrification ': *Region 10 Conference (TENCON), 2016 IEEE* (2159–3450), 1270–1273

Roos, J. (2014) *Energy Infrastructure Development in East Africa: Big Potential Meets Big Roadblocks* [online] available from <https://www.renewableenergyworld.com/articles/2014/06/energy-infrastructure-development-in-east-africa-big-potential-meets-big-roadblocks.html> [17 June 2019]

Rousis, A.O., Tzelepis, D., Konstantelos, I., Booth, C., and Strbac, G. (2018) 'Design of a Hybrid Ac/Dc Microgrid Using Homer pro: Case Study on an Islanded Residential Application'. *Inventions* 3 (3), 1–14

Rowell, D.P., Booth, B.B.B., Nicholson, S.E., and Good, P. (2015) 'Reconciling Past and Future Rainfall Trends over East Africa'. *Journal of Climate* 28 (24), 9768–9788

Royston, P. (1992) 'Approximating the Shapiro-Wilk W-Test for Non-Normality'. *Statistics and Computing* 2 (3), pp 117–119

Ruiter, A. (2012) *Delta-Change Approach for CMIP5 GCMs. Internship Report*. 36

Rwagaju, D. and Intwali, J.P. (2010) *One Laptop per Child Rwanda* [online] available from <https://www.rencp.org/about/member-organizations-1/one-laptop-per-child-rwanda/> [17 July 2019]

Sailor, David J., Smith, M., and Hart, M. (2008) 'Climate Change Implications for Wind Power Resources in the Northwest United States'. *Renewable Energy* 33 (11), 2393–2406

Sailor, David J, Smith, M., and Hart, M. (2008) 'Climate Change Implications for Wind Power Resources in the Northwest United States'. *Renewable Energy* 33 (11), 2393–

2406

Santos, L., Thirel, G., and Perrin, C. (2018) *Technical Note: Pitfalls in Using Log-Transformed Flows within the KGE Criterion*. 4583–4591

Savelsberg, J., Schillinger, M., Schlecht, I., and Weigt, H. (2018) 'The Impact of Climate Change on Swiss Hydropower'. *Sustainability (Switzerland)* 10 (7)

Scheck, C. and Simazine, F. (2004) 'Variability of the Recent Climate of Eastern Africa'. *International Journal of Climatology* 24 (6), pp.681-701

Schneider, U., Becker, A., Ziese, M., and Rudolf, B. (2011) 'Global Precipitation Analysis Products of the GPCC'. *IEarth System Science Data* (May), 1–13

Schreck, C.J. and Semazzi, F.H.M. (2004) 'Variability of the Recent Climate of Eastern Africa'. *International Journal of Climatology* 24 (6), 681–701

Schwartz, R.D. (2012) 'An Astrophysicist Looks at Global Warming'. *GSA Today* 22 (1), 44–45

Scirocco, E. (2012) *Choosing a Wind Turbine*.

Seager, R., Naik, N., and Vecchi, G.A. (2010) 'Thermodynamic and Dynamic Mechanisms for Large-Scale Changes in the Hydrological Cycle in Response to Global Warming'. *Journal of Climate* 23 (17), 4651–4668

Segele, Z.T., Lamb, P.J., and Leslie, L.M. (2009) 'Seasonal-to-Interannual Variability of Ethiopia/Horn of Africa Monsoon. Part I: Associations of Wavelet-Filtered Large-Scale Atmospheric Circulation and Global Sea Surface Temperature'. *Journal of Climate* 22 (12), 3396–3421

Sen, R. and Bhattacharyya, S.C. (2014a) 'Off-Grid Electricity Generation with Renewable Energy Technologies in India: An Application of HOMER'. *Renewable Energy* 62, 388–398

Sen, R. and Bhattacharyya, S.C. (2014b) 'Off-Grid Electricity Generation with Renewable Energy Technologies in India: An Application of HOMER'. *Renewable*

Energy [online] 62, 388–398. available from <http://dx.doi.org/10.1016/j.renene.2013.07.028>[12 March 2017]

Serdeczny, O., Adams, S., Baarsch, F., Coumou, D., Robinson, A., Hare, W., Schaeffer, M., Perrette, M., and Reinhardt, J. (2017) 'Climate Change Impacts in Sub-Saharan Africa: From Physical Changes to Their Social Repercussions'. *Regional Environmental Change* 17 (6), 1585–1600

Setiawan, A. and Nayar, C. (2006) 'Design of Hybrid Power System for a Remote Island in Maldives *of the HOMER Webcast-NREL USA* [online] 1–5. available from <http://www.homerenergy.com/webcast-downloads/Webcast_HOMER-Ahmad.pdf> [04 May 2018]

Shahzad, U. (2012) 'ITEE Journal'. *International Journal of Information Technology and Electrical Engineering* 16–18

Shapiro, S.S. and Wilk, M.B. (1965) 'An Analysis of Variance Test for Normality (Complete Samples)'. *Biometrika* [online] 52 (3/4), 591. available from <http://www.jstor.org/stable/2333709?origin=crossref> [16 March 2017]

Shongwe, M.E., van Oldenborgh, G.J., van den Hurk, B., and van Aalst, M. (2011) 'Projected Changes in Mean and Extreme Precipitation in Africa under Global Warming. Part II: East Africa'. *Journal of Climate* 24 (14), 3718–3733

Sidibe, M., Dieppois, B., Mahé, G., Paturel, J.E., Amoussou, E., Anifowose, B., and Lawler, D. (2018) 'Trend and Variability in a New, Reconstructed Streamflow Dataset for West and Central Africa, and Climatic Interactions, 1950–2005'. *Journal of Hydrology* 561, 478–493

Silva, A.R., Pimenta, F.M., Assireu, A.T., and Spyrides, M.H.C. (2016) 'Complementarity of Brazils Hydro and Offshore Wind Power'. *Renewable and Sustainable Energy Reviews* 56, 413–427

Sinha, S. and Chandel, S.S. (2014) 'Review of Software Tools for Hybrid Renewable

Energy Systems'. *Renewable and Sustainable Energy Reviews* [online] 32, 192–205. available from <http://dx.doi.org/10.1016/j.rser.2014.01.035> [18 June 2016]

Sohoni, V., Gupta, S.C., and Nema, R.K. (2016) 'A Critical Review on Wind Turbine Power Curve Modelling Techniques and Their Applications in Wind Based Energy Systems'. *Journal of Energy* 2016 (region 4), 1–18

SolarGIS (2015) *Global Horizontal Irradiance* [online] available from <http://solargis.info/doc/free-solar-radiation-maps-GHI#B> [29 November 2016]

Souverijns, N., Thiery, W., Demuzere, M., and Lipzig, N.P.M.V. (2016) 'Drivers of Future Changes in East African Precipitation'. *Environmental Research Letters* 11 (11)

Sridharan, V., Broad, O., Shivakumar, A., Howells, M., Boehlert, B., Groves, D.G., Rogner, H.H., Taliotis, C., Neumann, J.E., Strzepek, K.M., Lempert, R., Joyce, B., Huber-Lee, A., and Cervigni, R. (2019) 'Resilience of the Eastern African Electricity Sector to Climate Driven Changes in Hydropower Generation'. *Nature Communications* [online] 10 (1), 1–9. available from <http://dx.doi.org/10.1038/s41467-018-08275-7> [13 March 2019]

Stadler, M. (2017) *A THREE PROJECT*. (31), 14–15

Stephens, M.A. (1986) 'Tests Based on EDF Statistics. Goodness-of-Fit Technique'. *Marcel Dekke* 68 (97–193)

Stiel, A. and Skyllas-Kazacos, M. (2012) 'Feasibility Study of Energy Storage Systems in Wind/Diesel Applications Using the HOMER Model'. *Applied Sciences* 2 (4), 726–737

Sturman, A. (2008) 'Weather and Climate'. *The Natural History of Canterbury* 119–142

Taylor, K.E. (2001) 'Summarizing Multiple Aspects of Model Performance in a Single Diagram'. *Journal of Geophysical Research* 106 (D7), 7183–7192

Taylor, K.E., Stouffer, R.J., and Meehl, G.A. (2012) 'An Overview of CMIP5 and the

Experiment Design'. *Bulletin of the American Meteorological Society* 93 (4), 485–498

Teutschbein, C. and Seibert, J. (2012) 'Bias Correction of Regional Climate Model Simulations for Hydrological Climate-Change Impact Studies: Review and Evaluation of Different Methods'. *Journal of Hydrology* [online] 456–457, 12–29. available from <http://dx.doi.org/10.1016/j.jhydrol.2012.05.052> [10 May 2015]

Thomson, A.M., Calvin, K. V., Smith, S.J., Kyle, G.P., Volke, A., Patel, P., Delgado-Arias, S., Bond-Lamberty, B., Wise, M.A., Clarke, L.E., and Edmonds, J.A. (2011) 'RCP4.5: A Pathway for Stabilization of Radiative Forcing by 2100'. *Climatic Change* 109 (1), 77–94

Thornthwaite, C.W. (1948) 'American Geographical Society An Approach toward a Rational Classification of Climate Author (s): C . W . Thornthwaite Published by : American Geographical Society Stable URL : Http://Www.Jstor.Org/Stable/210739 Accessed : 11-08-2016 18 : 02 UTC'. *Geographical Review* 38 (1), 55–94

Tobergte, D.R. and Curtis, S. (2013) 'No Title No Title'. *Journal of Chemical Information and Modeling* 53 (9), 1689–1699

TRAORE, V.B. (2014) 'Calibrating the Rainfall-Runoff Model GR4J and GR2M on the Koulountou River Basin, a Tributary of the Gambia River'. *American Journal of Environmental Protection* 3 (1), 36

Türkay, B.E. and Telli, A.Y. (2011) 'Economic Analysis of Standalone and Grid Connected Hybrid Energy Systems'. *Renewable Energy* 36 (7), 1931–1943

U.S.Energy Information Administration (2016) *International Energy Statistics* [online] available from <http://www.eia.gov/cfapps/ipdbproject/IEDIndex3.cfm?tid=2&pid=2&aid=2> [15 March 2016]

Ugirimbabazi, O. (2015) 'Analysis of Power System Options for Rural Electrification in

Rwanda'. *Master Thesis, University of Agder* 1.5 (May), 1–95

Uluyol, O., Parthasarathy, G., Foslien, W., and Kim, K. (2014) 'Power Curve Analytic for Wind Turbine Performance Monitoring and Prognostics'. *Proceedings of the Annual Conference of the Prognostics and Health Management Society 2011, PHM 2011* 435–442

UN-Energy (2005) 'The Energy Challenge for Achieving the Millennium Development Goals Energy and the MDGs'. *UN-Energy* 1–16

UNDP (2005) 'Energizing the Millennium Development Goals A Guide to Energy ' s Role in Reducing Poverty'. *Development* 24

UNECA (2018) *POLICY BRIEF 18: Accelerating SDG 7 IN Africa*.

UNECA (2014) *Energy Access and Security in Eastern Africa. Status and Enhancement Pathways* [online] available from <http://www.uneca.org/sites/default/files/publications/energy_access_and_security_in_ea_eng_fin_lowres_27dec2013.pdf> [16 May 2017]

UNFCCC (2015) *Convention on Climate Change: Climate Agreement of Paris.* [online] 1–25. available from <https://unfccc.int/process-and-meetings/the-paris-agreement/the-paris-agreement> [16 May 2017]

UNHCR (2016) *North-West Tanzania: Mtendeli Refugee Camp Profile* [online] Arlington, VA, USA. available from <https://reliefweb.int/sites/reliefweb.int/files/resources/65652.pdf> [16 May 2017]

University of East Anglia (2017) *Climatic Research Unit* [online] available from <http://www.cru.uea.ac.uk/data> [16 November 2017]

USAID (2019) *RWANDA: POWER AFRICA FACT SHEET* [online] available from <https://www.usaid.gov/powerafrica/rwanda> [17 September 2019]

USAID (2011) 'Powering Health: Electrification Options for Rural Health Centers'. *Power On: Electrification of Rural Health, Education and Tourism Facilities* 1–41

Valentin, G. (2013) *PV*SOL Advanced*.

Veilleux, J.C. (2017) *Water Conflict Case Study – Ethiopia's Grand Renaissance Dam: Turning from Conflict to Cooperation* ☆ [online] Elsevier Inc. available from <http://dx.doi.org/10.1016/B978-0-12-409548-9.09445-8> [13 May 2018]

van Vuuren, D.P., Edmonds, J., Kainuma, M., Riahi, K., Thomson, A., Hibbard, K., Hurtt, G.C., Kram, T., Krey, V., Lamarque, J.F., Masui, T., Meinshausen, M., Nakicenovic, N., Smith, S.J., and Rose, S.K. (2011) 'The Representative Concentration Pathways: An Overview'. *Climatic Change* 109 (1), 5–31

Wassie, Y.T. and Adaramola, M.S. (2019) 'Potential Environmental Impacts of Small-Scale Renewable Energy Technologies in East Africa: A Systematic Review of the Evidence'. *Renewable and Sustainable Energy Reviews* [online] 111 (September 2017), 377–391. available from <https://doi.org/10.1016/j.rser.2019.05.037> [17 September 2017]

Wayne, G.P. (2015) *The Beginner's Guide to Representative Concentration Pathways* [online] available from <http://www.skepticalscience.com/docs/RCP_Guide.pdf> [18 September 2018]

Welland, A. (2017) *Education and the Electrification of Rural Schools Smart Villages*. [online] (April). available from <www.e4sv.org%7Cinfo@e4sv.org%7C@e4SmartVillages> [18 September 2018]

Weyant, J., Azar, C., Kainuma, M., and Kejun, J. (2009) 'Report of 2.6 versus 2.9 Watts/M2 RCPP Evaluation Panel'. *Integrated Assessment* ... [online] available from <http://ipcc.ch/meetings/session17/doc3d.pdf%5Cnhttp://scholar.google.com/scholar?hl=en&btnG=Search&q=intitle:Report+of+2.6+Versus+2.9+Watts/m2+RCPP+Evaluation+Panel#0> [17 May 2018]

Whitlock, R. (2015) *Gigawatt Global Develops $23.7 Million Solar Farm for Rwanda* [online] available from <http://www.renewableenergymagazine.com/article/gigawatt-global-develops-23-7-million-solar-20150209> [11 February 2016]

Wild, M., Folini, D., Henschel, F., and Fischer, N. (2015) ‘Projections of Long-Term Changes in Solar Radiation Based on CMIP5 Climate Models and Their Influence on Energy Yields of Photovoltaic Systems’. *Solar Energy* 116, 12–24

WMO (2017) *WMO Guidelines on the Calculation of Climate Normals*. [online] (1203), 1–29. available from <https://library.wmo.int/doc_num.php?explnum_id=4166> [03 April 2018]

World Bank (2008) *New Data Show 1.4 Billion Live On Less Than US$1.25 A Day, But Progress Against Poverty Remains Strong* [online] available from <https://www.worldbank.org/en/news/press-release/2008/09/16/new-data-show-14-billion-live-less-us125-day-progress-against-poverty-remains-strong> [4 July 2018]

World Meteorological Organisation (2015) *Emission Scenarios* [online] available from <https://www.wmo.int/pages/themes/climate/emission_scenarios.php> [11 October 2015]

World Rivers Review (2012) ‘Dam Greenwashing Flows at World Water Forum’. *International Rivers,* 27 (1)

World Watch Institute (2010) ‘Greenwashing Hydropower’. *World Watch Magazine* [online] 23 (1). available from <http://www.worldwatch.org/node/6344> [04 July 2018]

Wu, M.L.C., Reale, O., and Schubert, S.D. (2013) ‘A Characterization of African Easterly Waves on 2.5-6-Day and 6-9-Day Time Scales’. *Journal of Climate* 26 (18), 6750–6774

Yang, W., Andréasson, J., Phil Graham, L., Olsson, J., Rosberg, J., and Wetterhall, F.

(2010) 'Distribution-Based Scaling to Improve Usability of Regional Climate Model Projections for Hydrological Climate Change Impacts Studies'. *Hydrology Research* 41 (3–4), 211

Yang, W., Seager, R., Cane, M.A., and Lyon, B. (2015a) 'The Rainfall Annual Cycle Bias over East Africa in CMIP5 Coupled Climate Models'. *Journal of Climate* 28 (24), 9789–9802

Yang, W., Seager, R., Cane, M.A., and Lyon, B. (2015b) 'The Annual Cycle of East African Precipitation'. *Journal of Climate* 28 (6)

Yang, W., Seager, R., Cane, M.A., and Lyon, B. (2014a) 'The East African Long Rains in Observations and Models'. *Journal of Climate* 27 (19)

Yang, W., Seager, R., Cane, M.A., and Lyon, B. (2014b) 'The East African Long Rains in Observations and Models'. *Journal of Climate* 27 (19), 7185–7202

Yuemei, H., Xiaoqin, Z., Jianguo, S., and Jina, N. (2008) 'Conduction between Left Superior Pulmonary Vein and Left Atria and Atria Fibrillation under Cervical Vagal Trunk Stimulation'. *Colombia Medica* 39 (3), 227–234

Zadoks, J.C. (1985) *This Week ' s Citation Classic* ®. 1985

Zayas, J., Derby, M., Gilman, P., Ananthan, S., Lantz, E., Cotrell, J., Beck, F., and Tusing, R. (2015) *Enabling Wind Power Nationwide*. (DOE/EE-1218), 43

Zhou, W., Lou, C., Li, Z., Lu, L., and Hongxing, Y. (2010) 'Current Status of Research on Optimum Sizing of Stand-Alone Hybrid Solar-Wind Power Generation Systems'. *Applied Energy* 87 (2), 380–389

Ziegler, L., Gonzalez, E., Rubert, T., Smolka, U., and Melero, J.J. (2018) 'Lifetime Extension of Onshore Wind Turbines: A Review Covering Germany, Spain, Denmark, and the UK'. *Renewable and Sustainable Energy Reviews* [online] 82 (October 2017), 1261–1271. available from <http://dx.doi.org/10.1016/j.rser.2017.09.100> [05 May 2018]

Zou, C., Zhao, Q., Zhang, G., and Xiong, B. (2016) 'Energy Revolution: From a Fossil Energy Era to a New Energy Era'. *Natural Gas Industry* 36 (1), 1–10

Appendices

Appendix A: Precipitation spatial changes over the EAC under RCP4.5

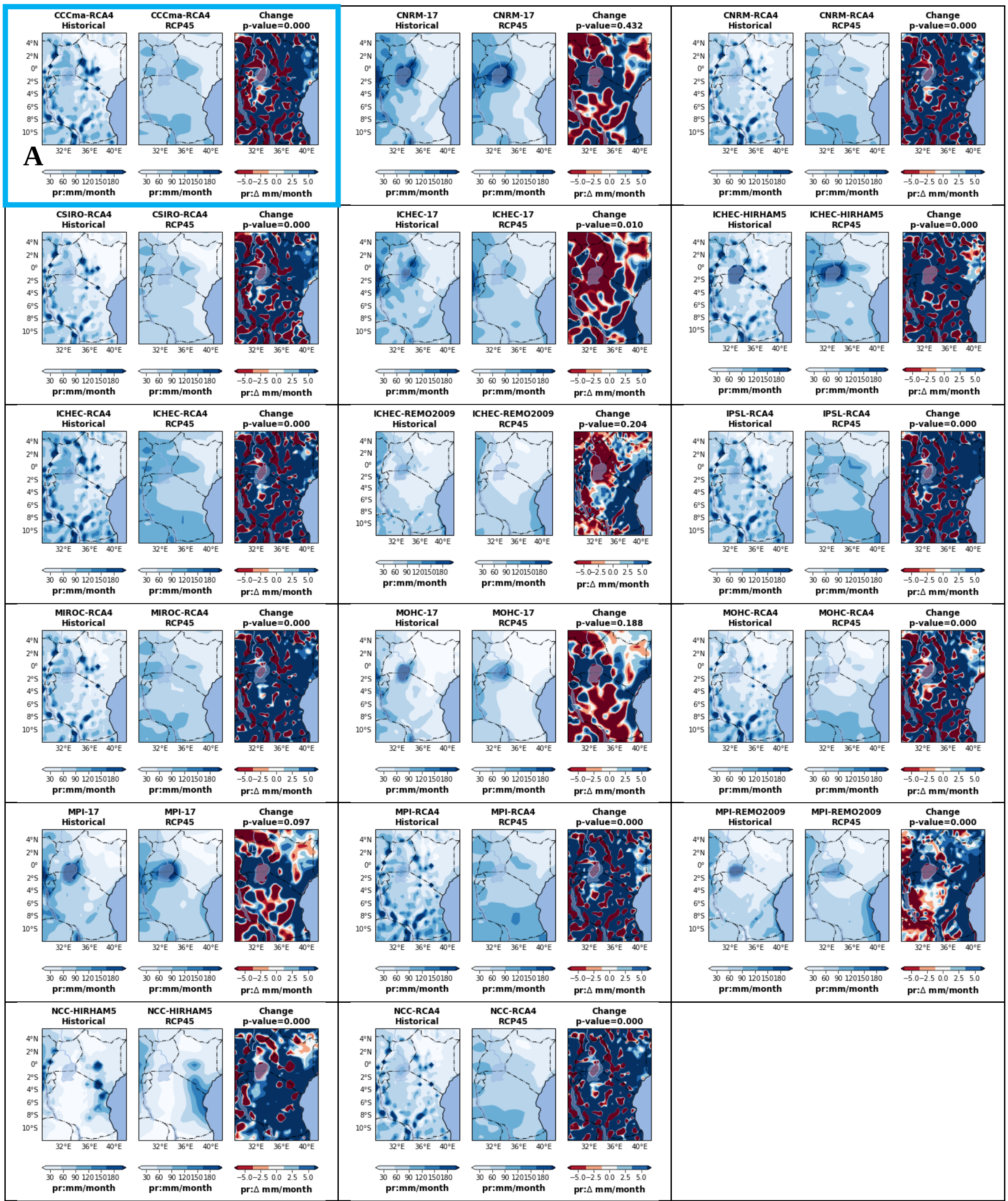

Three maps for precipitation are provided for each of the seventeen models and these maps are in one cell of as per cell[A] where this cell contains cccma-RCA4 model: The first map represents the historical, second map represent the future and the third map is the projected changes between historical and future precipitation under RCP4.5 scenario over the EAC. Changes in the third map are represented by a colour bar made of light to dark blue representing the field where changes are positive (wet conditions) and the white colour means that there is no change while the red colour representing the fields where changes are negative (dry conditions). Statistical significance of the changes is computed and the P-value is provided.

Appendix A2: Precipitation spatial changes over the EAC under RCP8.5

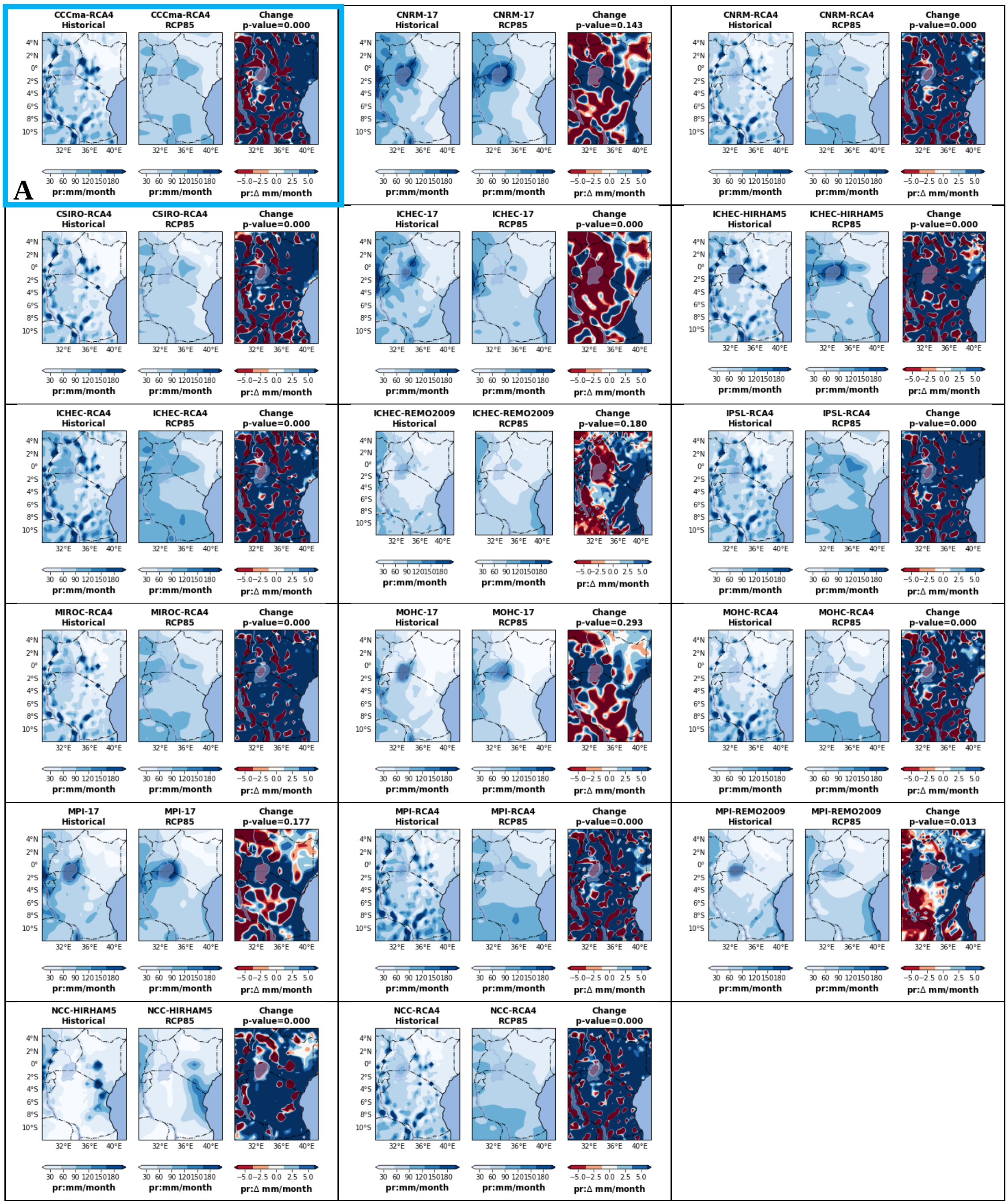

Three maps for precipitation are provided for each of the seventeen models and these maps are in one cell of as per cell[A] where this cell contains cccma-RCA4 model: The first map represents the historical, second map represent the future and the third map is the projected changes between historical and future precipitation under RCP8.5 scenario over the EAC. Changes in the third map are represented by a colour bar made of light to dark blue representing the field where changes are positive (wet conditions) and the white colour means that there is no change while the red colour representing the fields where changes are negative (dry conditions). Statistical significance of the changes is computed and the P-value is provided.

Appendix A3: Annual cycle monthly precipitation changes over the EAC under RCP4.5&8.5

RCP4.5 **RCP8.5**

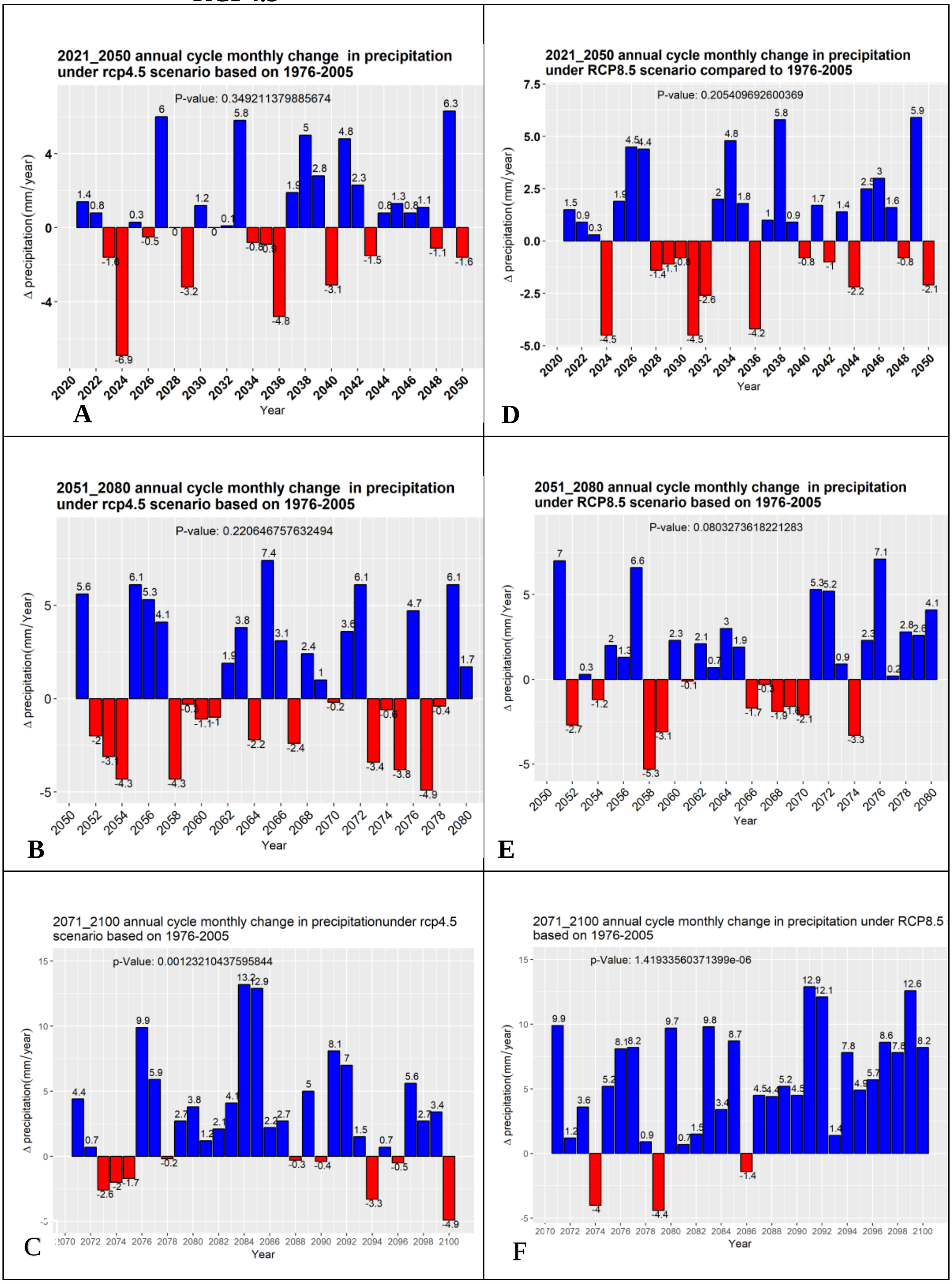

A, B, C, D, E and F are MME annual cycle monthly precipitation changes under RCP4.5 1st column &RCP8.5 2nd column based on the period of 1976-2005

Appendix A4: Monthly cycle changes in precipitation over the EAC under RCP4.5&8.5

RCP4.5 **RCP8.5**

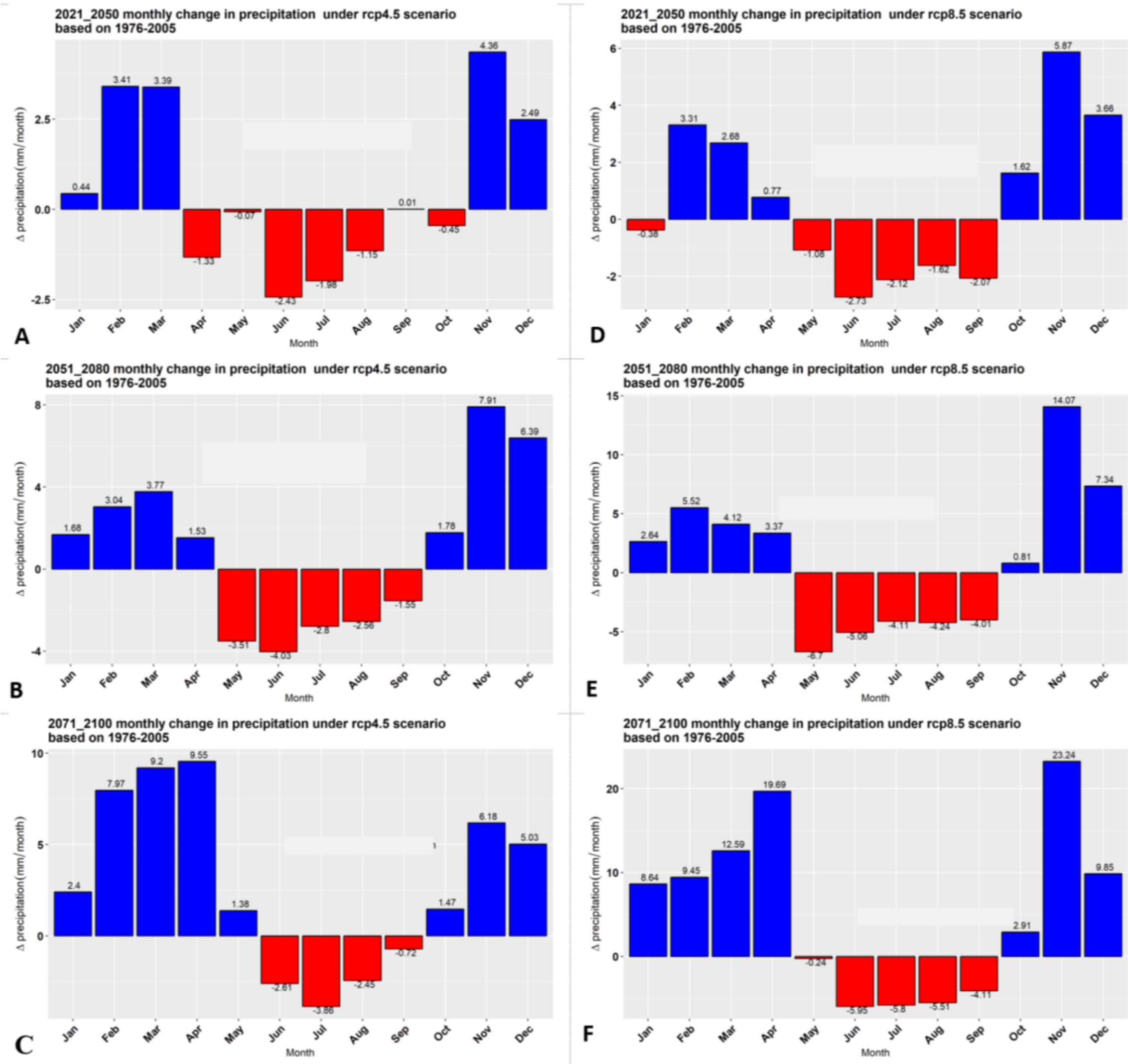

A, B, C, D, E and F are MME monthly cycle changes in precipitation under RCP4.5 1st column &RCP8.5 2nd column based on the period of 1976-2005.

Appendix B1: Temperature spatial changes over the EAC under RCP4.5

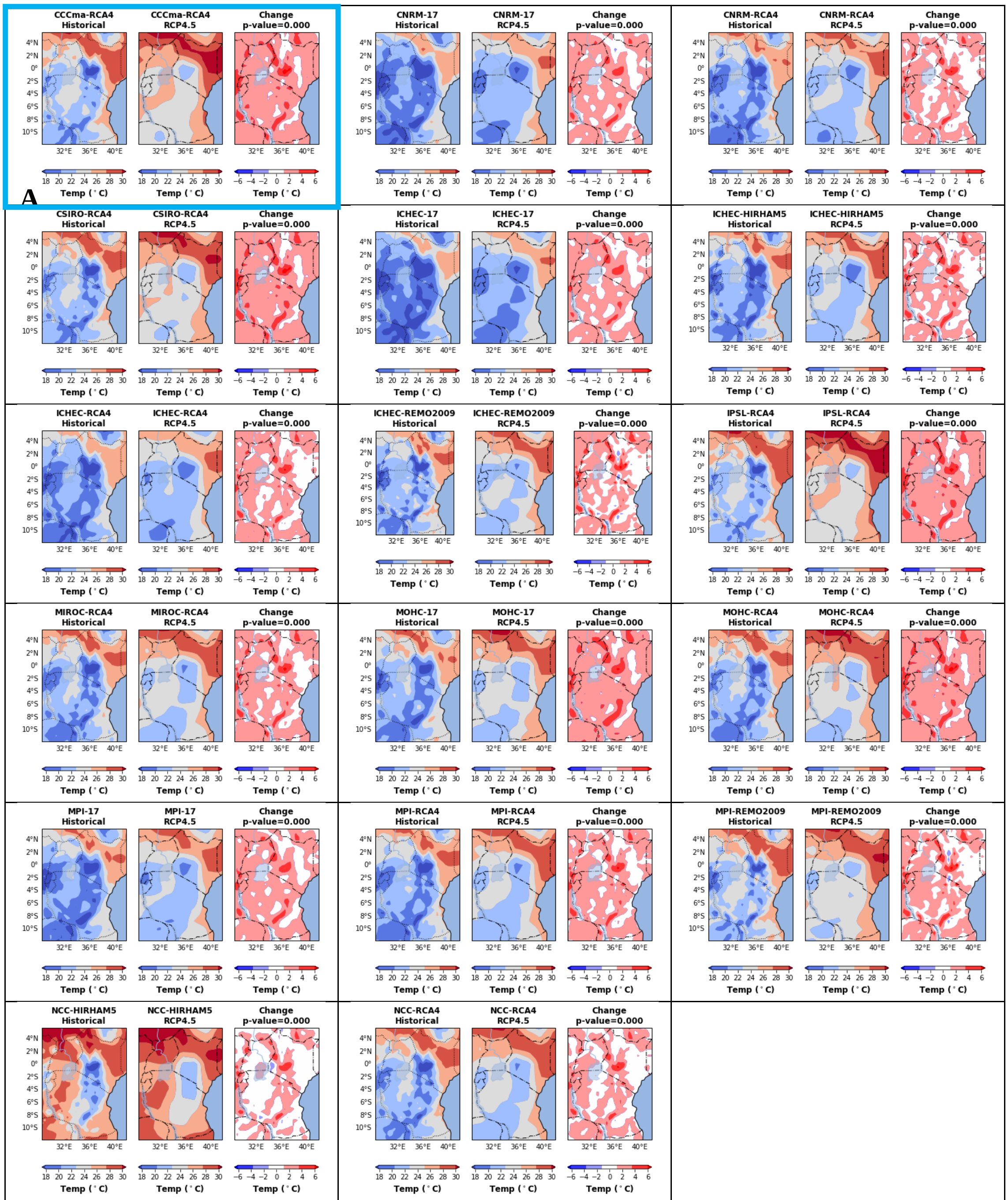

Three maps for temperature are provided for each of the seventeen models and these maps are in one cell of as per [A] where this cell contains cccma-RCA4 model: The first map represent the historical, second map represent the future and the third map is the projected changes between historical and future temperatures under RCP8.5 scenario over the EAC. Changes in the third map are represented by a colour bar made of light to dark blue representing the field where changes are negative(cool condition), and the white colour means that there is no change while the red colour (warm condition) representing represent the fields where changes are positive. Statistical significance of the changes is computed and the P-value is provided.

Appendix B1: Temperature spatial changes over the EAC under RCP8.5

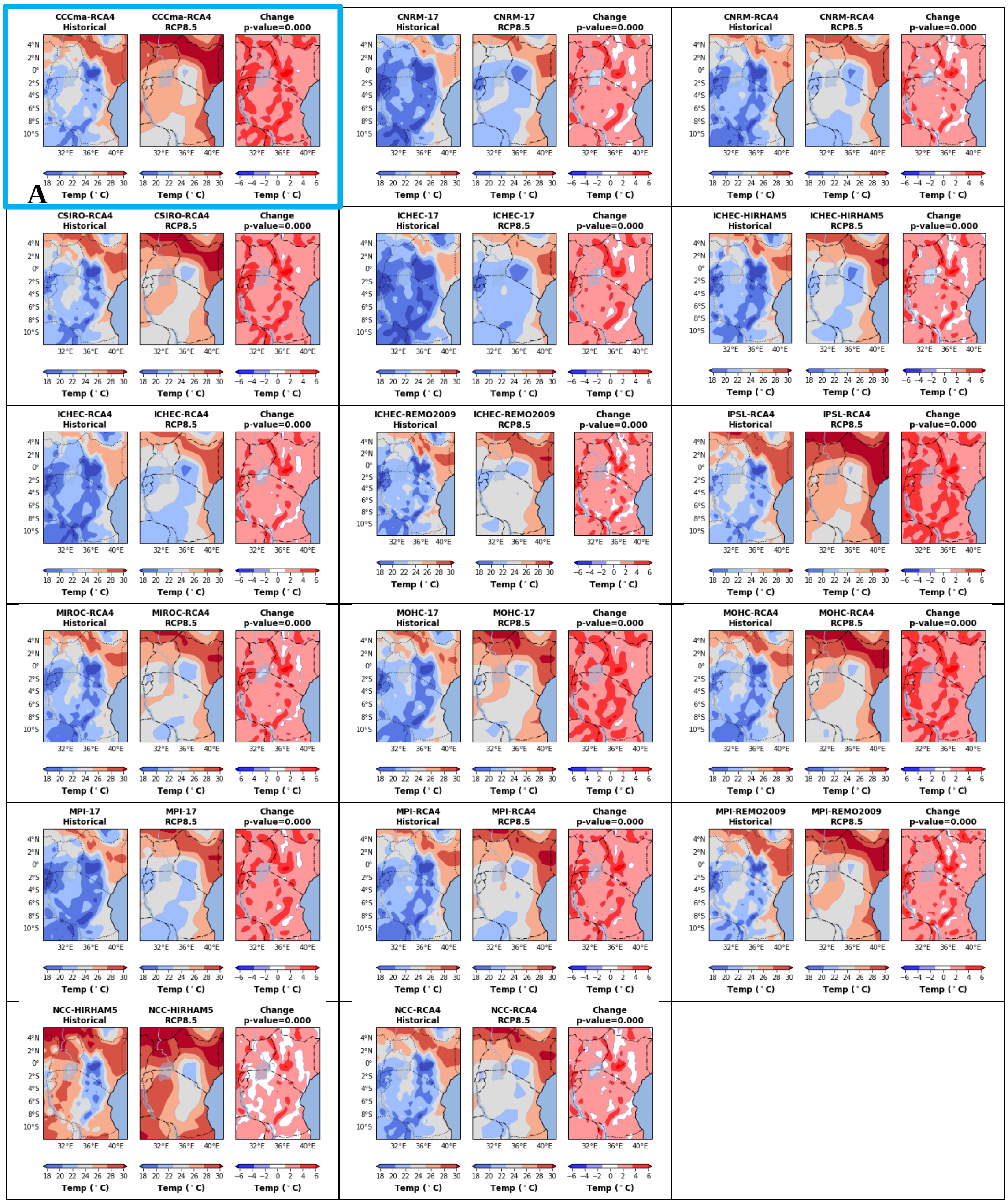

Three maps for temperature are provided for each of the seventeen models and these maps are in one cell of as per cell[A] where this cell contains cccma-RCA4 model: The first map represents the historical, second map represent the future and the third map is the projected changes between historical and future temperatures under RCP8.5 scenario over the EAC. Changes in the third map are represented by a colour bar made of light to dark blue representing the field where changes are negative(cool condition), and the white colour means that there is no change while the red colour (warm condition) representing the fields where changes are positive. Statistical significance of the changes is computed and the P-value is provided.

Appendix B3: Annual cycle temperature changes over the EAC under RCP4.5&8.5

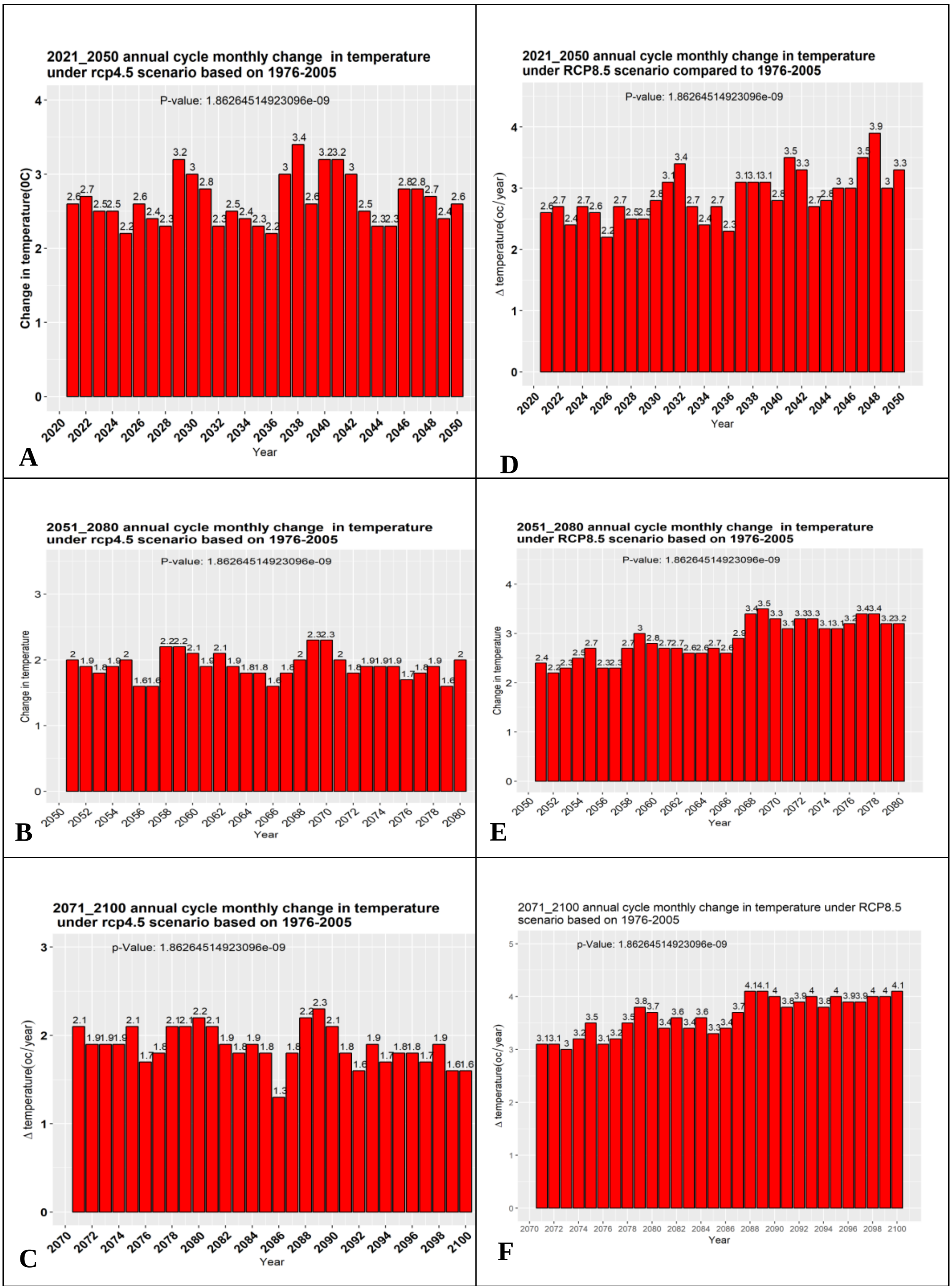

A, B, C, D, E and F are MME annual cycle monthly temperature changes under RCP4.5 1st column &RCP8.5 2nd column based on the period of 1976-2005.

Appendix B4: Monthly cycle changes in temperature over the EAC under RCP4.5&8.5

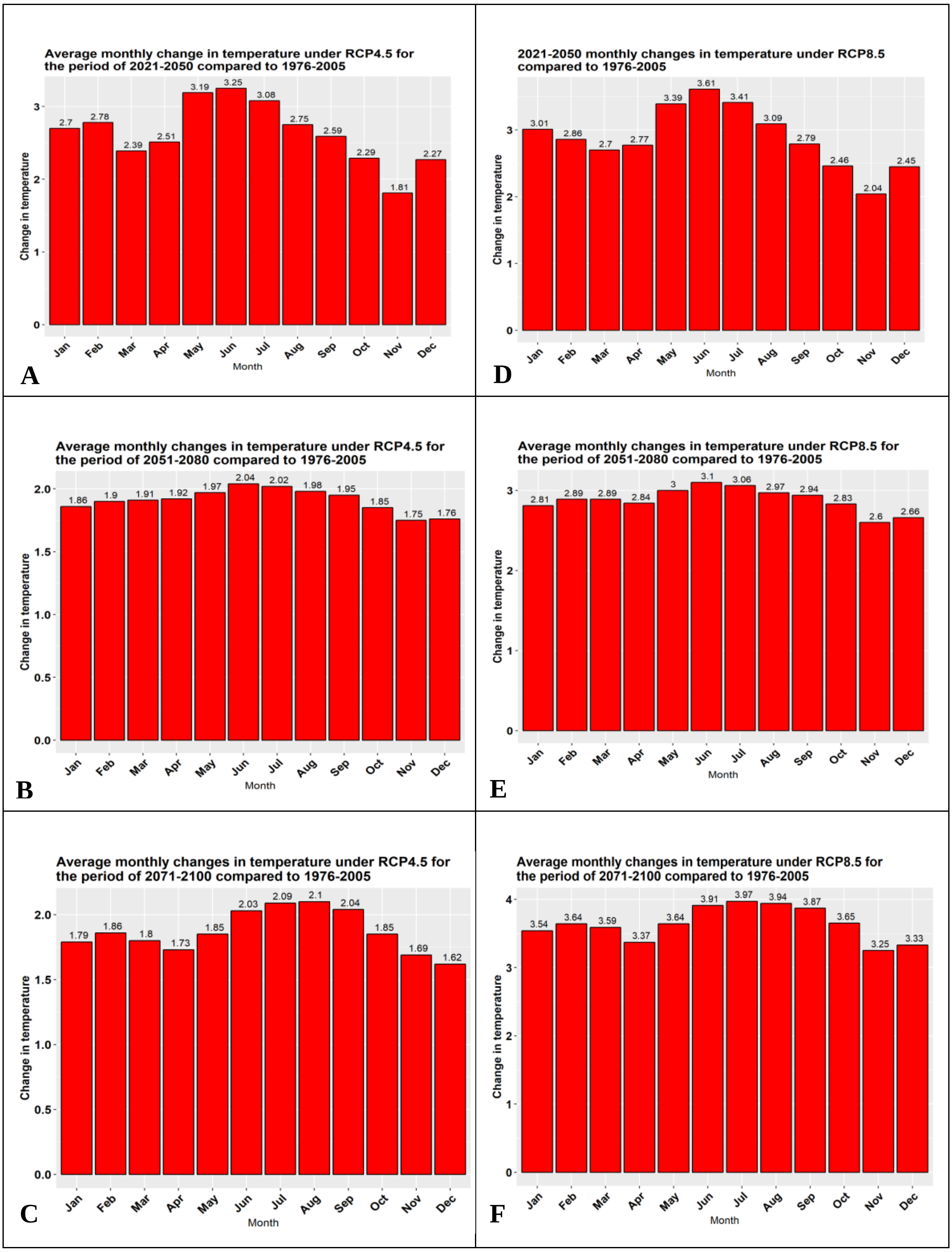

A, B, C, D, E and F are MME monthly cycle changes in temperature under RCP4.5 1st column &RCP8.5 2nd column based on the period of 1976-2005.

Appendix C1: Solar radiation spatial changes over the EAC under RCP4.5

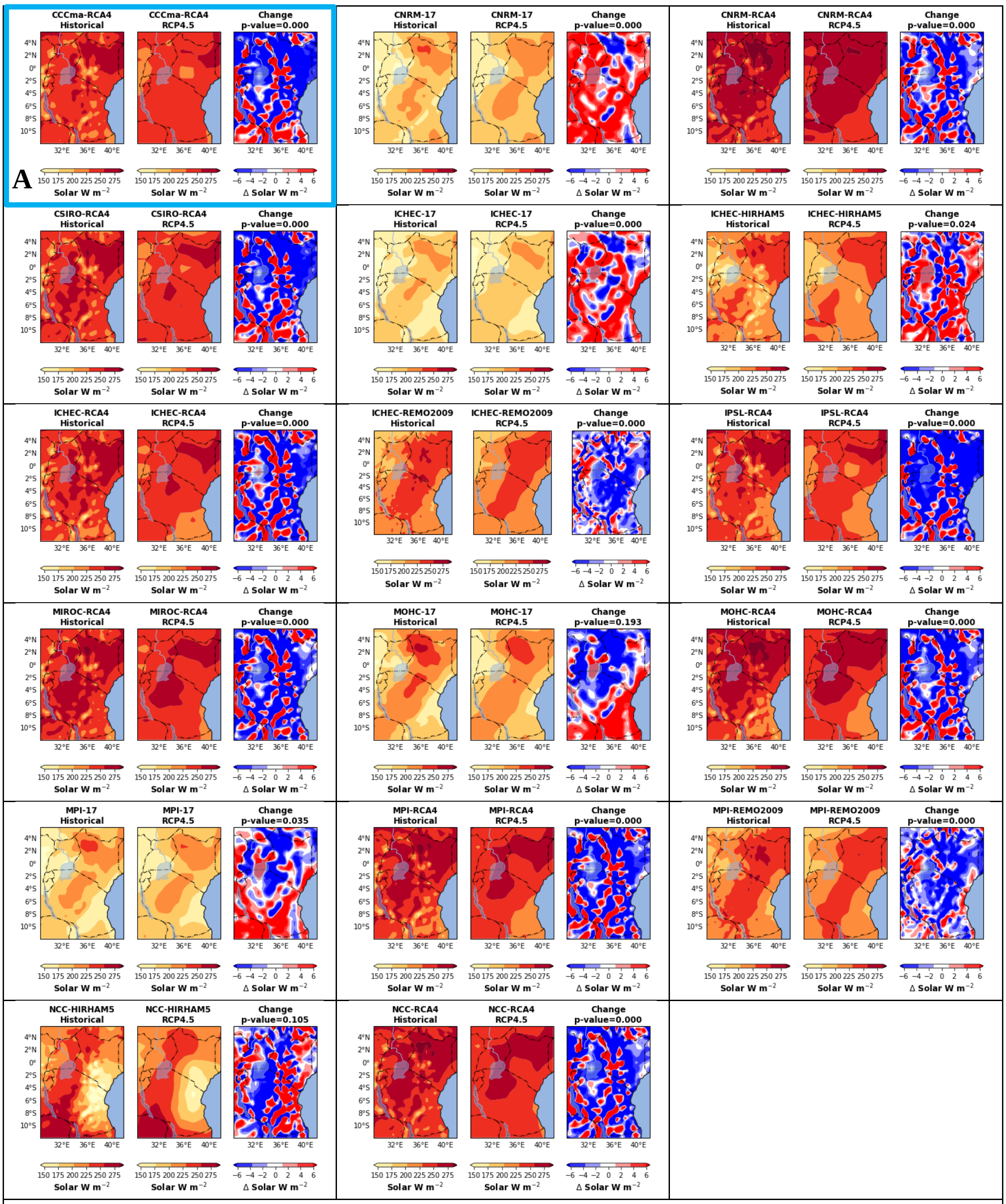

Three maps for solar radiation are provided for each of the seventeen models and these maps are in one cell of as per cell[A] where this cell contains cccma-RCA4 model: The first map represents the historical, second map represent the future and the third map is the projected changes between historical and future solar radiation under RCP4.5 scenario over the EAC. Changes in the third map are represented by a colour bar made of light to dark blue representing the field where changes are negative and the white colour means that there is no change while the red colour representing the fields where changes are positive. Statistical significance of the changes is computed and the P-value is provided.

Appendix C2: Solar radiation spatial changes over the EAC under RCP8.5

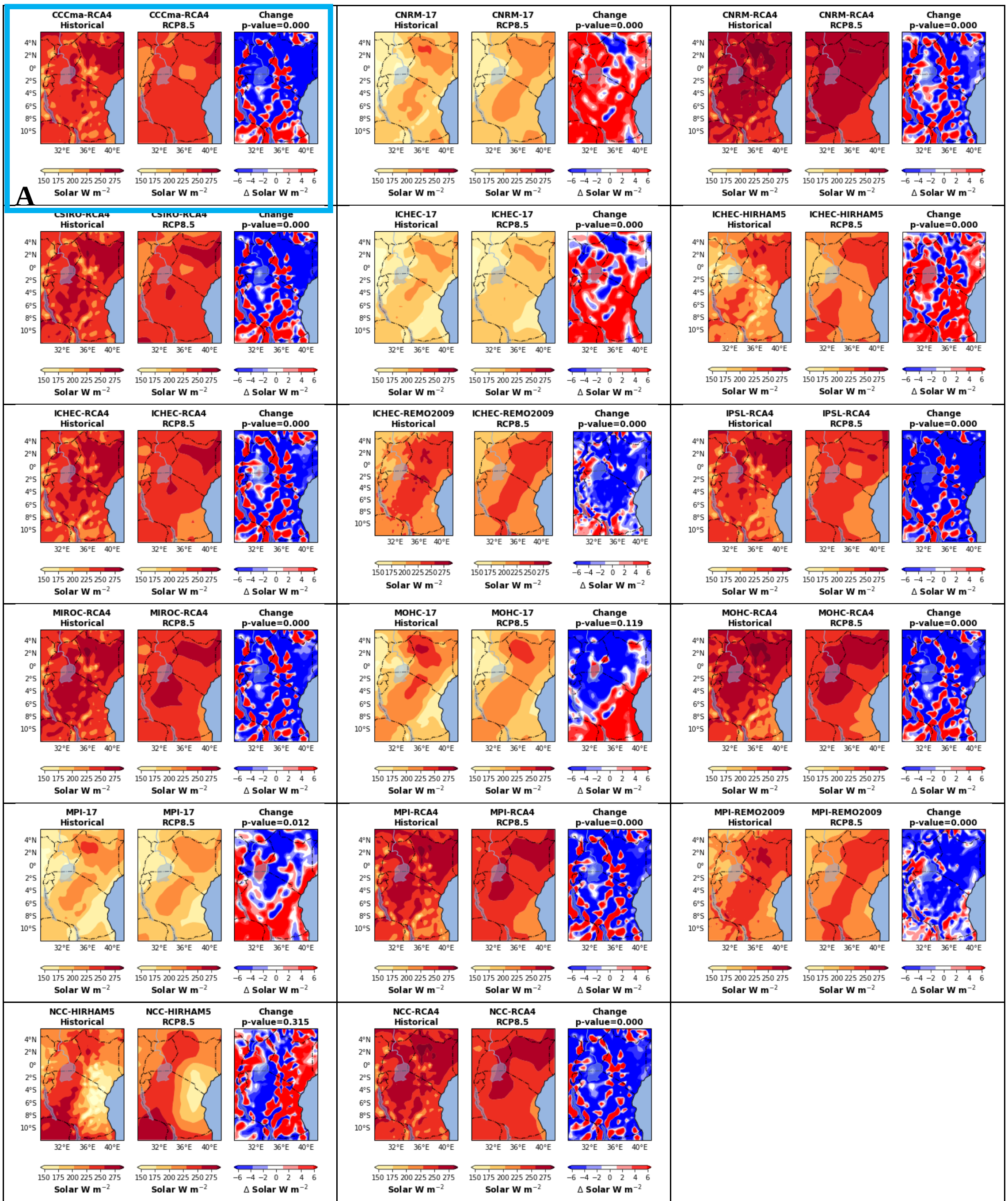

Three maps for solar radiation are provided for each of the seventeen models and these maps are in one cell of as per cell[A] where this cell contains cccma-RCA4 model: The first map represents the historical, second map represent the future and the third map is the projected changes between historical and future solar radiation under RCP8.5 scenario over the EAC. Changes in the third map are represented by a colour bar made of light to dark blue representing the field where changes are negative and the white colour means that there is no change while the red colour representing the fields where changes are positive. Statistical significance of the changes is computed and the P-value is provided.

Appendix C3: Annual cycle monthly mean solar radiation changes under RCP4.5&8.5

RCP4.5 **RCP8.5**

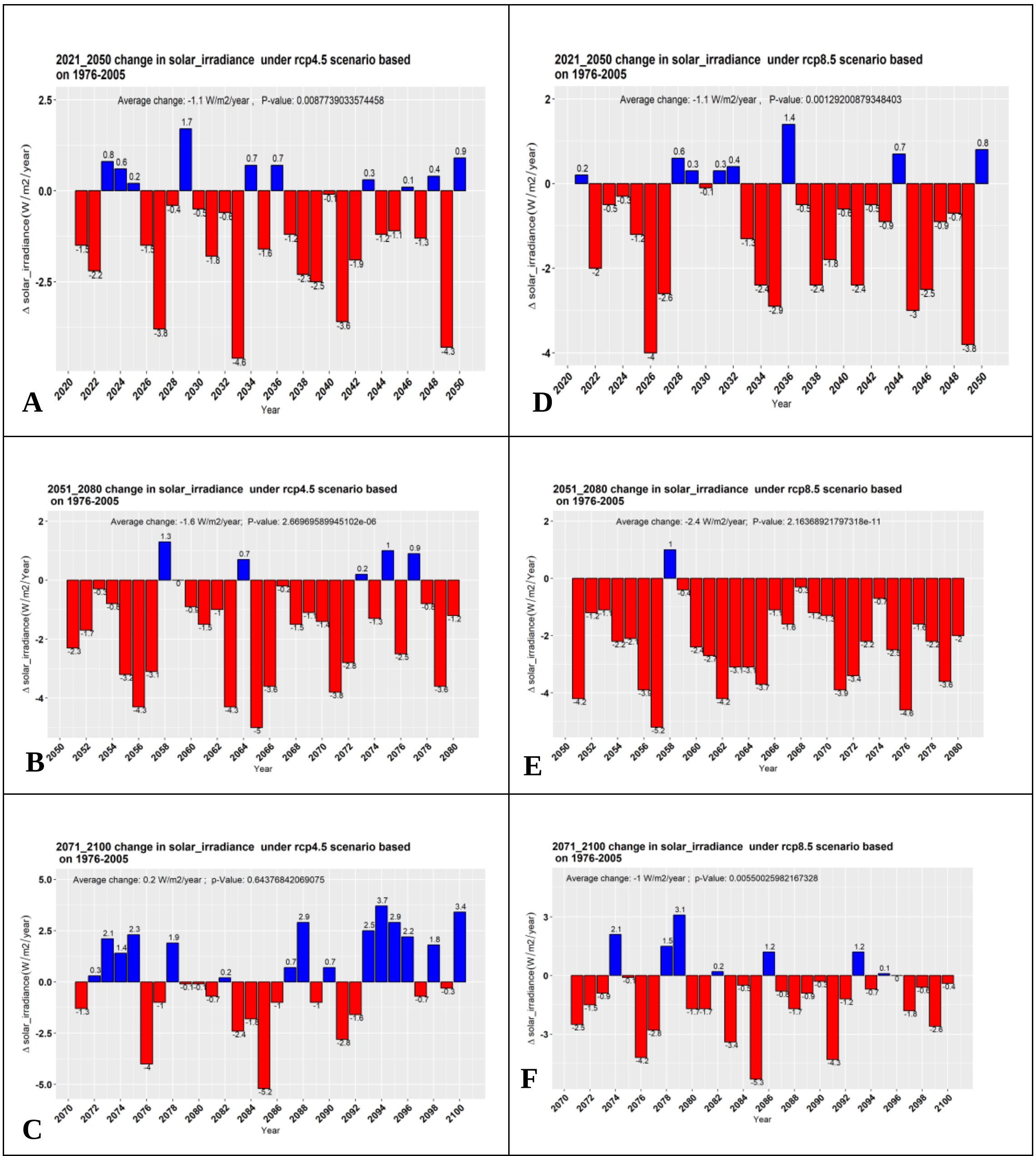

A, B, C, D, E and F are MME annual cycle solar radiation changes over the EAC under RCP4.5 1st column &RCP8.5 2nd column based on the period of 1976-2005

Appendix C4: Monthly cycle changes in solar radiation over the EAC under RCP4.5&8.5

RCP4.5 **RCP8.5**

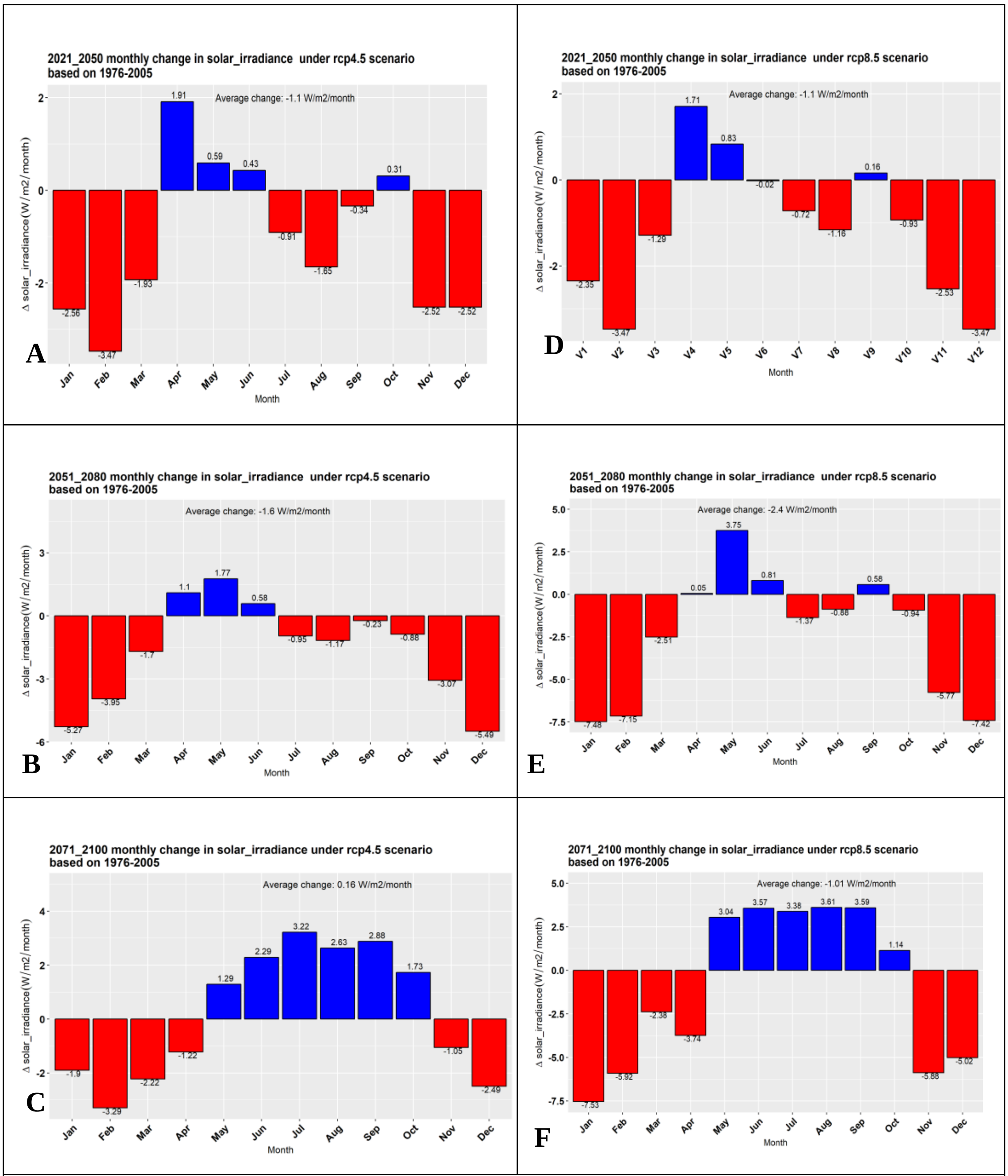

A, B, C, D, E and F are MME monthly cycle changes in solar radiation under RCP4.5 1st column &RCP8.5 2nd column based on the period of 1976-2005.

Appendix D1: Wind speed spatial changes over the EAC under RCP4.5

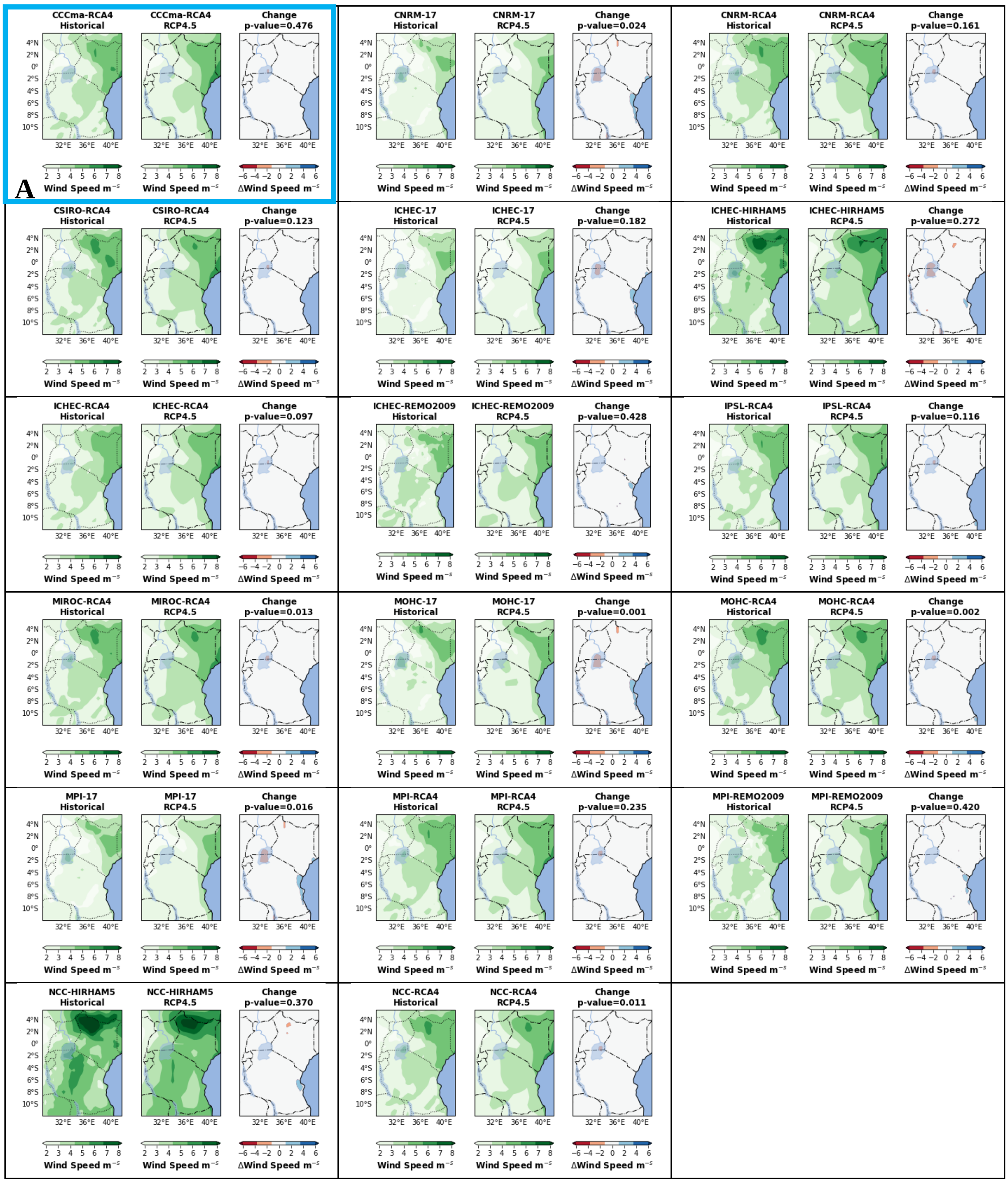

Three maps for wind speed are provided for each of the seventeen models and these maps are in one cell of as per cell[A] where this cell contains cccma-RCA4 model: The first map represents the historical, second map represent the future and the third map is the projected changes between historical and future wind speed under RCP4.5 scenario over the EAC. Changes in the third map are represented by a colour bar made of light to dark blue representing the field where changes are positive and the white colour means that there is no change while the red colour representing the fields where changes are negative. Statistical significance of the changes is computed and the P-value is provided.

Appendix D2: Wind speed spatial changes over the EAC under RCP8.5

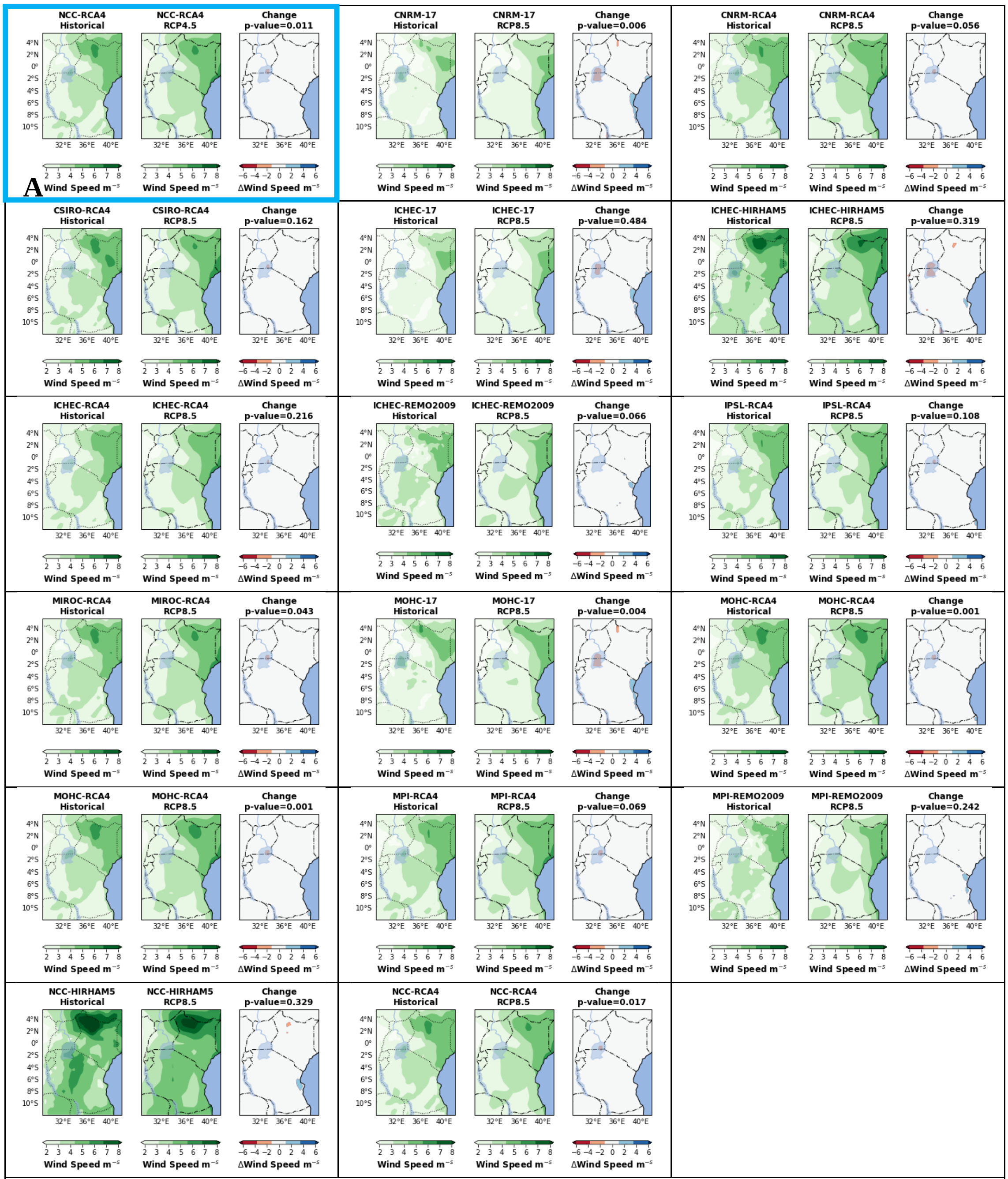

Three maps for wind speed are provided for each of the seventeen models and these maps are in one cell of as per cell[A] where this cell contains cccma-RCA4 model: The first map represents the historical, second map represent the future and the third map is the projected changes between historical and future wind speed under RCP8.5 scenario over the EAC. Changes in the third map are represented by a colour bar made of light to dark blue representing the field where changes are positive and the white colour means that there is no change while the red colour representing the fields where changes are negative. Statistical significance of the changes is computed and the P-value is provided.

Appendix D3: Annual cycle monthly wind speed changes over the EAC under RCP4.5&8.5

RCP4.5 **RCP8.5**

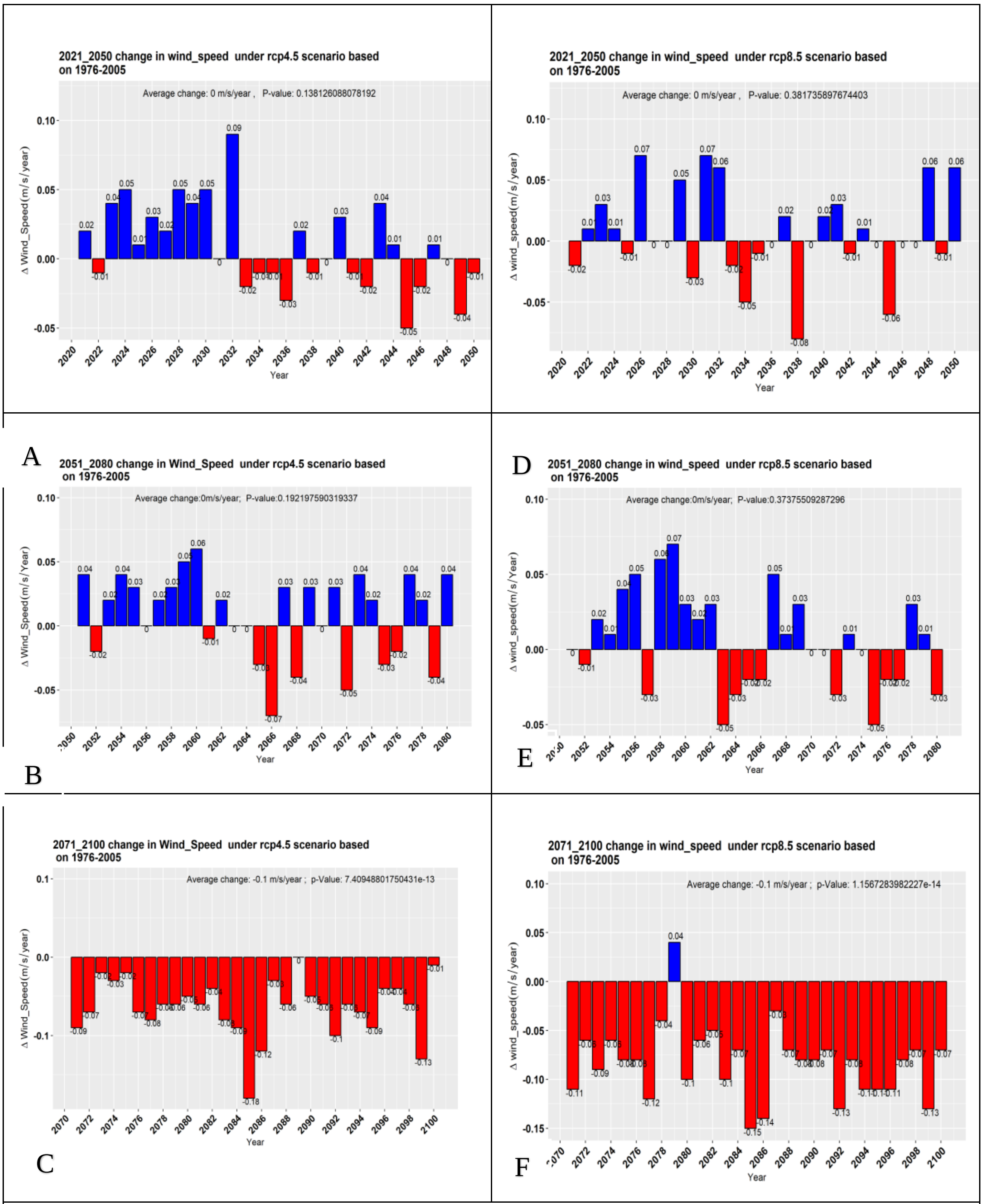

A, B, C, D, E and F are MME annual cycle monthly wind speed changes under RCP4.5 1st column &RCP8.5 2nd column based on the period of 1976-2005.